A METHODOLOGY FOR RAPID VEHICLE SCALING AND CONFIGURATION SPACE EXPLORATION

A Thesis
Presented to
The Academic Faculty

by

Davis Balaba

In Partial Fulfillment
of the Requirements for the Degree
Doctorate of Philosophy

School of Aerospace Engineering
Georgia Institute of Technology
May 2009

A METHODOLOGY FOR RAPID VEHICLE SCALING AND CONFIGURATION SPACE EXPLORATION

Approved by:

Professor Dimitri Mavris
Committee Chair
Department of Aerospace Engineering
Georgia Institute of Technology

Professor Daniel Schrage
Department of Aerospace Engineering
Georgia Institute of Technology

Dr. Danielle Soban
Aerospace Systems Design Laboratory
Georgia Institute of Technology

Dr. Sriram Rallabhandi
National Institute of Aerospace

Dean Ward
PACE Aerospace and IT GmbH

Mathias Emeneth
PACE Aerospace and IT GmbH

Date Approved: 8 January 2009

ACKNOWLEDGEMENTS

It was a gray Tuesday morning when I received a call from one Dr. Dimitri Mavris. After a brief "interview" he informed me that Christmas had come early for me as I had been admitted to Georgia Tech's prestigious Aerospace Systems Design Laboratory. I ran up to my room-mate's room shouting-laughing-yelling euphorically. She thought I had ingested something. But that demeanor, in a nutshell showed how much the news meant to me. Six years later, I have come to the end of this journey. I have been humbled by the number of times Dr. Mavris has gone beyond the call of duty to help me out of some sticky situations. Thank you, Doc.

I would also like to thank my URETI team-mates Dr. Taewoo Nam and Dr. Taeyun Choi for their multi-faceted assistance and support through this journey. To our leader, Dr. Soban, thank you for guiding us through our evolution from hyper-energized undergrads to exhausted, accomplished and sometimes disillusioned researchers.

To my Latex/LyX support team, Dr. Stephane Dufresne and Mandy Goltsch, merci bocoup and vielen dank!

I would also like to thank Dr. Elmer Gilbert of the University of Michigan and Professor Ong Chong Jin of the National University of Singapore for their invaluable support regarding all things "collision detection". Your work was a key enabler for my idea.

To my family, thank you mother for inspiring me to reach for the stars. Without you, none of this would have been. Ps. 20 years later, I still think you should have been mad at Mrs. Nakanwagi, my 3rd grade teacher, for spanking me because I got 99% (read failed to get 100%) in a math test.

To my wife Millie thank you for sticking with me and supporting me through my thesis-induced virtual absence.

To my son, Daren D.B. family tradition dictates that each generation raises the benchmark. Over to you now.

Contents

List of Tables

List of Figures

LIST OF ACRONYMS

AC	Aerodynamic Center
CAD	Computer Aided Design
CESM	Configuration-space Exploration and Scaling Methodology
CG	Center of Gravity
f	Fitness Function
FC	Fuel Cell
FLOPS	Flight Optimization System
GA	General Aviation
GAs	Genetic Algorithms
GB	Gigabytes
K	Boltzman Constant
M	Mach Number
MHz	Mega Hertz
NSGA	Non-dominated Sorting Genetic Algorithm
OEC	Overall Evaluation Criterion
OML	Outer Mold Line
P	Power
PC	Personal Computer
PDE	Partial Differential Equation
PEM	Proton Exchange Membrane
PMAD	Power Management and Distribution unit
QFD	Quality Function Deployment
RAM	Random Access Memory

RFP	Request For Proposal
SA	Simulated Annealing
SFC	Specific Fuel Consumption
SOFC	Solid Oxide Fuel Cell
T	Installed Thrust
URETI	University Research : Engineering and Technology Institute
VSP	Vehicle Sketch Pad

SUMMARY

Drastic changes in aircraft operational requirements and the emergence of new enabling technologies often occur symbiotically with advances in technology inducing new requirements and vice versa. These changes sometimes lead to the design of vehicle concepts for which no prior art exists. They lead to revolutionary concepts. In such cases the basic form of the vehicle geometry can no longer be determined through an ex ante survey of prior art as depicted by aircraft concepts in the historical domain. Ideally, baseline geometries for revolutionary concepts would be the result of exhaustive configuration (or subsystem layout) space exploration and optimization. Numerous component layouts and their implications for the minimum external dimensions of the resultant vehicle would be evaluated. The dimensions of the minimum enclosing envelope for the best component layout(s) (as per the design need) would then be used as a basis for the selection of a baseline geometry. Unfortunately layout design spaces are inherently large. The process must thus be automated. Automation makes a key contributing analysis i.e. automated detection of collisions between subsystems imperative. This key analysis can be very expensive. When an appropriate baseline geometry has been identified, another hurdle i.e. vehicle scaling has to be overcome. Through the design of a notional Cessna C-172R powered by a liquid hydrogen Proton Exchange Membrane (PEM) fuel cell, it was demonstrated that the various approaches to vehicle scaling i.e. photographic and historical-data-based regression can result in highly sub-optimal results even for very small $O(10^{-3})$ scale factors. Building complete CAD mock-ups for each of what could be thousands of designs and then analysing the scaling behavior of each can also be computationally prohibitive. Therefore, there is a need for higher fidelity and relatively inexpensive vehicle scaling laws especially since emergent technologies tend to be volumetrically and/or gravimetrically constrained when compared to incumbents.

The Configuration-space Exploration and Scaling Methodology (CESM) is postulated

herein as a solution to the above-mentioned challenges. This bottom-up methodology entails the representation of component or sub-system geometries as matrices of points in 3D space. These typically large matrices are reduced using minimal convex sets or convex hulls. This reduction leads to significant gains in collision detection speed at minimal approximation expense. (The Gilbert-Johnson-Keerthi algorithm [79] is used for collision detection purposes in this methodology.) Once the components are laid out, their collective convex hull (from here on out referred to as the super-hull) is used to approximate the inner mold line of the minimum enclosing envelope of the vehicle concept. A sectional slicing algorithm is used to extract the sectional dimensions of this envelope. An offset is added to these dimensions in order to come up with the sectional fuselage dimensions. Once the lift and control surfaces are added, vehicle level objective functions can be evaluated and compared to other designs. The size of the design space coupled with the fact that some key constraints such as the number of collisions are discontinuous, dictate that a domain-spanning optimization routine be used. Also, as this is a conceptual design tool, the goal is to provide the designer with a diverse baseline geometry space from which to chose. For these reasons, a domain-spanning algorithm with counter-measures against speciation and genetic drift is the recommended optimization approach. The Non-dominated Sorting Genetic Algorithm (NSGA-II) [60] is shown to work well for the proof of concept study.

There are two major reasons why the need to evaluate higher fidelity, custom geometric scaling laws became a part of this body of work. First of all, historical-data based regressions become implicitly unreliable when the vehicle concept in question is designed around a disruptive technology. Second, it was shown that simpler approaches such as photographic scaling can result in highly suboptimal concepts even for very small scaling factors. Yet good scaling information is critical to the success of any conceptual design process. In the CESM methodology, it is assumed that the new technology has matured enough to permit the prediction of the scaling behavior of the various subsystems in response to requirement changes. Updated subsystem geometry data is generated by applying the new requirement settings to the affected subsystems. All collisions are then eliminated using the NSGA-II algorithm. This is done while minimizing the adverse impact on the vehicle packing density.

Once all collisions are eliminated, the vehicle geometry is reconstructed and system level data such as fuselage volume can be harvested. This process is repeated for all requirement settings. Dimensional analysis and regression can be carried out using this data and all other pertinent metrics in the manner described by Mendez [124] and Segel [173]. The dominant parameters for each response show up as in the dimensionally consistent groups that form the independent variables. More importantly the impact of changes in any of these variables on system level dependent variables can be easily and rapidly evaluated. In this way, the conceptual design process can be accelerated without sacrificing analysis accuracy. Scaling laws for take-off gross weight and fuselage volume as functions of fuel cell specific power and power density for a notional General Aviation vehicle are derived for the proof of concept.

CESM enables the designer to maintain design freedom by portably carrying multiple designs deeper into the design process. Also since CESM is a bottom-up approach, all proposed baseline concepts are implicitly volumetrically feasible. System level geometry parameters become fall-outs as opposed to inputs. This is a critical attribute as, without the benefit of experience, a designer would be hard pressed to set the appropriate ranges for such parameters for a vehicle built around a disruptive technology. Furthermore, scaling laws generated from custom data for each concept are subject to less design noise than say, regression based approaches. Through these laws, key physics-based characteristics of vehicle subsystems such as energy density can be mapped onto key system level metrics such as fuselage volume or take-off gross weight. These laws can then substitute some historical-data based analyses thereby improving the fidelity of the analyses and reducing design time.

Chapter I

MOTIVATION

From 1-g flight in the early 1900s to radar transparency in the 1950s to today's increasing emphasis on green transport, significant changes in aircraft requirements or technologies have manifested themselves in major topological changes in the affected vehicles. Today, aircraft conceptual design methods have advanced to such a level that reliable assessments and predictions of technology impacts on vehicle systems can be made analytically. There are instances, however, when incumbent and emerging technologies exhibit such disparate volumetric and gravimetric properties that the geometric treatment of vehicles in the aforementioned analytical methods must be buttressed with vehicle-specific information in order to reach acceptable and defensible conclusions. The emergence of fuel cells as a candidate technology for alternative aircraft propulsion is one such instance.

Attempts to retrofit a General Aviation (GA) vehicle with this technology as a way of assessing its potential, revealed that the typical GA vehicle geometry does not leverage the technology's key strong suit, that is modularity. For this and similar technologies, the appropriate baseline geometry can no longer be easily identified by performing a cursory evaluation of the geometric concept space as depicted by prior art. The designer must explore a multitude of subsystem layouts in order to identify the portion of the geometric concept space that is best suited for the technology.

The emergence of new technologies and changes in operational requirements often occur symbiotically with advances in technology inducing changes in requirements and vice versa. Emissions concerns have, for example, led to policy changes in the US and around the world inducing a stronger focus on cleaner fuels. In his 2006 state of the union address, President George Bush noted:

> *"Here we have a serious problem: America is addicted to oil, which is often imported from unstable parts of the world... We will increase our research in*

better batteries for hybrid and electric cars, and in pollution-free cars that run on hydrogen".

The onus is thus now on the scientific community to develop innovative solutions to this imminent problem. Alternative fuels also come with the promise of cleaner exhaust which could help mitigate global warming effects. The CO_2 emission coefficient of some popular and prospective aviation fuels is shown in Table 1 below. With no CO_2 emissions LH_2 makes a very desirable candidate for green transport.

Table 1: Emission Coefficients of Various Aviation Fuels

Fuel	***Emission Coefficient*** ($\frac{lbCO_2}{gal}$)
Aviation Kerosene	21.5
Jet A	21.1
Aviation Gasoline	18.4
LH_2	0.0

Typically, there is more than one technology vying to fill an identified gap or to satisfy an emergent need e.g. Solid Oxide Fuel Cells, Proton Exchange Membrane Fuel Cells and batteries for greener transport. In such scenarios the question becomes, "to which prospective sources should the limited human and financial resources be dedicated?". A definitive answer to this question can only be reached by comparing the performance of the optimal vehicle platforms for each technology.

An end to the global "addiction" to oil comes with a promise of not only more stable economies but perhaps a more peaceful world where the need to stabilize oil prices is not a key influence on the foreign policy of developed nations. As seen in Figure 1 below, the highly volatile prices seem to be headed for the record levels of the early 1980's. Buoyed by the increasing consumption of the new "tiger" economies like China and India, the demand for oil is growing much faster than the supply. The rumination of this trend paints a bleak picture for the state of the global economy in the coming decades. Increased use of alternative energies will not only reduce the demand for and dependency on oil but it may also help increase price stability thereby assuaging these fears. Concerns about oil use are not just economic in nature but they are also environmental. Global warming, though still a contentious issue among scientists and politicians, is becoming increasingly self-evident

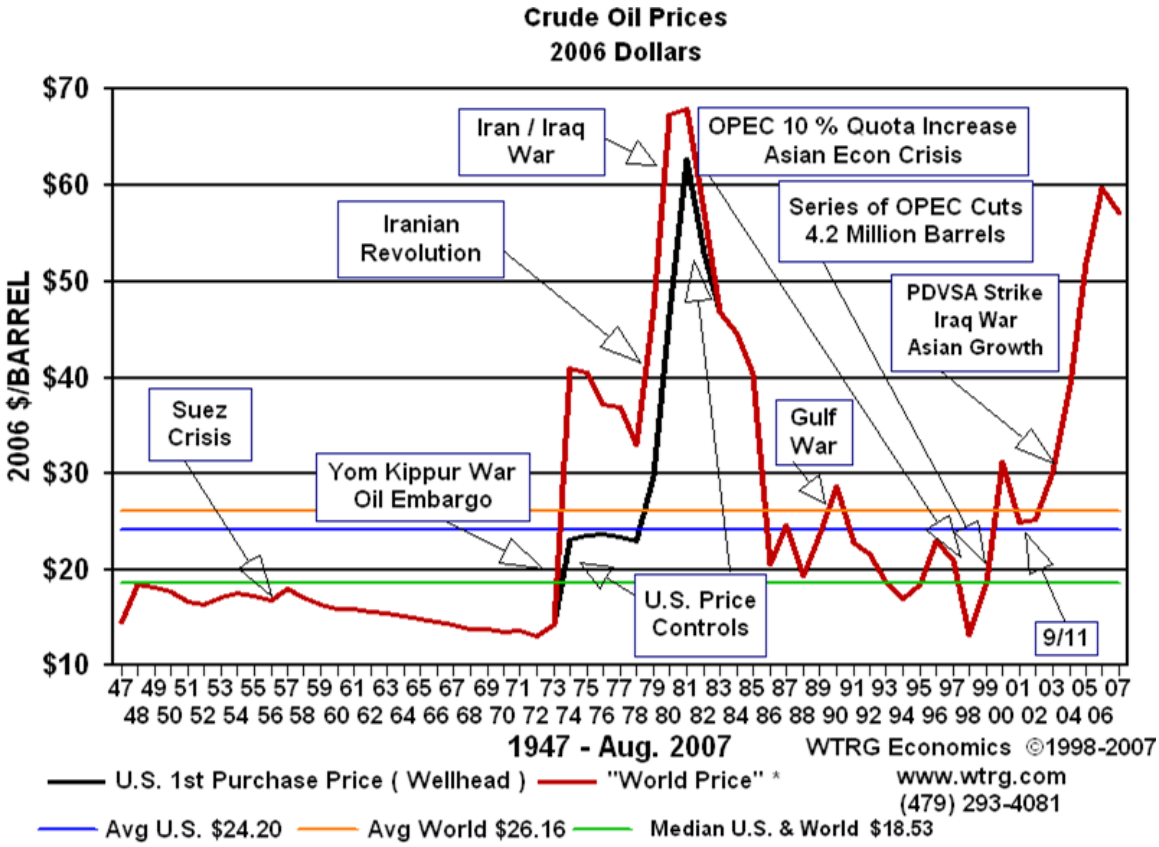

Figure 1: Oil Price Volatility [65]

even to the untrained eye. This claim is evident in the pictures of the Mount Kilimanjaro shown in Figure 2 below.

Some of the research funding that President George Bush alluded to in his address came in the form of the University Research : Engineering and Technology Institute (URETI). As part of the URETI Task 2.1.2, Georgia Institute of Technology's Aerospace Systems Design Laboratory undertook the task of formulating and developing physics-based methods for the analysis and design of revolutionary concepts, architectures and technologies. This task involved the identification of challenges that revolutionary architectures or technologies present to conventional design methodologies as well as the development of solutions or methodologies that overcome these impediments. An overview of the research vision for the project is shown in Figure 3 . This project is the core source of the motivation behind the thesis described herein.

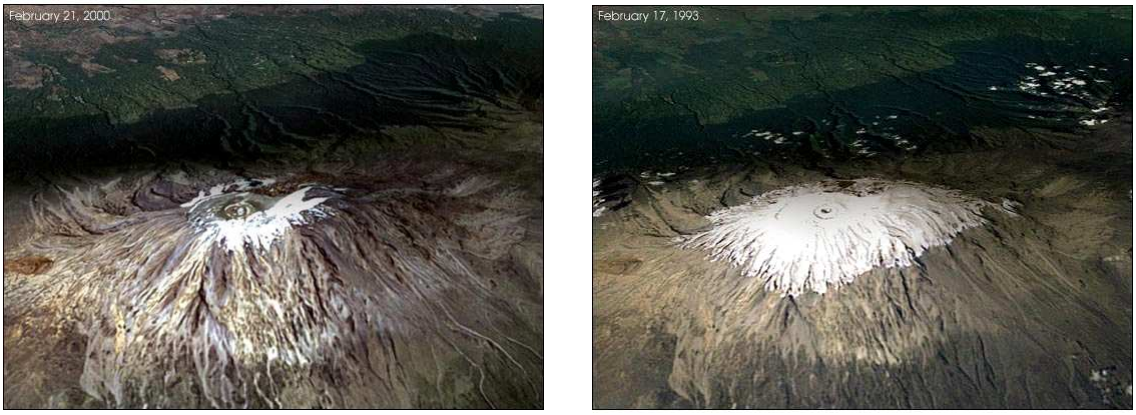

Figure 2: Mount Kilimanjaro Ice Cap 20^{th} Century and 21^{st} Century [145]

The first phase of the research plan involved the application of the revolutionary technologies to conventional aircraft architectures. The goal was to identify deficiencies in conventional design methods and to eventually plug these holes in the second phase of the project. The major areas of research included electric propulsion modeling, revolutionary concept sizing and synthesis as well as volumetric sizing. Dr. Taeyun Choi [48] addressed the area of electric propulsion system modeling, while Dr. Taewoo Nam [137] addressed revolutionary concept sizing using a generalized power-based approach. Dr. Eric Upton [193] and the author tackled the volumetrics aspect with the goal of devising inexpensive methodologies for the direct integration of volumetric analyses in vehicle conceptual design. The synthesis of these three areas would involve an iterative process where aircraft geometry and propulsion system specifications were fed into a volumetric analysis module which compared available to required volume. The geometry would be scaled until a concept that satisfies all three balances is achieved. In attempting to identify the holes or challenges that disruptive technologies pose to conventional design methods a three-step process was followed i.e. retrofit, rescale and redesign. This study was performed using a notional Cessna C-172R baseline vehicle powered by a Proton Exchange Membrane (PEM) fuel cell power plant as a test-bed.

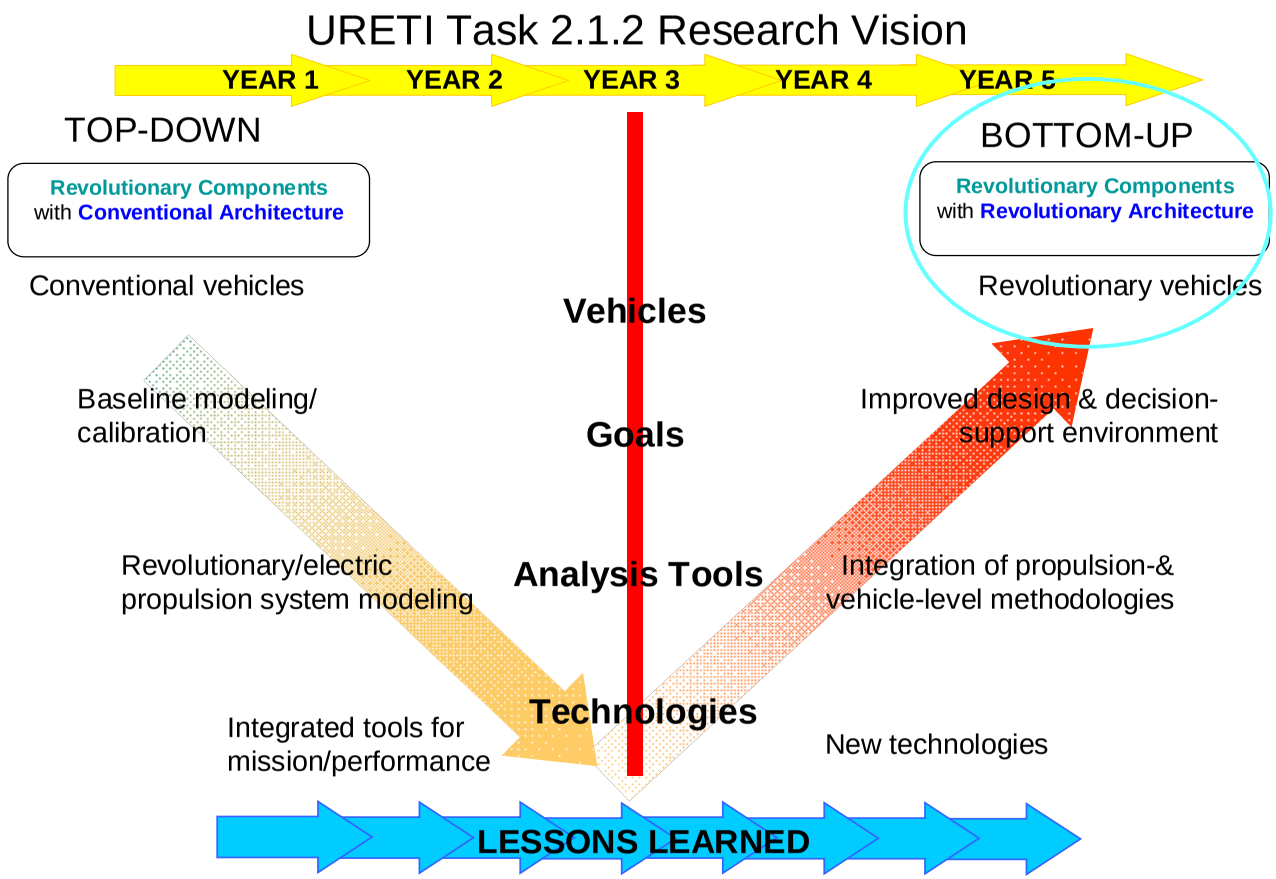

Figure 3: Overview of URETI Task 2.1.2 Vision [179]

1.1 *Disruptive Technologies Case Study: PEM Fuel Cell powered Cessna C-172R [188]*

Coined by Harvard Business School professor, Clayton M. Christensen, the term disruptive technology refers to:

> *"A technology that introduces a very different package of attributes from the one mainstream customers typically value, and often performs worse along some dimensions that are particularly important to those customers"* [34].

Christensen proceeds to note that as customers continue to streamline and increase their demands, the superior performance attributes of a disruptive technology become key players in the customer's decision to buy. At this point, he contends, it is usually too late for the reluctant adopters that most incumbent firms tend to be. This metaphor can be extended to the national level. Nations that desire to remain at the leading edge of technological innovation must continually invest in the disruptive technologies of tomorrow. Fuel cells are one example of a possible disruptive technologies.

Like any new technology, fuel cells have been faced with the challenge of winning over the hearts and minds of both end-use customers and the businesses that could use the technology to power their products. The enthusiasts and visionaries described in Figure 4 have mainly come from the automotive industry [73, 93, 189]. As the effects of climate change become more explicit, this technology could garner the interest and demand that would fuel the investment in research and development (R&D) that could take it over the chasm into the mainstream market.

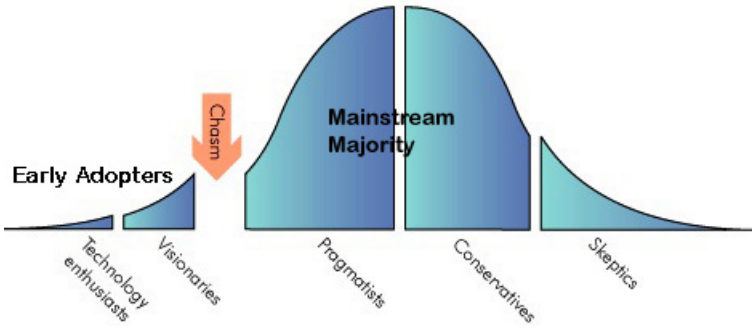

Figure 4: Diffusion of Technologies [165]

1.1.1 Background

The logical approach to investigating the feasibility of new technologies is first to attempt to retrofit an existent vehicle, then to rescale the concept in case some constraints are violated or over-satisfied and eventually to design a new concept if two previous steps do not produce a feasible or viable concept. In reaching valid conclusions at each of the three steps a number of tools and metrics are necessary.

In the preliminary assessment of the feasibility of a propulsion system the most important metrics are the specific thrust or power $\frac{T}{W}$ or $\frac{P}{W}$ ratio and the overall efficiency of the propulsion system. The fuel specific density and specific weight are equally critical especially when dealing with unconventional fuels. Shown in Figure 5 and Figure 6 respectively are the gravimetric and volumetric comparisons of internal combustion engines and a PEM fuel cell engine model at three technology levels. Figure **7** shows the disparate properties of two alternative fuels when compared to Aviation Kerosene, a popular general aviation fuel. As a result, a PEM fuel cell-based vehicle design is likely to be constrained by the propulsion system weight and the propellant volume. The use of hydrogen fuel reduces the weight requirement by a factor of $\sim 2:5$ assuming constant efficiency for the two systems. This can be improved even further if the new system has superior operating efficiencies. However, hydrogen as a fuel introduces severe volume constraints by increasing the volume requirements by a factor of $\sim 4:1$. Thus a cursory determination of the feasibility and promise of an alternative propulsion concept comes down to technology forecasting, a trade-off between operating efficiencies, weight and volume requirements. The current rate of advancement in PEM fuel cell technology makes PEM fuel cells one of the leading prospects for the alternatively powered air-vehicle of the future. In this study an attempt was made to retrofit a notional C-172R General Aviation vehicle with a Liquid Hydrogen (LH_2) powered PEM fuel cell power plant. Though similar studies have been done before [53, 201], the goal here was to reach a solution that was as close to the mission capability of an everyday manned general aviation vehicle as possible.

By doing so, the key showstoppers to an all-electric GA concept could be identified. This power plant and propellant combination has drastically different gravimetric and volumetric

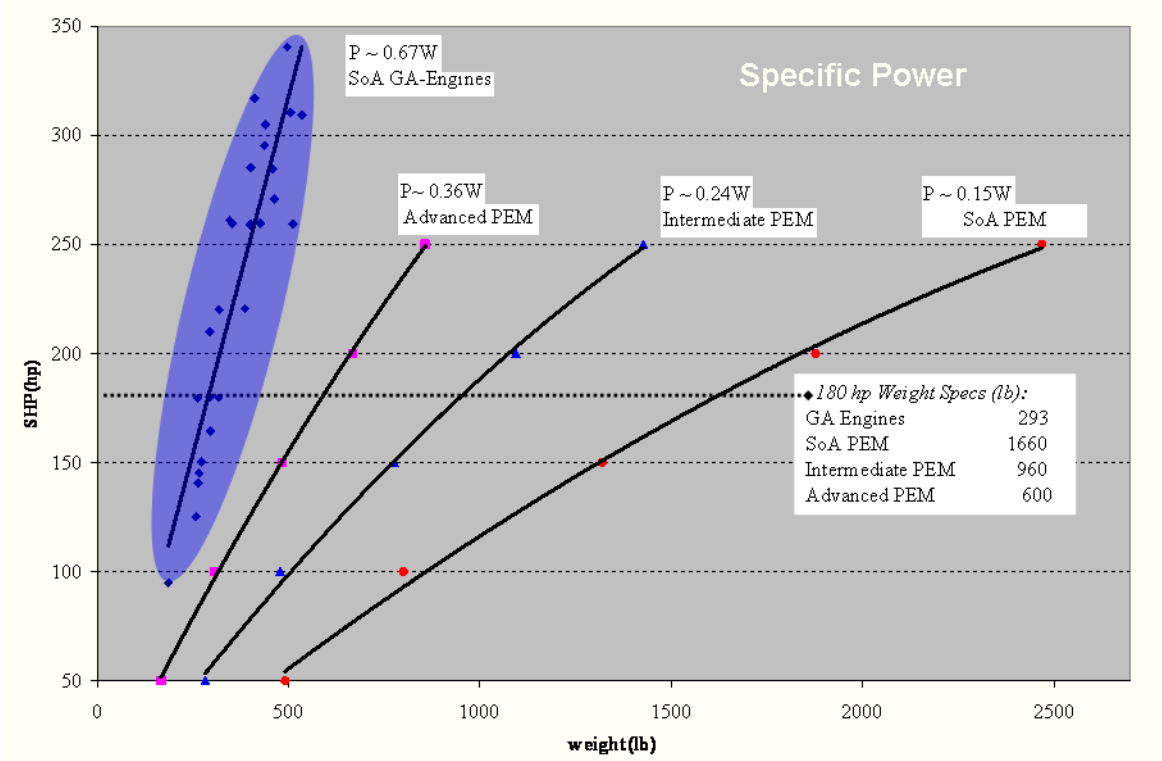

Figure 5: Gravimetric Comparison of IC-Engines to PEM engines [46, 47, 217]

properties compared to those of the aviation-gas-powered, 180 BHP Avco-Lycoming 0360 engine in the C-172R. Because of these conflicting and competing attributes, a number of trade-offs must be made in the search for the optimal solution. For example the PEM system has the potential to operate at relatively high fuel efficiencies, but this comes with a significant weight penalty. Since the maximum take-off gross weight is fixed as a basis for comparison, system efficiency and therefore weight can be traded off for more on-board fuel. This seems like a sensible trade because LH_2 has a high energy density hence more energy can be brought on-board while incurring disproportionately low weight penalty. But the amount of LH_2 carried is also limited by a volume constraint and since LH_2 has a very low gravimetric density, another trade-off must be considered here. The vehicle range is a direct function of the amount of fuel on board where as the rate of climb and the service ceiling are directly related to the excess power available. A design process in which these trade-offs can be made rapidly while exploiting the inherent advantages of the PEM system was used in the study. The technical feasibility and economic viability of the best concept

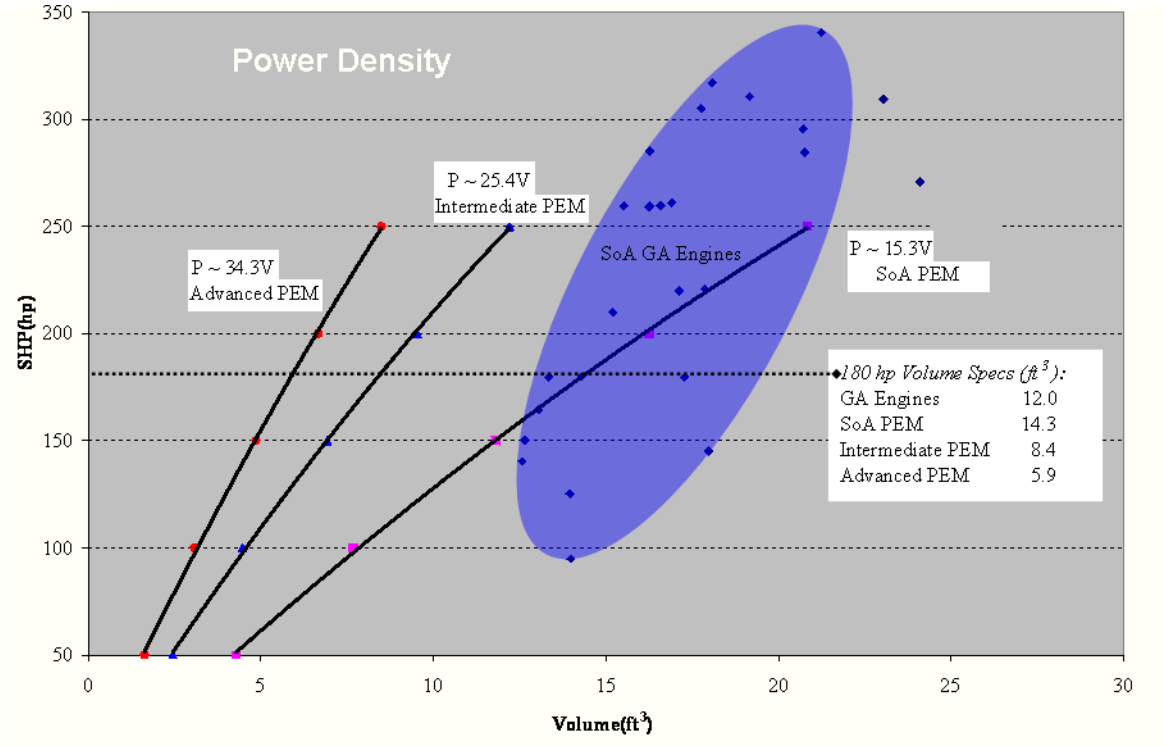

Figure 6: Volumetric Comparison of GA-engines to PEM engines [46, 47, 217]

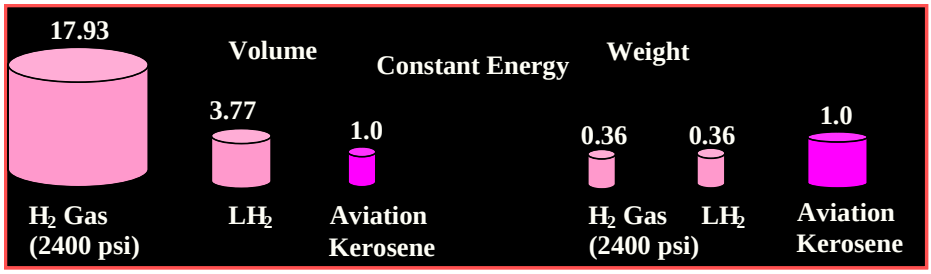

Figure 7: Gravimetric and Volumetric Comparison of Fuels (constant energy content) [182]

was assessed by comparing it to the C-172R specifications. A brief technical description of the PEM power plant follows.

1.1.2 The PEM Power Plant

A schematic of the power-plant is shown in Figure 8 below. Hydrogen fuel and pressurized humid air are fed into the fuel cell stack. The fuel cell produces electrical energy via electro-chemical processes across the Proton Exchange Membranes. The Power Management and Distribution (PMAD) unit contains circuitry that distributes power to the main motor and other power consuming auxiliaries like compressors and pumps. Heat produced by the fuel may be expelled using a cooling circuit that could dabble as a heating circuit for the cabin. The engine decks used in the eventual performance analysis are generated by a physics-based environment based on the above schematic and described in detail by Choi [47]. Component weight estimates are based on three levels: the state-of-the-art (SoA), the intermediate (2010) level technology and advanced (2015) level technology as prognosticated in [194, 25].

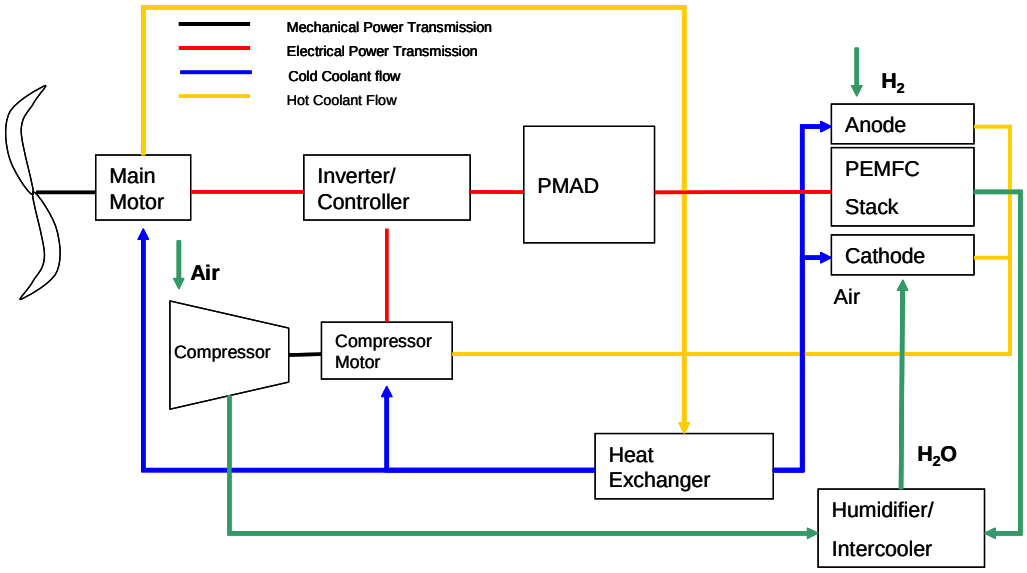

Figure 8: Schematic of Electric Propulsion System [46]

Component topologies are modeled after the prototypes described in [18, 20, 21]. The liquid hydrogen tank is modeled using the "non-cryo-cooling" approach [128]. Here, some of the LH_2 is bled off as the temperature of the tank rises. This tank-model is more

suitable for a weight-constrained problem since cryo-coolers come with a significant weight penalty. Results from the aforementioned physics-based environment were incorporated into a comprehensive vehicle analysis process described in detail below.

1.1.3 Retrofit Design Environment and Process

The design process begins when the mission requirements are fed into the PEM engine modeler which generates an engine deck. See Figure 9 . It also outputs a matrix of geometric and inertial attributes for all major engine components. These include basic shape and dimensions. This data is fed into the volumetric analysis tool which attempts to fit these components inside the aircraft based on their individual matrix of attributes.

A survey of contemporary component representation and layout techniques [183, 220, 167] revealed that these approaches would be prohibitively expensive to set up and run for the large design spaces that are typically explored in conceptual design. For this study, this process was sped up significantly by exploiting the fact that aircraft geometry in NASA Langley's VSP® [113] is defined in a discretized format based on top level engineering metrics such as aspect ratio. See Figure 10 .

The portability of the XML geometry definition file is exploited via a Perl-script that employs XMLsmart® [151] to rapidly browse the nodal input file and find candidate storage areas without invoking the CAD package. Significant savings in time and computational expense are realized. While attempting to fit the PEM system components inside the notional C172-R the author observed that :

> *I. For any vehicle geometry there are potentially thousands of layouts depending on the degree of modularity of the vehicle subsystems.*
>
> *II. The utility (and acceptance) of a mass and volume allocation methodology in conceptual design is highly dependent on the degree to which the methodology mitigates the computational expense incurred.*

Geometry representation is one avenue through which this reduction in expense could be achieved. Unlike conventional power-plants that have strict mechanical connectivity constraints i.e. all components must lay in contiguous spaces, the PEM power plant's reliance

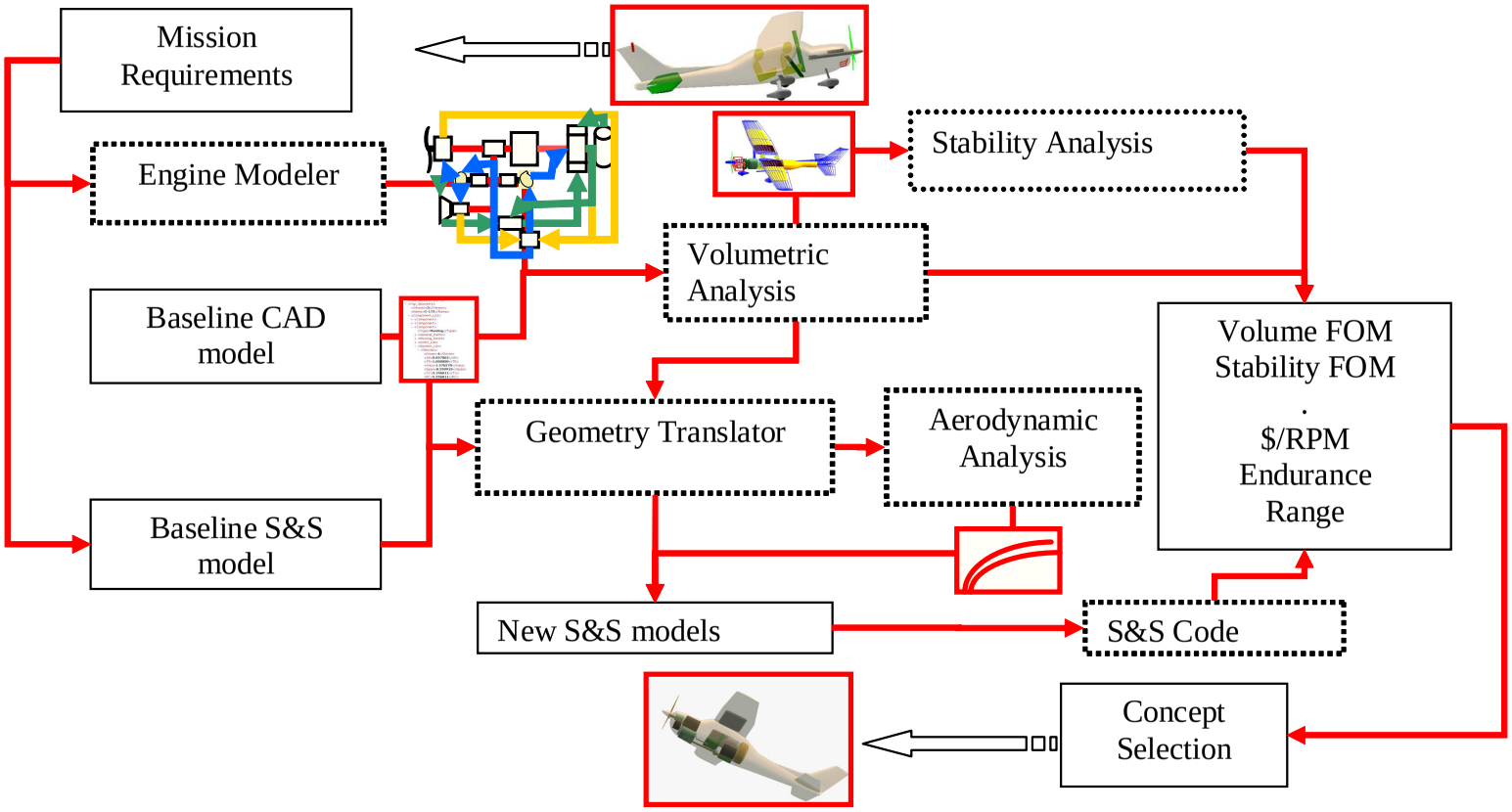

Figure 9: The Retrofit Design Process

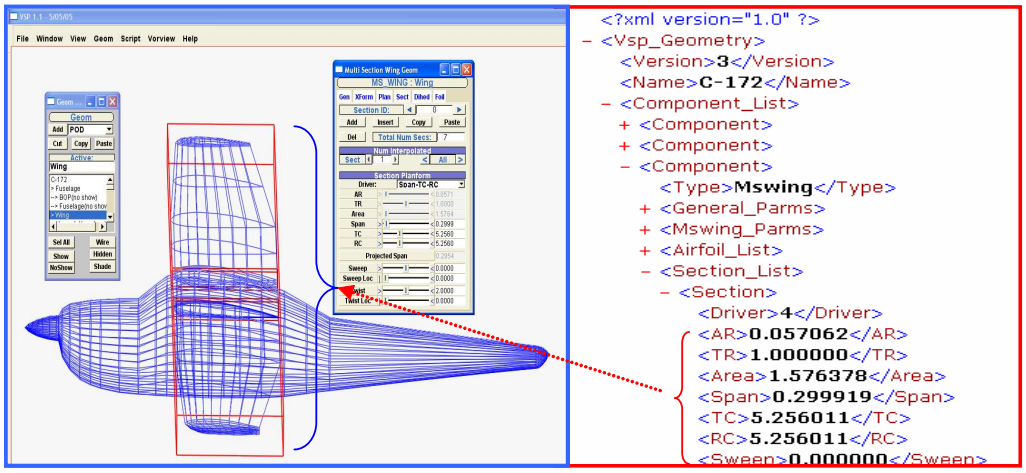

Figure 10: Top-level geometry definition in VSP® [15]

on electrical power makes it highly modular. As such, many of the subsystems have a high degree of location freedom. This means that, save for the main motor, which must be directly and mechanically connected to the propeller, all other components of the system could be located in many different parts of the aircraft as long as they can be connected via current-paths (cables) as shown in Figure 11 below. The designer's choice would of course be tempered by considerations such as safety and maintainability.

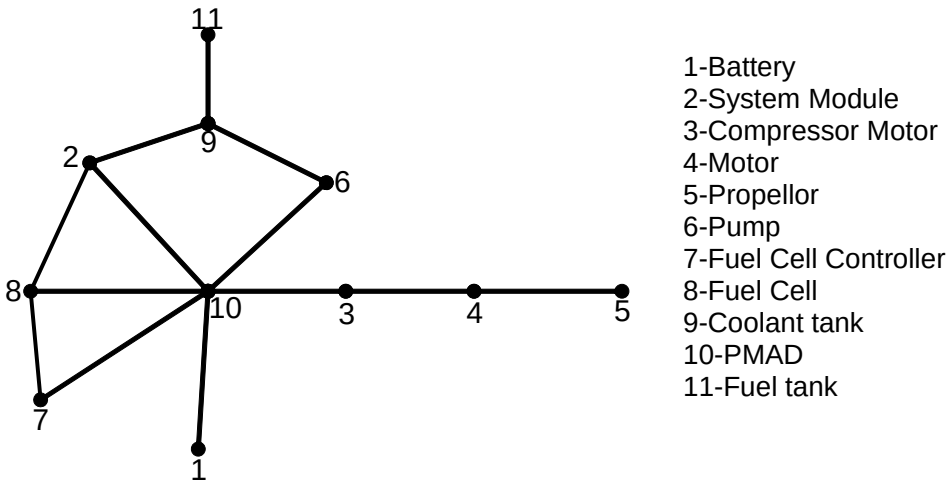

Figure 11: Connected tree schematic of fuel cell engine

In a typical scenario, the designer would have to explore a plethora of possible layouts

in order to identify the most ideal layout. The author was unable to find any published literature regarding a methodology that tackles the problem while sufficiently mitigating the computational expense to such an extent that it could be used for large concept-space exploration. There is therefore a need for a generalized mass and volume allocation methodology to tackle this challenge without necessitating assumptions that over-simplify the problem. The volumetric analysis module determines possible layouts by sweeping through the discretized model of the aircraft and comparing extreme sectional dimensions of components to those of the vehicle. This module then feeds inertial and geographical data for each layout to the stability analysis code which outputs a stability figure of merit based on the location of the center of gravity. This was deemed sufficient for stability analysis since the aircraft geometry remained unchanged and the load distributions remained within the vehicle's operational envelope. Other criteria such as the need to minimize wiring and dead volume could also be included but are neglected here since they are only ancillary to the overall objective. Inertial data is also fed to the geometry translator which updates the FLOPS® model. The geometric data is then passed on to the aerodynamics tools Vorlax® and a skin friction estimation tool. The resulting data is written into the sizing and synthesis (S&S) model which is analyzed by FLOPS®. The performance data is then passed onto the concept evaluation phase.

1.1.4 Solution-space Exploration

Theoretically a technically equivalent solution exists if a PEM fuel cell option can effectively replace the internal combustion engine and in the process match or beat the original performance of the vehicle. The three key design drivers, i.e. weight, power and volume, are manifested in six key metrics. The specific power $\frac{BHp}{power\,plant\,weight}$, power density $\frac{BHp}{power\,plant\,volume}$, and overall efficiency are critical for the power plant. For the propellant: the fuel system's weight-specific density $\frac{System\,weight}{fuel\,weight}$, volume-specific density $\frac{System\,volume}{fuel\,weight}$ and the fuel's energy density are the key drivers. State-of-the-art PEM fuel cells are advertised at about $0.67\,\frac{Hp}{lb}$ [18, 19], (not including auxiliary system components) whereas internal combustion engines generally give $\sim 0.67\,\frac{Hp}{lb}$ (most major system components included See

Figure 5). Liquid hydrogen at a temperature of $20K$ is approximately ten times less dense than aviation kerosene [146] but carries at least three times more energy per unit weight. A trade-off between weight and volumetric requirements presents a couple of challenges to the contemporary design process. First of all, volumetrics traditionally takes a back-seat to thrust and weight balance in preliminary sizing methodologies such as Mattingly's [121] master equation approach. This approach works well for evolutionary designs where significant knowledge can be ploughed back from existent and similar designs. This skill has been fine-tuned and homed over time. The same geometries, with the same propulsion system architectures, and essentially gravimetric and volumetrically similar fuels continue to be used. Here, the new propulsion systems and new fuels pose new challenges to the traditional design process.

The third observation follows:

> *III. Any new technology that exhibits significant volumetric and/or gravimetric disparity to its predecessor will render the contemporary design process wanting in many historical-data-based analyses. These aspects include but are not limited to vehicle scaling laws and the identification of optimal geometries.*

As seen in Figure 7 above, there is a strong disparity in volumetric and gravimetric properties when alternative fuels such as LH_2 are considered as propellant. The introduction of a different power plant with disparities such as those highlighted in Figure 7 and Figure 6 for the PEM engine below can further exacerbate the problem. When all the components of the PEM engine are considered the overall specific power drops to $0.15\,\frac{Hp}{lb}$. This is 20% of the GA-engine value. Using these linear approximations it is seen that fuel cells become competitive below the values of 0.8 Hp, 5.4 Hp and 24 Hp for the state-of-the-art, intermediate and advanced technology levels respectively. In fact Georgia Tech flew a compressed hydrogen fuel-cell powered demonstrator in this power range. See [35, 129, 130, 132, 131]. Also, at 180 Hp the advanced, intermediate and SoA concepts are also 307 lb, 667 lb and 1367 lb over-weight respectively. It can be deduced from Figure 6 and Figure 7 that a 560% improvement in PEM system specific power and 20% improvement in specific

volume are required for the PEM system to compete with the original engine. Weight is therefore a more critical constraint than volume. With this disparity in power plant weight and volume requirements it is clear that simply swapping the GA-engine for a PEM system can not generate a feasible solution. As seen in Figure 5 and Figure 6 , weight and volume requirements are directly proportional to the power required. To ease the weight constraint alternative sources of supplemental power were explored.

1.1.4.1 Mitigating Weight Constraint

During its mission, a typical general aviation aircraft only uses close to the maximum power during the take-off, climb and perhaps missed approach segments. This fact can be exploited to downsize the power-plant either by providing higher specific power supplemental power sources or by relaxing the mission requirements for these segments. The former option is employed here since the original goal was for the retrofitted vehicle to be able to fly a mission as close as possible to that of the C-172R.

Batteries are a good candidate for a supplemental power source. A variety of candidate battery types such as lead-acid, nickel-cadmium and lithium ion [49, 218, 185] are considered. Unlike the PEM engine the battery weight and volume are directly proportional to the energy storage requirements. The available power, service time and system efficiency are state properties whereby if one is defined, the other two become fall-outs given the energy capacity of the system. Batteries have a generally lower specific energy than fuel cells. See Figure 12. But for durations of less than one hour, some batteries have a higher specific energy than fuel cells. Thus batteries could be used to relieve system requirements during the shorter climb segment where more power is required.

The stage is therefore set for a trade-off study where, given power and performance requirements, fuel cell power, LH_2 fuel volume, battery power and service time can be varied to ascertain the existence of a volumetrically and gravimetrically superior hybrid solution. To further assuage the gravimetric constraints the back seat is removed thereby reducing the passenger capacity of the vehicle to one passenger and one pilot. See Table 2 for other configuration changes.

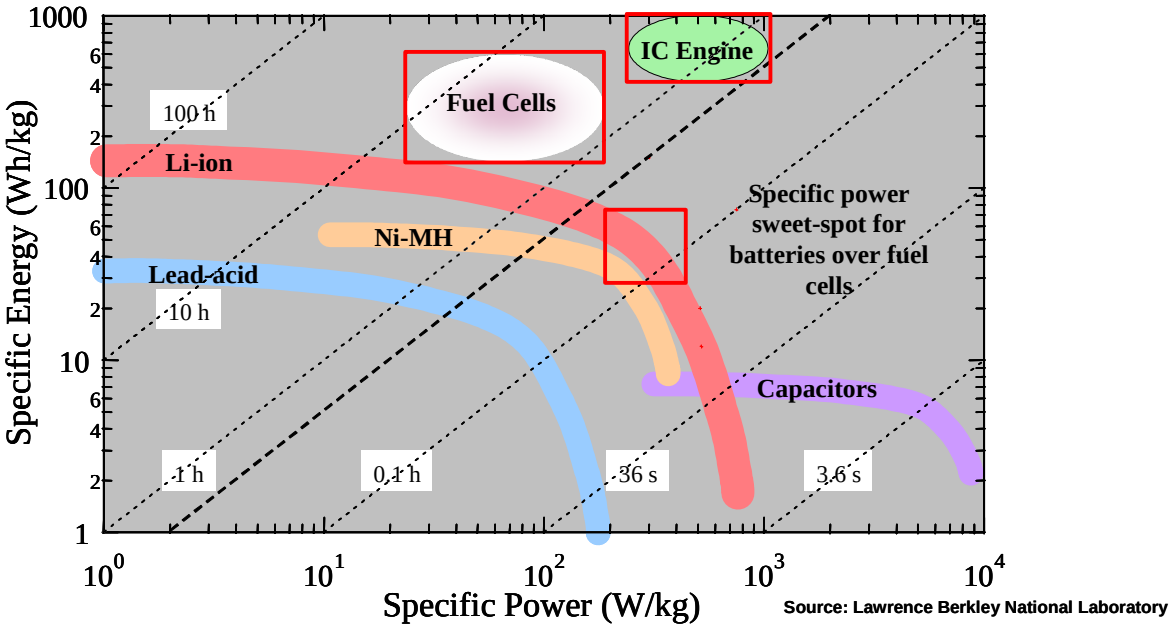

Figure 12: Comparison of potential propulsive technologies

Table 2: Summary of Retrofit changes

Item	*Weight (lb)*
2 small passengers	250
Back Seat	43
Engine	298
Baggage	120
Aviation kerosene	330
Miscellaneous	40

Hence 1081 lb is available for the propulsion system, the fuel and fuel tank if gross weight is maintained. The total available volume for storage of the new system is estimated at 118 ft^3. A brief discussion of the modelling and simulation environment created for this design problem follows.

1.1.4.2 The Optimization Problem

The optimization problem is set up in the following manner:

$$Maximize: Range$$

$Subject\ to:$

$TOGW < 2568 lb$

$Total\ Volume\ Required < 80\ ft^3$

$Power\ available \geq Power\ required$

$By\ varying:$

Fuel cell volume required

Fuel tank volume and shape

Battery power required (continuously for 14 minutes)

Technology level

A schematic of the trade-off environment is shown in Figure 13 .

1.1.5 Results

The results from the three models at each technology level are shown in Table 3 below.

It is seen that only the advanced technology concept meets the take-off gross weight constraint at the minimum fuel capacity condition. The advanced technology concept was marched through the entire design process so as to verify the results. The best retrofit layout as determined by the volumetric and stability analyses is shown in Figure 14 below.

One of the major challenges of analyzing the performance of an unconventional retrofit vehicle using a conventional analysis tool was the generation of a hybrid engine deck. This challenge arises from the fact that the consumption of battery energy does not result in a change of mass. This means the specific fuel consumption (SFC) of the battery can not be conventionally defined. The tool used here i.e. NASA's Flight Optimization System

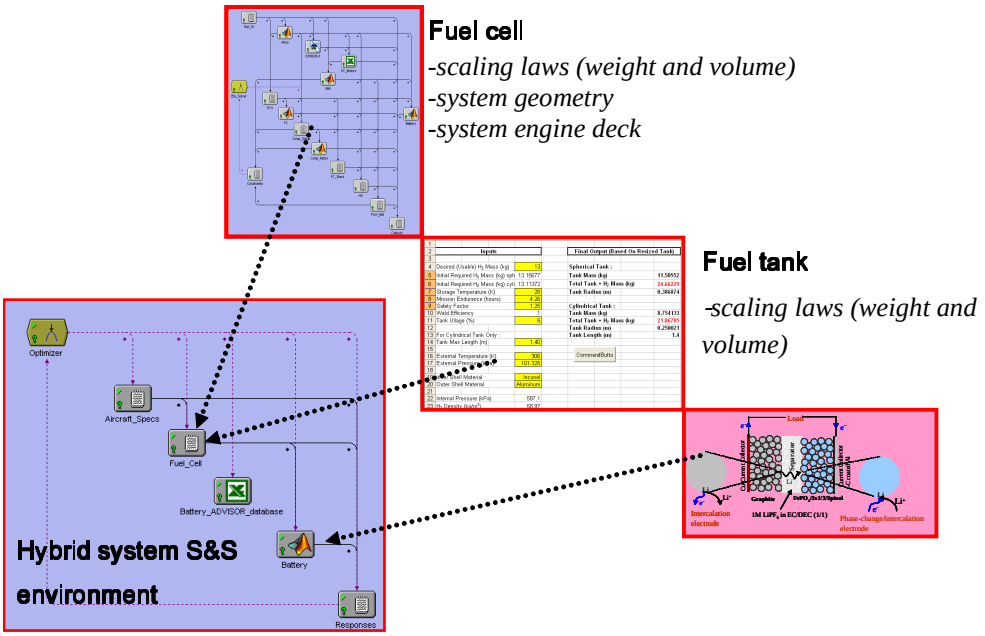

Figure 13: Integrated Power Trade-off Environment

Table 3: Optima at each Technology Level

Response	***C -172R***	***SoA Tech Retrofit***	***Intermediate Tech Retrofit***	***Advanced Tech Retrofit***
TOGW(lb)	2558	3268	2673	2558
Volume Required (ft^3)	12	71	40	30
Fuel Cell Engine Weight (lb)	293	630	501	347
Max Power (BHP)	180	111	117	80
Fuel Weight (lb)	330	22	22	24
Battery Weight (lb)	-	128	93	51
Battery Power (BHP)	-	20	18	20
Battery Time ($minutes$)	-	10	10	13

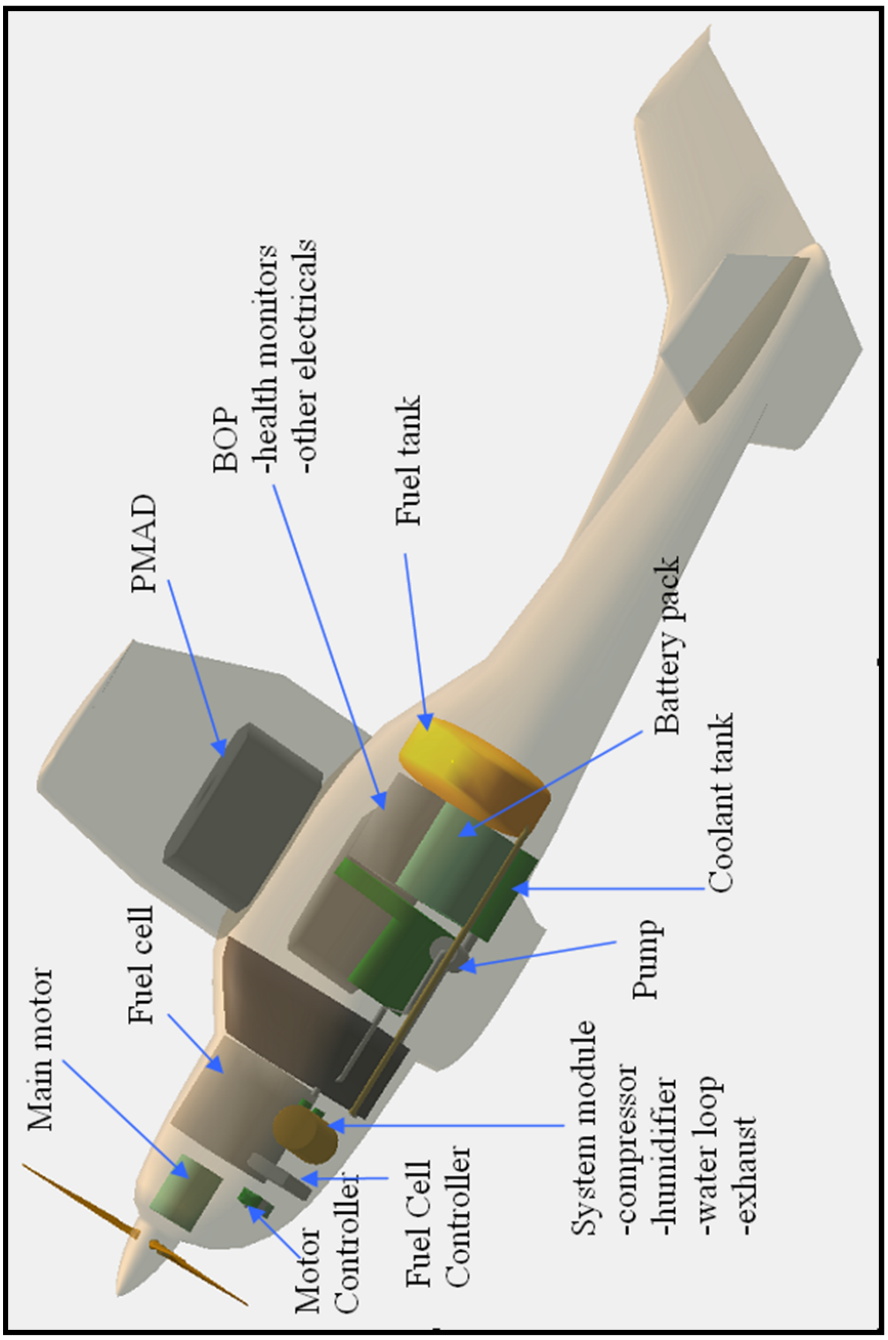

Figure 14: Retrofit Configuration

(FLOPS) does not take multiple decks simultaneously and uses a traditional mission analysis approach that has SFC as the core parameter in vehicle weight calculations during the mission. This challenge was circumvented by aggregating power-supply from the two sources and using a pseudo-SFC for all climb-altitudes during which battery power is consumed. For a given setting $P = P_{battery} + P_{FC}$, the pseudo-SFC is given as the specific fuel consumption of the fuel cell at power setting P_{FC}. The relevant assumptions are summarized in Figure 15 below.

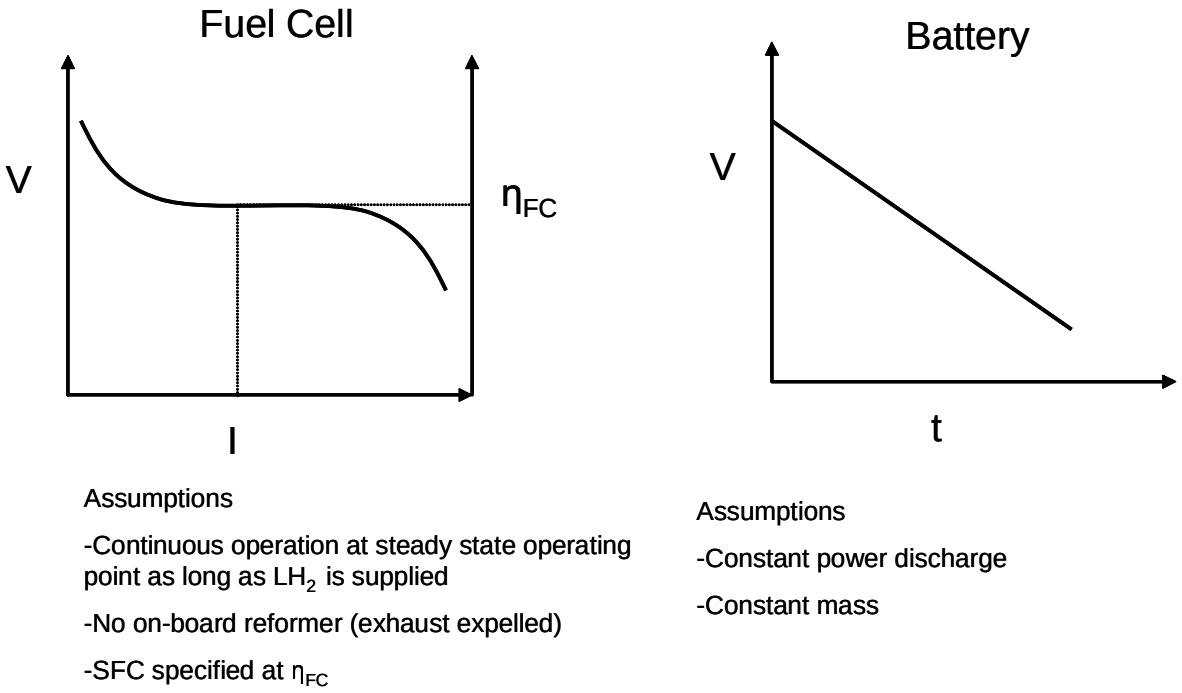

Figure 15: Assumptions in the generation of a hybrid engine deck

The mission analysis tool was fed a modified engine deck in which battery-supplemented segments of the mission had higher power for the same fuel cell fuel consumption rate. It was also essential that the hybrid power settings were not used by the analysis tool beyond the maximum allowable power supply time for the battery at a given setting. This was enforced by limiting mission-freedom for the sizing and synthesis tool and manually checking output files. In Figure 16 the results of the performance analysis of the conventional C-172R are compared to those of the retrofit.

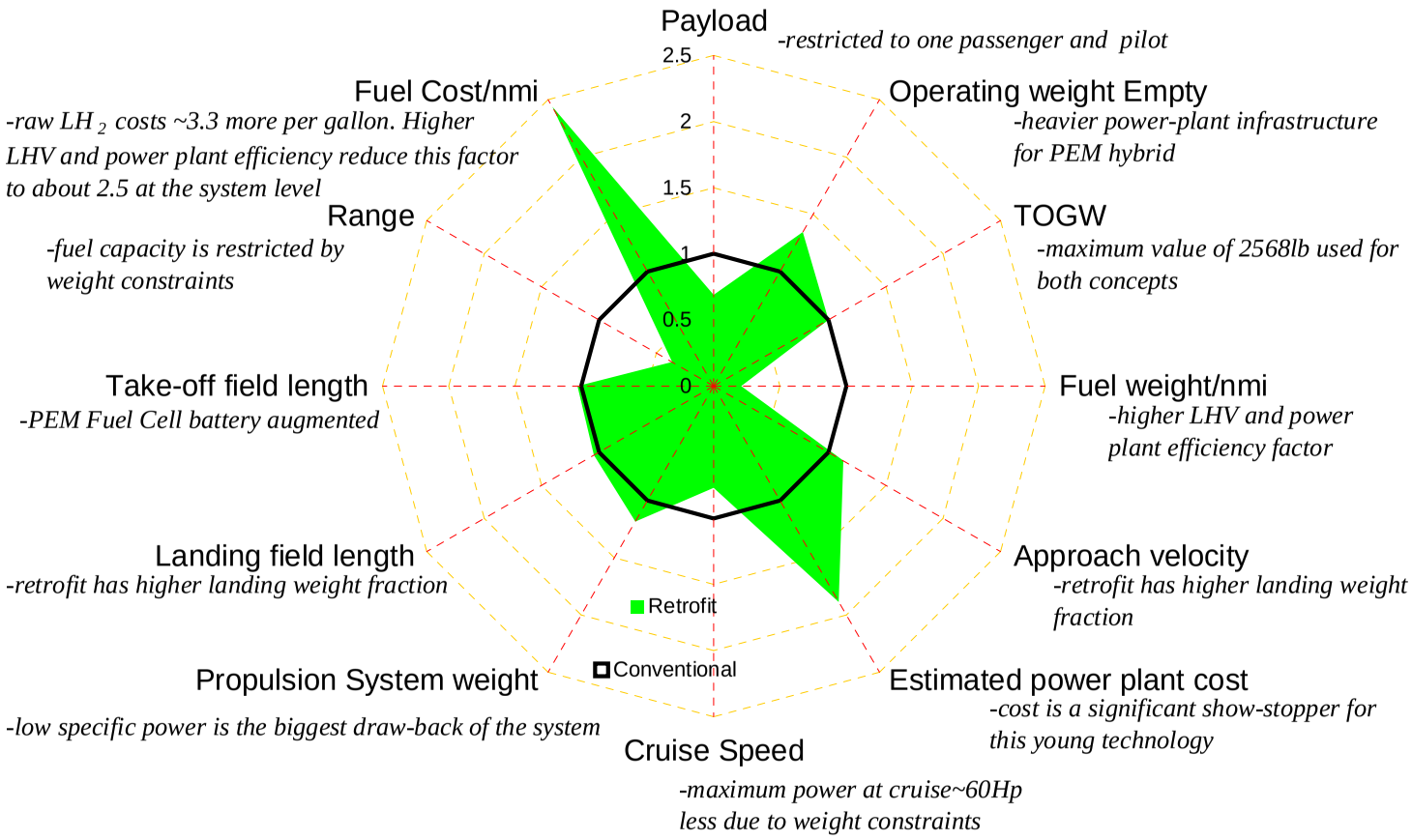

Figure 16: Comparison of conventional and retrofit vehicle specifications

The major sore-spots for the hybrid concept are economic in nature. The estimated cost of the power plant is almost twice as high as that of the Lycoming O-360 ($49,000: $25,000 in year 2006) [25, 194]. This is equivalent to ∼544:140 $/hp. Estimated well-to-wing costs of LH_2 are 3.3 times as high as those of aviation gas. Fuel cells have been hailed for their promise of highly efficient transport. And even though the efficiency reduces the fuel cost ratio from ∼3.3:1 to 2.5:1 [25, 194], further reduction in costs is necessary before this fuel can become an attractive option. As mentioned earlier, the specific power of the system is quite low; this manifests itself in decreased available weight for fuel and payload. Part of this weight penalty is relieved by the higher heating value, hence lighter LH_2 propellant. As seen in Figure 16, the fuel weight consumed per nautical mile is ∼20% of the conventional configuration value. Due to the limitation in available fuel, the range falls from 630 nmi at $8500 ft$ to 228 nmi at a cruise altitude of 4000 ft. The most appealing aspect of this vehicle, however, is that it is a zero-emissions (green) vehicle. In sum the benefits of a superior overall efficiency power-plant coupled with a higher energy density fuel are out-weighed by the low specific power of the PEM-battery hybrid, low gravimetric density of the fuel and the high costs associated with the power plant and the fuel.

This study not only demonstrated the potential of fuel cells as alternatives to conventional power plants, it also highlighted the need to bring volumetrics forward in the design of revolutionary vehicle concepts. The analysis was greatly simplified by the fact that the top-level geometry was already defined and fixed. The designer would not have this luxury if the nature of the technology was such that total redesign provided the best chance of attaining a feasible and viable design. Consideration of total redesign of a fuel cell powered General Aviation vehicle led to a forth observation:

> IV. *In the design of a truly revolutionary concept, no knowledge of the final shape would exist ex ante. The logical approach would be a bottom-up design process where major component sizes, shapes, inertial properties, locations and connectivity requirements are taken into account when coming up with the appropriate baseline geometry.*

1.1.6 Summary of Challenges Identified

1.1.6.1 Size of layout / Configuration Space

It is implicit in the nature of a layout problem that a huge number of configurations is possible within the limits of the design constraints. The enormity of the design space creates the impetus for automated layout space exploration. The preceding two factors, together create the impetus for a fast and automated collision detection method. This method would form the core of any methodology that aims to bring volumetrics forward in the design process.

1.1.6.2 Vehicle Scaling

As with the design of any novel concept, all aspects of the design process that strongly rely on historical data are rendered less reliable and sometimes totally useless. In this particular case, the sizing and synthesis process as well was rendered wanting. To this end Dr. Taewoo Nam [137] developed a power-based sizing and synthesis methodology that is generic enough to handle to hybrid propulsion technologies with esoteric fuel "consumption" behavior among other things. Within the sizing and synthesis routine a variety of scaling laws for component mass and volume are employed. These critical pieces of the process have to be custom-generated. The evaluation of new scaling laws requires knowledge about each major vehicle component as well as its scaling behavior. This individual scaling behavior varies from component to component as determined by the physics of the component, manufacturing limitations or practices and financial considerations. A turbofan engine could scale linearly and continuously based on the inlet area to outlet area ratios as dictated by the amount of thrust, noise levels etc. However, if the design requirement were to use an off-the-shelf design, then the scaling behavior would be a discrete distribution. Likewise a modular component like fuel cell would scale discretely based on the size of the smallest unit that can be manufactured. Evaluating new system-level scaling laws is not as trivial as consolidating the various subsystem-level scaling laws. The eventual behavior of a containing body is a function of the layout of its components and their scaling response to changes in requirements. This is in turn a function of the component shapes and volume requirements.

Therefore replacement scaling laws must capture not only the scaling behavior of a given layout but also the thresholds beyond which alternative layouts offer more optimal solutions per the designer's requirements.

1.1.6.3 Identification of volumetrically feasible baseline geometry

When designing a new aircraft concept around a new technology, the choice of baseline geometry is usually driven by the similarity of the replacement technology to the current technology. This similarity can usually be quantified by comparing the volumetric and gravimetric properties of the technologies in question. Whenever, these properties are of comparable magnitudes, it is plausible to assume that the new concept would be similar to the current concept. The choice of baseline geometry is clear. However, when there is significant disparity between the incumbent and the emergent technology, more rigor is required to design a new concept. A methodology that simplifies this problem would be very useful in this situation.

1.1.7 Role of Disruptive Requirements

The advent of new, disruptive technologies is not always the only impetus toward the design of revolutionary vehicles. Other events such as changes in the legal operating environment of the vehicle can lead to new requirements. For example, tougher emissions regulations might lead to changes in propulsion systems and propellants of choice. Changes in the social and political environment may also require new performance standards in terms of range, maneuverability and maximum speed. See Figure 17 for a synopsis of vehicle geometry and requirement co-evolution.

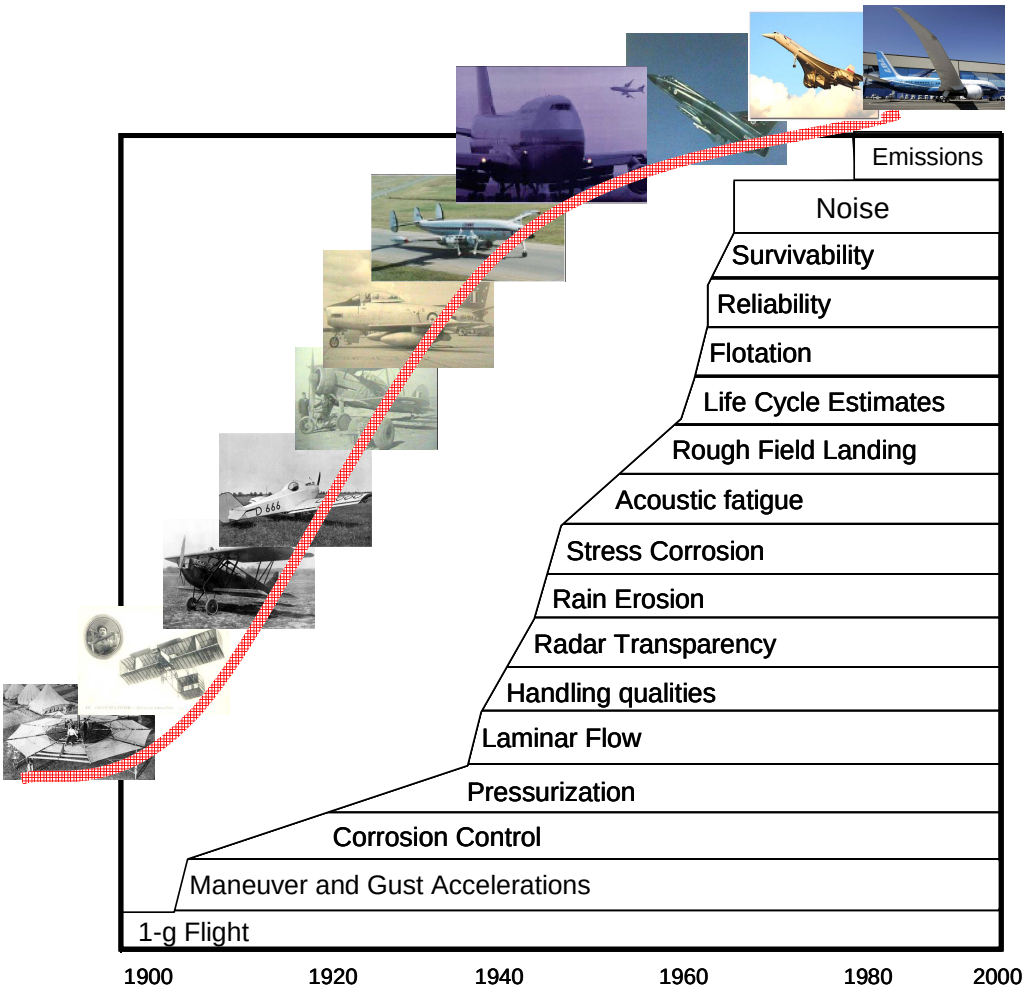

Figure 17: Evolution of Aircraft Design Requirements [11, 12, 13, 51, 96, 97, 98, 99]

Changes in requirements may also be accompanied by changes in the relative importance of the system performance metrics. For example endurance and range can be more important metrics in the design of a border surveillance vehicle than say speed. The change in the relative importance of these metrics translates into a change in the overall objective function and eventually a change in the geometric attributes of the optimum configuration. Often in these situations, the inability to quantify the effect of the disruption on the design leads only to a cursory treatment of such effects in design. In cases where some of the effects can be quantified, scenario analysis and/or probabilistic treatments can be employed to identify more robust solutions. But as Carty [43] stated:

"A design has no physical foundation without an analysis, and similarly, an analysis has no path to realization without a practical design".

Thus the full impact of a disruptive technology can only be realized once the analytical and design impacts are consolidated and harmonized. Methods such as TIES by Kirby [105] could effectively quantify the analytical impact of a technology. This is sufficient when the volumetric or gravimetric impacts of the technology are not severe enough to warrant major geometric changes to the vehicle. The purpose of this thesis is to find a conceptual design solution for scenarios such as the PEM fuel cell powered general aviation aircraft when disruptive technologies impose major volumetric and gravimetric changes to the chosen vehicle class.

1.2 Inputs to Traditional Design Approaches

A number of classical results on the optimal shapes of aerodynamic bodies use physical geometric attributes of the body as inputs. These include the Sears-Haack body [84, 171] , the *von Kármán ogive* [143, 200] and ideal hypersonic bodies [114, 202, 221] .

Equation 1 [10]shows the area distribution of the Sears-Haack result for optimal slender bodies of revolution. Two of the three inputs on the right hand side of this equation refer to physical dimensions of the body. These inputs could take on a wide range of settings especially for highly modular systems.

$$S(\theta) = \frac{4V}{\pi l}(sin(\theta) - \frac{sin(3\theta)}{3}) \tag{1}$$

$where:$

$V: Total\,Internal\,Volume$

$l: Length\,of\,Body$

$0 \leq \theta \leq \pi$

Similarly, for a known base area $S(l)$ a minimum drag distribution known as the *von Kármán ogive* can also be derived. The area distribution for this body is described by [10]:

$$S(\theta) = \frac{S(l)}{\pi}(\pi - \theta + \frac{1}{2}sin(2\theta)) \tag{2}$$

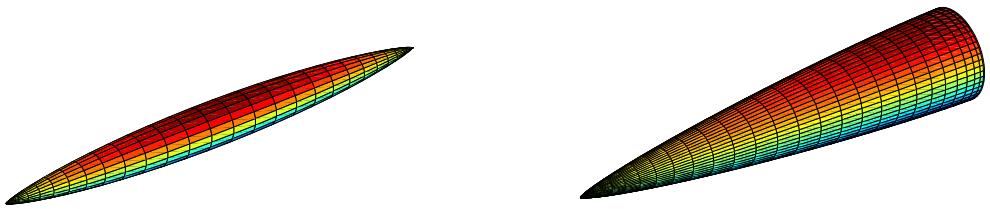

(a) (b)

Figure 18: Sears-Haack Body(a) and Von Karman Ogive (b)

Equation 3 shows the Lapygin [114] result for a high velocity body with prescribed base area and shape. These properties are direct functions of the layouts of the subsystems within the body. Thus an "optimal" layout must be prescribed before a body shape can be defined and analyzed.

$$S(\varphi) = 2\frac{C_f}{K}\left\{1 + \frac{1}{sin(\varphi)}\right\}^{\frac{2}{3}} \tag{3}$$

$where:$

$C_f : Frictional\,Coefficient$

$K : Lift\,to\,Drag\,Ratio$

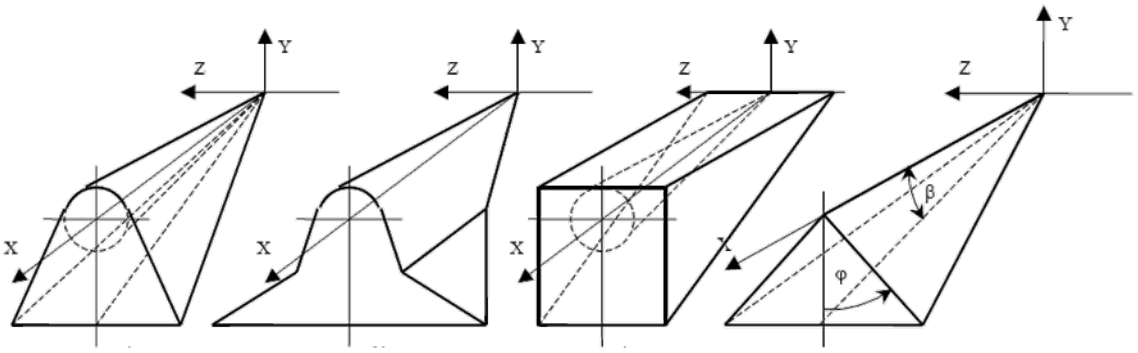

Figure 19: "Absolutely" Optimal High Speed Body [114]

Traditional sizing and synthesis tools such as FLOPS© take in inputs such as fuselage length, and diameter. These values are typically derived from historical data. However, as mentioned earlier these same values are not readily available in the design of revolutionary concepts.

All of the approaches discussed above depend on some geometric parameters of the body in order to completely define the vehicle. In cases where expert opinion or historical data provide at best a zero-order estimate of these values, a scientific methodology by which the optimal values of these parameters can be determined is necessary.

1.3 Guiding Policy/Decision Makers

The regulations alluded to above are usually accompanied by increased public and sometimes private investment in the corresponding enabling technologies. As is the case with green propulsion, there are a number of competing technologies ranging from batteries, to solid oxide fuel cells (SOFC's) to the PEM fuel cells described earlier. Before funding or investment decisions can be made, the decision makers must be equipped with information regarding the potential of each technology. When it comes to fuel cells for example, it would be useful to know the minimum specific power or power density required for each fuel cell type in order to produce a feasible vehicle for a given set of mission requirements. Such information can be gathered by designing optimal conceptual platforms around each technology and thereafter comparing the performance of each platform to the design targets.

Armed with such technology and vehicle specific information, policy makers can then decide to fund the technology that offers the best chances of meeting their goals at minimal cost and maximal return on investment.

Chapter II

RESEARCH OBJECTIVES

Based on the observations outlined in the preceding discussion, two major research goals were established. These objectives are aimed at creating an enabler for revolutionary geometry identification, selection and optimization through fast design space exploration and a capability to generate requirement-based geometric scaling laws.

2.1 Research Objective 1: Devise a methodology for the identification and selection of volumetrically feasible baseline vehicle geometries

A disruptive technology which manifests itself in significant volumetric or gravimetric disparity to its antecedent renders most historical-data based weight and volume regressions at best unreliable as design and decision-making tools. In such cases, the designer must pursue a bottom-up approach i.e. building the aircraft from the subsystem level outwards. This approach entails the exploration of subsystem layouts. Exploring layouts in 3D space can be a daunting task as there can be a plethora of possible combinations even within a constrained space. Also, the level of detail provided by a given component layout is not directly useful in conceptual design. This information must thus be consolidated into a form that has some utility to the conceptual designer. A good approach to solving this problem is to generate a minimum enclosing envelope for the layout. This envelope should be a good approximation for the inner mold line of the vehicle being considered so that its dimensions can be used as constraints to the external geometry of the vehicle. These constraints will be based on a set of parameters commonly used as inputs in traditional sizing and synthesis codes. In his doctoral thesis [162], Dan Raymer identified the basic five or six variables that are most useful in aircraft conceptual design. These are the thrust-to-weight ratio $\frac{T}{W}$ or the power-to-weight ratio $\frac{P}{W}$, the wing loading $\frac{W}{S}$, the Aspect Ratio AR, the Taper

Ratio (TR), Sweep and airfoil thickness-to-chord ratio. Of these, the latter three are directly dependent on various aspects of aircraft geometry. Popular sizing and synthesis tools such as FLOPS© [122] employ these and other variables to define aircraft geometry. For example, the namelist "CONFIN" in a FLOPS© input file contains a variety of variables that describe various geometric attributes of the aircraft. The fuselage is defined using the geometric variables listed in Table 4. These dimensions can be evaluated for a minimum enclosing envelope as well. The values can then form the basis for the constraints by which a feasible design must comply. By so doing, the chances of volumetric feasibility are improved for all compliant designs.

Table 4: FLOPS® Fuselage Geometry Variables[122]

Variable Name	***Description***
NFUSE	Number of fuselages
XL	Fuselage total length
WF	Maximum Fuselage Width
DF	Maximum Fuselage Diameter
XLP	Length of passenger compartment

An analysis of modeling approaches in aircraft sizing and synthesis led to a fifth observation:

> V. *The limited number of geometric variables input variables can only uniquely define an aircraft configuration in the context of an apriori definition of the vehicle class e.g. commercial transport, general aviation or fighter. Implicit in this definition is an assumption of fuselage shape.*

As demonstrated earlier, the designer may not always be in a position to choose a good baseline geometry by basing her choice solely on a consideration of prior art. The designer must either be equipped with an aid that will guide the configuration selection process or the number of geometry input variables must be increased in such a way that various classes of aircraft can be analyzed by varying the same set of design variables. Since effective geometry parametrization typically requires a prohibitively large number of unintuitive variables [32, 166], it is deemed wiser to take the former approach i.e. enabling robust configuration selection. The above objectives will be deemed to have been achieved if the

design information is delivered to the decision-maker in a "ready-to-eat" format at an acceptable computational expense. By combining a fast layout exploration technique with a methodology that consolidates layout metrics into a compact and useful set of system level parameters, this approach will bring volumetric visibility forward in the design process. The success criteria are described in more detail below.

1. Deliver configuration data in the form of useful conceptual design variables

   A good conceptual design variable must have intuitive meaning to the designer. Intuitive meaning is a key tool in shortening design cycle. It enables the designer to make good decisions without first having to run an analysis. The design variable should also be measurable either as a numerical value or one of a set of discrete choices. It should also have a quantifiable effect on the final objective function but not on individual items of specific end-worth to the client e.g. range, speed and cost [161]. This effect should be in such a way that the variable can not be optimized independently. Variables that reflect current and historical design parameters and vocabulary are preferred [161]. A successful methodology will convey variables that carry intuitive and useful meaning to the designer. These variables will be fed into a demonstration tool that will also output metrics that are quantifiable, intuitive and relevant to the conceptual designer.

2. Mitigate computational expense

   The methodology will be benchmarked against other conceptual design disciplines such as aerodynamics, structural analysis, propulsion and stability and control. Figure 20 and Figure 21 below show the preliminary results of a survey of graduate students at the Aerospace Systems Design Laboratory (ASDL) at the Georgia Institute of Technology [1]. Despite the fact that many of these students have varied and international design experience, no claim can be made as to the statistical validity of this study in representing the design industry as a whole. However, since these subjects are well-versed in cutting edge design methodologies, they provide satisfactory expert opinion for this survey.

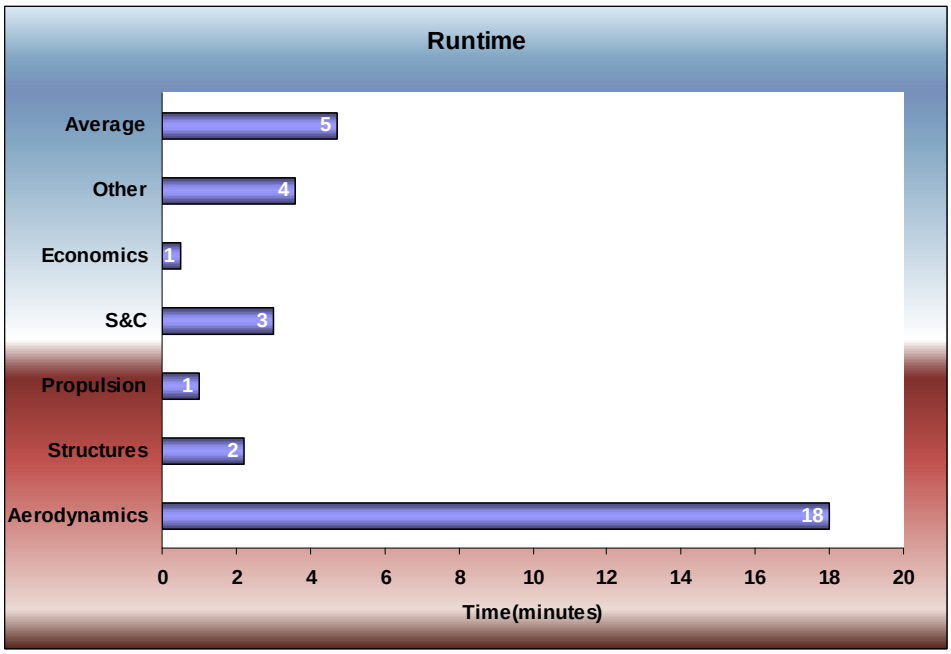

Figure 20: Benchmarking Disciplinary Run Time Expense [14]

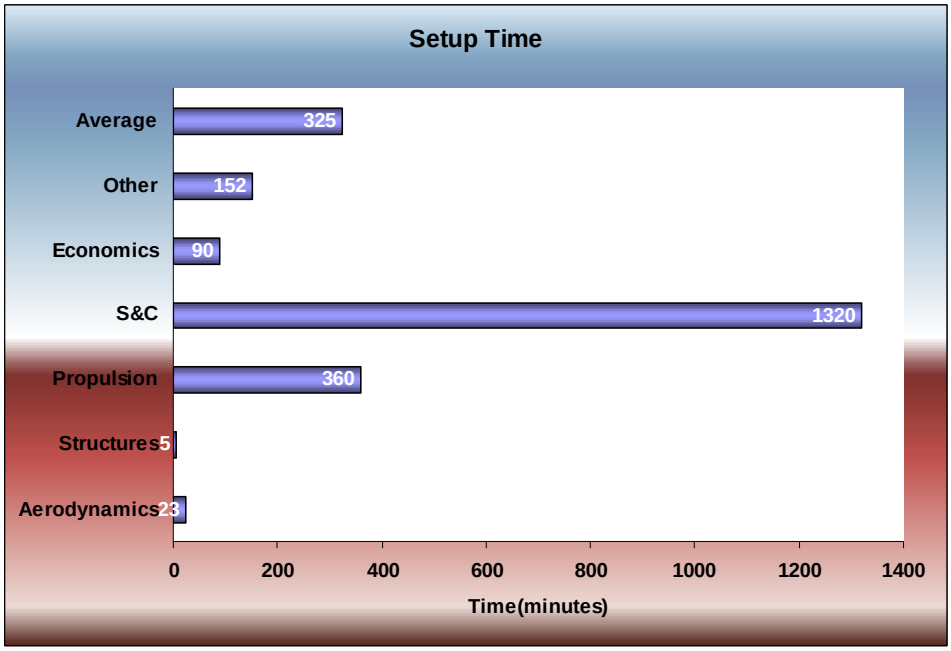

Figure 21: Benchmarking Disciplinary Set Up Time Expense [14]

The methodology will be deemed to be fast enough if it requires at most the same order of magnitude as the slowest conceptual design discipline to set and run.

2.2 Research Objective 2: Use methodology as enabler for the derivation of custom scaling laws

The methodology for identifying optimal geometries will also be used as enabler for the derivation of the most important scaling laws as determined by the designer. The need to scale a vehicle geometry can result from the violation or over-satisfaction of one or more design constraints. Scaling studies are also necessary in situations where trade-offs on requirements need to be made. During the sizing and synthesis process there is a need to balance the required power, volume and weight against the available amounts. For example insufficient range leads to an increase in the amount of required fuel on-board. This in turn leads to a proportionate scaling of the containing vessel i.e. the fuel tank in this case. This scaling may or may not have some ripple effects on other subsystems. To reach the best possible solution as fast possible, there is a need to accurately quantify the system level effect of such a change in requirements. This is the second objective of this research.

Chapter III

BENCHMARKING

3.1 The Contemporary Design Process

In his 1969 study, W.E. Caddell [39] concluded that:

> *"The writer is convinced after many years of work generating, using and improving generalized weight estimating methods that more of aircraft components are size dependent than load dependent. The corollary to that thesis is that the smallest size aircraft that will contain the required equipment and meet the required performance will be the lightest, and the least expensive."*

Yet in contemporary design, volumetrics: the field that deals with aircraft size seems to play only a supporting role to gravimetrics: the field that deals with aircraft weight and load. In light of this, the ensuing discussion of the contemporary design process will shed some light on how designers are still able to reach optimally sized solutions.

Like any other product, the design of an aircraft usually begins with the identification of a need. This need may be conveyed to the designer in the form of a Request For Proposal (RFP). Within this RFP are a set of performance requirements and expectations which the design must meet or beat in order to fulfill the mission goals. The designer, with the help of tools such as Pugh matrices, Quality Function Deployment (QFD) etc translates these into a set of engineering requirements which can be directly mapped to meaningful and quantifiable design metrics. Armed with this knowledge the designer will perform sizing studies so as to identify an "optimal" design point. This process is illustrated in Figure 22 . The designer's goal is to identify the point at which the "best" balance of available and required power or thrust, energy (and volume) occurs.

This point is usually described by a power-to-weight $\frac{P_{SL}}{W_{TO}}$ ratio or a thrust-to-weight ratio $\frac{T_{SL}}{W_{TO}}$ and a wing loading $\frac{W_{TO}}{S}$. These metrics, coupled with RFP requirements, are

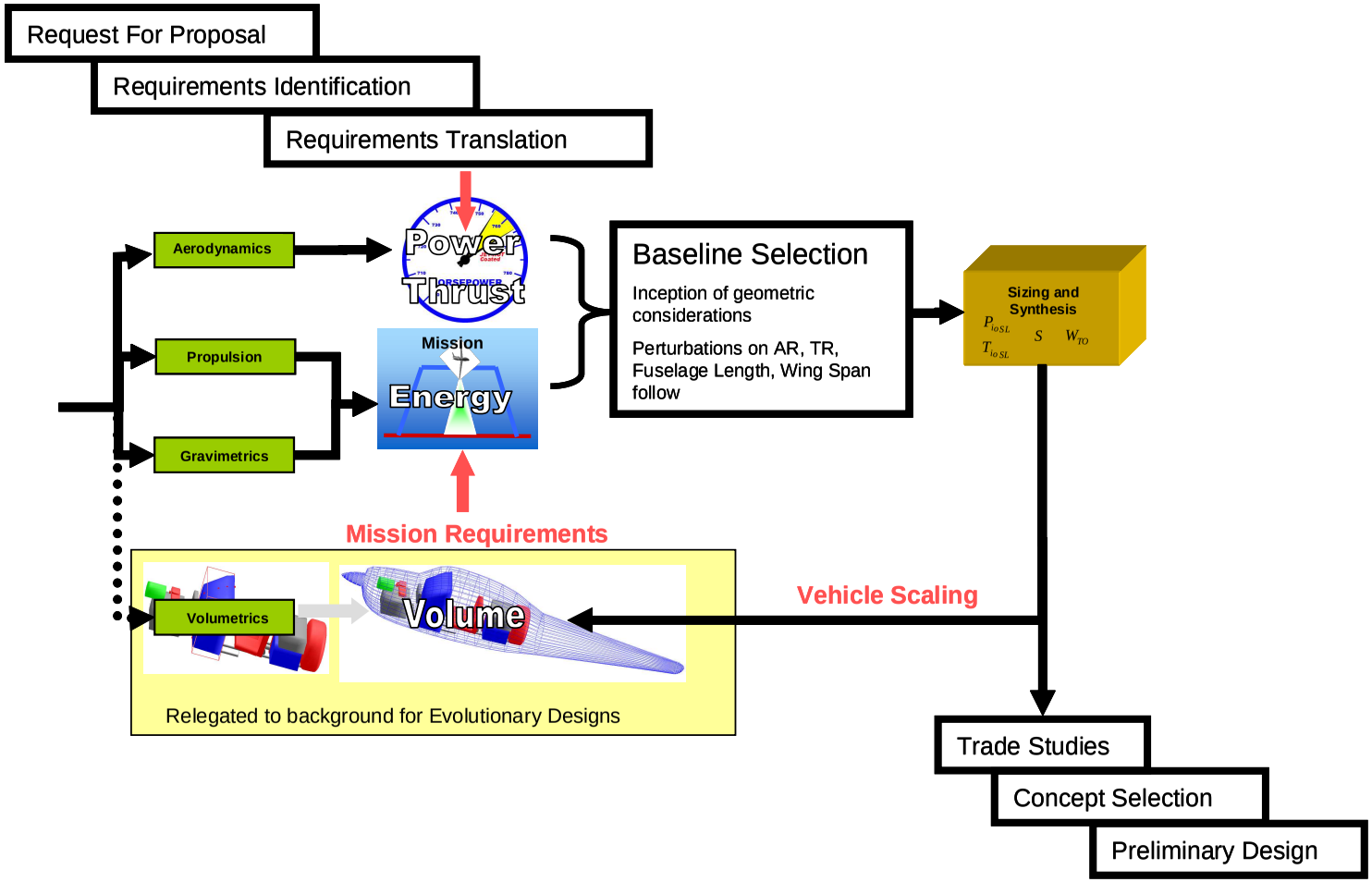

Figure 22: Contemporary Design Process

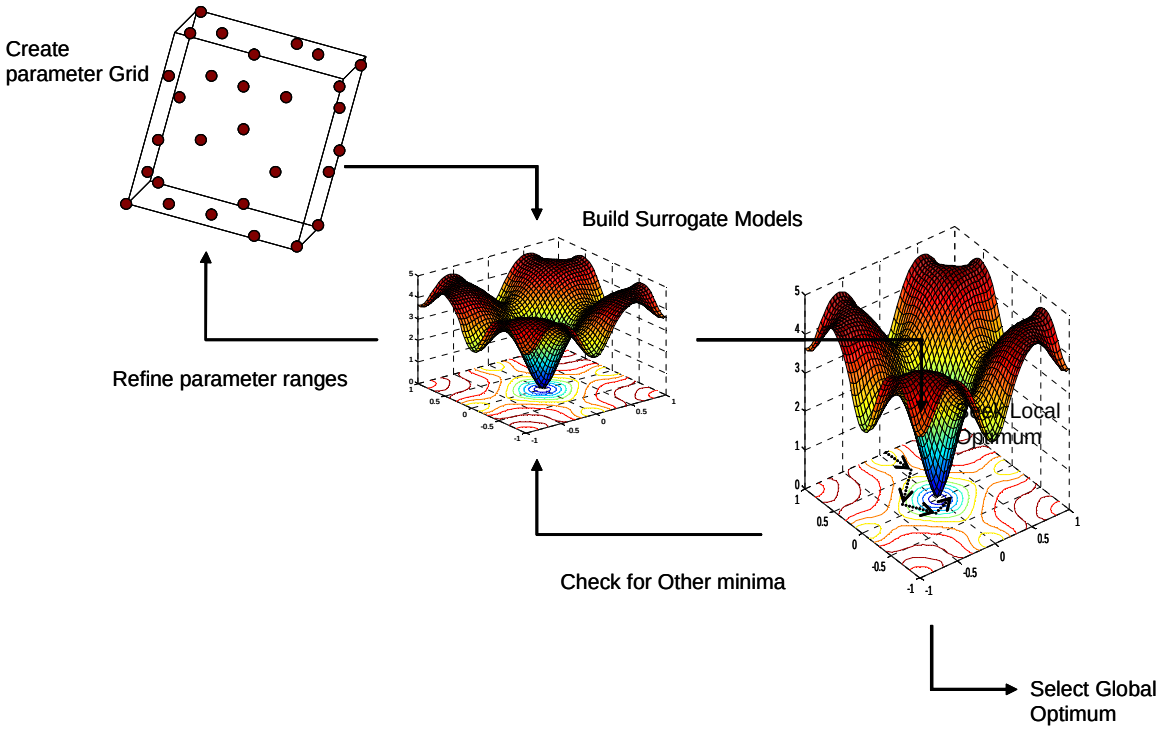

Figure 23: Design Space Exploration in Conceptual Design

used to select a baseline concept. In most cases, the baseline vehicle is a known entity that can be effectively modeled both analytically and geometrically. The baseline vehicle specifications and performance characteristics form the benchmark for the exploration of the design space. Design parameter ranges are set as percentage changes in these benchmark figures sometimes using ratios of baseline to optimal design performance specifications. The process then follows the process shown in Figure 23 below.

Surrogate models help accelerate the design process by replacing expensive disciplinary codes with faster regressions of the key metrics as functions of the variables of interest. Other optimization techniques can also used at this stage of the design process. The optimum combination of the design variables is then passed on to the preliminary design team for further refinement.

Evident in the two design point metrics described earlier, i.e. $\frac{P_{SL}}{W_{TO}}$ and $\frac{T_{SL}}{W_{TO}}$, is the fact that the volume balance aspect is left in the background. The designer can usually get away with this for highly evolutionary designs i.e. designs for which a significant amount

of historical data warrants the replacement of "physical" models with sufficient fidelity regressions. In the absence of such regressions, the designer is left with little recourse outside of a rigorous volumetric treatment of the concept. "Philosophies" that will lead the leap to a new "S-curve" in aircraft conceptual design have been postulated by Beukers [26] among others. However, a conceptual design methodology that bridges the gap between changes subsystem level volume requirements and their impacts on key system level metrics is still lacking.

3.1.1 Gaps in the Contemporary Design Process

A number of challenges in the contemporary design of air vehicles are yet to be definitively solved. Some of these challenges are highlighted in Table 5 .

When it comes to design of revolutionary concepts, the gap under the geometry section of Table 5 is of critical importance. This is because the traditional approach of selecting a baseline from prior art in a class similar to that of the vehicle being designed can no longer be applied. In fact in many cases, even if a geometry that might be close to the final solution existed in prior art, the designer would be hard-pressed to point it out without performing a detailed design study. In performing this study, the designer will need fast, low-fidelity tools that would enable him to identify a good baseline geometry. Additionally, knowledge of the scaling behavior of this geometry in response to requirement changes would be invaluable in the search for an optimum. The fast, low-fidelity tools typically yield to slower, higher fidelity tools as the design process progresses. This approach is referred to herein as the *analytical paradigm*.

3.1.1.1 The Analytical Paradigm

The choice of disciplinary analysis tool in each phase of the design process is driven by the trade-off between speed and accuracy. As illustrated in Figure 24 below, the large number of design points (cases) to be analyzed in the conceptual design phase dictates that faster, lower fidelity tools be used. As this number is trimmed down through trade studies and optimization, the emphasis then shifts from speed to accuracy. Initial assumptions on higher order effects are replaced with higher fidelity tools capable of reliably predicting these effects.

Design Process			Tool	Discipline						
Phase	No. of Designs	Analysis Speed	Fidelity	Aerodynamics	Structures	Propulsion	Controls	Geometry	Cost	Manufacturing (& PLM)
Conceptual	many	Fast	Low	Empirical methods e.g. EDET	Empirical methods e.g. FLOPS	Empirical methods e.g. FLOPS	Empirical methods e.g. FLOPS	V S P / G A P	Piano	GAP
Preliminary	Few	Slow	Medium	Vortex Lattice e.g. Vorlax	Basic Structures e.g. ELAPS	Basic Noise e.g. ANOPP	GAP	Vortex Lattice e.g. VORSTAB	GAP	GAP
Detailed	Very Few	Even Slower	High	CFD e.g. Fluent	FEM Analysis e.g. NASTRAN	Advanced Noise e.g. AVATAR	GAP	CAD systems e.g. CATIA	GAP	Virtual Manufacturing e.g. DELMIA

Table 5: Gaps in the Contemporary Design Process[142, 156]

The fact that these tools take longer to run per case is offset by the fact that there are then less design cases to analyze.

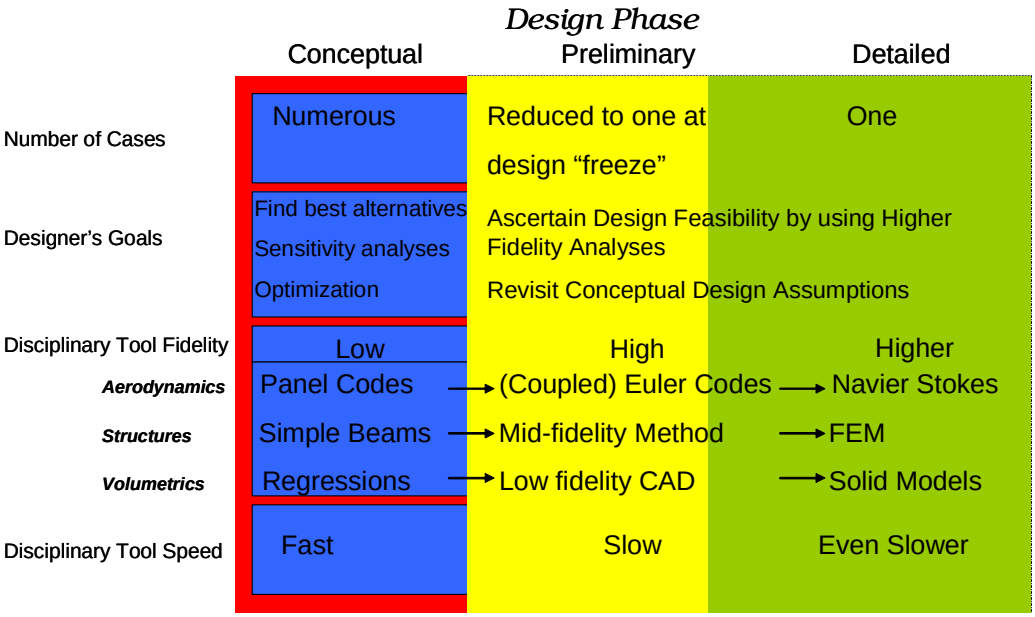

Figure 24: The Analytical Paradigm in Contemporary Design

As alluded to earlier, a conceptual design tool or methodology with similar fidelity as other disciplinary design tools is necessary for the continued use of this paradigm in the design of non-traditional vehicle concepts.

3.2 Volumetrics in Design

Volumetrics as used here describes any method or tool that is used in the analysis of vehicle volume with the aim of balancing the required and available volume. Balancing available volume against required volume does not, however, guarantee volumetric feasibility of a vehicle as the shape and location of the volume are equally important. As previously discussed, designers can usually get away with ignoring the last two criteria for volumetric feasibility until the latter stages of the design process. When new technologies are infused the need to consider these factors early on in the design process becomes imperative. Worse still, in

the absence of both historical data and component placement information within a vehicle configuration, intelligent scaling would be impossible to execute. When volumetric analysis is implemented in conceptual design, in an automated way, automated collision detection becomes a necessity.

3.2.1 Component Layout and Collision Detection

Aerodynamics, payload requirements and structural capability and cost play a key role in determining the final shape of an aircraft fuselage. Fuselages with lower fineness ratios also generally have lower wet area to volume ratios. However, if the diameter is relatively constant along the fuselage length then the inverse is true [180]. Trades such as this and many more have to be considered early in the conceptual design of revolutionary concepts.

It is imperative that a sized concept have the right amount of volume in the right location and in a shape that is congruent with the components that constitute the vehicle's subsystems. Typically, as alluded to earlier, this analysis is relegated to the preliminary and detailed design phases. In these phases one of the key challenges is to identify the optimal layout of components inside the pre-selected vehicle geometry. "Optimality" here is based on metrics and requirements such as minimizing dead volume, static margin considerations, maximizing payload capacity etc. Component layouts are typically explored in CAD packages such as Dassault Systemes' Catia® [56] and PACE's PaceLab Suite® [149]. Aircraft companies typically stitch additional modules on top of these packages to make them more aircraft design friendly. One such example is Lockheed Martin Tactical Aircraft Systems' Computer Mock-up (COMOK) [183]. Traditional volumetric analysis in such packages is inherently computationally expensive. This is because the process involves detailed modeling of both aircraft and component geometries. This extensive modeling is necessary for accurate collision detection analysis. This unparalleled accuracy is of little use in conceptual design if it can not be implemented in a methodology that is fast enough to analyze thousands of designs within an acceptable time frame. The author has been unable to find any information in the public domain regarding a methodology that exploits fast layout and collision detection algorithms as a basis for external geometry definition and selection. Such

a methodology would be very useful in vehicle conceptual design because as Torenbeek [190], stated:

> *"The fuselage should be designed "from the inside outwards" and the skin should envelope the load in such a way that the wetted area is minimum, thus avoiding breakaway of airflow as far as possible."*

Furthermore, it goes without saying the better a baseline concept is, the faster the design optimization process arrives at the final design solution. Where, there is no historical data to choose from, this baseline must be "built" around the new technology. These statements further highlight the need for a tool that trades off analysis speed against accuracy so as to become an enabler for rapid conceptual configuration space exploration. For evolutionary designs, volumetric analysis is usually reduced to a series of regressions. This approach has some advantages and some short comings.

3.2.2 Regression Approach

The regression approach is a fast and simple approach that is easily applicable to conceptual design. Based on the dimensions of the body the net usable volume can be determined using regressions of various, similar class aircraft. See Figure 25. In fact, in the design of many freighter and long haul aircraft, the cargo density takes on predetermined settings which are based on designer experience and mission requirements among other things. The volume then becomes a fall-out once the maximum take-off gross weight is fixed.

However, since volumetric feasibility must be assessed in three dimensions i.e. quantity, shape and location, this approach only works for predetermined geometries for which sufficient historical data is available for regression. As seen in Figure 25 such an approach would be inapplicable to the Airbus A300-600 and the Airbus A380 concepts. Predetermination of geometry means that the two additional metrics i.e. shape and location can be evaluated with reasonable accuracy. It is worth noting, however, that predetermining aircraft class and geometry eliminates or at least limits a sometimes critical degree of freedom i.e. aircraft shape. It was seen from the C-172R study that the conventional GA aircraft shape could not exploit the advantages of the new propulsion system such as modularity. There was a need

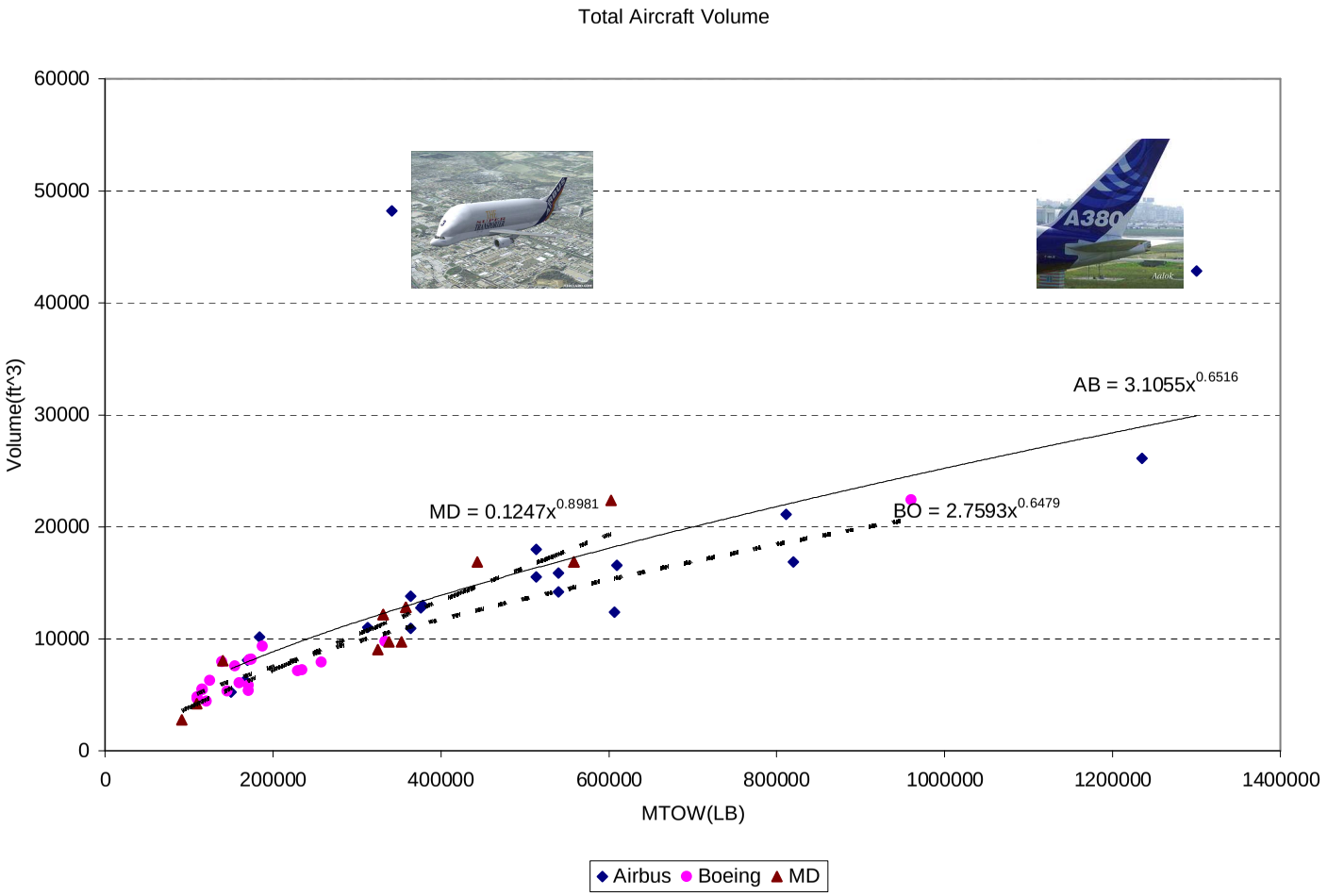

Figure 25: Volumetric Regression for commercial transport aircraft [9, 187, 11, 12, 13, 51, 96, 97, 98, 99, 190]

to identify the optimal shape for a vehicle powered by this technology. Therefore in the design of a truly novel concept, a conceptual design process that must predetermine geometry becomes more cumbersome and vulnerable to the designer's biases as to what the optimal shape should look like. Even when all the above hurdles are somehow overcome, there is significant variability or error in the regression because different aircraft are optimized to different overall evaluation criteria (OEC's) as seen in Figure 25. And, the contribution of design and technology advances through time e.g. in materials are not accounted for. Thus the introduction of a new item that creates new volumetric or gravimetric constraints say a different fuel type renders this approach very unreliable as is. The traditional approach must therefore be reinforced with a capability for reliable volumetric analysis even at the conceptual level. To achieve this , both the components and the containing body must be modeled in 3D space.

3.3 Geometry Modeling

The choice of geometry modeling technique is usually driven by factors such as set-up time, run time, typical number of design variables per model, cost of collision detection, learning curve, ease of geometry scaling, portability and consistency across disciplines. For this work, the choice of modeling approach is based on the typical number of design variables, degree of complexity and the inherent ease/complexity of collision querying for a given geometry modeling approach as these are deemed to be the most critical factors in performing a fast moderate fidelity volumetric analysis.

3.3.1 Geometry Model Representation

A number of methods for the representation of geometry in computational space exist in literature. Some of the most popular methods are described following.

3.3.1.1 Basis Vector Approach

This approach is based on the notion that given a response t and a design variable vector v , a sensitivity derivative can be expressed as

$$\frac{dt}{dv} = \frac{dt}{dR_f}\frac{dR_f}{dR_s}\frac{dR_s}{dR_g}\frac{dR_g}{dv} \tag{4}$$

$where:$

R_f : $volume\,grid$

R_g : $geometry\,model$

R_s : $Surface\,grid$

Based on this fundamental equation Picket [155] proposed a technique that combined the second, third and forth right hand terms of Equation 4 into a set of basis vectors. New geometries can be generated as a series of perturbations to the basis vector shown in Equation 5 below.

$$R = r + \sum_n v_n U_n \tag{5}$$

$where:$

U_n : $Perturbation\,vector$

v_n : $Design\,variable\,vector$

The major advantage of this approach is that it lends itself naturally to the generation and transfer of sensitivity derivatives [167]. Additionally grid generation can be automated thereby yielding significant reductions in design time. Shape changes can be parametrized using a manageable set of design variables even though these may not necessarily lend themselves to effortless understanding on the designer's part. The scope of allowable shape changes is, however, limited by the fact that the reduced basis must remain constant all through the optimization cycle [166]. The designs must thus be relatively similar in shape. Design freedom is therefore artificially constrained.

3.3.1.2 Domain Element Approach

In this approach shapes are represented using a set of points that is connected to a generic shape model called a macroelement. Shape modification is achieved by systematically deforming the macroelement by applying a transformation to points of interest [8]. See Figure

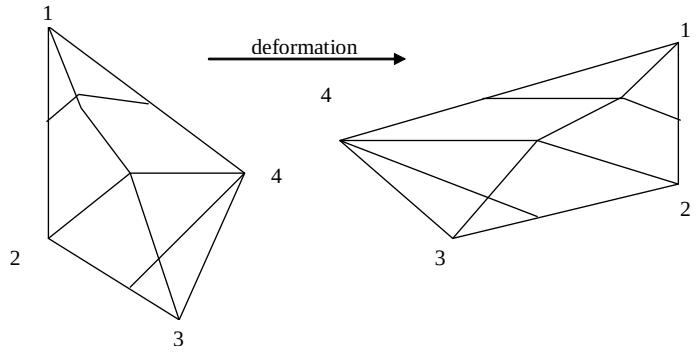

Figure 26: Domain Element Deformation

26. Like other methods in this genre, however, the parameters used to represent the shapes do not convey direct intuitive meaning to the designer. The designer will therefore be subject to a learning curve every time that he introduces a new shape into his system.

This method is relatively simple and is as a result, easy to implement. Other advantages of this approach are that it conserves the grid i.e. the grid does not have to be regenerated for every new shape or deformation. This conservation also makes it well suited for MDO applications where automation of shape deformation and generation is critical.

3.3.1.3 Partial Differential Equation Approach

In this approach geometry definition is achieved through the formulation of a boundary-value problem. The surfaces that define the geometry are the solutions to the corresponding elliptic partial differential equations (PDE's) [108, 166] of the form shown in Equation 6.

$$\left\{ \frac{d^2}{du^2} + \frac{d^2}{dv^2} \right\}^2 X(u,v) = 0 \tag{6}$$

$where:$

$X(u,v) = \{x(u,v), y(u,v), z(u,v)\}$

$x, y, z:\ Euclidean\, coordinate\, functions.$

$u, v\ :\ Parameters\, of\, function\, X$

$a\ :\ smoothing\, factor\, in\, u, v\, directions$

The boundary conditions are imposed on the function $X(u,v)$ and the normal derivative $\frac{dX(u,v)}{dn}$ are imposed at the edges of the surface. Boundary conditions imposed on $X(u,v)$ determine the physical shape of the surface. The rate at which that surface shape moves away from the boundary is determined by the boundary conditions on the derivative function $\frac{dX(u,v)}{dn}$.

Bloor et al [32] successfully demonstrated the use of this approach in what he called the "efficient parametrization of a generic aircraft". In his formulation the fuselage was described as a body of revolution obeying the equation:

$$y^2 + x^2 = a^2$$

$$a(\chi) = a_0 sin[\tfrac{\pi}{18}(17\chi + 1)] + a_1 sin[\tfrac{3\pi}{18}(17\chi + 1)]$$

$where:$

$a_0, a_1 : constants$

$\chi : non - dimensional\, fuselage\, parameter$

The wings were described using a series of airfoil sections described using the simple equations:

$$x(\theta) = ch.sin(\tfrac{\theta}{2})$$

$$y(\theta) = -\tfrac{t}{2}.sin(\theta) + 6.75.cam.x(\theta)\tfrac{[ch - x(\theta)]^2}{ch^3}$$

$$z = a_0 + h_1$$

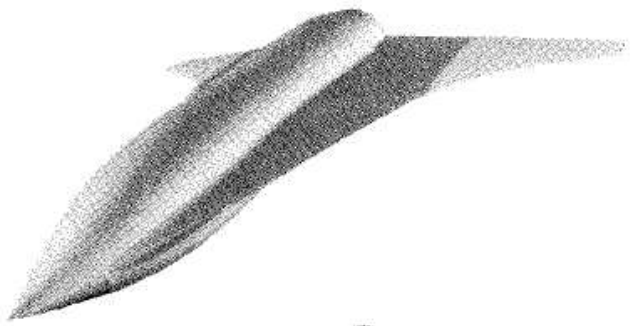

Figure 27: Baseline Parametrized Geometry [32]

$where:$

$ch: airfoil\ chord\ length$

$cam: cubic\ camber\ control\ parameter$

$\theta: radial\ variation\ parameter\ \theta | 0 \leq \theta < 2\pi$

With this formulation Bloor et al successfully parametrized a supersonic blended wing-body concept (See Figure 27) using a set of twenty parameters.

Of this set, about six make direct intuitive sense to a designer and can thus be manipulated to achieve predictable effects. Some experimentation would therefore be necessary before a novice could effectively manipulate the entire variable set and achieve the desired results.

3.3.1.4 Discrete Approach

Here the geometry is represented with a set of coordinates which also dabble as design variables. See Figure 28. Thus the degree of geometric flexibility is only limited by the number of design variables. The tradeoff is that increasing geometric flexibility; hence the number of design variables increases the complexity of the design problem especially if it involves optimization. This approach is relatively easy to implement with the only challenge being how to maintain a smooth geometry. Smoothing is particularly critical for the external aircraft geometry definition due to the inherent aerodynamic implications. At the component level, however, this easy and high degree of geometric freedom method is still relatively attractive. As an added bonus, the computation of shape sensitivity derivatives

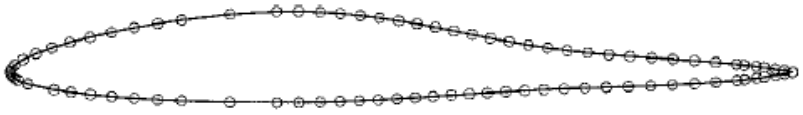

Figure 28: Discretized Airfoil

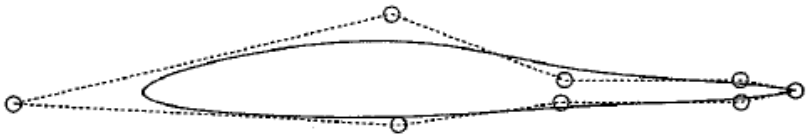

Figure 29: Airfoil Shape Definition using control points [167]

is almost trivial since all the necessary values are always known at every point.

3.3.1.5 Polynomial and Spline Methods

This approach provides one of the most effective ways of reducing the number of design variables. Polynomials can essentially be defined with $(n+1)$ coefficients where n is the degree of the polynomial. This representation is fundamentally represented below as:

$$S(x) = a_0 + a_1 x + a_2 x^2 + ... + a_n x^n \tag{7}$$

where a_i and x represent a numerical constant and a simple variable respectively in the case of a monomial. These may take on more advanced forms such as Lagrange or Hermite polynomials in cases where shapes are represented as sums of more than one complex function. See Figure 29 for a sample airfoil design using only nine control points or design variables.

However, each of these representations comes with its own set of challenges. Monomial design variables do not deliver any intuitive meaning to the designer. Only an analysis of the effect of variation on the final shape can build this intuition in the designer's mind. Lagrangian interpolation curves may exhibit unwanted oscillation along the shape especially for higher order polynomials [94]. A polynomial form that overcomes most of these difficulties is the Bezier curve [108] . In this form are the points on the Bezier polygon a_i and x are the

Bezier or Bernstein polynomials . Problems with round-off error as the degree of the Bezier curve increases for example when representing non-simple shapes, drive designers to adopt the composite curves known as splines. B-splines are special form of these functions where the segments are lower order Bezier curves. These curves typically take the form:

$$R(u) = \sum_{i=1}^{n} \overline{P}_i N_{i,p}(u) \tag{8}$$

where :

$\overline{P_i}$ *are the* $B-$*spline control points*

P *the degree of the* $i-th$ $B-$*spline basis function of degree* P.

B-spline modeling also faces some challenges such as the inability to represent conic sections accurately. Various adaptations of splines such as Non-Uniform Ration B-Splines (NURBS [68]) are used to overcome this stumbling block since conic sections are high utility shapes in aircraft design.

3.3.1.6 CAD-Based Approach

CAD-based modeling is implemented through either boundary/surface representation or solid object construction. Parametrizing CAD models for purposes such as design automation is usually a daunting task and even when this is achieved, parameter sets can break down after the slightest of modifications to the model as imperfections such as gaps and slivers emerge. To put the "Design" back in "CAD" [167] a new approach, commonly known as Feature-Based Solid Modeling (FBSM) was developed and is quickly gaining acceptance. Here dimensions or features form the foundation of the any solid model. As a result, modifying any object "template" is as easy as modifying the values corresponding to its features. Thus automation and design exploration are better facilitated in FBSM CAD tools than the earlier standards in CAD. There are other challenges to the use of CAD-based models. These include: portability, integration and automation of sensitivity derivative calculation. Portability issues arise because the codes and the models they generate tend to require significant amounts of storage space. When multiple instances of a baseline are created for design space exploration purposes this problem can be further exacerbated. This creates

additional computational expense in both run-time and storage. Most CAD tools require special plug-ins to enable integration with external tools and this combined with the aforementioned computational expense makes such tools less attractive for conceptual design studies for example where multitudes of possibilities must be explored before a choice is made. With the exception of the special case where the solid topology is kept constant, any other changes to a model present significant computational challenges when calculating sensitivity derivatives. CAD integration presents other challenges too. These include computational speed, random bugs, crashes and memory leaks [220]. Even with the current levels of computational power for an average PC platform the use of CAD tools is still limited due to the inherent overhead. Stumbling blocks such as memory leaks and random bugs that occur as a result of the automation/batching that is implicit in most conceptual design computational processes still need to be overcome as well.

3.3.1.7 Analytical Approach

Particularly useful in wing design, the analytical approach attempts to define (airfoil) shapes using closed-form equations e.g. Equation 9 below describing a NACA 0012 [7].

$$y(x) = \pm 5t[0.2969\sqrt{x_{int}x} - 0.3516(x_{int}x)^2 + 0.2843(x_{int}x)^3 - 0.1015(x_{int}x)^4] \qquad (9)$$

$$\begin{aligned} &where: \\ &X_{int} = 1.0089 \\ &t = thickness\ to\ chord\ ratio \end{aligned}$$

As expected, not all shapes can be defined in smooth, differentiable closed form solutions as that discussed above. Other approaches use piece-wise shape definition for more complex shapes. However, this approach runs into the same challenges as the spline forms discussed earlier i.e. ensuring smooth continuity at the transition points. One solution to this challenge is the superposition of a number of functions. The shape co-ordinate at each location is therefore defined by an equation of the form:

$$y_{new} = y_{basic} + \sum_{i=1}^{n} a_i P_i \qquad (10)$$

Table 6: Polynomial Design Variable Ranges

Coefficient	Upper Bound	Lower Bound
A	3.75	2.75
B	0.1	0
	0.1	0
D	0.01	0

where :

$a_i = weighting\ factor\ for\ shape\ function\ P_i$

Using a generic or known shape such as the NACA 0012, a number of shape functions each targeted at modifying a specific section of the airfoil can be aggregated to form the new shape. For example, using the three polynomials listed in Equation 11, Equation 12 and Equation 13 the ranges listed in Table 5, the shapes shown in Figure 30 can be generated.

$$P(1) = \frac{B \cdot (1-x)x^4}{e^{20x}} \tag{11}$$

$$P(2) = \frac{C \cdot (1-x)\sqrt{x}}{e^{3x}} \tag{12}$$

$$P(3) = D \cdot sin^5(\pi x) \tag{13}$$

This approach can be extended to 3D by extrapolating between cross-sections along the span of the wing. Kulfan [110] of the Boeing Commercial Airplane Group recently (September 2007) extended the Class function/Shape Function Technique (CST) from 2D to 3D.

In this approach the airfoil is modeled using the round noose/closed-loop shape function $\sqrt{\psi}$ as follows :

$$\varsigma(\psi) = \sqrt{\psi}(1-\psi)\sum_{i=0}^{N} A_i \psi^i + \psi\varsigma_T \tag{14}$$

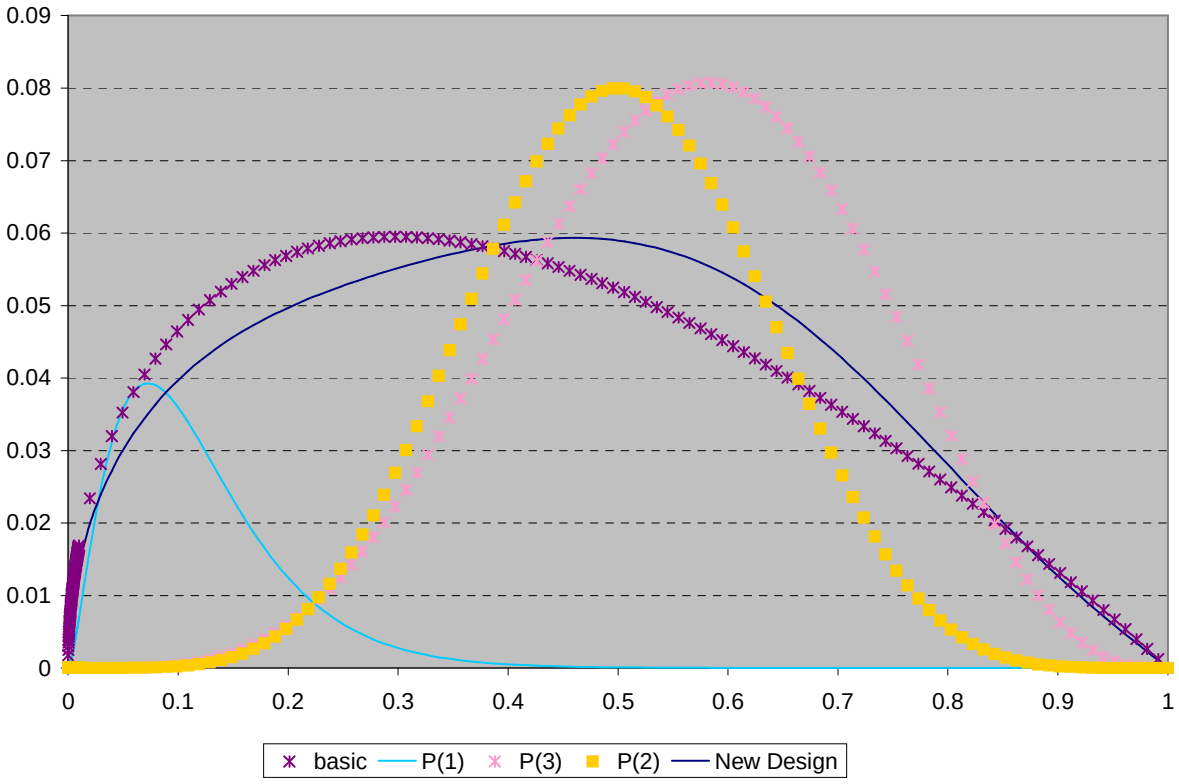

Figure 30: Analytically Generated Airfoil

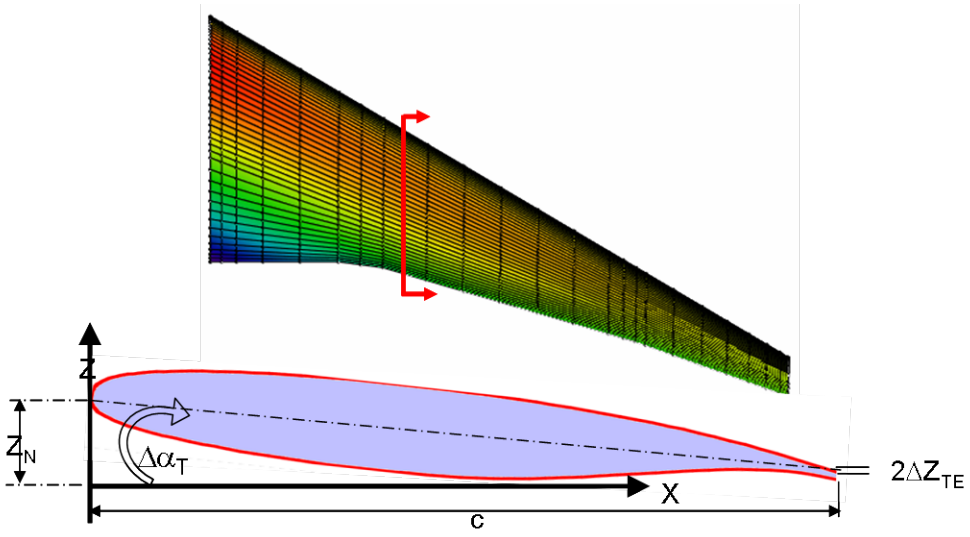

Figure 31: Extension of CST methodology to 3D [110]

$$where:$$

$$\psi = \frac{x}{c}$$

$$\varsigma = \frac{z}{c}$$

$$\varsigma_T = \frac{\triangle \varsigma_{TE}}{c}$$

The extension to 3D is achieved by adding two parameters for local wing shear and twist as shown in Equation 15 and Equation 16 below.

The upper surface is represented by:

$$\varsigma_u(\psi,\eta) = \varsigma_n(\eta) + C_{1.0}^{0.5}(\psi)S_u(\psi,\eta) + \psi[\varsigma_T(\eta) - tan[\triangle\alpha_T(\eta)]] \tag{15}$$

Similarly the lower surface is given by:

$$\varsigma_L(\psi,\eta) = \varsigma_n(\eta) + C_{1.0}^{0.5}(\psi)S_L(\psi,\eta) + \psi[\varsigma_T(\eta) - tan[\triangle\alpha_T(\eta)]] \tag{16}$$

$$where:$$

$$Fraction\ local\ chord: \psi = \frac{x - x_{LE}(\eta)}{c(\eta)}$$

$$Normalized\ Semi-spanstation: \eta = \frac{2y}{b}$$

$$Local\ leading\ edge\ coordinates: x_{LE}(\eta)$$

$$Local\ chord\ length: c(\eta)$$

$$Normalized\ Upper\ Surface\ Coordinates: \zeta(\eta) = \frac{z_u(\eta)}{c(\eta)}$$

$$Normalized\ local\ wing\ shear: \zeta(\eta) = \frac{z_N(\eta)}{c(\eta)}$$

$$Local\ wing\ twist: \triangle\alpha_T(\eta)$$

Like most methods discussed so far the most challenging aspect of this method is that the design parameters do not deliver any intuitive meaning to the designer. Thus the selection of design variable ranges must be preceded by some trial and error perturbations on the values to get some sense of their effect on geometry. Naturally this becomes more complex and more challenging as the number of variables increase. In most cases, however, this number can be limited to a manageable set. The selection of the base function set can be challenging as well.

A summary of the identified methodological challenges follows.

3.4 Summary of Technical and Philosophical Challenges to Early Volumetric Analysis

3.4.1 Computational Expense

Computational expense is incurred in the form of storage requirements and processing time. The dramatic increases in computing power over the past decades have rendered time expense less of a problem. However, even at the current speeds design problems still have the potential to become prohibitively expensive especially in cases where multitudes of different configurations must be analyzed in the search for an optimum. An alternative solution to this problem may be the use of simplified algorithms and geometry abstractions that offer sufficient fidelity for the conceptual design phase while minimizing the storage and computational expense

3.4.2 Uncertainty in Component Sizes

The placement of components in 3D space is based on the principle that no two components can occupy the same space. However, when there is uncertainty in the size of any component due to technology immaturity, a treatment of the possible changes in component size is necessary in order to improve the robustness of the final outcome. Collision could occur if actual component sizes differed from design sizes. Uncertainty is not confined to volumetric analysis alone. Many disciplines within aircraft design such as aerodynamics and structures all rely upon low fidelity approximations during the preliminary design stages. To maximize, the chances that the chosen design meets all performance requirements designers usually choose the robust solution i.e. the solution that exhibits the least sensitivity to the various forms of design noise while meeting performance expectations. A similar approach could be taken to deal with uncertainty in component sizes in design.

3.4.3 Design Variables Numerous and not Intuitive

Even the most efficient geometry representation methods require a typically high number of non-intuitive design variables. In addition to exacerbating the aforementioned computational expense, this issue further complicates the design optimization process. The designer would have to investigate the effect of all the variables on the design metrics of interest in order to screen out the less important variables. In cases where the majority of the variables have comparable effects on the output metrics, the problem may become computationally prohibitive. The magnitude of this problem can be some what lessened if the variables and their impacts on the geometry lend themselves to designer intuition. In such cases the designer can narrow down the design space to a few critical areas prior to setting up and running experiments thereby saving some design time. Multiple parameters can sometimes be lumped into a scaling law thereby reducing the number of design variables while preserving the intuitive value of the lumped parameters. Thus a successful methodology must minimize the number of design variables while maximizing their intuitive appeal to the designer.

3.4.4 Restrictions on Scalability of Component Models

The scaling of aircraft and component geometries to meet unsatisfied constraints is an integral part of the aircraft design process. Many high fidelity geometry representations usually produce odd shapes when scaled up or down. This limits the utility of such models across disciplines and through the design process. In designs where much variation in component sizes is to be expected due to either low technology maturity or the absence of sufficient knowledge about the design space, the robustness of a geometry representation technique to changes in component sizes is of paramount importance.

3.4.5 Implications for Design Methodologies

Since computational expense in terms of collision detection time and storage resources is the key technical barrier to the implementation of explicit volumetric analysis during conceptual design, a successful methodology must apply the right combination of geometry representation techniques and geometry manipulation algorithms so as to overcome this problem.

Figure 32 summarizes the strengths and weaknesses of the various component representation methods.

3.5 Scaling in Design

Scaling refers to the systematic alteration of vehicle geometry in response to the violation of design constraints or over-satisfaction of performance requirements. Popular approaches to scaling include full photographic scaling where the entire vehicle geometry is scaled by the same scale factor; decoupled photographic scaling where fuselage and wing surfaces are scaled independently based on the cause of the scaling need and scaling laws where regressions of historical data are used as a basis for geometry modification.

3.5.1 Photographic Scaling

Typically, scaling in conceptual design is performed photographically. In this approach the dimensions of the vehicle are scaled linearly using a scale factor λ such that:

$$\overline{D}_{new} = (1 + \lambda)\overline{D} \tag{17}$$

The total aircraft volume thus changes by a factor of $(1 + \lambda)^3$. This approach is very simple and easy to implement since it requires no further volumetric analysis on the new body. The simplicity arises from the assumption that critical similarity laws such as Mach number, $M = \frac{V}{C}$ and Reynolds number, $Re = \frac{\rho V L}{\mu}$ match across aircraft of different sizes. As a result, key aerodynamic performance parameters also remain constant. In practice, however, it is nearly impossible to match similarity parameters [38]. Factors such as transitional flow influences [66, 85] , vorticity dynamics [87, 107] and real gas effects for hypersonics [67] can tremendously alter the flow characteristics in real flight. For a sufficiently small , the change in the similarity factors is usually negligible and as such these factors are assumed to be essentially constant. Thus, it is still plausible to assume that the performance of the body remains unchanged. However, it is still questionable whether the new body lies at the optimal point for a vehicle of the new size. This doubt arises from the fact that typically scaling is invoked by the violation of a few but not all

Method	CAD based	Domain Element	PDE	Discrete + Convex Hull	Polynomial and Spline	Basis Vector	Analytical
Number of Variables	–	–	✓	✓	✓	✓✓	✓✓
Do variables lend themselves to designer intuition?	–	–	–	–	–	–	–
Tolerance for large geometric changes	✓✓	✓	✓✓✓	✓✓✓	✓✓✓	–	–
Allowable complexity of geometry changes	✓✓✓	✓	✓	✓	✓✓	✓	✓
Consistency across disciplines	✓✓✓	✓	✓✓	✓	✓✓	✓	✓✓
Collision detection expense	–	–	–	✓✓	✓	✓✓	✓
Require reverse engineering of original design?	–	✓✓	–	✓✓✓	–	✓✓	✓✓✓

✓✓✓ Excellent ✓✓ Good ✓ Poor - Very Poor

Figure 32: Strengths and Weaknesses of various approaches to Efficient Geometry representation [167, 220]

of the volumetric constraints governing the body. Also, not all of the aircraft components scale photographically: a fuel tank could scale photographically but a passenger box would scale in discrete units dictated by the number of passengers. The nature of the scaling law is determined by factors such as physics-based laws, technology and manufacturability. Sometimes, budget constraints dictate that an off-the-shelf component be used. For such components as an engine, it would take a stroke of luck to find an exact match for the desired design point. Thus the designer can choose engines at various discrete design points. The effective scaling law for this situation would be a step-function. Discerning the impact of this and other subsystem level scaling patterns on the optimal geometry requires some rigor.

Thus the question arises that given dissimilar scaling laws for the major components of a vehicle, is photographic scaling still optimal? If not, then beyond what threshold ε would photographic scaling result in a volumetrically feasible but not necessarily optimal solution? Photographic scaling is fast and efficient approach in the special case where all subsystems scale photographically in response to the impetus for scaling otherwise there is a risk of leaving the optimal region of the design space by scaling blindly.This phenomenon is notionally illustrated in Figure 33 below.

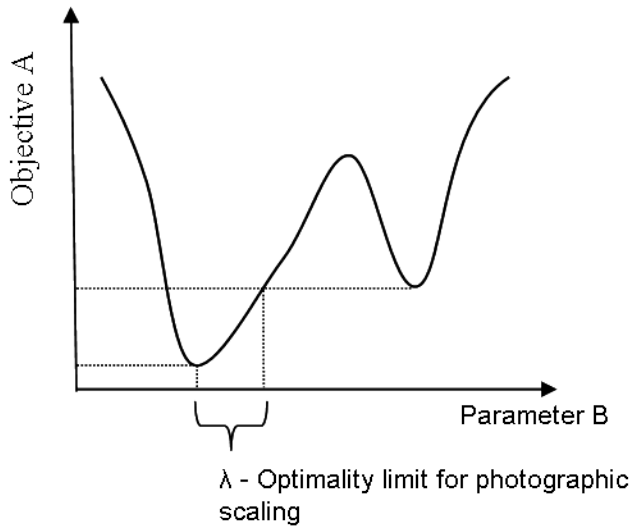

Figure 33: Limitations of Photographic Scaling

This behavior can explained with the help of differential calculus. Suppose a vehicle with total internal volume V, constituted of three components : A, B and C. That is to say, $V = V_A + V_B + V_C + V_R$ where R is the residual volume resulting from the relative arrangement of the subsystems as well as the shape of the fuselage. Then the rate of change of V with respect to a change in a performance metric M, can be quantified as shown in Equation 18 :

$$\frac{dV}{dM} = \frac{dV_A}{dM} + \frac{dV_B}{dM} + \frac{dV_C}{dM} + \frac{dV_R}{dM} \tag{18}$$

Scaling a vehicle photographically is tantamount to reducing Equation 18 to Equation 19 below :

$$\frac{dV}{dM} = \frac{V_o}{M_o} \tag{19}$$

$$where :$$

$$*_o = reference\ value\ of\ metric\ *$$

Thus in practice, scaling of aircraft based either on incremental innovations or a need for extra capacity is targeted primarily at the affected sub-systems and then propagated to the rest of the dependent sub-systems. As noted earlier, photographic scaling while useful may fall short of the optimum in many cases. A new term i.e. smart scaling is thus introduced here to describe a bottoms-up methodology by which the impact of subsystem scaling is propagated onto other subsystems and further onto the overall vehicle geometry. By this approach, vehicle scaling will not be confined to a predefined set of rules but to an adaptive set of methods that will be robust to large changes in geometry resulting from large changes in components. With sufficient acceleration, this methodology will not only be useful in vehicle scaling but also in bringing information regarding component contribution to vehicle inertial properties forward in the design process. This information may be especially useful for concept volumetric feasibility analysis as well for preliminary stability analysis.

3.5.1.1 Quantifying the "sufficiently small" λ

Even though the phrase "sufficiently small" is commonly used in literature [45, 123, 204, 224]] in reference to the upper limit of in Equation 17 , the author has been unable to come across

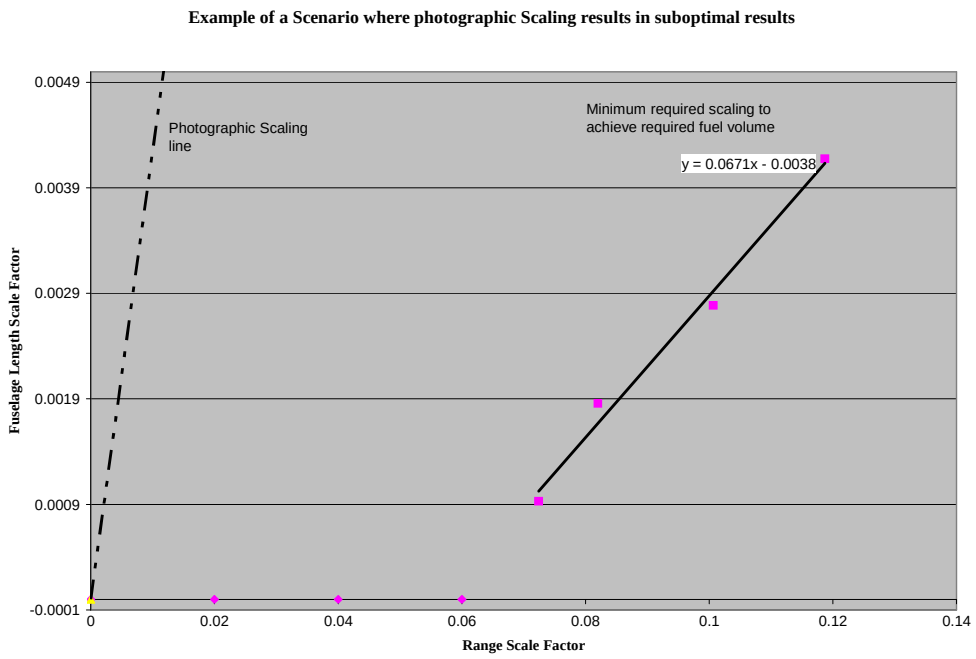

Figure 34: Shortcomings of Photographic Scaling

a quantification of a generalized theorem on the upper limit or threshold for the parameter. This is mainly because the optimality of photographic scaling depends on the percentage of total internal volume that is accounted for by components that exhibit a scaling behavior that is close to photographic. The higher this percentage is, the more optimal this approach. In many cases, however, this approach results in sub-optimal results even for small scale factors as shown in Figure 34 . In this scenario, the notional PEM powered C-172 does not meet the range requirement. The study is based on the layout in Figure 14 . The fuel tank is therefore scaled to increase its fuel capacity. Note that the photographic scale factor is usually calculated as $\sqrt[3]{\frac{R_{required}}{R_{available}}}$ where R corresponds to the volume of the insufficient resource. Because the concept is not volumetrically constrained, the fuel tank can be scaled up by a factor of up to 6% before changes in the fuselage dimensions become necessary. And even at and beyond this point, a $0.067 : 1$ ratio of change in fuselage length to change in range is seen.

It is therefore evident that if this fuselage were scaled photographically, there would be an unnecessarily large increase in dead volume and fuselage size. This is often the case in many real-world applications because most subsystems either do not scale at all or scale in a discontinuous manner in response to a given change in requirements.

Figure 35: Batteries 4.5V, D, C, AA, AAA, 9V, SR41, SR44 [214]

A further examination of the volumetric (Figure 36) and gravimetric (Figure 37) properties of typical alkaline batteries painted the same picture as seen in Figure 35.

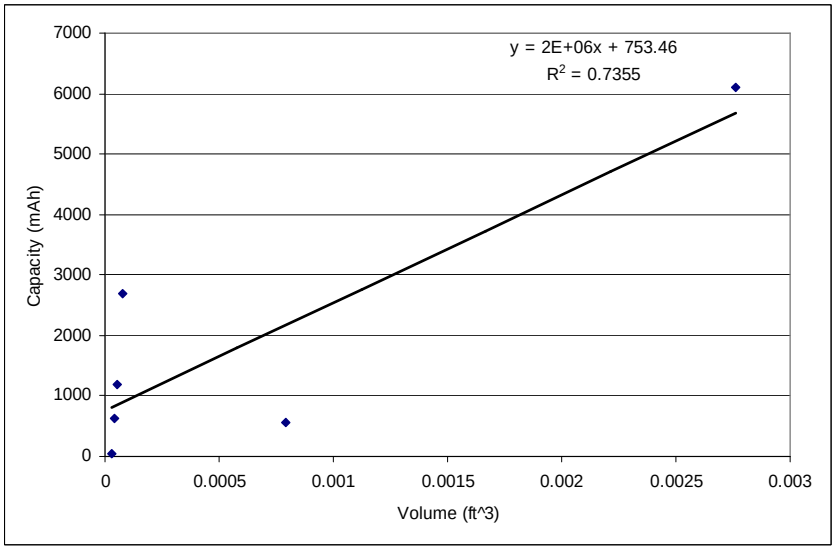

Figure 36: Battery Capacity Scaling [209, 210, 213, 212, 211]

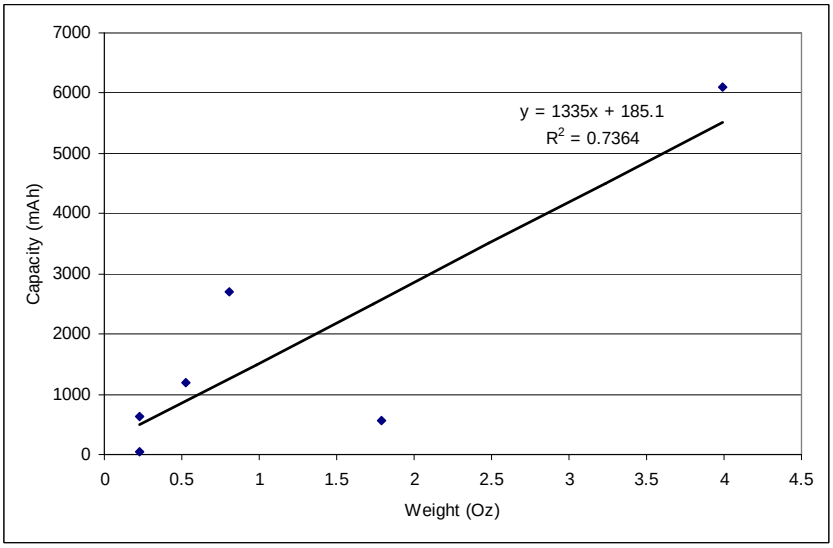

Figure 37: Battery Capacity Scaling [209, 210, 213, 212, 211]

Here most regression approaches can not satisfactorily model the property changes with capacity. Factors ranging from technology to materials to manufacturing practices influence the outcome in this case. Once this and similar scaling effects are propagated to the system level, the impact on the system can not be easily predicted through the use of such assumptions as photographic scaling.

The above analyses led to a sixth observation:

> VI. *Photographic and regression-based scaling can result in highly sub-optimal results even for very small scaling factors.*

3.5.2 Scaling Laws

3.5.2.1 Definition and Utility

The early phases of any design process are characterized by a high degree of design freedom. Implicit in this high degree of freedom is a high number of variables that could take on multiple settings. From this multitude of possible configurations, the designer must identify the "best" solution in the shortest possible time. This task usually boils down to the identification of the most dominant variables and the quantification of their impact on the overall system metrics. Scaling laws are one of the more popular methods by which the impact

of dominant variables on the behavior of complex systems. These laws usually take the form of a power law (shown in Equation 20 below) mainly because many observed physical phenomena such as the population growth rate of bacteria follow power laws.

$$y = k\frac{x_1^i x_2^j}{x_{n-1}^l x_n^m}... \tag{20}$$

$$\overline{\begin{array}{l} where: \\ i, j, k, l, m, n \, are \, constants \end{array}}$$

Also, many empirical regressions are best fit using power laws [124] . Furthermore dimensional consistency is easily attained when using power laws. More concisely, a scaling law can be defined as:

> *A law stating that two quantities are proportional, which is known to be valid at certain magnitudes and is used to calculate the value of one of the quantities at another magnitude. [64, 154]*

Scaling laws can be derived in various ways as discussed in the following section.

3.5.2.2 Derivation

Philosophical Foundations

A significant amount of literature [36, 115, 173, 181] exists on the derivation of scaling laws for systems that range from virus infection rates to ceramic-metal bonding . Generally scaling laws are derived either by abstraction or physical scaling. The abstraction approach employs a combination of mathematical rigor and sparse knowledge of the system in question to come up with metrically consistent laws that exhibit low prediction errors outside of the known regions of the system. Physical scaling provides the most accurate scaling laws as it minimizes the effects of averaging across noise-induced system dissimilarities. An aircraft body scaled up in response to a fuel requirement violation would respond differently from one scaled up in response to a "payload volume" violation. Linear scaling approaches such as those used in photographic scaling approaches do not respond directly to the impetus for scaling. For evolutionary designs whose solutions occur as interpolations within a wealth of

historical data, these effects are averaged out. For the revolutionary concepts, the process would more often than not fail to update the configuration to the most optimal point in the design space due to the sparsity of knowledge. Physical scaling is not always feasible. Factors such as time and economic expense could become prohibitive. It is therefore desirable that analytically derived scaling laws mirror the accuracy of physically derived scaling laws without a significant accompanying computational expense.

One key condition for the validity of any scaling law is the "single regime" requirement [124, 173]. This requirement stipulates that the relative influence of the independent parameters on the response being tracked should remain relatively constant. A regime could be a flight regime but it could also be a technology regime. A change from a low Reynolds number regime to a high Reynolds number regime changes the relative influence of inertial and viscous effects on vehicle performance. The relative importance of wet area and thus volumetric packing efficiency changes accordingly. These effects trickle down to the various subsystem configurations and their optimality ratings. Likewise substituting a higher heating value fuel such as LH_2 for aviation kerosene can diminish the importance of parameters such as weight fraction on performance metrics such as range.

A number of studies on scaling and the effects of scale effects exist in literature [51, 85, 206, 161]. A discussion of some results from these studies follows.

Examples in Literature

Werner and Wislicenus [206] used the physics based laws such as the Froude number and historical data on various vehicle classes to derive scaling laws such as:

$$S = K\{\frac{TOGW}{\rho g}\}^{\frac{2}{3}} \tag{21}$$

$where:$

$K: Constant$

$\rho: Aircraft\ Mass\ Density$

$g: Gravitational\ Acceleration$

$S: Vehicle\ Characteristic\ Area$

Raymer [160, 162] used the abstraction approach to derive a set of scaling laws for use in the multi-disciplinary optimization of vehicles. Some of these laws are shown below.

$$S_{tail} = K_1 (S_{wing})^{\frac{3}{2}} \tag{22}$$

$$S_{X-section\,max} = K_2 S_{wing} \frac{t}{c} cos(\triangle) \tag{23}$$

$$Fuel\,Volume_{\,wing} = K_3 S_{wing}^{\frac{3}{2}} \tag{24}$$

$$S_{wet_{nacelle}=K_4 \frac{T}{W}} \tag{25}$$

$where:$

$S_i: Component\ Reference\ Area$

$\frac{t}{c}: Thickness - to - chord\ ratio$

$\triangle: Sweep$

$K_i: Constant$

Big aircraft companies such as Boeing and Cessna are also said to have large sets of scaling laws by virtue of their having access to large detailed aircraft databases. However, even with access to the historical data, one encounters significant scatter in the data for some key parameters even within the same class of aircraft as will be seen later. This scatter is a result of technology and requirement changes, improvement in design and manufacturing practices and variance in design objectives among others. When questioned about this issue, Dr. Dan Raymer replied:

> *"... Those scaling laws are the best I can do, and I think are actually pretty good. The next step up would probably be a really detailed, design-specific program that would take ages to define and load. The big companies used to have huge programs that did this - it took a full-time expert about a month to load and run! ..."* [163]

This excerpt implicitly acknowledges the issue and hints a possible solution i.e. the customization of the laws to a specific vehicle. It also suggests that the accompanying time and computational expense would be high. Also, like other historical data based analyses, such laws become questionable where novel concepts are being considered.

The above survey led to a series of research questions pertaining to the best way to enhance the conceptual design process so that novel concepts can be handled comfortably within the methodology.

Chapter IV

RESEARCH QUESTIONS

1. ***How can the contemporary treatment of geometric aspects in conceptual design be enhanced to facilitate the design of revolutionary concepts?***

   (a) *How can the baseline configuration space for a vehicle concept based on a disruptive technology be defined?*

   As Haldane [86], one of the pioneers of "systems-thinking" approaches so insightfully put it :

   "*For every type of animal there is a most convenient size, and a large change in size inevitably carries with it a change in form.*"

   Faced with a design process disruption that imposes significant variance in the volumetric and gravimetric properties of the target vehicle class, the designer must identify the new "most convenient" size and form of the vehicle. This form may not necessarily lie within the domain of the prior art. When this disruption is imposed by new and perhaps immature technologies the designer must overcome a significant hurdle namely uncertainty in component sizes. This leads to the next research question:

   (b) *How should the subsystems be modeled in order to facilitate fast configuration definition?*

   Which component transformation approach does this approach permit?

   Which collision detection approaches does it permit?

   How fast must a configuration space exploration method/ tool be in order to permit configuration space exploration at the conceptual design level?

   The choice of subsystem modeling technique can not be made independently of

a consideration of the implications of the technique for the cost of automated transformation and collision detection.

(c) *How can information at the component level be mapped onto meaningful and useful system level metrics?*

As mentioned earlier, the more "ready-to-eat" the information delivered by any conceptual design discipline, the shorter the design cycle time and longer the design process' capacity to absorb this information.

Not all the significant factors affecting the final form of an aircraft are physics-based laws. Other factors commonly referred to as "real-world" effects also influence aircraft design. Therefore this area merits some further research.

(d) *How can the volumetric uncertainty inherent in new technology immaturity or revolutionary designs be accommodated?*

Which volume requirement does the designer design for?

Examples such as the PEM fuel cell engine model demonstrate how factors such as low technology readiness level introduce uncertainty in the sizes of major components. This uncertainty can be further compounded by the fact that the probability distributions on size may vary wildly from component to component. A deterministic layout analysis is intrinsically much faster than its probabilistic equivalent. How then can the inherent uncertainty be accommodated? Also, information at the component level does not lend itself well to the decision-making paradigms used in conceptual design. A solution to this challenge must be identified. This begs the question:

(e) *How can real-world effects such as maximum practical density, subsystem connectivity requirements and aesthetics be incorporated into the configuration space search methodology ?*

How can they be modeled and quantified in order to be considered in conceptual design?

Practical considerations such as manufacturability and maintainability sometimes play as critical a role in determining the final form of an aircraft as key disciplines like aerodynamics. It is therefore imperative that the designer integrate these in design loop when searching for optimal configurations to the extent possible.

The search for the optimal geometric form of a vehicle does not end at the identification of the optimal baseline geometry. This baseline must be sized and synthesized. This iterative sizing and synthesis process involves the scaling of the vehicle. New vehicle concepts do not necessarily exhibit the same scaling behaviors as known concepts. The effective identification of an optimal form of the vehicle necessitates that the best attainable scaling laws be used in the sizing process. This leads to the question:

2. ***How can the evolution of vehicle geometry with requirement changes be captured in conceptual design?***

In identifying the new form of a vehicle, the designer will often have to decide whether to go wider, longer or to simply to scale up the entire system. Good answers to these questions can only result from synergistic information exchange between all key disciplines. Here, volumetrics plays a key role in mediating the proverbial battle between the aerodynamicist's "pencil" vehicle and the structural analyst's I-beam body. This mediation can be quantified in the form of scaling laws. These scaling laws must be based on as compact a set of vehicle parameters as possible. This leads to the question:

(a) *How the dominant drivers of system level geometric change be identified? Do these vary from concept to concept?*

The quality of the scaling laws derived is contingent upon the identification of key parameter sets that exhibit high correlation with or influence on the aircraft

geometry under consideration. If it is determined that the key parameters do not vary from concept to concept, the designer can save time in latter design process by harvesting and reusing this knowledge.

(b) *At what threshold does photographic scaling become less viable than "smart scaling" based on scaling laws?*

The disparate scaling behavior of aircraft subsystems implies that it is almost impossible to derive a universally applicable scaling law for most vehicle concepts. Recall that smart scaling as used here refers to the systematic variation of individual component sizes and dimensions in response to requirement changes or constraint violation while concurrently allowing the containing body to respond geometrically. Since smart scaling will require more effort on the designer's part, it is worth investigating if there is indeed a general threshold of vehicle scale factor less than which photographic scaling consistently yields acceptable results. In sum this research question is aimed at identifying the gaps that need to be plugged in order to make the contemporary design process more geometrically accommodating to revolutionary concepts. To address these questions, a number of hypotheses have been formulated. These hypotheses are spelled out below.

Chapter V

HYPOTHESES

Preliminary research on contemporary methods of dealing with both uncertainty and scaling issues in decision making has yielded the following hypotheses:

Hypothesis I: *Defining Custom Baseline Configuration Space*

The custom baseline configuration space for a given technology can be defined by implementing a bottom-up approach to vehicle geometry definition.

This approach entails:

1. the exploration of various layouts of subsystem geometric models in 3D space

2. the definition of the basic shape of the vehicle geometry based on the layouts

3. the identification and selection of the candidate baselines based on a defined set of metrics

Hypothesis I.I: *Subsystem Modeling Technique*

Reduced complexity convex component models with a fast simplex-based collision detection algorithm to enable the rapid exploration of a large configuration space.

Hypothesis I.II: *Mapping Component level data to system level Metrics*

Subsystem to system level mapping can be achieved by :

1. Evaluating the minimum enclosing envelope in the form of a convex hull of the subsystems i.e. a "super-hull" for each layout.

2. Sectional slicing of the super-hull by exploiting triangular facets and interior angle

sum constraint

3. Using the sectional data to define the external geometry

Hypothesis I.III: *Configuration Space Exploration*

A domain spanning algorithm acting on the location and orientation variables of the subsystems with respect to a fixed axis can be used to explore the design space.

Hypothesis I.IV: *Incorporation of Real-world effects*

Density : Rule of thumb Regression of historical trends in vehicle packing efficiency and inertial density coupled with adjustments for technology impacts can be used to check candidate geometries for historical reasonableness.

Connectivity : Proximity Preferences Between Subsystems A connectivity metric that is a weighted sum of a designer-defined weighting factor and the actual distance between subsystem-pairs may be used to drive subsystems towards desired proximity.

Aesthetics : Symmetry A symmetry metric defined by the mean Balinsky [17] distance of the super- hull half-sections in the plane perpendicular to the flow direction may be used to quantify symmetry.

Hypothesis I.V: *Handling geometric uncertainty*

Geometric uncertainty can be incorporated into the search for an optimal geometry by first quantifying the expected uncertainty costs of a volume

surplus or deficit either in the design cycle or even in the system life-cycle and then choosing the geometry that minimizes total expected cost of

not meeting requirements.

This cost can be quantified either in the form of redesign costs or changes in vehicle

life-cycle costs. A surplus or deficiency in the volume available in a final concept can result increased design and/or life cycle costs. These costs can come in the form of increased design cycle time as design assumptions are re-examined and many analyses are repeated. If the sunk cost is already too great, the selected concept may pass on to prototyping and final design testing. The costs resulting from this decision recur all through the life-cycle of the system. The cost of flying an oversize aircraft will manifest itself in higher operating costs such as fuel and maintenance. Likewise a vehicle that is too small for its intended mission may have to perform multiple sorties to achieve the mission requirements for which it was intended. Thus the designer must do all he can to ensure that by the time the sunk cost is so high that the process' absorptive capacity for design information is really limited all expected uncertainty costs have been minimized.

Hypothesis II: *Capturing Requirement-change Induced Geometric Scaling Laws*

Configuration scaling laws can be used to capture the geometric evolution of a given concept. These laws can be derived through a combination of dimensional analysis and statistical regression techniques. Custom data for the statistical regressions can be obtained via an automated bottom-up parameter space exploration approach.

Hypothesis II.I: *Identification of Dominant Parameters*

The dominant variables will form the dependent variable portion of the dimensionally consistent scaling law that minimizes the predictive error of the scaling law.

Hypothesis II.II: *Threshold for photographic scaling*

This threshold depends on: The scaling behavior of major subsystems: The closer this behavior is to the photographic, the higher the threshold.

The converse applies as well. The impact of individual requirement changes on major

subsystems The "<5%" rule does not hold across different vehicle configurations.

Chapter VI

RESEARCH PLAN

6.1 Towards Proving Hypothesis I: Devise a fast methodology for component location/relocation and collision detection

1. Identify the best combination of geometry representation technique and collision detection algorithm for the unique needs of the conceptual design process.

2. Identify/Devise a methodology to evaluate the minimum enclosing envelope for these components once a layout is defined.

3. Implement a sample test case based on the notional PEM fuel cell. This step tests the preliminary collision detection performance of the chosen algorithm and its behavior as the complexity (number of surface points) of the subsystems increases.

4. Implement an automated component placement procedure in 3D space.
   i. Choose technique with which to define component location
   ii. Devise method to compose transformation matrix from layout settings

5. Attempt to use historical data through dimensional analysis with regression to determine "transcendent" metrics or properties. Transcendent metrics as used here refers to metrics that exhibit remarkable consistency in behavior across technologies, time and manufacturers. Such metrics if identified can be used to evaluate the practical soundness of a design without necessary compromising the fact that the concept is revolutionary.

6. Identify the volumetric, gravimetric and aerodynamic metrics that can be used to select between various component layouts.

7. Couple the above metrics with the transcendent metrics (if any) to come up with a generalized overall evaluation criterion for layouts in 3D space.

8. Investigate the existence of a plausible yet reasonably inexpensive treatment for uncertainty in component sizes.

9. Investigate how to best propagate dimensional constraints from the minimum enclosing envelope to the external geometry in order to aid baseline geometry selection.

6.2 Towards Proving Hypothesis II: Derive Scaling Laws for Chosen Concept

1. Implement automated scaling law derivation methodology that takes in statistical data and dimensional information and outputs scaling laws.

2. Create integrated modeling and simulation environment.

3. Generate necessary statistical data through a design space exploration approach.

4. Derive analytical expressions or scaling laws for the behavior of the system i.e. PEM fuel cell powered GA vehicle in response to changes in requirements or failure of concept to meet original requirements.

5. Validate these laws by comparing the actual data of the scaled vehicle dimensions to predictions from scaling laws.

6. Draw conclusions and make recommendations for future work.

Chapter VII

METHOD FORMULATION

7.1 Overview of Methodology

In line with the original goal of letting the technology drive the nature of the vehicle, a new methodology is being developed, which while enforcing volumetric feasibility at any design point, will also allow selective scaling of components resulting from feedback from other contributing analyses. This methodology will from here on out be referred to by the acronym CESM for Configuration space Exploration and Scaling Methodology.

7.1.1 Key Assumptions

7.1.1.1 System modularity

It is assumed that the number of vehicle subsystems is sufficiently large and that there is sufficient design freedom in the relative location of the subsystems. The combination of modularity and a high degree of location freedom often results in a problem of such high complexity that identifying the "best" solution is a non-trivial problem.

7.1.1.2 Knowledge of Aircraft Subsystems

It is also assumed that there is sufficient geometric knowledge of major aircraft subsystems. This knowledge includes basic shape, basic size with some quantifiable uncertainty and subsystem scaling behavior in response to changes in requirements.

7.2 Definitions

7.2.1 Convexity

In lay terms, a body can be said to be convex if it consists of surfaces that either bulge outwards or remain neutral. Furthermore a line drawn through such a body can only cross its boundary two times or less. This is further illustrated in Figure 38 below.

More rigorously and generally, a set in Euclidean space R^d is convex if and only if it

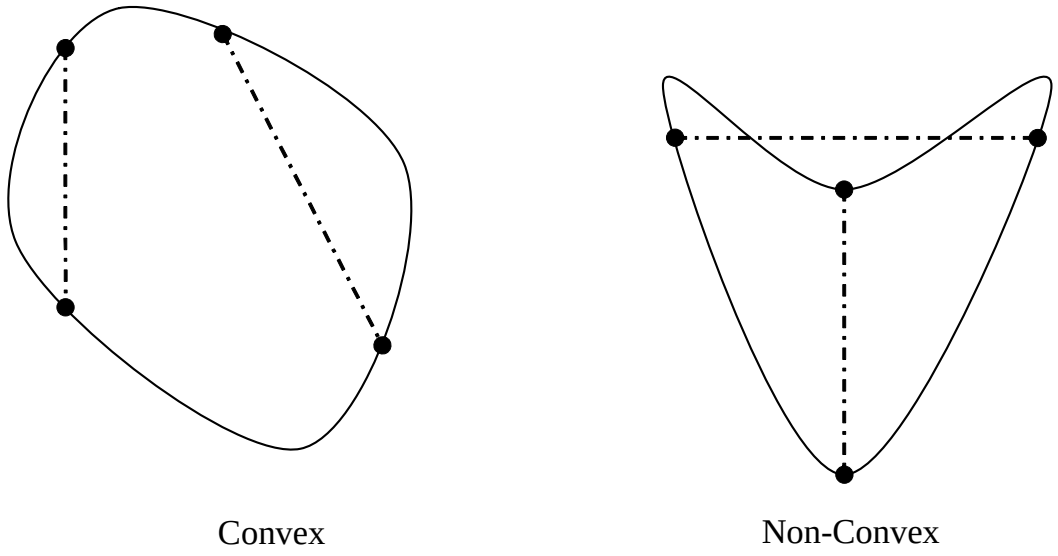

Figure 38: Illustration of Convexity

contains all the line segments connecting all its points.

Thus: A set S is convex iff for $I, J \epsilon S : \alpha I + (1-\alpha) J \, \epsilon \, S$ as well [57]. The convex hull of S in a given dimension is the intersection of all convex sets containing S. Thus the convex hull C of S is given by:

$$C = \left\{ \sum_{i=1}^{n} \alpha_i P_i \right\} \tag{26}$$

where:

$\alpha_i \geq 0 \, , \sum_{i=1}^{n} \alpha_i = 1$

P_i *is a convex set in* S

7.2.2 Voronoi regions

Officially postulated, formalized and generalized by Georgy Voronoi in 1908, the Voronoi diagram is a special decomposition of any metric space (any space where the notion of distance is defined) based on the distances to a specified discrete set of objects in the space

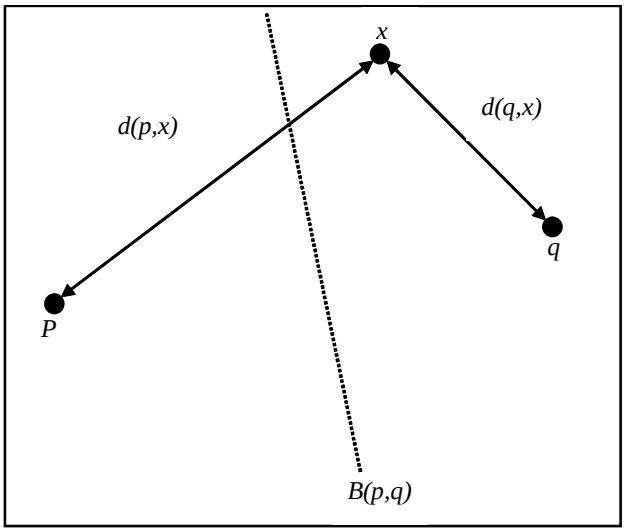

Figure 39: Illustration of fundamentals in 2D

[50]. Applications predating 1908 include John Snow's study of the correlation between the effect of the cholera epidemic on a neighborhood and its proximity to an infected pump. Today, Voronoi applications range from video games [177] to geophysics [168] and even to condensed matter physics [144]. Mathematical Definition of Voronoi regions

Let S be a space of dimension $n \geq 3$ and let points $p, q, r \ldots$ belong to space S.

For points $x = (x_1, x_2)$ and $p = (p_1, p_2)$ let

$$d = \sqrt{(x_1 - p_1)^2 + (x_2 - p_2)^2} \tag{27}$$

be their Euclidean distance apart.

For $p, q \epsilon S$ let

$$B(p, q) = \{x | d(p, x) = d(q, x)\} \tag{28}$$

be the perpendicular bisector of the line segment $\overline{pq}$. (See Figure 39) Being the bisector, it separates the halfplane containing p such that $D(p, q) = \{x | d(p, x) < d(q, x)\}$ from the halfplane containing q.

Extending this to multiple points (and dimensions) the Voronoi region of p with respect to S is defined as the intersection of the $n - 1$ halfplanes containing the site p.

$$VR(p,s) = \bigcap_{q \epsilon S\,,\, p \neq q} D(p,q) \tag{29}$$

The Voronoi region of S is thus defined as the intersection of the Voronoi regions of p and q. It is denoted as

$$VR(p,s) = \bigcup_{p,q \epsilon S,\, p \neq q} \overline{VR(p,S)} \bigcap \overline{VR(q,S)} \tag{30}$$

Figure 40 below shows a sample Voronoi diagram.

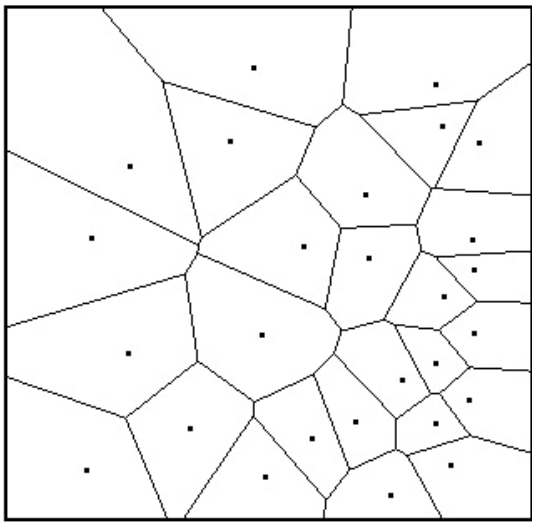

Figure 40: Sample Voronoi Diagram

7.2.2.1 Polyhedron

The term polyhedron as used herein will refer to any geometric object with flat faces and straight edges.

7.2.3 Computational Complexity key terms

1. Polynomial Time

   This refers to the computation time of a problem of dimension n, where the run time is less or equal to the polynomial function of order n. [90]

2. NP

NP or Non-deterministic Polynomial time problems refers to the set of decision problems solvable in polynomial time in a non-deterministic environment i.e. an environment where there are multiple end-state possibilities for any given input. [90]

3. NP-Complete

   A problem is said to be np-complete if every other problem in NP is reducible to it. This subset of computational problems is widely believed to be unsolvable in polynomial time due to the degree of complexity. [90]

7.2.3.1 Minkowski Difference

The Minkowski difference of two convex objects is the object that results when one object is "grown" by the shape of the other. In mathematical terms the Minkowski difference is the vector space created by subtracting each point on convex object A, from its most opposite point on convex object B. This abstraction is perhaps best illustrated with the help of two circles where circle C is the Minkowski difference $A - B$. See Figure 41. The set of vector differences between the two objects is referred to as the configuration space.

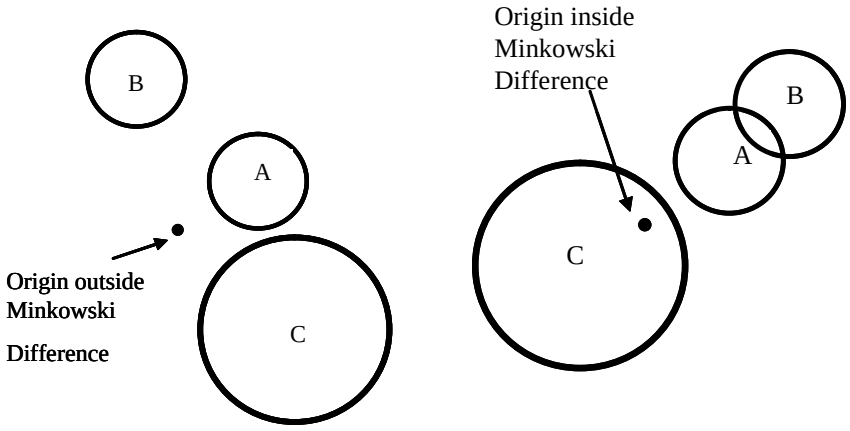

(a) No Collision (b) Collision Case

Figure 41: Scenarios for two Convex Polytopes in Space

The key take away here is that the origin of the configuration space will always lie inside the Minkowski difference if the two objects collide or overlap. The inverse of this statement is also true i.e. if the origin of the configuration space lies outside the Minkowski polygon,

then the two objects do not intersect. An even more useful fallout from this fact is that the separation between the Minkowski difference and the origin also equals the separation or overlap between the two objects.

7.2.4 The importance of Convexity and Voronoi regions

One of the key showstoppers to any attempts at bringing any inertial information forward in the design process is the time and computational expense described earlier. The urgent need for a methodology that brings information of optimal reliability forward in the design process at minimal expense has been shown to be self evident in the design of revolutionary concepts. Bringing inertial/volumetric information forward in the design process entails performing collision detection tests among the various objects in the space. Collision detection problems typically fall in the complexity range of NP-complete problems. Inherent in this property is the fact that time expense rises rapidly as the number of components and their complexity increases. Per the conceptual design analytical paradigm discussed earlier, accuracy is traded-off for some gains in computational speed in order to efficiently explore the conceptual design space. Thus a conceptual design methodology that fits this paradigm must circumvent the $O(n^2)$ problem via a faster and acceptably accurate method. Voronoi regions of a space in which aircraft components lay can be used to identify and track the closest features of any pair of components. These diagrams can be generated rapidly for convex objects. The analyses in Figure 47, Figure 48 and Figure 49 gave rise to a seventh observation:

VII. Many major aircraft components as well as axial cross-sections are either convex in shape or can be efficiently approximated as convex objects.

This observation is illustrated in Figure 42 and Figure 43 below. The evolution of the F-18 family in the quest to enhance range as seen in [6, 5] will later be used as a case study for the scaling methodology.

Furthermore, objects that do not show any intersection of Voronoi regions need not be tested for collision. These two preprocesses put together can yield significant improvements in the computational time required per case.

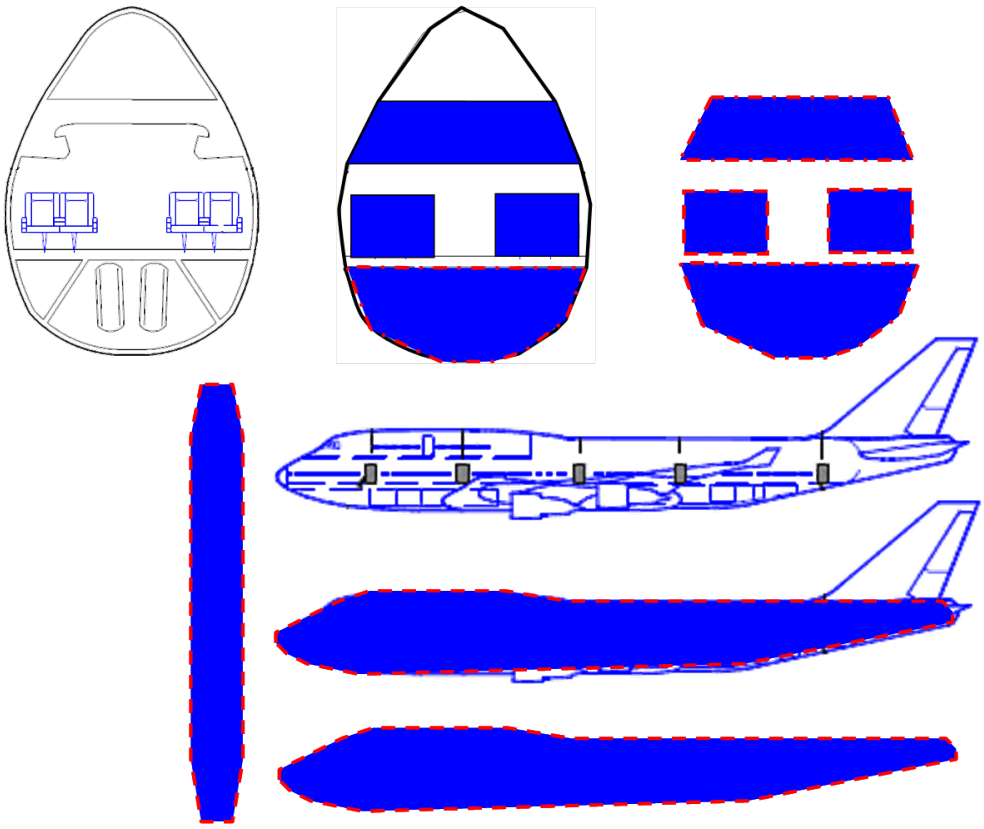

Figure 42: Boeing 747 Cross-sectional profiles 42

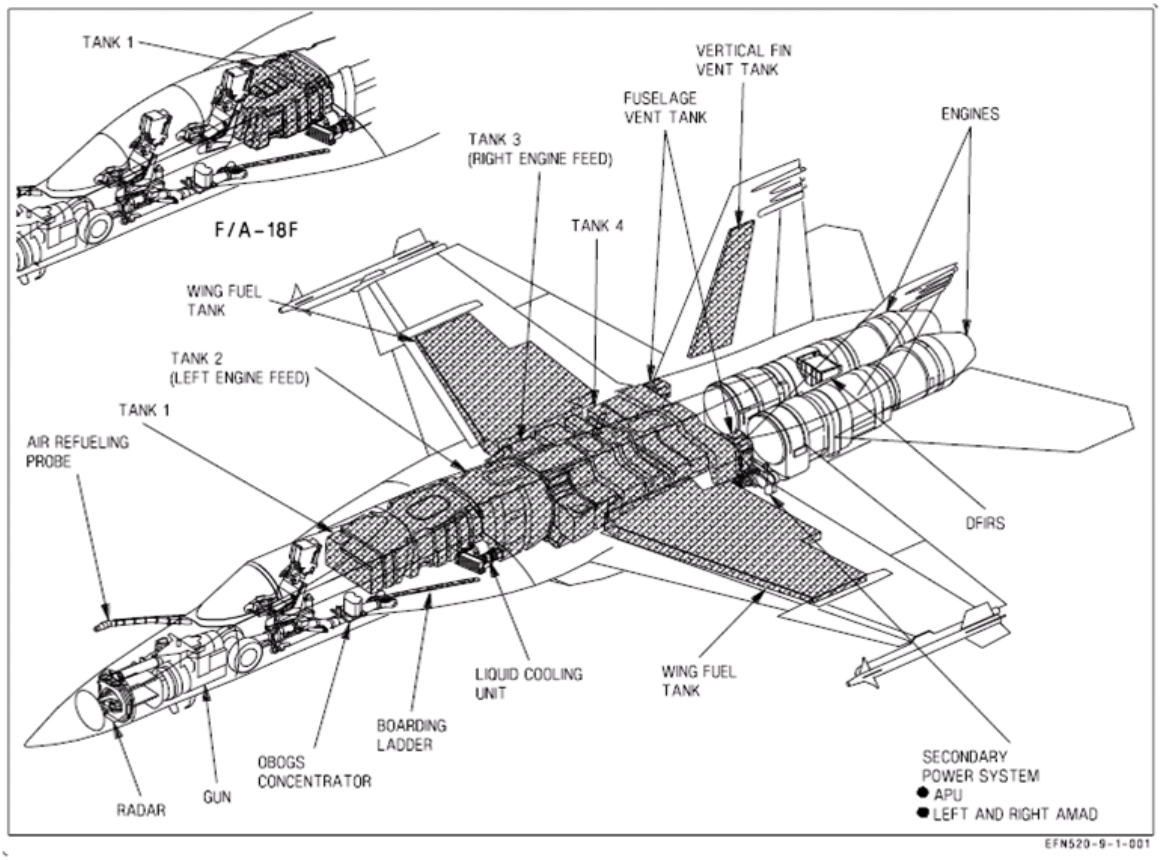

Figure 43: F-18 Subsystems [5]

Convex hulls have been widely studied and a number of good options for easily "codeable" algorithms exist in literature. Perhaps the fastest and most popular algorithm for problems of this nature is the University of Illinois at Urbana-Champaign's Qhull [2]. Also, the since most fuselages are designed to approach the convex minimum wave drag ogive described by Haack [84], convex envelopes provide a good first order approximation or inner mold line for a fuselage design. The feasibility of a layout is contingent upon the fact that the components do not collide. In an environment where layout formulation is automated, collision detection algorithms play a key role in ascertaining feasibility.

7.2.5 Convex Hull Algorithms

A brief description of some of the key algorithms used in the computation of convex hulls follows.

7.2.5.1 Gift-wrapping algorithm

Also called the Jarvis march after R. A Jarvis, the gift wrapping algorithm [101] is so-named because its core procedure is similar to the procedure of wrapping a gift. The algorithm is initialized at an extreme point P_0. If P_0 were say the leftmost point, then P_1 would be chosen so that all other points P_i were to the right of the line segment connecting P_0 and P_1. This is achieved by comparing the polar angles of all other points as measured at P_0. This is an $O(n)$ time process where n is the number of vertices in the set. The point with the smallest angle is added to the convex hull and the process is repeated at the new point until $P_i = P_0$.

7.2.5.2 Graham Scan

Published by Ronald Graham in 1972 [82], this $O(n \log n)$ algorithm operates on a set of points sorted by one of the co-ordinate axes. Starting with the first two points, the algorithm determines whether moving to the next point, constitutes a right or left turn. The direction of the turn is determined by computing the tangent of the angle that the vector to the point from the origin make with respect to the reference axis. A right turn implies that the previous point is not in the convex hull of the set. A left turn causes the algorithm to

proceed to the next point. This procedure is repeated until the algorithm returns the first point in the convex set.

7.2.5.3 Divide and Conquer

The divide and conquer algorithm [106] decomposes the original point set into smaller subsets whose convex hulls can be rapidly evaluated. The solutions to these subsets are then recomposed into a "next level" problem that is simpler to solve in comparison to the original problem. This process is successively repeated until the convex hull of the entire set is determined.

7.2.5.4 Quickhull Algorithm

The Quickhull algorithm [2] is one of the most popular algorithms in the geometry community today because of its efficiency and robustness. The algorithm works by recursively partitioning a set-space into several groups. At each step line segments are drawn from a feature known to be on the convex hull to the furthest point in the set-space. All points enclosed by the resulting triangle are automatically excluded from consideration for subsequent convex hull candidacy analysis. This process is repeated until all points are either contained in the convex hull set or the excluded set. The algorithm is expected to require $O(n \log r)$ time where r is the number of vertices on the convex hull.

7.2.6 Collision Detection Algorithms

It is a fundamental physical law that disjoint physical objects can not occupy the same physical space. This law makes it imperative that collision be investigated every time one attempts to automatically place more than one component in a defined space. There is a bevy of collision detection algorithms in the public domain ; each with its particular strengths and weaknesses. These algorithms can be classified into two major categories i.e. feature-based and simplex-based.

7.2.6.1 Feature-based Collision Detection Algorithms

Polyhedra are defined by the features that define their boundaries. These features can be faces, edges, vertices or some combination thereof. Feature-based collision detection exploits

the inherent mathematical properties of lines and planes to determine if a pair of objects does not intersect. The Lin-Canny algorithm [117] is perhaps the fastest published feature-based algorithm that calculates the distance between the closest features of any two disjoint polyhedra.

7.2.6.2 Simplex-based Collision Detection Algorithms

Instead of operating directly on polyhedra and their features, these algorithms operate on "reduced" representations called simplices. These simplices (usually planes) are formed from subsets of points that constitute the convex hulls of the polyhedra. Most of the algorithms available in the public domain today are descendants of the Gilbert-Johnson-Keerthi algorithm (GJK) [79]. The elegance of the algorithm lies in the fact that it exploits the properties of the Minkowski Difference of two convex polyhedra to calculate their separation distance without explicitly calculating the Minkowski difference itself. The GJK procedure intelligently queries the simplices of this polyhedron until it establishes whether or not the origin of the configuration space lies inside the polyhedron. As discussed earlier, the separation or overlap distance of the two polyhedra is calculated in this manner. Some of the more popular GJK descendants include the Rabbitz Algorithm [157] and Stephen Cameron's "Enhanced GJK" [40]. The key need is for a collision detection algorithm that can output the minimum separation distance between two convex polyhedra. In the case where there is collision, knowledge of the maximum penetration distance or minimum translational distance to uncollide the two objects is useful but not critical. Buckley [37] showed that this problem is inherently complex. Buckley [37] and Cameron et al [41, 40] suggested estimates for the penetration distance as :

$$D_p \leq -min\,\{|z| \,:\, z\,\epsilon\, Minkowski\, Difference\, of\, Polyhedra\} \tag{31}$$

$where$:

$D_p = Penetration\ Distance$

Based on the criteria outlined above, the GJK algorithm was selected as the best candidate for the proof of concept implementation of the CESM methodology.

7.2.6.3 The Gilbert-Johnson-Keerthi Algorithm

Named after its postulators : Elmer *G*ilbert, Daniel *J*ohnson and Saathiya *K*eerthi, this algorithm can efficiently calculate the Euclidean distance between convex polyhedra. A few key equations are outlined below. A FORTRAN implementation of the algorithm can be found in §Appendix A.

A synopsis of the algorithm follows.

The algorithm basically iterates through the logic described in the pseudo-code [40, 79, 118] below until a termination criterion is satisfied.

$$X_0 = initial\ point\ set$$

$$k = 0\ counter$$

$$Do\ \{$$

$$V_k = affinely\ independent\ subset\ of\ X_0$$

$$Compute\ v\ as\ in\ Equation\ 35$$

$$Compute\ S_k\ and\ H_k\ as\ in\ Equation\ 34$$

$$V_{k+1} = V_k \bigcup S_k$$

$$k = k + 1$$

$$\}\ until\ (v_k \cdot v_k + H_k) = 0$$

The GJK algorithm essentially searches point-pairs one from each body, to establish which pair has the minimum distance apart. The distance is defined as the Euclidean distance:

$$d_{A,B} = min\,|a - b|,\ a\,\epsilon\,A\,, b\,\epsilon\,B \tag{37}$$

It is clear that the closest points on A and B will also satisfy the condition $min(\varphi)$ as defined in Equation 32. However, if object A contains m points and object B contains n points then the pair selection problem becomes an $O(mn)$ problem. The algorithm circumvents this "problem" by sequentially constructing simplices whose vertices are points on the

Term	Description
$\psi = X_1 \pm X_2 = \{x_1 \pm x_2 : x_1 \epsilon X_1, x_2 \epsilon X_2\}$ (32)	$Minkowski\ Difference\ in\ m-dimensional\ Space$
$co\ X = \left\{ \sum_{i=1}^{l} \lambda_i x_i \ : x_i \epsilon X,\ \lambda_i \geq 0,\ \sum_{i=1}^{l} \lambda_i = 1 \right\}$ (33)	$Convex\ Hull\ of\ X$
$h_x(\eta) = max\{x \cdot \eta \ :\ x \epsilon X\}$ (34)	$Support\ Function$
S_x	$Any\ Solution\ to\ Equation\ 34$
$\upsilon(X) \epsilon X\ \lvert\upsilon(X)\rvert = \{min\lvert X\rvert :\ x \epsilon X\}$ (35)	$Nearest\ Point\ in\ X\ to\ the\ Origin$
$V_k = \{y_1, \cdots, y_\upsilon\},\ 1 \leq \upsilon \leq m+1$	$A\ subset\ of\ Minkowski\ set\ K$
$g_k(x) = \lvert x \rvert^2 + h_k(-x)$ (36)	$if\ x \epsilon K\ then$ 1. $g_k(x) < 0 \Rightarrow \exists z \epsilon Co\{x, S_k(-x)\}\ \lvert\ \lvert z\rvert < \lvert x\rvert$ 2. $x = \upsilon(K)\ \ iff\ \ g_k(x) = 0$ 3. $\lvert x - \upsilon(K)\rvert^2 \leq g_k(x)$

Table 7: Main Equations in the GJK Algorithm [40, 79, 118]

Minkowski difference [58]. On initialization, the initial is set to empty as no points on the Minkowski difference have been chosen. A point x_0 on the Minkowski difference is then arbitrarily selected as seen in Figure 44. The auxiliary point η_0 is then calculated using the support function defined by Equation 34. Since the Minkowski difference is not explicitly calculated, the support function is evaluated as the difference between the supporting functions of A and B relative to the selected point. At the next iteration, $x_1 = \eta_0$ as shown in Figure 44 *(b)*. This process goes on until a termination condition that characterizes the event shown in Figure 44 *(c)* is satisfied.

A commonly used termination criterion [58] is :

$$|x_i| - L_b \leq \mu \tag{38}$$

$$\begin{aligned} &where: \\ &L_b = max\left\{0, \overline{d}_i\right\} \\ &\overline{d}_i = x_i \cdot \eta_i \end{aligned}$$

Alternative termination criteria were suggested by Cameron [40]. Van den Bergen [195] later showed that even these were not as universally robust as earlier thought. For purposes of this work, the original the original termination criteria will be used.

7.2.7 Component Complexity

For the purpose of this work, the working definition for component complexity will be the minimum number of surface points required to represent the component to achieve of a volume approximation error of less than 5% of actual component volume.

7.3 CESM Formulation

Before CESM is outlined, some key terms must be explained. Based on the qualitative assessment of geometry representation techniques summarized in Figure 32 and collision detection algorithm speed considerations, it was decided that a discretized geometry representation technique would be ideal for this methodology. The need was for a portable

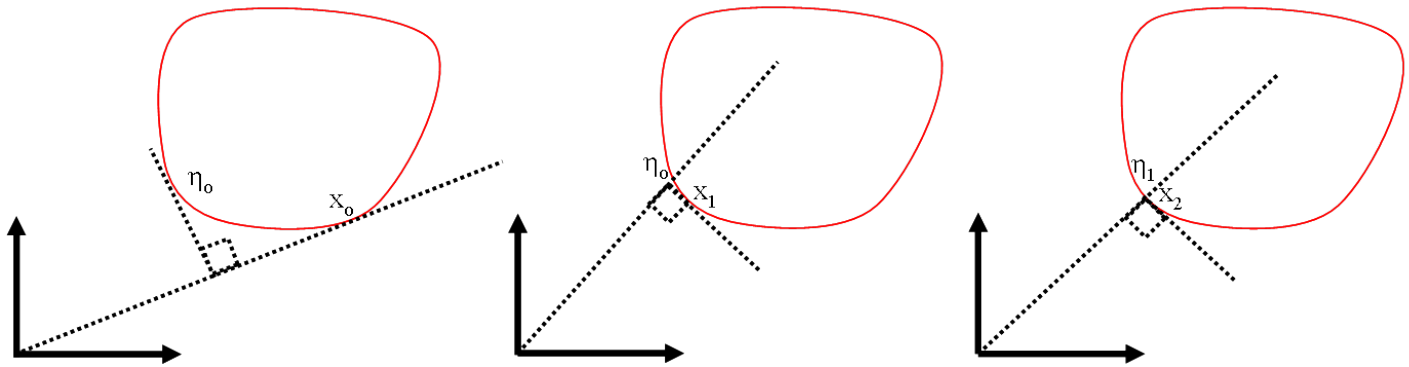

Figure 44: Illustration of GJK Algorithm

representation of the component geometries that allowed for easy scaling and fast collision detection. Discrete representation best satisfies these requirements. Convex approximation is used to approximate the interrelationships between these points for purposes of collision detection. The key blocks that make up the methodology are discussed below.

7.3.1 Key Process Blocks of Methodology

CESM is based on mathematical abstractions of complex geometries and is summarized in the six steps below.

1. Model major vehicle components e.g. engines, passenger boxes

   The test case for this methodology is built in VSP (R). This tool was chosen because of the built-in capability to represent a wide variety of shapes using a very limited number of geometric primitives. Furthermore as shown in Figure 10 , the interface variables are directly relevant aerodynamic parameters. The geometry files are also stored in XML format, which renders them ease to manipulate in an automated manner.

2. Reduce component models to matrices of shape-critical points

   Reduction of components to critical points reduces the computation expense per pair of components. The best known collision detection algorithms exhibit linear behavior for run time as a function of the number of vertices that describe each component. The less points used to represent the components the faster the collision detection procedure but care must be taken to not overly simplify and thereby misrepresent the component geometry.

3. Create shape-aware convex hulls from the vectors

   To further accelerate the collision detection process, the objects are further reduced to points that lie on the border of the minimum enclosing convex object also called a convex hull. The convex hull is the component abstraction of choice because it lends itself well to fast collision detection as discussed earlier. But, as previously explained, not all aircraft components come in convex shapes. In the few cases where a singular convex representation proves inadequate in representing the body, a decomposition

procedure is suggested. The body can be represented as a union of convex objects that represents the various pieces into which it was decomposed. Figure 45 illustrates a "convex model" of a non-convex object. This model is derived by first decomposing the convergent-divergent object into three convex objects. Convex hulls are then generated for each of the objects. The object model exists in mathematical space as the union of the three convex objects. This process can be fully and inexpensively automated and therefore poses no real challenge to the methodology as a whole.

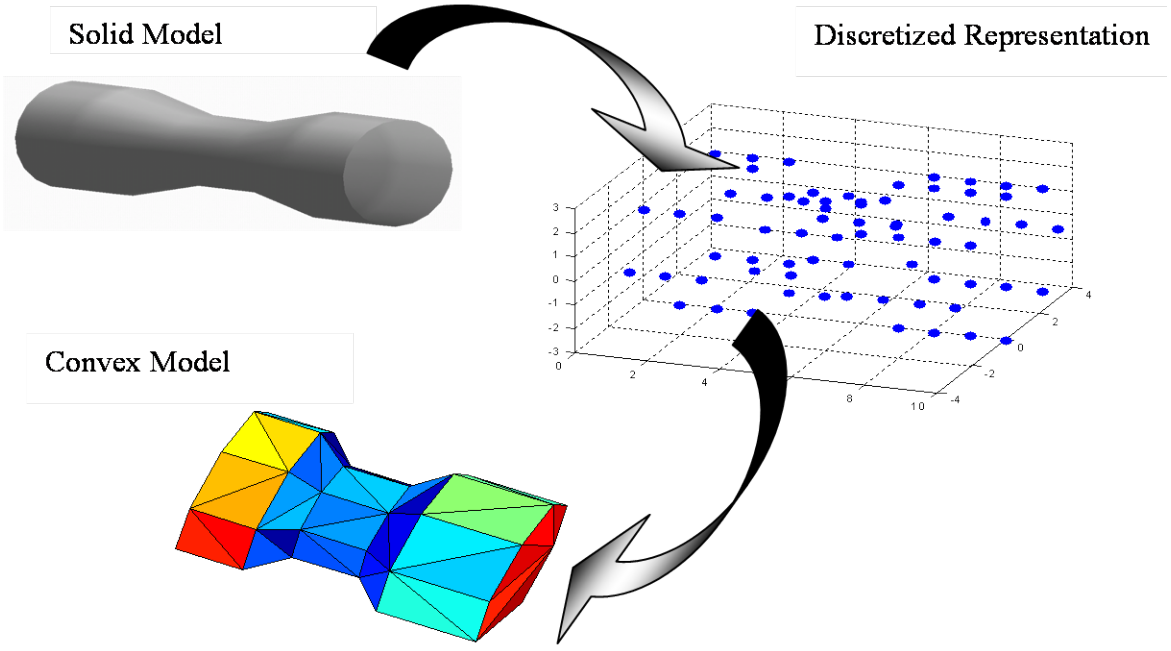

Figure 45: Geometry Abstraction Process

4. Combine fast layout and collision detection algorithms to establish minimum volume superhull

   The points on the convex hull of the component are represented as vectors from the component's centroid. Creating a layout is hence reduced to the application of a transformation matrix which is the sum a translation and a rotation. The process may be sped up further by culling the number of component pairs on which collision detection must be performed. This may be done through either Voronoi tracking or

projective geometry to determine which component pairs are within line of sight from each other and hence warrant collision querying. Once this is achieved, the last major challenge will be the linking of the super-hull metrics to geometry metrics.

5. Create a component-aware superhull i.e. hull of component hulls for feasible layouts

   The superhull is the convex hull of the convex hulls of the aircraft components. Its shape is dependent on the layout of the components. Based on the component layouts, the super-hull forms the minimum enclosing enveloped for the components. This property works well for the goals of the identifying the minimum size vehicle that can carry the specified components.

6. Select best layouts

   Design requirements and their relative importance vary from concept to concept depending on the aircraft mission. The considerations for selecting the best layouts can be broadly grouped into three categories i.e. aerodynamic, volumetric and gravimetric. Aerodynamic considerations take into account the impact of the dimensions of the minimum enclosing envelope on the external shape of the aircraft. The parameters of interest here include the ratio of the length to the maximum diameter of the body also called the slenderness ratio and the cross-sectional area distribution.

   The gravimetric considerations include the effective density of the containing body and stability considerations such as contribution to the center of gravity location and the moments of inertia. The optimal density usually balances out the two conflicting attributes of cost and maintainability. The volumetric considerations include packing efficiency and residual volume. The packing efficiency is the ratio of total component volume to the total volume of the containing body i.e:

$$\eta_p = \frac{Total\,Component\,Occupancy\,Volume}{Total\,Hull\,Volume} \tag{39}$$

   This is a non-dimensional measure of the amount of dead volume in a given configuration and can thus be used as selection criterion. Since only the major aircraft components are considered, some volume has to be set aside for minor components

such as wiring and small avionics boxes. This volume is sometimes referred to as residual volume [161]. The percentage of total aircraft volume taken up by the residual component volume varies from aircraft to aircraft as seen in Figure 46 below. Torenbeek [190] states that, "The analytical approach used in ref 3-3[1] indicates that it is not so much the fuselage drag but more particularly the weight which is the deciding factor where the optimum shape is concerned." Even though the study alluded to here, pertained to a low Reynolds number subsonic vehicle, it is implicit in the study's conclusions that the relative importance of key disciplines such as aerodynamics may vary with vehicle class or target mission.

Identifying the ideal objective function for the selection of the optimal layout (hence vehicle shape) entails finding and quantifying the right balance of importance between the three categories of considerations mentioned above. The final nature of such a function is likely to be concept-dependent since the relative importance of vehicle performance metrics varies with vehicle class. Additionally since the sizing and synthesis process is iterative, the preferred layout at the inception of the iteration may not necessarily be the best or most optimal layout at the point of convergence. The natural solution to this problem is to carry as many layouts as possible through the design process. However, this is inherently expensive because, as stated in observation II, there are potentially thousands of layouts. Thus the designer must make an initial down-selection in layouts based on the considerations described above. The selected layouts will be considered simultaneously through the iterative process, selecting the best candidate at each iterative update.

7. Constrain top-level geometry metrics with superhull metrics

   This step creates the information linkage between the contemporary design process and the volumetrics discipline. The set of design variables that need to be constrained depends on the nature of the geometry being analyzed. The methodology by which

[1] Ref 3-3 : A. A. Badiagin "Concerning an efficient slenderness ratio for the fuselage of civilian aircraft"

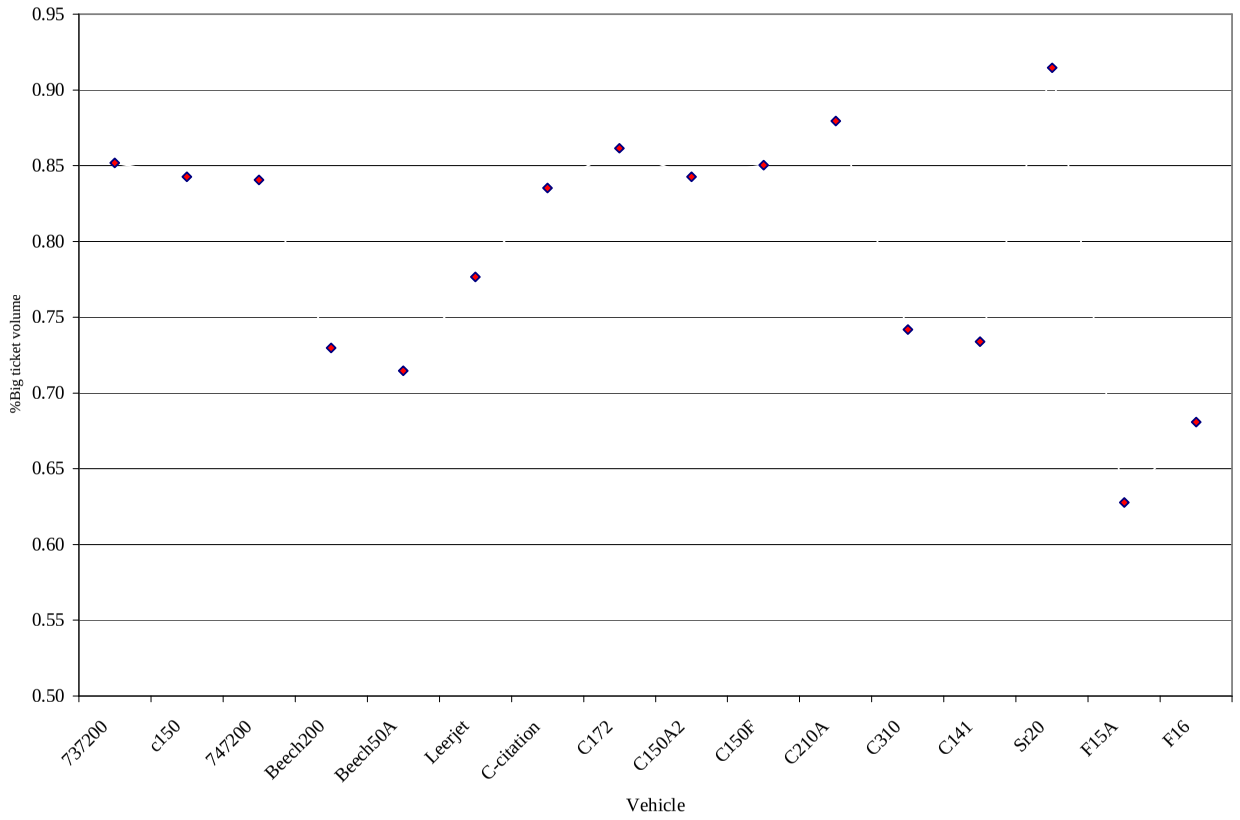

Figure 46: "Big Ticket" Volume as a percentage of total Volume for a select set of Aircraft [11, 12, 13, 96, 97, 98, 99]

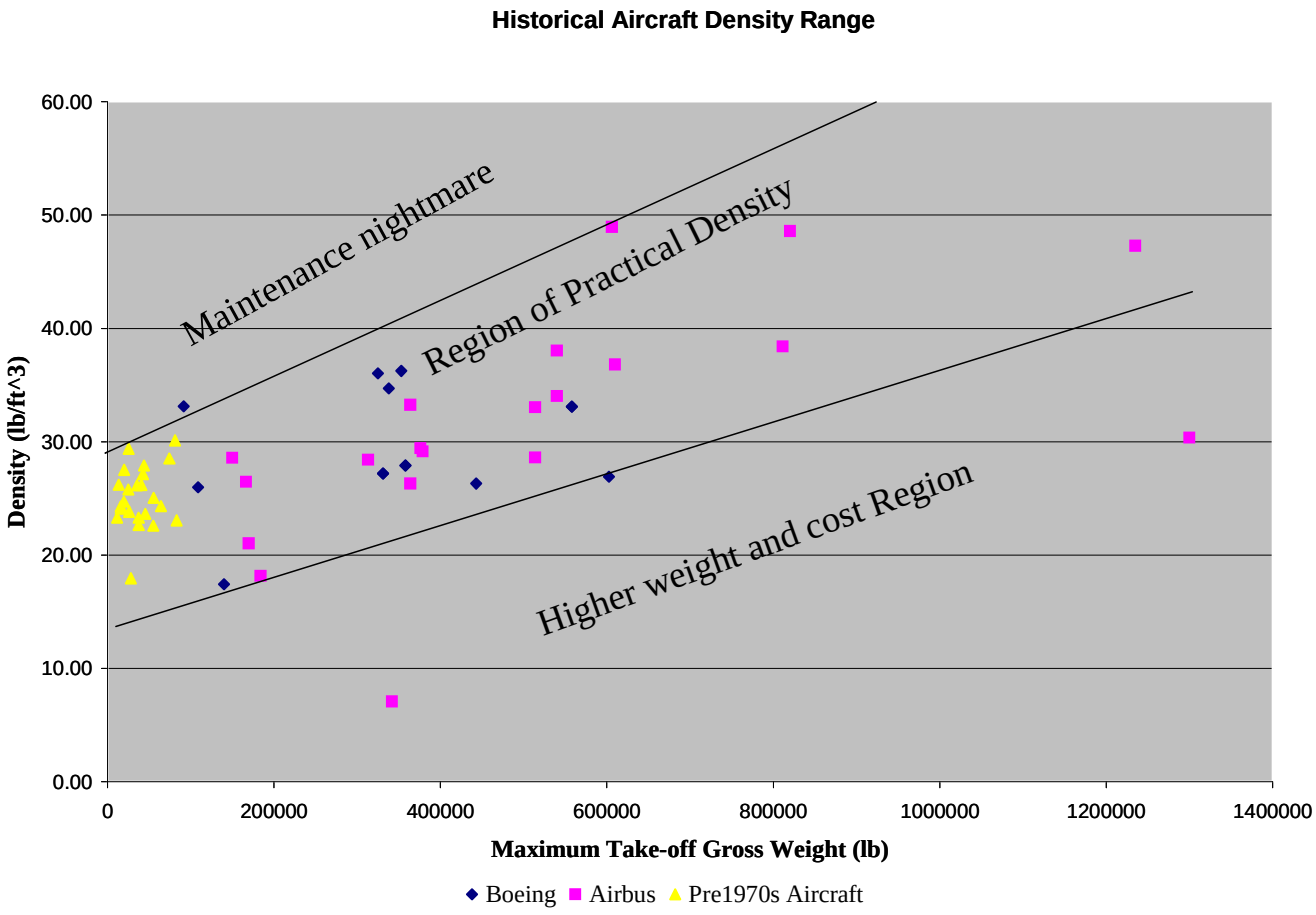

Figure 47: Aircraft Densities [11, 12, 13, 96, 97, 98, 99, 174]

scaling laws are derived can be used to easily identify these key parameters.

8. Integrate some real-world effects

   Vehicle density is a useful metric in checking the historical reasonableness of a vehicle design. However, the premise that new technologies impose significant volumetric and gravimetric changes to the vehicle implies that traditional bounds on vehicle density (seen in Figure 47 below) can not be used as is. A rule of thumb is therefore postulated. A design will warrant further investigation if the density of the proposed design lies significantly out of the expected density range specified by D_e as defined below. The range specified by this metric is deemed to be a good ball-park figure for the eventual density of the vehicle as it incorporates the effect of the technology while at the same time accommodating "real world" effects such as manufacturing practices and maintenance requirements.

Define*:*

D_i, D_e : *Density range for vehicles designed around incumbent and emergent technologies respectively*

V_i, V_e : *Volume range for vehicles designed around incumbent and emergent technologies respectively*

M :*Vehicle gross weight*

V_{Ti}, V_{Te} :*Volume requirement for incumbent and emergent technologies respectively*

m_{Ti}, m_{Te} :*Volume requirement for incumbent and emergent technologies respectively*

Then $D_i = [25, 40]\frac{lb}{ft^3}$ and $V_i = [\frac{M}{25}, \frac{M}{40}]ft^3$. Data for this range was collected from a number of sources namely: [11, 12, 13, 39, 97, 99, 96, 98, 174].

Thus $V_e = [\frac{M}{25} - V_{Ti} + V_{Te}, \frac{M}{40} - V_{Ti} + V_{Te}]$.

Therefore the expected density range for the new vehicle is:

$$D_e = [\frac{\frac{M}{25} - V_{Ti} + V_{Te}}{M - m_{Ti} + m_{Te}}, \frac{\frac{M}{40} - V_{Ti} + V_{Te}}{M - m_{Ti} + m_{Te}}] \tag{40}$$

Partial justification for this approach is shown in Figure 48 and Figure 49. It is observed that for the aircraft studied here, there is remarkable consistency in structural layout practices across time and gross weight regimes. Sensmeier [174] demonstrated similar consistency in fuselage frame-spacing as well. Since the aircraft structure typically constitutes a significant portion of its gross weight, there is some plausibility to assuming similar structural characteristics for new vehicle concepts as a way of capturing this "real world" effect.

9. Analyze scaling behavior of superhull

   Perturbations in system requirements such as maximum power induce changes in size of the affected subsystems. These size changes are then propagated to the super-hull geometry and eventually to the geometry constraints. This procedure is illustrated in Figure 50 .

This procedure can be done off-line and integrated into the design process as a series of scaling laws. For any given setting of say maximum power required, a corresponding value for the minimum size vehicle is passed on to system level design process.

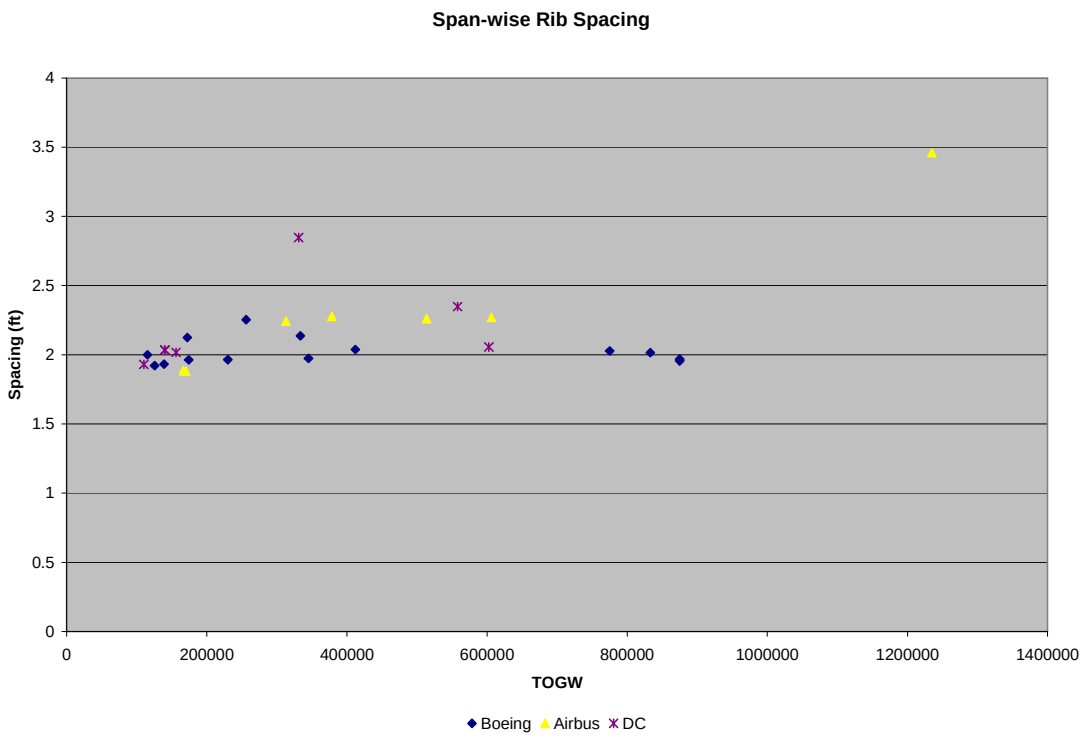

Figure 48: Span-wise Rib Spacing for various Aircraft [11, 12, 13, 96, 97, 98, 99, 174]

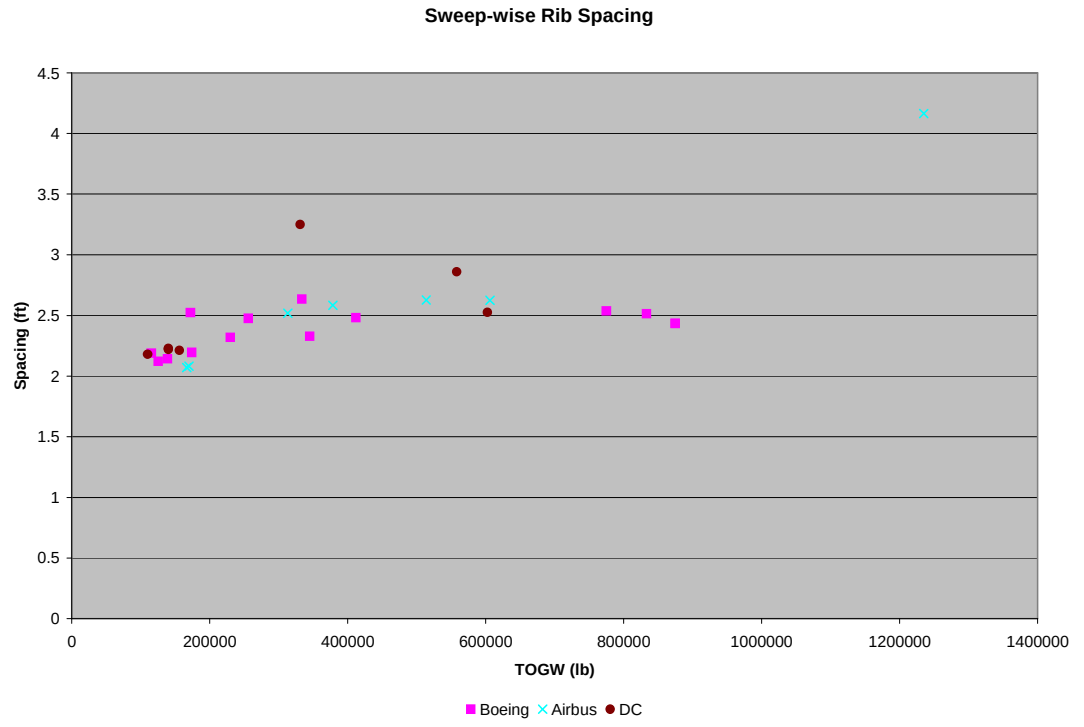

Figure 49: Sweep-wise Rib Spacing for various Aircraft [11, 12, 13, 96, 97, 98, 99, 174]

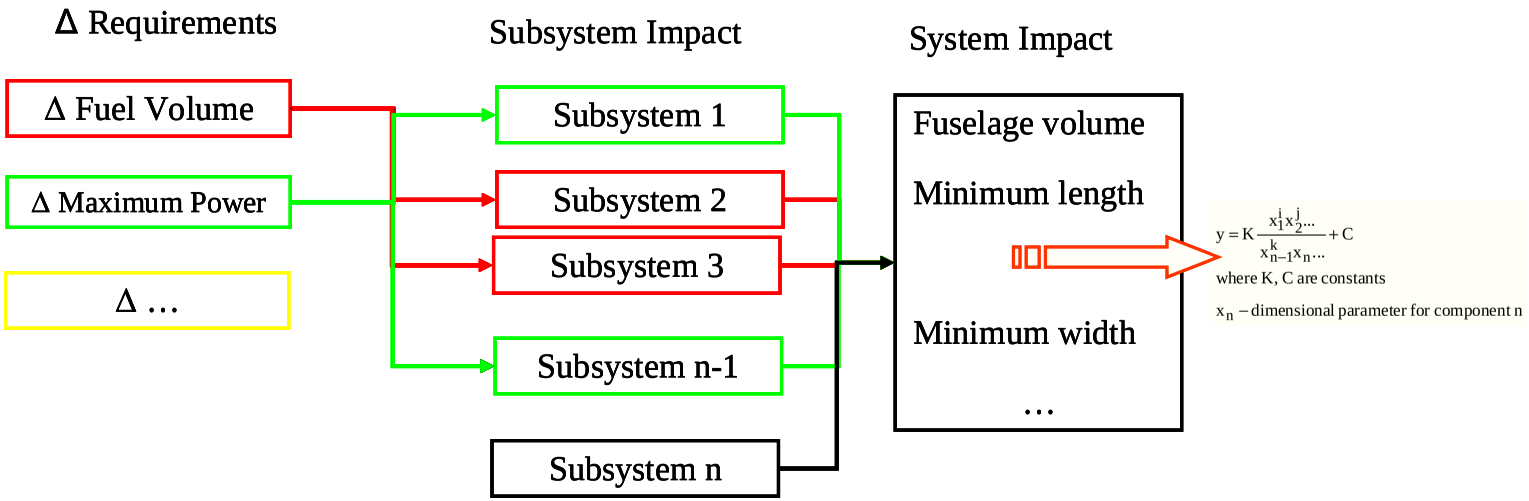

Figure 50: Super-hull Scaling Procedure

7.3.2 Minimum Enclosing Envelope

7.3.2.1 Derivation

The idea of using convex models to represent geometries is taken one step further by generating the minimum enclosing envelope in the form of a super-hull. The super-hull is the collective convex hull of the aircraft components. The key dimensions of this hull can now be ported to the system level as the minimum requirements to ensure volumetric feasibility as shown in Figure 51 . The super-hull is generated using only the points that belong to the convex hulls of the components. This is because the space is convex and as such, points that do not belong to the convex hull of their corresponding subsystem can not belong the convex hull of the system. This follows from the fact that a set of vertices S such that:

$$S = S_1 \bigcup S_2$$

It follows that [106] :

$$H(S) = H(S_1 \bigcup S_2) = H\left(H(S_1) \bigcup H(S_2)\right)$$

where :

$H(S)$: *is the convex hull of* S

Thus the benefit of convex reduction is felt here as well as less points have to be considered.

With the enclosing envelopes of various layouts defined, a domain spanning algorithm may be used to identify the sweet-spots within the design space. These spots will be defined by using gravimetric, aerodynamic and volumetric measures of merit.

7.3.3 Evaluation of Aerodynamic characteristics through slicing

Some of the aerodynamic metrics of interest are the fineness ratio, which is the quotient of the maximum cross-sectional diameter and the length of the body, the shape of fuselage cross-sections in comparison to the ideal shape and the rate of growth of the streamwise cross-sectional area profile. These metrics can be evaluated by slicing the body. The fact

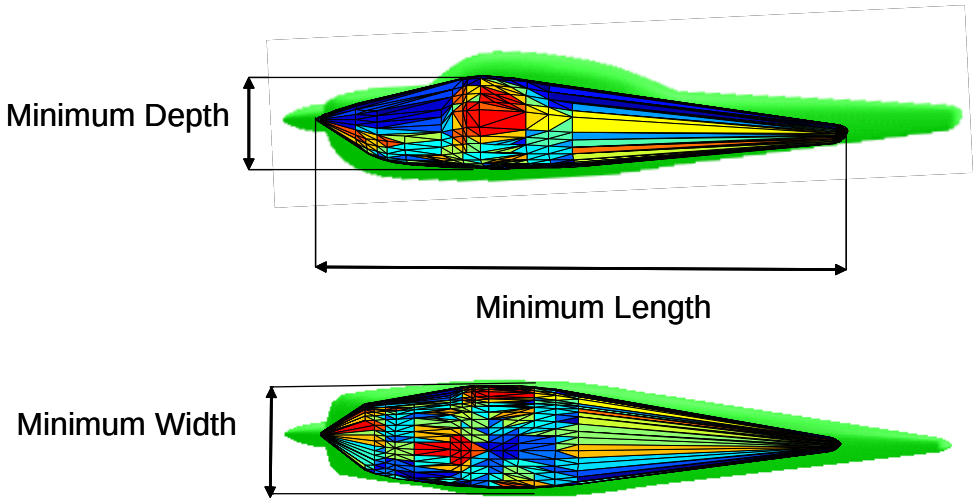

Figure 51: Use of Super-hull to constrain external geometry

that the superhull consists of triangular facets is exploited to come up with an efficient slicing algorithm. The pseudo code is described below.

$For\ each\ hull\ facet,\ define\ bounding\ box,\ BB$

$Find\ Xmin\ and\ Xmax\ over\ entire\ hull$

$Set\ up\ n\ slice\ stations\ between\ Xmin\ and\ Xmax$

$For\ each\ i \leq n$

$Find\ Ymin\ and\ Ymax\ for\ all\ facets\ spanning\ X(i)$

$Set\ up\ K\ slice\ stations$

$For\ each\ j \epsilon K$

$Define\ lines\ through\ [X(i), Y(j), \pm\ Large\ constant\ C]$

$\forall\ facets\ i\ where\ plane\ containing\ facet(i) \cap Line(i,j)\ \neq \varnothing$

$Calculate\ vectors\ from\ facet\ vertices\ to\ intersection\ point$

$Calculate\ corresponding\ interior\ angles$

$If\ sum\ of\ interior\ angles\ =\ 2\pi$

$Add\ intersection\ point\ to\ slice\ profile.$

7.3.4 Scaling Law Derivation

For a problem with n design variables $X_1 \cdots X_n$ the designer would not only like to know the key variables that impact any system characteristic C, but also the dimensionless groups into which they could be lumped. Such knowledge enables the designer to advance further into the design process without necessarily assigning fixed values to the variables. The first step in this process is the identification of the dimensionless groups that describe the system.

7.3.4.1 Dimensional Analysis

Dimensional analysis is premised on the $Buckingham - \pi$ theorem [36, 173]. Two fundamental assumptions must be made in order for this theorem to be mathematically valid. Firstly all the parameters that affect the characteristic in question must be accounted for. Secondly, the relative importance or influence of the independent on the characteristic must remain unchanged. In other words, the system must be in a single regime. For example the relative influence of viscous forces on the aerodynamic characteristics of a vehicle varies greatly from low subsonic flight to high supersonic flight. This means that the Reynolds number as a scaling law may not be used across these regimes.

This $Buckingham - \pi$ theorem states that a physically meaningful system (equation) with n independent variables and m fundamental dimensions can be alternatively expressed as an equation of $n - m$ dimensionless groups $(\pi - groups)$. Per this theorem any system represented by $C = f(X_1 \cdots X_n)$ may be rewritten as [124]:

$$C = a_0 \prod_{j=1}^{n} X_j^{a_{0j}} f(\Pi_1 \cdots \Pi_{n-m}) \tag{41}$$

$$\begin{array}{l} where: \\ a_i = Constant \\ \prod_i = a_i \prod_{j=1}^{n} X_j^{a_{ij}} \end{array}$$

If it is further assumed that most of the behavior of characteristic C is captured within the power law portion of Equation 41 and that f exhibits small, smooth and monotonic variations within a regime [124, 199], Equation 41 can be further simplified as follows:

$$C = a_0 \prod_{j=1}^{n} X_j^{a_{0j}} \prod_{i=1}^{n-m} \left(a_i \prod_{j=1}^{n} X_j^{a_{ij}} \right) = a \prod_{j=1}^{n} X_j^{\sum_{i=0}^{n-m} a_{ij}} \tag{42}$$

7.3.4.2 Regression

Regression becomes a necessary addendum to the system simplification process whenever (which is almost always) there is uncertainty arising from the values of the independent variables used to determine the constants and also when the system is not understood well enough for the designer to determine if all influential variables have been accounted for. Some of the more popular works combining regression techniques and dimensional analysis in order to simplify systems include the works of *Vignaux* et al [199] and *Mendez* et al [124]. The key difference between these techniques is the sequence in which the dimensionless groups are generated. Whereas the latter generates the $\pi - groups$ apriori, the former uses actual statistical data from the system in question to determine and refine the dimensionless groups. The latter approach is favored here, since the system has a large number of variables whose order of relevance can not be easily determined apriori.

To mitigate the uncertainty, a dependent variable transformation (usually the logarithm) is applied to Equation 41 to yield :

$$log\ C = \beta_0 + \sum_{j=1}^{n} \beta_j log X_j + \varepsilon \tag{43}$$

$where:$

$\beta_0 = log\, a$

$\varepsilon\ :\ Residual$

$\beta_i = \sum_{i=0}^{n-m} a_{ij}$

Thus for k experimental observations of the parameters a system

$$\tilde{y} = \left\{ \begin{array}{c} log\, C_1 \\ \vdots \\ log\, C_k \end{array} \right\} \tag{44}$$

and

$$\tilde{X} = \begin{matrix} 1 & log\, X_{11} & \cdots & log\, X_{1n} \\ \vdots & \vdots & \ddots & \vdots \\ 1 & log\, X_{k1} & \cdots & log\, X_{kn} \end{matrix} \tag{45}$$

such that:

$$\tilde{X}^t \tilde{X} \beta = \tilde{X} \tilde{y} \tag{46}$$

$\hat{\beta}$, the solution to Equation 46 minimizes the residual sum of square errors. This solution, however does not always result in a dimensionally consistent system. Mendez [124] solved this problem by reformulating the problem as follows :

$$min_\beta\ (\tilde{y} - \tilde{X}\beta)^t (\tilde{y} - \tilde{X}\beta) \tag{47}$$

$$such\ that\ : R\beta = b \tag{48}$$

$where$:

R_{ij} : $Exponent\ of\ unit\ i\ in\ variable\ X_j,\ i = 1, \cdots, n,\ j = 1, \cdots, k+1$

b_i : $Exponent\ of\ unit\ i\ in\ C$

The constraint defined by Equation 48 is used to ensure that each parameter set that is considered results in a dimensionally consistent system.

7.4 Layout Space Exploration

The component configuration space is inherently multimodal because for example axial rotations of the minimum enclosing envelope will have the same value for the packing efficiency but different design variable settings. This observation implies that domain-spanning "optimization" techniques must be used in the search for an optimum. An optimization problem with m and n equality and inequality constraints respectively, will generally take the form:

$$Minimize:\ f_p = f(\overline{x}) \tag{49}$$

$Subject\ to:$

$g_i \leq 0.0\ i = 1, ..., m$

$h_j = 0.0\ j = 1, ..., p$

7.4.1 Domain-Spanning Optimization Techniques

Domain-spanning techniques include grid searches, Genetic Algorithms (GAs) and Simulated Annealing (SAs). In general, genetic algorithms and simulated annealing techniques tend to be more efficient for large scale problems [147]. These methods are sometimes "contentiously" referred to as stochastic optimization techniques. This is due to the fact that they both include a probabilistic element in the optimization routine.

7.4.1.1 Genetic Algorithms (GAs)

The origins of genetic algorithms date back to 1954 when Nils Aall Baricelli [215] first executed a computer simulation of evolution. Evolutionary behavior or "Darwinism" is the philosophical basis for GA-based optimization. The works of Holland [92], DeJong [61] and more recently Goldberg [80] contributed to the popularization of the application of genetic algorithm approaches to the solution of multi-modal problems.

Holland [92] introduced two key concepts:

1. Schema: A generalization of an interacting coadpted set of genes. This concept enabled the analysis of non-linear interactions of "subsystems".

2. Crossover, Inversion and Mutation as genetic operators for the simulation of an evolutionary process with applications such as optimal learning and complex system design.

DeJong [61] further extended the application sphere of genetic algorithms to software design and artificial systems. Goldberg [80] formalized a number of concepts many of which were already out there in the public domain. The main difference was that his work came on the eve of the meteoric growth in desktop computational power that would increase interest in evolutionary techniques in solving complex problems. He demonstrated that if a reproductive probability was assigned per the ratio $P_i = \frac{f_i}{\sum f_j}$ then m, the number of samples of a

particular chromosome H in population A, would grow according to the progression $m(H, t+1) = m(H,t)\frac{f(H)}{\overline{f}}$. Thus the subsequent generations of a genetic search routine are always "fitter" than their predecessors as seen in Equation 50.

$$m(H, t+1) > m(H,t)\frac{f(H)}{\overline{f}}[1 - P_c\frac{\delta(H)}{t-1} - P_m O(H)] \tag{50}$$

Genetic searches/ optimizations are built on three fundamental pillars namely the population, environmental conditions and transformations. The population is defined by a set of chromosomes. The chromosomes are composed of genes which are mapped onto design variable settings either by binary coding or real coding [54]. In order to survive, the population must harness and conquer the (changing) environmental conditions. The mechanisms or transformations by which the population can survive are reproduction, crossover and mutation. Reproduction enables "fitter" species to propagate. Crossover enables the exchange of specific characteristics with the hope that better designs will emerge. After several generations, a dominant species may emerge. This is not necessarily good for the long term survival of the population as new changes in the environment could lead to extinction. To preclude this scenario, a third mechanism; mutation; is used to maintain diversity within the population through random changes in the chromosome. Higher chances of identifying "optima" in the neighborhood of the true global optimum are realized by using an approach that is built on these mechanisms.

Because the method depends solely on function evaluations and not gradients, it is not locally convergent. Once the "neighborhoods of interest" have been identified an additional optimization routine must be performed in order to move the points closer to the true local minima. The global minimum can then, with some certainty, be selected from this limited set of stationary points.

7.4.1.2 Simulated Annealing (SA)

Evolution is to genetic algorithms as thermodynamic cooling is to Simulated Annealing techniques[147]. The approach mimics the thermodynamic process of slowly cooling down hot metal to relieve thermodynamic stress. The algorithm begins with a random population

or set of points, $\overline{X}$ within the design space at an initial high temperature, T. For each point, $\overline{X}_{new} = \overline{X}_{old} \pm \overline{\rho}$ where $\overline{\rho}$ is a random move limit within the design space. If fitness function $F(\overline{X}_{new}) < F(\overline{X}_{old})$ then $\overline{X}_{new}$ is accepted. However, the unique aspect of this algorithm is that it allows hill-climbing by accepting inferior settings with a probability:

$$P(Accept) = e^{\{\frac{-|F(\overline{X}_{new}) - F(\overline{X}_{old})|}{KT}\}} \tag{51}$$

$$\overline{\quad where: \quad}$$

$$\overline{\quad K: \, Boltzman\, constant \quad}$$

By permitting hill-climbing in a minimization problem, the SA approach increases the chances of finding the true global minimum in problems akin to that notionally described in Figure 33. However, simulated annealing techniques generally require a higher investment in computational resources than genetic algorithms [55].

Simulated Annealing algorithms and genetic algorithms are unconstrained optimization techniques but inherent in the nature of the aircraft component layout problem is that a number of constraints must be satisfied. For example aircraft must typically fit in a defined "box" for example the $80\,m$ [127] box for commercial airliners. There are therefore some side constraints resulting from operational considerations. Additionally, as discussed in §7.2.6 the components can not overlap. Also due to physics-based properties e.g thermodynamic heating or structural support requirements, components can be allocated a minimum clearance requirement. This minimum requirement for each component must also be satisfied. As the clearance requirement is not a side constraint, the only way it can be integrated into a domain-spanning optimization process is through a penalty function. The choice of penalty function is critical to the success and efficiency of the optimization.

7.4.2 Penalty Functions

Penalty functions can be broadly divided into exterior and interior penalty functions. With a penalty function applied, the minimization problem generally takes the form:

$$Minimize: \; f_p = f(\overline{x}) + P(\overline{x}) \tag{52}$$

$Subject\ to:$

$g_i \leq 0.0\ i = 1, ..., m$

$h_j = 0.0\ j = 1, ..., p$

7.4.2.1 Interior Penalty Functions

The interior penalty method works by successively improving feasible designs. Infeasible designs are precluded from consideration by virtue of the severity of the penalty as the design point approaches the constraint. The penalty function is given by [198]:

$$P(\overline{x}) = \sum_{j=1}^{m} \frac{-1}{g_j(\overline{x})} \tag{53}$$

The key disadvantages of this method are that interior penalty functions tend to lead to more complex unconstrained minimization problems [198] and also that an infeasible solution may indeed be closer to the true optimum than a feasible solution. This approach could indeed be more efficient if the ability to "look over the fence" was integrated into the optimization. This Achilles heel may be overcome by using approaches such as Linear and Quadratic Extended penalty functions [198]. However, the success rate varies from case to case.

7.4.2.2 Exterior Penalty Functions

Exterior penalty functions are employed to penalize the objective function whenever constraints are violated. The appropriate form of the penalty function depends on the nature of the objective function. It takes some iterative tuning in order to identify the ideal form of this function for a given problem. Exterior penalty functions can be broadly subdivided into three major categories. These are static, dynamic and adaptive penalty functions. Each category has some advantages and disadvantages.

Static Penalty Functions

In this approach, a constant penalty C is added or subtracted from the objective function

for a minimization or maximization problem respectively. Some sophistication is usually added onto the penalty in order to distinguish between designs that violate more constraints than others. The penalty function takes the form [111]:

$$P(\overline{x}) = \sum_{i=1}^{m} C_i \delta_i \tag{54}$$

$$\begin{array}{l} where: \\ \delta_i = 1 \, if \, constraint \, is \, violated \\ \delta_i = 0 \, if \, constraint \, is \, satisfied \end{array}$$

Goldberg [80] proposed the use of a "distance to feasibility" metric as the basis for the penalty. This approach has been shown to be generally more effective [178]. Static penalty functions are relatively simple in that they do not incorporate in temporal or stochastic effects. However, the key weakness in static penalty functions is that they often require significant investment of effort in the "iterative tuning" alluded to earlier. In some cases, the globally robust set of constants C that the user is searching for may not exist. Also there is some implicit philosophical conflict in allowing the optimization routine to explore infeasible solutions yet requiring that the final solution be feasible.

Dynamic Penalty Functions

Dynamic penalty functions overcome some of the weaknesses of static penalty functions by incorporating a temporal component $S_i(t)$. This component must be a monotonically non-decreasing function of time in order to increase the severity of the penalty as the optimization progresses [52]. This increases the probability that the final solution is feasible .

$$P(\overline{x}) = \sum_{i=1}^{m} S_i(t) d_i^k \tag{55}$$

$where:$

$\delta_i g_i(\overline{x}) = 1 \quad for \;\; i = 1, ..., m$

$|h_i(\overline{x})| = 0 \quad for \;\; i = m+1, ..., q+m$

$t = temporal \;\; effect \, e.g. \, generation \, number$

But like other penalty functions, some iterative tuning of $S_i(t)$ is necessary. An overly lenient $S_i(t)$ may result in infeasible final solutions while an excessively severe $S_i(t)$ could cause premature convergence to sub-optimal solutions.

Because, as pointed out in §7.4.1.1, genetic algorithms are solely function dependent and because these functions rely on values from often random initializations, there is also a need to further guide the algorithm away from less attractive regions and towards more attractive regions. In cases such as the optimization of packing efficiency, where the optimal value i.e. 1 is known, adaptation of the penalties based on on-going success or lack thereof could significantly improve performance.

Adaptive Penalty Functions

In these functions adaptation is achieved by selecting two constants β_1 and β_2 such that $\beta_1 < \beta_2 < 1$ and evaluating feasibility every N_f generations. The adaptive penalty is defined as follows [178] :

$$P(\overline{x}) = \sum_{i=1}^{m} \lambda_k d_i^k \tag{56}$$

$where: \; d_i =$

$\lambda_k \beta_1 \quad if \, previous \, N_f \, generations \, have \, infeasible \, best \, solution$

$\frac{\lambda_k}{\beta_2} \quad if \, previous \, N_f \, generations \, have \, feasible \, best \, solution$

$\lambda_k \quad otherwise$

Assigning good values to the constants in Equation 56 requires a fair amount of knowledge about the design space. This can be acquired through experience with the subject matter or through experimentation. Adaptive penalty functions have also sometimes been referred to as non-stationary penalty functions [102]. However, the basic idea and its origin

i.e. simulated annealing remain the same.

The preceding steps i.e. component modeling, convex hull evaluation, creation of layouts and collision detection all build up to the layout selection phase. This phase is a critical piece of the CESM process as the quality of the final solution is directly dependent on the ability to identify the right spots in the design space for secondary local optimization studies.

7.4.3 Layout Selection

As with any other optimization routine, the layout selection process is built on two key pillars i.e the objective function(s) and the evaluation function(s). The former is *a mathematical statement of the task to be achieved.* The latter, on the other hand, is *a mapping from the space of possible candidate solutions under the chosen representation to a set of numbers where each element from the set of possible solutions is assigned a numeric value that indicates its quality.* [125] The nature of the objective function has an obvious and explicit influence on the final solution. Down-selecting from the multitude of designs is a multi-objective problem as alluded to earlier in section §7.3.1. These objectives can be broadly classified into three categories i.e. volumetric, gravimetric and aerodynamic. The ideal component layout would be one that best harmonizes the competing interests of the three categories.

7.4.3.1 Formulation of Evaluation Functions

Volumetric Function

The objective of a subsystem layout process is to place the components in such a way that the volume of the containing body is minimized [190]. This objective can be quantified in the form of a ratio of total subsystem volume to total hull volume. This ratio is typically referred to as the packing efficiency, η_p. Implicit in its definition is the fact that the theoretical optimum for this parameter is 1. However, since only the major aircraft subsystems are considered in the layout exploration process, an allowance is made for a residual volume [161] based on the vehicle class. The information in Figure 47 and the methodology embodied in Equation 40 are used to come up with the target density ranges. These ranges are in turn used to evaluate the expected packing efficiency range as follows:

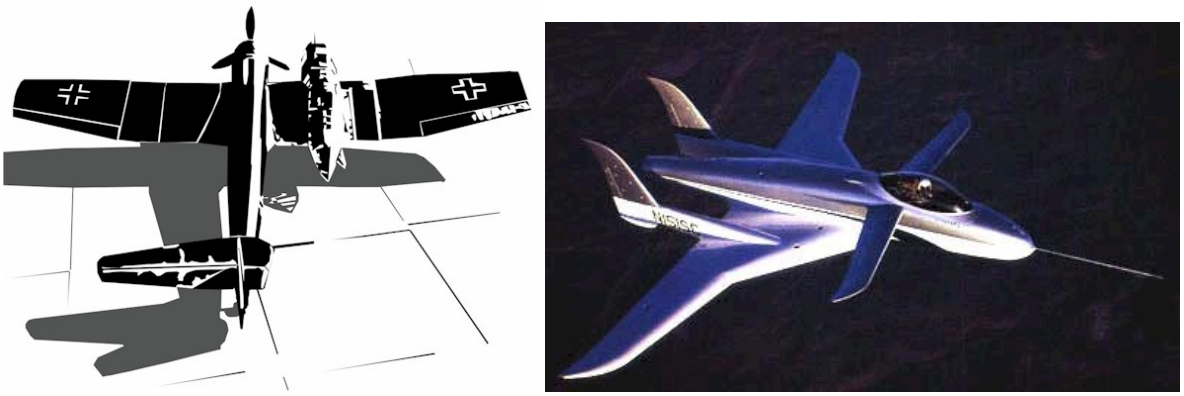

(a) BV-144 (b) ARES

Figure 52: Asymmetric Aircraft Concepts

Let:

$$vehicle\,density,\ \rho_v = \frac{Total\,Component\,Mass}{Total\,Vehicle\,Volume} \tag{57}$$

Substituting total vehicle volume in Equation 57 for total hull volume in Equation 39 yields:

$$\overline{\eta}_p = \frac{Total\,Component\,Volume}{Total\,Component\,Mass} \cdot \overline{\rho_v} \tag{58}$$

$where:$

$\overline{\eta}_p:\ Target\,packing\,efficiency\,range$

$\overline{\rho_v}:\ Historical\,density\,range\,for\,vehicle\,class$

Another volumetric consideration is symmetry. This may or may not be a design requirement based on the nature of the target vehicle. Asymmetric vehicles were proposed and built in the 1930s by Blohm and Voss [28, 29, 30, 31] and more recently by Scaled Composites Inc. [175, 169] . See Figure 52.

However, since this is likely to be a requirement for a significant percentage of new vehicle concepts, the quantification of symmetry must be investigated.

A number of approaches towards the quantification of object symmetry exist in literature [17, 109, 116, 153, 222, 197]. These typically employ Fourier coefficients to evaluate some distance metrics which are used as indicators of shape symmetry. van Otterloo [197]

discussed a number of contour based approaches. Heijmans [89] introduced new measures tailored to convex objects. Such measures are of particular interest since convex approximation is the method of choice for object representation in this work. However, Balinsky [17], introduced an even more elegant and straight forward approach to symmetry quantification that is particularly well-suited to convex objects. This is because the hull and the convex hull of the objects' vertex sets are one and the same. Evaluating axial symmetry for such components can therefore be reduced to determining the symmetry of the set of all point pairs derived from the vertex set. This is generally an $O(n!)$ complexity problem [17, 216]. Given a set of n point pairs $\widetilde{s} = \{\{x_1, y_1\}, \ldots, \{x_n, y_n\}\}$ and an axis of symmetry $y = y_A$ then the scaled co-ordinates $\widetilde{x}_i$ and $\widetilde{y}_i$can be defined as:

$$\widetilde{x}_i = \frac{x_i - x_c}{max_{i=1,\ldots,n}\{|x_i - x_c|\}} \tag{59}$$

$$\widetilde{y}_i = \frac{y_i - y_A}{max_{i=1,\ldots,n}\{|y_i - y_A|\}} \tag{60}$$

$$\begin{array}{l} where: \\ \widetilde{x}_c = \frac{1}{n}\sum_{i=1}^{n}\widetilde{x}_i \end{array}$$

As a result, $-1 \leq x_i \leq 1$ and $-1 \leq y_i \leq 1$ and the axes of symmetry coincide with the X and Y axes. The set $\widetilde{s}$ is now mapped onto s in the complex plane such that $s = \{z_1, \ldots, z_n\}$ where $z_i = x_i + Iy_i$, $1 \leq i \leq n$. Since complex numbers and their conjugates are symmetrical with respect to the real axis, a symmetrical set must contain only real numbers and pairs of complex conjugates. The symmetry problem is solved by using the results of the "Fundamental Theorem of Algebra" [192] which states that an $n-$*degree polynomial has exactly* n *complex roots*. By this theorem a $1-to-1$ correspondence between the subsets $\frac{\mathbb{C}^n}{S_n}$ (where $\mathbb{C}^n$ is an n-dimensional linear complex space and S_n is a permutation group of n elements) and the space containing complex polynomials of order n can be represented as:

$F : (z_1,\ldots,z_n) \mapsto z^n + a_{n-1}z^{n-1} + \ldots + a_1 z + a_0$ [17]

$P_n(z) = \Pi_{i=1}^{n}(z - z_i) = \sum_{i=0}^{n} a_i z^i$

---

where :

$a_n = 1\,,\,, a_i = a_i(z_1,\ldots,z_n)$ as defined by the Vieta polynomials [33, 196]

Balinsky also suggested a more elegant way to compute the the polynomials P_n as the evaluation of each coefficient using the Vieta polynomials is inefficient. In this approach, each polynomial P_n can be represented by a string of polynomials $S_i = \{a_0,\ldots,a_1\}$. This string can be evaluated by sequentially multiplying the preceding polynomial by the monomial $(z - z_{i+1})$. This operation is tantamount to shifting the elements of S_i one position to the left to get $\{a_0,\ldots,a_1,0\}$ and then adding $(-S_i \cdot z_{i+1}) = \{-a_0 \cdot z_{i+1},\ldots,-a_i \cdot z_{i+1}\}$. The string set $S_{i+1} = \{a_0, a_1 - a_0 \cdot z_{i+1} - \ldots, a_{i-k+1} - a_{i-k+1} \cdot z_{i+1}, a_i \cdot z_{i+1}\}$. Thus the symmetry of the object can be measured using the Euclidean distance metric given by :

$$D(z_1,\ldots,z_n) = \frac{1}{n}\sqrt{\sum_{i=0}^{n}(im(P_n(i))^2} \tag{61}$$

The volumetric symmetry objective based on this measure can be mathematically stated as follows:

$$Minimize:\ D(z_1,\ldots,z_n) \tag{62}$$

The key volumetric objective function deals with the packing efficiency of the layout. The packing efficiency as defined earlier is the ratio of total component volume and residual volume [139, 161] to the containing body's volume. Thus for any non-colliding layout, the maximum value of this objective is 1. This objective can be mathematically formulated in the following manner:

$$Maximize:\ \frac{Total\,Component\,Volume + R}{Total\,Super\,Hull\,Volume} \tag{63}$$

$Subject\,to:$
$Number\,of\,collisions = 0$
$where:$
$R:\ Residual\,Volume\,Provision$

Aerodynamic Function

The analysis of the aerodynamic merits of a given configuration is complicated by a number of factors. First of all, at the point where the designer must select from the multitude of layout options, the Outer Mold Line (OML) is not yet defined. Because there is, potentially, a very large number of subsystem configurations, it would be prohibitively expensive to first invest resources in fully defining the OMLs over the entire configuration space and then narrowing down to a select few. To circumvent this issue a generic baseline geometry based on an ideal body of revolution is used. The cross-sections are defined in such a way that they can take on circular, oval or rectangular dimensions based on the values of the dimensions. These dimensions are determined by adding an offset to the dimensions of the super-hull. These customized vehicles must now be evaluated against each other in order to narrow down the design space.

Vehicle cruise mach regimes play a critical role in influencing the vehicle's external geometry. Mach regimes can be broadly broken down into four categories namely: Subsonic, Transonic, Supersonic and Hypersonic. In subsonic flow, the Mach number is less than 1 at every point in the flow field. As a result, flow disturbances propagate to every point in the flow field. Thus subsonic flow streamlines are smooth i.e. there are no discontinuities in their gradients [133]. Inertial forces are typically dominated by viscous forces resulting in the low Reynolds number flow characteristics. At high subsonic Mach numbers i.e. $0.8 \lesssim M \lesssim 1.2$, isolated pockets of the flow field may experience sonic or supersonic flows. The flow field is then said to experience transonic flow. These pockets are encased in weak shock waves that transition the flow back to subsonic characteristics [83]. As flow speed is increased even further, these pockets expand up to a point where flow is supersonic ($M > 1$) everywhere in the field. Shock waves result from the fact that flow disturbances can not propagate

upstream. Supersonic flow is generally characterized by sharp discontinuities in streamlines induced by shock waves [42, 126]. As the Mach number increases further the shock layer becomes thinner [24], thereby trapping a smaller volume of fluid between itself and the body. High temperature gas effects such as rarification, viscous dissipation, ionization and dissociation [63, 91]. These effects are typically observed around $M \gtrsim 5$ although this threshold varies depending on the geometry of the body and the properties of the fluid in which it is immersed.

Analytical expressions exist for the optimal shapes of some body classes in specific Mach regimes. For example, for slender bodies in supersonic flow, the Sears-Haack body is said to be optimally shaped [10, 84, 171].

Optimality from an aerodynamic perspective translates into having the maximum lift-to-drag ratio ($\frac{L}{D}$). The ease with which this optimality can be quantified depends on the geometric attributes of the body. These attributes can be broadly classified into slender and non-slender bodies.

Slender bodies Slender bodies are vaguely defined as bodies whose maximum cross-section is much less than their length [10]. Non-slender bodies on the other hand are bodies that fail to satisfy this criterion. The wave drag on the Sears-Haack body can for example be calculated using the relatively simple expression in Equation 64 [172].

$$D_w = \frac{64V^2}{\pi l^4}\rho_\infty U_\infty^2 \tag{64}$$

$where:$

$V : Total\,Volume$

$l : Vehicle\,Length$

$\rho_\infty : Ambient\,Density$

$U_\infty : Ambient\,Velocity$

Thus for vehicles that are designed to cruise in flight regimes where the wave drag is a dominant factor, this equation could be a good representative measure of the aerodynamic

merits of a vehicle. These figures have indeed been used in the estimation of volume wave drag before the detailed geometry is known [176].

Non-slender bodies Methodologies for the evaluation of flow properties for generalized bodies range from Euler equations to full potential equations to Navier-Stokes equation [203]. Generally the computational expense increases is lowest at the Euler end of the spectrum and highest at the Navier-Stokes end. There is an inverse relationship between the number of simplifying assumptions (and thus the fidelity of the analyses) and the computational expense. For conceptual design purposes, the goal is not to accurately predict the lift-to-drag ratio of each vehicle concept but rather to eliminate those concepts that are expected to have inferior or unacceptable performance. To this end, and in line with the analytical paradigm discussed in §3.1.1.1, faster, lower fidelity models are used. Panel codes based on potential equations are usually used as the compromise between low fidelity and prohibitive computational expense. Potential flow equation codes are based on a modified version of the full potential equation [27, 191]:

$$\nabla^2\phi - \frac{1}{a^2}\left\{\frac{\delta^2\emptyset}{\delta t^2} + \frac{\delta q^2}{\delta t} + \overrightarrow{q}\cdot\nabla\left(\frac{q^2}{2}\right)\right\} = 0 \tag{65}$$

$where:$

$\phi : Velocity\,Potential$

$\overrightarrow{q} : Freestream\,Velocity$

$t : Time$

The major assumptions on which this equation is based are that the flow is irrotational, momentum is conserved and that continuity equation holds [176]. When used in conjunction with the perfect gas law and an additional assumption of isentropic flow [27], the relationship between the pressure distribution and the velocity potential can be derived. Based on these relationships, coefficients of aerodynamic forces such as lift and drag can be estimated [203]. For example, when the flow is assumed to be incompressible, which is reasonable at a low Reynolds number, the equation reduces to:

$$\nabla^2 \phi = 0 \tag{66}$$

A unique solution to this equation may be found by enforcing boundary conditions such as the fact the flow must remain tangent to the body at all points.

The author's previous experience with panel codes indicates that it would take $O(10)$ seconds to analyze a body of average complexity. An average of between 8 seconds was observed for a blended wing-body configuration [16]. It is worth investigating if alternative measures the aerodynamic merits of a body that are cheaper to evaluate exist. Two measures are investigated here. One is the geometric similarity to the ideal body of the same fineness ratio and the other is the best possible performance, of an ideal body of the same fineness ratio.

Similarity to ideal When analyzing the merits of the supersonic area rule, Whitcomb [208] noted:

> *The range and relative magnitude of the favorable effects of body comparisons of shaping based on the supersonic area rule are markedly influenced by the wing configuration, as pointed out in reference 2.[207] a number of experimental results (ref. 4, for example) [62] have indicated that the general overall effectiveness of body shaping is usually greater with increased wing or tail leading-edge sweep.*

Per this observation, a similarity to ideal approach may be taken for concepts which are designed for Mach regimes that dictate high sweep angles. For lower sweep concepts where the lift and control surfaces cause major "bumps" in the cross-sectional area distribution, a different approach is taken. A control surface area distribution is assumed for the wing and empennage. This distribution is moved aft from the estimated forward limit of the center of gravity to the aft limit until an optimal location is identified. The location of the empennage is fixed relative to that of the wing by using the desired tail volume coefficient.

The cross-sectional similarity to ideal is quantified in terms of the Hausdorff distance [164] of the super hull point set to the point set of the ideal body of equal length and volume.

	Slender Body	Non-slender Body
High Speed	Analytical Equations Sears [171] Haack [84] *von Kármán* [200]	Analytical Equations Hypersonic- Min(D*) Yakunina [221] Waldo [202]
Transonic	Whitcomb[208] Heaslet and Lomax [88]	Minimum Drag Closed Body for given maximum cross-sectional area and length Parker [150] Potential Flow Methods
Low Speed	Analytical Equations Sears [171] Haack [84] *von Kármán* [200] Virtual wing and empennage	Hausdorff Distance to Ideal [22, 134] Potential Flow Methods Virtual wing and empennage

Table 8: Taxonomy of Aerodynamics Approaches

Postulated , by Felix Hausdorff, the Hausdorff distance metric measures the distance of a point set A, to the nearest point in another point set B [3]. That is to say:

$$h(A,B) = max_{a \epsilon A} \{min_{b \epsilon B} \{d(a,b)\}\} \tag{67}$$

where :

$d(a,b)$: *Euclidean Distance between a and b*

Because the Hausdorff distance is measured at each cross-section and no information from the preceding or subsequent sections is used, the metric must be reinforced with a smoothness measure. This measure is important because even when the vehicle cross-sections match up exactly with the ideal body, they could be staggered in such a way that the vehicle concept is less attractive than a better laid out concept. This measure can be formulated as the symmetry of the body about the plane parallel to the freestream and perpendicular to the freestream direction as described in Equation 61.

Performance of Equal Fineness Ratio Ideal Body In this approach it is assumed the ideal streamlined body of with length and maximum cross-sectional area equal to those

of the superhull is the fuselage. This assumption enables the use of idealized equations to quickly come up with a drag-based measure of merit. A minimax strategy is employed in formulating the aerodynamic objective function for a given layout. The goal is to minimize the maximum possible drag coefficient value based on frontal area, $C_{D_{frontal}}$, wet area, $C_{D_{wet}}$, or volume $C_{D_{volume^{\frac{2}{3}}}}$. The idea here is that if the superhull were to be enclosed in fuselage that is a streamlined into a perfect body of revolution, the drag coefficients used here are the best that the designer could effect. The aerodynamic measure of merit for the proof of concept can thus be mathematically represented as:

$$Obj_{aero} = Min\left(Max\left(C_{D_{frontal}}, C_{D_{wet}}, C_{D_{volume^{\frac{2}{3}}}}\right)\right) \tag{68}$$

The methodology for the derivation of the three C_D curves depends on the expected attributes of the final design.

For non-slender bodies, the Hausdorff distance described in Equation 67 is used in conjunction with the symmetry metric in Equation 61 for the proof of concept study. Other metrics could also be derived based on the design goals.

Gravimetric Function

This function provides a yardstick by which the inertial merits of a given configuration can be evaluated. Attaching a value to any given layout is further complicated by the fact that at this point, the vehicle is "incomplete" as the structures nor the lift and control surfaces have not been fully defined due to the enormity of the design space.

The location of the center of gravity and its excursion range are of primary interest in evaluating the gravimetric merits of a given layout. The location has a direct impact on the aircraft's pitch, roll and yaw characteristics. Take for example, the pitching moment derivative shown in Equation 69 [140] below.

$$C_{m_\alpha} = C_{L_{\alpha w}}\left(\frac{X_{cg}}{\overline{c}} - \frac{X_{ac}}{\overline{c}}\right) + C_{m_{\alpha f}} - \eta V_H C_{L_{\alpha t}}\left(1 - \frac{d\varepsilon}{d\alpha}\right) \tag{69}$$

$where:$

$X_{cg}: Location\,of\,C.G$

$X_{ac}: Location\,of\,A.C$

$\overline{c}: Mean\,Aerodynamic\,Chord$

$C_m: Pitching\,Moment\,Coefficient$

$C_L: Lift\,Coefficient$

$\eta: Tail\,Efficiency$

$V_H: Tail\,Volume\,Coefficient$

$\varepsilon: Downwash\,Angle$

$\alpha: Angle\,of\,Attack$

$_t: tail$

$_w: wing$

$_f: fuselage$

The pitching moment derivative, $C_{m_{\alpha f}}$ just like the normalized location of the center of gravity $\frac{X_{cg}}{\overline{c}}$, contribute significantly to the aircraft's handling characteristics. These forces were first studied by Max Munk [136] who concluded that for a body of revolution, $\frac{dM}{d\alpha} = f\left(volume, \frac{1}{2}\rho v^2\right)$ under the assumption of invsicid ideal flow. His results were later improved upon by Multhopp [135] who added a correction for induced flow along the fuselage to come to the following equation:

$$C_{m0_f} = \frac{k_2 - k_1}{36.5 S \overline{c}} \int_0^{l_f} w_f^2 \left(\alpha_{0w} + i_f\right) dx \tag{70}$$

$where:$

$k_2 - k_1 : Correction\ factor\ for\ fineness\ ration$

$\bar{c} : Mean\ aerodynamic\ chord$

$S : Wing\ reference\ area$

$w_f : Average\ width\ of\ fuselage\ sections$

$\alpha_{0w} : Wing\ zero\ lift\ angle\ relative\ to\ fuselage$

$i_f : Fuselage\ camber\ line\ incidence\ angle$

$l_f : Length\ of\ fuselage$

Similarly the fuselage contribution to the rate of change of the pitching moment can be estimated as follows [140]:

$$C_{m0_f} = \frac{1}{36.5S\bar{c}} \int_{x=0}^{x=l_f} w_f^2 \frac{\delta\varepsilon_u}{\delta\alpha} dx \tag{71}$$

$where:$

$\frac{\delta\varepsilon_u}{\delta\alpha} : Local\ change\ in\ flow\ angle\ with\ \alpha$

To fully define the fuselage, an offset between the inner and outer mold lines must be decided upon by the designer. The outer mold line is then evaluated by adding the offset value to the sectional dimensions of the sliced super-hull. The new dimensions are then applied to a generic baseline fuselage in order to come up with a representative fuselage. A wing is initially sized based on lift requirements. Based on the wing dimensions and a desired tail volume coefficient as recommended by the stability and controls group, the empennage can then be sized as well.

Also of critical importance in the evaluation of the stability merits of any vehicle is the allowable excursion of the center of gravity as the quantity of the consumable elements and/or the loading change. The designer must ensure that the empty-to-full center of gravity locations lay within the desired forward and aft limits. This parameter is often quantified as the static margin. Its official definition is the distance between the center of gravity and the neutral point [140] .

$$Static\ margin = \frac{X_{NP}}{\bar{c}} - \frac{X_{cg}}{\bar{c}} \tag{72}$$

The location of the neutral point is calculated using the following formula:

$$\frac{X_{NP}}{\overline{c}} = \frac{X_{ac}}{\overline{c}} - \frac{C_{m_{\alpha f}}}{C_{L_{\alpha w}}} + \eta \frac{V_H C_{L_{\alpha t}}}{C_{L_{\alpha w}}} \left(1 - \frac{d\varepsilon}{d\alpha}\right) \tag{73}$$

The dynamic stability of a vehicle is also of critical importance to the overall handling merits of a vehicle. Dynamic stability can be quantified in several ways e.g. stability derivatives, non-dimensionalized radii of gyration etc. The latter are used here :

$$R_{xx} = \sqrt{\frac{4 \cdot I_{xx}}{b^2 \cdot M}} \tag{74}$$

$$R_{yy} = \sqrt{\frac{4 \cdot I_{yy}}{L^2 \cdot M}} \tag{75}$$

$$R_{zz} = \sqrt{\frac{4 \cdot I_{zz}}{(b+L)^2 \cdot M}} \tag{76}$$

---

where :

I_{ii} : *Mass Moment of inertia in i axis*

b : *Wing span*

L : *Fuselage Length*

Designs that best satisfy the overall design goals must be identified via an optimization routine such as the genetic algorithms described in section §7.4.1.1. However, any optimization routine is only as good as the objective function employed.

7.4.3.2 Formulation of Objective Function

Whenever there is more than one objective in an optimization process, the designer must decide on a methodology by which to drive his optimization process. As mentioned earlier, the quality of the final results is a direct function of the quality or appropriateness of the designer's decision. A number of approaches may be used in driving the optimization process. These include plain aggregation, Pareto optimality, population-based non-Pareto optimality and niched Pareto approaches.

Plain Aggregation By the aggregation approach the objective function is a weighted sum of the individual objectives as shown in Equation 77 below.

$$OBJ = \sum_{i=1}^{n} \lambda_i f_i \tag{77}$$

---

where :

λ_i : *weighting factor for objective* i

f_i : *objective* i

n_i : *number of objective functions*

The main advantages of this approach are that it can be used with traditional optimization techniques and that it always leads to one final solution. They thus do not require additional "tweaking" on the designer's part. However, the choice of the appropriate weighting factors for each objective is not an exact science. Any final solution is therefore only an optimum in the context of these weighting factors. The weighting should not only reflect the relative importance of each objective but also balance out scale disparities among the objectives. When some objectives vary significantly in order of magnitude, choosing the appropriate weighting factor is complicated even further. Partial solutions to this problem were demonstrated by Syswerda [184] , Jones [103] and [100] , however, the designer still faces an up-hill battle in determining the optimal set of weighting factors for any given problem [72, 71]. Because of these and other challenges, new population-based methods that preclude the need for the aggregation of conflicting objectives have been developed.

Pareto-Based Approaches A design point is said to be *Pareto Optimal* if all of its evaluation functions can not be improved simultaneously [125]. That is to say that improvement in one dimension results in degradation in another. More formally, a set of n objectives $f_i(\overline{X})$, $i = 1, \cdots, n$ on $X \epsilon D$ is said to be Pareto optimal iff $\forall \overline{X}^* \epsilon D \; f_i(\overline{X}) \succ f_i(\overline{X}^*)$. That is to say, the Pareto Optimal combination dominates every other combination in design space, D that does not lie on the Pareto front. When $f_i(\overline{X}) > f_i(\overline{X}^*)$ for at least one objective f_i then the design variable vector X is said to be at least weakly dominant [74].

Pareto-based fitness approaches assign sequentially lower ranks to sets of non-dominated solutions while removing them from the population pool. Individuals in every set are assigned an equal probability of reproduction. Therefore at the end of a Pareto-based optimization approach the designer must often choose a single design from within the Pareto optimal set. This decision can often be arrived at by including less critical design metrics that were omitted in the preliminary design process and sometimes on information that only becomes available later in the design process.

Pareto-based fitness can be amalgamated with "Game theory" [158, 159]. Game theory was developed by economist Amnon Rapoport in the mid 20^{th} century. The term broadly encompasses any scenario where two or more players with conflicting objectives make decisions or choose strategies that impact each other's goals. For the problem at hand, aerodynamics and stability are examples of players with conflicting goals and mutually impacting decisions or strategies.

Two sets of outcomes typically emerge in a "Game Theory" scenario i.e. the cooperative outcome, where players work together in order to maximize their collective "good" and the non-cooperative outcome where "everyone for himself and God for us all" is the law of the land [138]. In the cooperative scenario, a player may change his/her decision i.e. a chromosome can mutate, reproduce or crossover if and only if no player's goal deteriorates as a result. This way, the genetic algorithm inches closer and closer to the Pareto front with every generation. In the non-cooperative scenario, each player is assigned a subset of the design variables. The player then optimizes his objective by changing those variables and accepting fixed values from the other players for the rest of the design variables. These fixed values represent the settings for the best design in the previous generation [4]. A Nash equilibrium [138] is said to have been reached when no player can do better by changing their strategy if all other players stood pat. Nash equilibrium approaches show some promise for aerodynamic design applications, however, for the problem the allocation of variables to different players and its impact on the final solution are not well-understood. A more well-understood approach will therefore be utilized for the proof of concept. Not all population-based approaches are built around the Pareto-optimality, however. Some of these alternative

approaches are described below.

Population-based Non-Pareto Approaches These methods pioneered the idea of treating disparate objectives separately while searching for and monitoring all non-dominated solutions within a design space. Schaffer's approach [170], Vector Evaluated Genetic Algorithm (VEGA), employs a pseudo aggregation approach where the objectives are implicitly aggregated based on dynamic weighting factors. The expected number of offspring produced by each parent is the sum of the expected number of offspring per each parent's rating based on each objective. The population is thus broken down into sub-populations within which the dominant schema produce more offspring. The inevitable result of such an approach is that different clusters emerge along the design space, a phenomenon called *speciation*. For the aircraft design problem at hand for example, aerodynamically optimal configurations would lie in one sector of the design space while gravimetric efficiently configurations would be found in a different portion of the design space. This goes against the basic premise of multi-disciplinary design where the goal is essentially to search for the best compromise solution. In fact, Fleming and Pashkevich [69] noted that points in concavities within a design space could not be found using any linear combination of objectives.

Niche Induction aka Niched Pareto Genetic Algorithm Goldberg and Segrest [81] observed that when presented with multiple equivalent optima, finite populations tend to converge to just one of the optima. Thus Pareto-based methods do not guarantee results that uniformly sample the design space. This naturally occurring phenomenon is often referred to as *"genetic drift"*. To counter this phenomenon, Goldberg [80] and Nafpliotis [95] introduced fitness sharing and nested fitness sharing respectively. These methods essentially penalize individuals within a population for being too densely packed or too close together. By doing so, the algorithm is "encouraged" to explore more sparsely populated areas of the design space, thereby improving diversity within the population. Srinivas and Deb [59] formalized these ideas in the form of NSGA-I, a non-dominated sorting algorithm that offers a family of solutions that lay on or close to the Pareto frontier. Despite its promise, NSGA-I had a high computational complexity $O(mn^3)$ where m is the number of objectives and n

is the population size. It could also have benefited from the use of elitism to speed up its performance. Thirdly, the need to specify the niche sharing parameter σ_{share} *apriori* made it challenging for most design scenarios where the designer does not necessary have a rich enough understanding of the design space in order to be able to choose the appropriate value of the sharing parameter. These criticisms were addressed in NSGA-II [60] which precluded the need to specify a sharing parameter and incorporated elitism, thereby improving performance to $O(mn^2)$.

NSGA-II The NSGA-II algorithm is used in this research for the preliminary step in identifying points close to the many modes in the layout configuration space. The algorithm consists of three major blocks namely non-dominated sorting, crowding distance assignment and crowding distance comparison. These blocks are described below.

For each design point i, the non-dominated sort algorithm classifies the rest of the points into two sets S_i and n_i which contain the design points which dominate i and those which are dominated by i respectively. The points with $n_i = 0$ form the first Pareto front F_1. For each of these points, the size of its dominated set is reduced by one. If any n_j becomes empty as a result, then the corresponding point is put in a separate set H. The process is then continued with the members of H as the new front until all fronts have been identified. This process is illustrated in Figure 53.

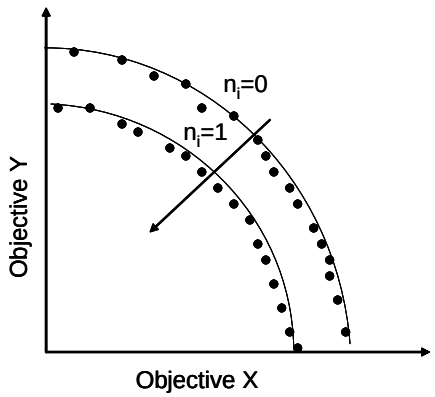

Figure 53: Illustration of NSGA-II

The pseudo-code [60] for a population P is shown below .

$for\ each\ p \epsilon P$

$for\ each\ q \epsilon P$

$if\ p \prec q\ then$

$S_p = S_p \cup \{q\}$

$else if\ (q \prec p)\ then$

$n_p = n_p + 1$

$if\ n_p = 0\ then$

$F_1 = F_1 \cup \{p\}$

$i = 1$

$while\ F_i \neq \emptyset$

$H = \emptyset$

$for each\ p \epsilon F_i$

$for\ each\ q \epsilon S_p$

$n_q = n_q - 1$

$if\ n_q = 0\ then$

$H = H\ \cup \{q\}$

$i = i + 1$

$F_i = H$

The crowding distance is a measure of how densely populated a design point's neighborhood is. This metric is quantified as the average side length of the enclosing cuboid whose extremities are defined by the two closest points on either side of the point in the question. The pseudo-code follows [60].

$$l = |I|$$

$$for\, each\, i$$

$$set\, I\,[i]_{distance} = 0$$

$$for\, each\, Objective\, m$$

$$I = sort\,(I, m)$$

$$I\,[1]_{distance} = I\,[l]_{distance} = \infty$$

$$for\, i = 2\, to\, (l-1)$$

$$I[i]_{distance} = I[i]_{distance} + (I\,[i+1]\,.m - I\,[i-1]\,.m)$$

7.4.4 Dealing with Uncertainty in Component Sizes

Uncertainty in component sizes results from factors such as low technology readiness as well as flexible requirements that are meant to accommodate unforeseen design and economic trade-offs. Scaling laws help to address the latter issue. A satisfactory treatment of the former is also critical piece to the usefulness of the methodology. The capacity optimization challenge is not unique to aircraft design. Production plants must continuously balance their capacity with cyclical and unpredictable demand patterns. Airlines have to balance between seats allocated to cheap (buy-early) fares and seats for high-end (last minute). Hotels face a similar quandary. Problems of this nature can be solved by employing the "News Vendor Model".

7.4.4.1 The News Vendor Model

This model derives its name from a decision the typical news vendor has to make every morning. He must purchase the "right" number of papers to meet a highly variable daily demand. If he purchases too many, then he will incur an overage cost, C_o (the cost of unsold papers). On the other hand purchasing too few will unnecessary limit the profit he can make that day. He suffers an underage cost C_u (the profit foregone). The News Vendor Model was specifically developed for this kind of problem. Two key assumptions are made in deriving this model:

Q : $Order Quantiy$
$G(Q,D)$: $Sum\ of\ Underage\ and\ Overagecost$
$E[G]$: $Expected\ Cost$
dd : $Actual\ Demand$

1. Single Product with measurable C_o and C_u.

2. Demand, dd, is a continuous non-negative random variable with density function $f(x)$and cumulative distribution function $F(x)$.

   Based on these assumptions, the model is derived as follows:

7.4.4.2 News Vendor Model Derivation [152, 186]

Definitions:

Thus:

$$G(Q,D) = C_o max\{0,(Q-dd)\} + C_u max\{0,(dd-Q)\}$$

and

$$G(Q) = E[G(Q,D)] = C_o \int_0^Q (Q-x)f(x)dx + C_u \int_0^Q (x-Q)f(x)dx \tag{78}$$

To find the optimum quantity, differential calculus is employed:

$$\frac{d}{dQ}G(Q) = C_o \int_0^Q (Q-x)f(x)dx - C_u \int_0^Q f(x)dx = C_o F(Q) - C_u(1-F(Q)) = 0\, at\ optimum$$

Therefore $(C_o + C_u)F(Q) - C_u = 0$ which implies that :

$$F(Q) = \frac{C_u}{C_o + C_u} = Probability(dd \leq Q_{optimal}) \tag{79}$$

Therefore once the overage and underage unit costs are quantified, a target optimal probability of meeting demand can be calculated. This can then be plugged back into an empirical distribution where data is available or an assumed distribution based on expert opinion to find the deterministic optimal quantity.

7.4.4.3 News Vendor Model Translation to Aircraft Design

Translation of Metrics

Q, the order quantity, becomes synonymous with the design volume i.e. the volume that minimizes the cost of redesign.

C_o, the overage cost, represents the expected cost of either sizing down an oversize concept or the extra costs incurred if such a concept were applied to the design mission.

C_u, the underage cost, represents the expected cost of either sizing up an undersized concept or the extra costs incurred if such a concept were applied to the design mission.

There are two main challenges in implementing the News Vendor model for purposes of aircraft design i.e. the quantification of overage and underage costs and the decomposition of the lump sum of optimal volume among the contributing components such that optimality is maintained. The approach to the quantification of overage and underage costs is dictated by the expected reaction to a design solution that does not meet all required performance specifications downstream in the design process. If there is no room for flexibility in the performance requirements then redesign would be the only recourse for the designer. In practice the sunk cost may be too high to warrant the luxury of redesign. Here other costing options must be explored. These options must be compare the cost of operating the sub-optimal solution to the cost of operating the theoretical optimum.

Estimation of Overage and Underage costs

To estimate C_o and C_u two approaches will be investigated. The first is an activity-based costing system that focuses on the cost of design and redesign in the period before prototyping and initial production begins. The other approach entails mission-based costing. As noted earlier, the sunk cost at the point when it is realized that the design does not meet all performance requirements may limit the process capacity to develop and/or absorb the new knowledge that would lead to a better design. Here the cost of flying an aircraft with excess capacity is traded-off against the cost of choosing an under-capacity design and perhaps having to do multiple sorties to deliver the same amount of payload. The cost of overage C_o and the underage cost C_u may be measured in terms of the resulting changes

in aircraft related costs amortized over the expected number of missions in the vehicles expected service life. The change in cost per mission may be broken down into change in cost to acquire, change in cost to operate and change in total non-operations-related Life Cycle Cost (LCC).

$$\triangle Cost\,to\,acquire\,per\,mission = \frac{\triangle Total\ Acquisition\ Cost}{Expected\ Number\ of\ Missions}$$

$$\triangle Cost\,to\,Operate\,per\,mission = \triangle(IOC + DOC)$$

$$\triangle LCC' = \frac{\triangle LCC}{Expected\ Number\ of\ Missions}$$

The optimal value of Q is obtained by applying the identified probability to the volume density function. However, per initial assumptions, this function is not known. Therefore it must be derived before Q can be evaluated.

1. Design Volume Density Function Derivation

   It is assumed here that the probability distributions of individual component volumes are known. The challenge is how to consolidate these into a system level probability function. The results of the News Vendor analysis are to be applied to this function in order to back out a robust design volume. The author has been unable to find any theorems on the derivation probability density functions for sums of random variables of known distributions. Two practical approaches to solving this issue are the use of inequalities or the use of simulation.

   Bennett [23] explored probability inequalities as a work around to this problem. Some of the better inequalities included, Bernstein's inequality, Berry's inequality and Uspensky's inequality. These inequalities provide an upper bound on probability that a density function of the sum of a set of density functions is greater or equal to some multiplier of the standard deviation. Simulation can also be used to derive a representative density function. Once Q has been evaluated, it must then be redistributed back to the subsystems.

2. Design Volume Decomposition

   The total design volume will be decomposed first into total component volume and residual volume. Residual volume is the fraction of total aircraft volume allocated to

the rest of the contents of the vehicle e.g. structural components, wiring, plumbing etc The total component volume ,$V_{optimal}$, will then be allocated to the individual components based on the fraction of expected total volume that the component accounts for as shown below.

$$V_i^* = \frac{E[V_i]}{\sum_{i=1}^{n} E[V_i]} V_{optimal} \tag{80}$$

7.4.5 Integration into Conceptual Design

7.4.5.1 How the Individual Pieces of CESM Fit Together

Figure 54 below shows the sequence in which the various contributing analyses are used in the CESM process. Automated conceptual structural topology generation methods such as that developed by Dr. Sensmeier [174] can be used in conjunction with the analytical approaches which have been postulated as part of this work to build the complete environment.

The results of the methodology must be further integrated into the contemporary design process in order to realize their usefulness.

7.4.5.2 CESM Integration into Conceptual Design Process

Figure 55 illustrates the information flow in the enhanced conceptual design process. Results from a CESM analysis will be integrated into the conceptual design process first by using the superhull as a skeleton around which the external geometry is wrapped. The dimensions of this minimal enclosing envelope are also used as constraints for the geometric variables used in concept sizing and synthesis. The designer could also use visual judgment and dimensional comparison to choose a suitable baseline configuration from known architectures.

Secondly, scaling will still take place in response to the output of the sizing and synthesis process but in accordance with the custom scaling laws derived using the CESM process. This output could include information on key performance metrics such as range, endurance, maximum power and so on. This and other information that carries direct implications for the size of aircraft subsystems is used as input for the CESM scaling laws and constraints. The CESM output is in the form of updated constraints for the vehicle as well and perhaps a change in layout.

As noted in observation V above, a number of different layouts could fit the aircraft

Figure 54: CESM Process Sequence Diagram

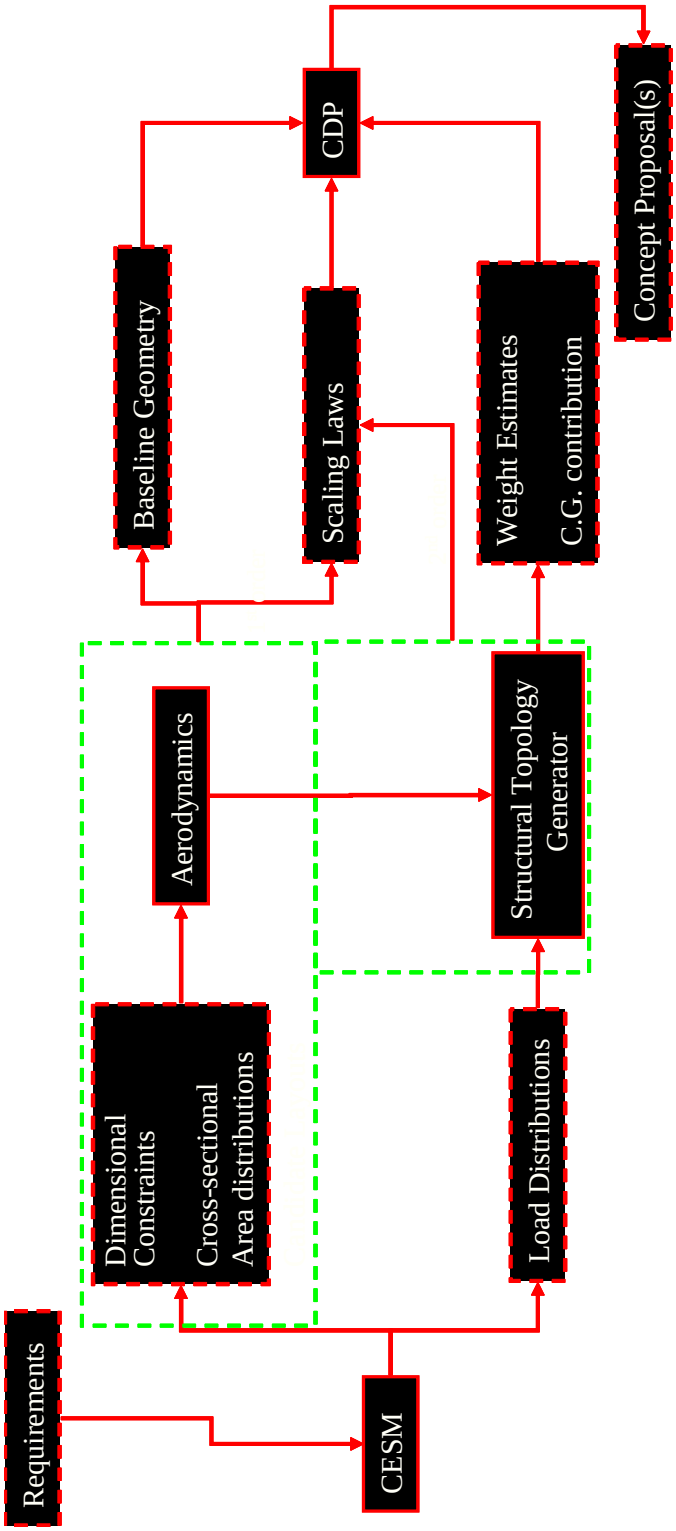

Figure 55: Enhanced Conceptual Design Process

mold as seen from the perspective of the sizing and synthesis tool, if the general form of the final configuration is not decided on, apriori. The relative optimality of these layouts could change during the sizing and synthesis process as various components are scaled up or down. To reduce the possibility of excluding a layout that could yield the smallest size vehicle for the final configuration, a number of configurations are carried forward simultaneously during the analysis. A treatment of volumetric uncertainty could be applied at this point.

In order to verify and validate the preceding claims, a proof-of-concept study was carried out. The study entailed the design of a PEM fuel cell powered general aviation aircraft using the CESM-enhanced design process.This aircraft was designed to meet the same operational requirements as a notional C-172R aircraft discussed in §1.1 . The verification and validation process was implemented as described following :

Chapter VIII

IMPLEMENTATION

8.1 Component Modeling

The surface models shown below were created in VSP® [113]. Figure 56 below shows some of the major components of the retrofitted C-172 discussed earlier. As described in §1.1.3 VSP® uses low-level primitives to create skin models of component geometries.

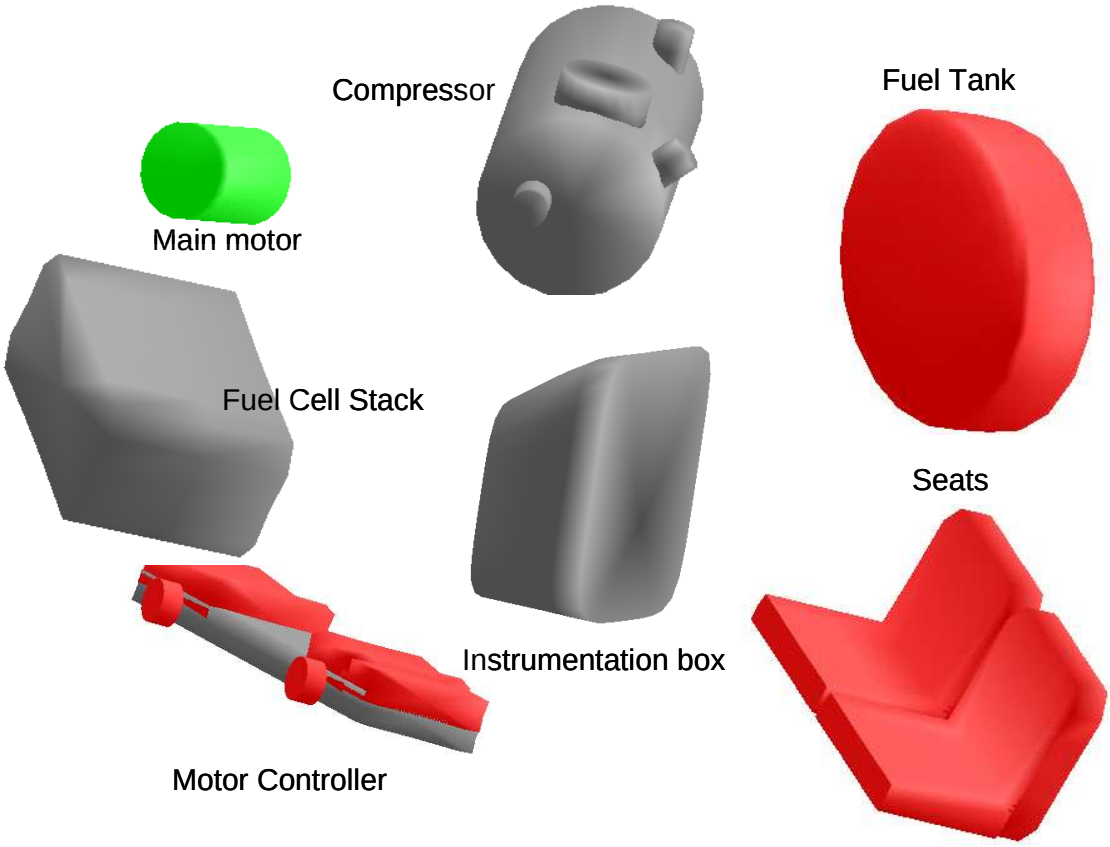

Figure 56: Component models in VSP®

8.2 Component Rotation, Translation and Scaling

As mentioned earlier, the ease of geometric manipulation was one of the major reasons why the author chose to represent components using the discretization approach. Each component is assigned a set of functions i.e $\lambda_{ix} = f(m)$, $\lambda_{iy} = g(m)\, and\, \lambda_{iz} = h(m)$ each describing the scaling behavior of the subsystem in the x, y and z directions in response to changes in metric m. A scaling matrix to represent the entire transformation can be formulated as follows:

$$Sc = \begin{bmatrix} \lambda_{ix} & 0 & 0 \\ 0 & \lambda_{iy} & 0 \\ 0 & 0 & \lambda_{iz} \end{bmatrix} [75, 77]$$

Object translation can be implemented using a basic transformation vector [76, 78]:

$$T = \begin{bmatrix} T_x \\ T_y \\ T_z \end{bmatrix} \tag{81}$$

This can either be defined by the designer or by an optimization routine. These two transformations may be combined by augmenting the scaling matrix as shown below:

$$Sc + T = \begin{bmatrix} \lambda_{ix} & 0 & 0 & T_x \\ 0 & \lambda_{iy} & 0 & T_y \\ 0 & 0 & \lambda_{iz} & T_z \\ 0 & 0 & 0 & 1 \end{bmatrix}$$

Thus the operation $Sc + T$ performed on subsystem model M yields the modified subsystem :

$$M* = [\lambda_{ix} M_x + T_x,\, \lambda_{iy} M_y + T_y,\, \lambda_{iz} M_z + T_z] \tag{82}$$

Other CESM processes such as collision detection and the construction of the super-hull follow as outlined earlier.

A number of additional transformations may be useful in optimizing a layout and the emergent shape of the corresponding containing body. These include rotation, for components whose physical nature does not mandate a particular orientation, and shearing for components that do not have a fixed predetermined shape such as cargo bays.

Rotational matrices [108] for a given angle θ can be defined as follows in a Cartesian co-ordinate system:

$$Rot_x = \begin{bmatrix} 1 & 0 & 0 \\ 0 & cos\,(\theta) & -sin\,(\theta) \\ 0 & sin\,(\theta) & cos\,(\theta) \end{bmatrix}$$

$$Rot_y = \begin{bmatrix} cos\,(\theta) & 0 & sin\,(\theta) \\ 0 & 1 & 0 \\ -sin\,(\theta) & 0 & cos\,(\theta) \end{bmatrix}$$

$$Rot_z = \begin{bmatrix} cos\,(\theta) & -sin\,(\theta) & 0 \\ sin\,(\theta) & cos\,(\theta) & 0 \\ 0 & 0 & 1 \end{bmatrix}$$

It is worth noting that the rotational matrix is commutative only up to two dimensions. Thus an item that has more than two degrees of rotational freedom increases analysis complexity by a factor of six. The designer could screen out of one of the dimensions in order to mitigate the resulting computational expense.

Likewise, a shear-matrix [219] can be formulated by changing one of the zero values in the identity matrix of any order to the shear factor γ for example:

$$Sh = \begin{bmatrix} 1 & 0 & \gamma \\ 0 & 1 & 0 \\ 0 & 0 & 1 \end{bmatrix}$$

Such a matrix would be applicable to components such as cargo bays where shape is not a fixed requirement.

The following subsystem power (P) scaling laws as determined from the analysis environment developed by Choi [48], were used in the derivation of system scaling laws.

Subsystem	Power Scaling Law
Fuel Cell	$0.0225 \cdot P^{0.965}$
PMAD	$0.4371 \cdot e^{0.0058P}$
BOP	$1.6933 \cdot e^{0.0058P}$
Main Motor	$0.251 \cdot e^{0.0059P}$
Compressor	$0.5297 \cdot e^{0.000006P}$

Table 9: Power Scaling Laws for Major PEM Subsystems

As seen in Figure 57, Figure 58, Figure 59, Figure 60 and Figure 61 there is significant noise in the subsystem sizing data. This is partially a result of attempts to capture uncertainty in some design parameters as detailed in Dr. Choi's recourse-based methodology [48]. Another source of noise is the optimization process by which the data is arrived at.

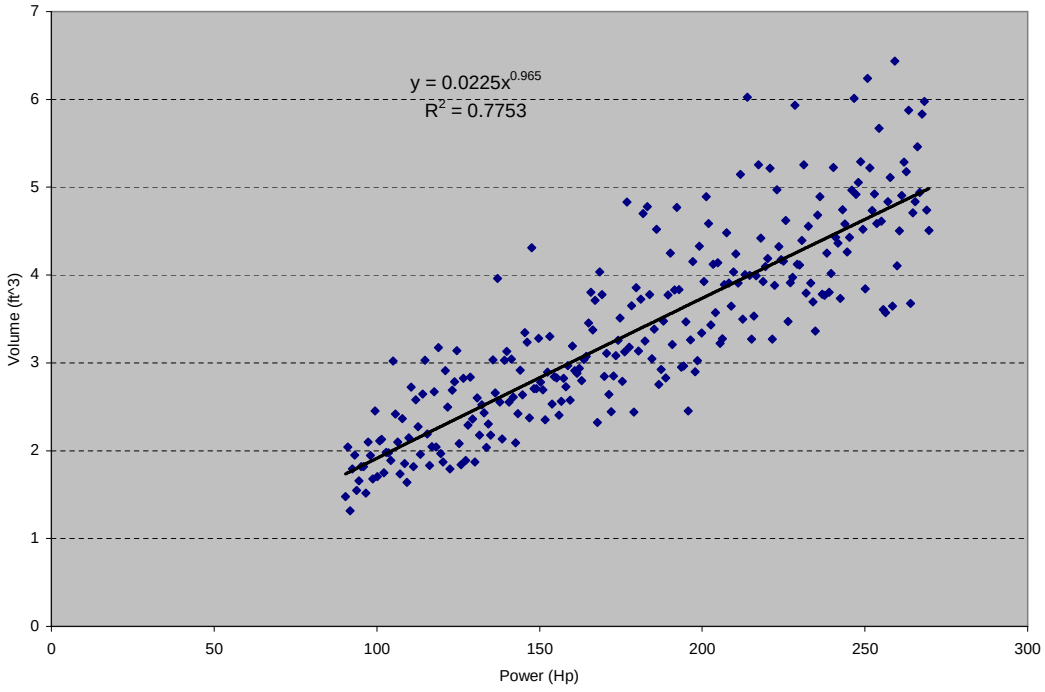

Figure 57: Fuel Cell Stack Scaling Data

The fuel cell equation shown in Table 9 refers to the ideal case where the fuel cell stack can be continuously scaled to meet a given power requirement. In "real world" design, however, this is almost never the case. Technological and financial limitations usually limit designers to discrete choices. A fuel cell is indeed a stack of basic units . A representative

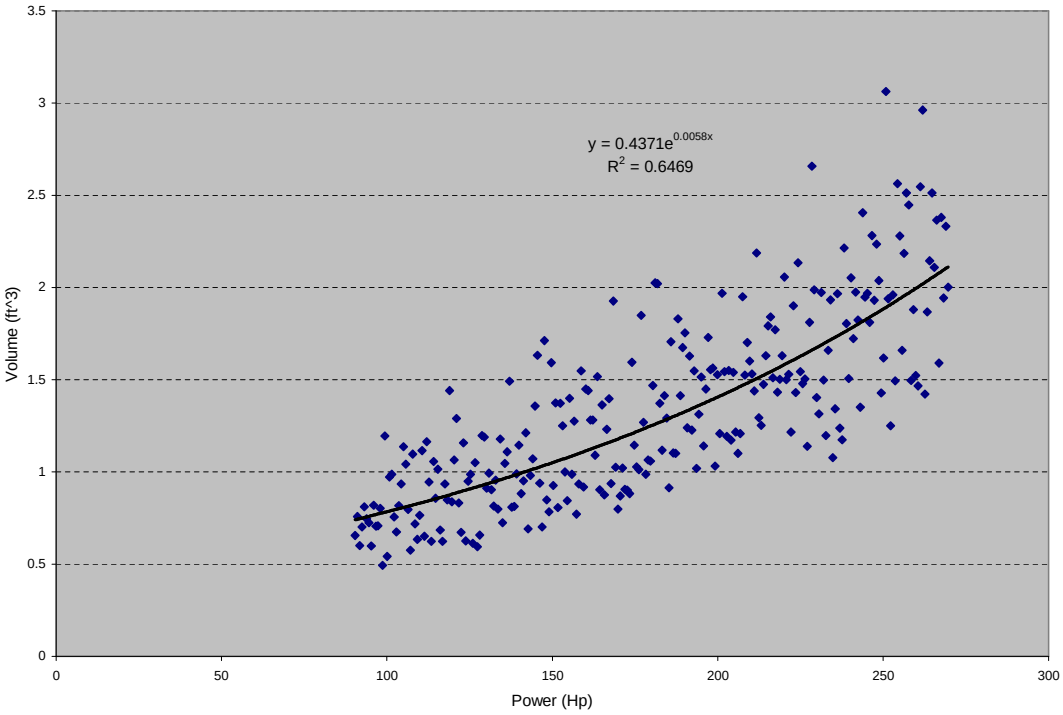

Figure 58: PMAD Scaling Data

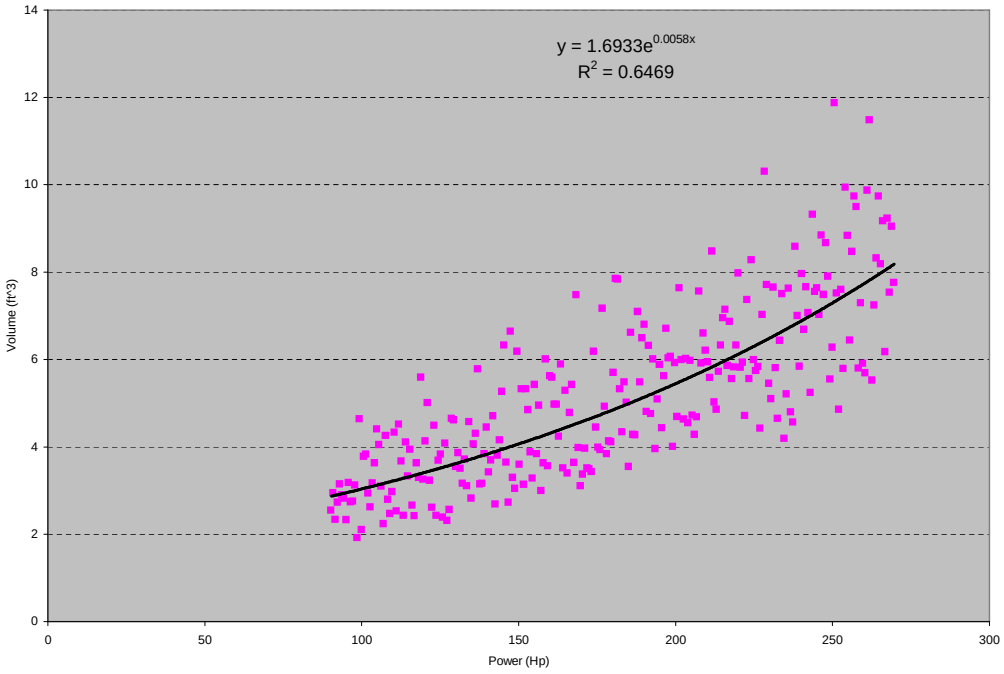

Figure 59: BOP Scaling Data

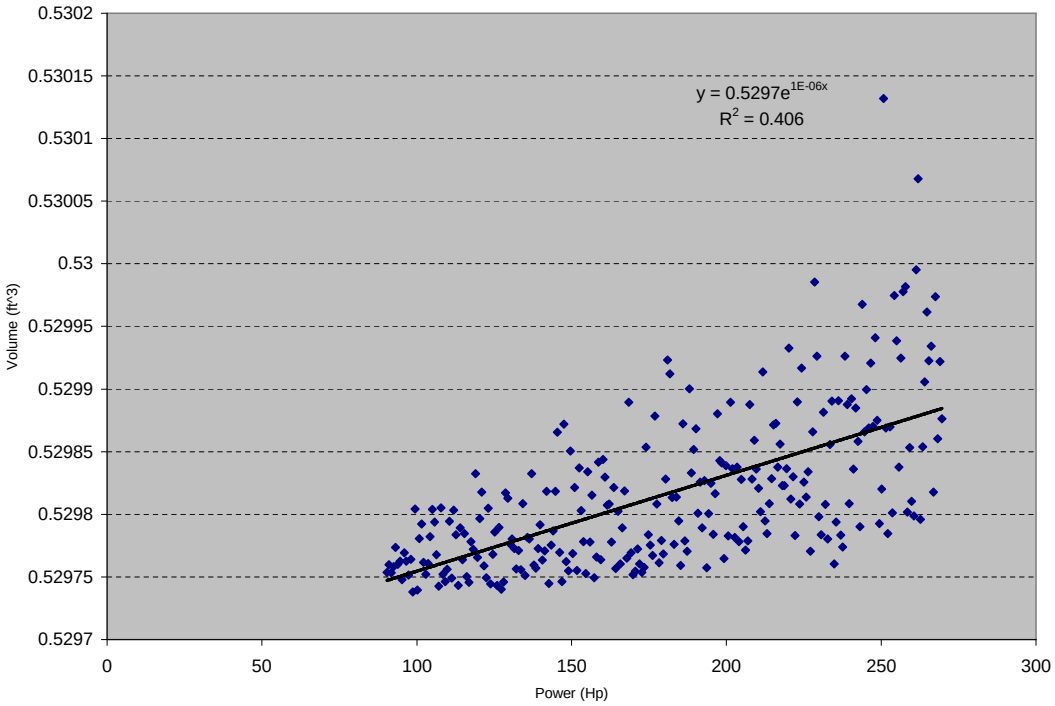

Figure 60: Compressor System Scaling Data

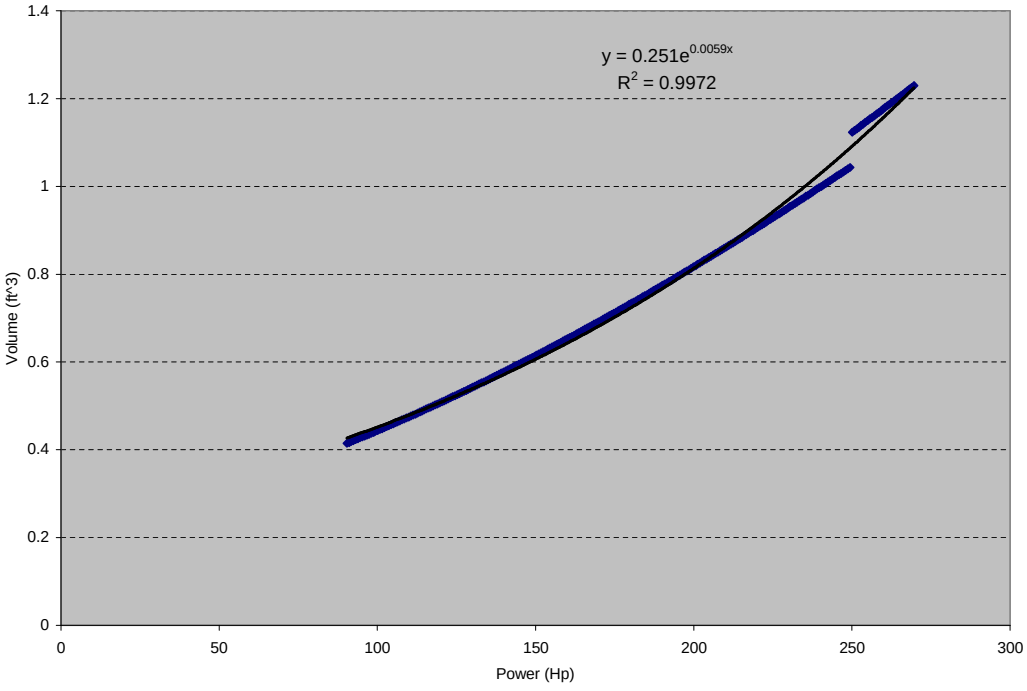

Figure 61: Main Motor Scaling Data

scaling law would take the form of a step function.

A function $f : \mathbb{R} \rightarrow \mathbb{R}$ is a step function if [205]

$$f(x) = \sum_{i=0}^{n} \alpha_i \chi_{A_i}(x) \tag{83}$$

$where:$

$\chi = Indicator\, Function$ [70]

$A = Unit\, subsets\, along\, \mathbb{R}$

$$\chi_{A_i} = \begin{cases} 1 & if\, x \epsilon A \\ 0 & Otherwise \end{cases}$$

$\alpha_i : Real\, Numbers$

$n \geq 0$

Furthermore the intervals A_i are disjoint. That is to say, $A_i \cap A_j = \phi\, for\, i \neq j$. Also the union of all intervals forms the real domain $\mathbb{R}$. Thus, a fuel system with basic power unit of specification P_u and a power requirement P_r will consist of $P_r\, modulo\, P_u$ (rounded up) stacks. The volume scaling function can thus be expressed as:

$$V = V_u \cdot P_r\, modulo\, P_u \tag{84}$$

Evident in Equation 82 is the fact that cost of the component relocation operation is a direct function of the size of the component surface matrix. Since computational speed is a key showstopper in this area, innovative ways to down-size this matrix must be explored.

8.3 Component Reduction

Surface points can be harvested from most forms of geometry representation techniques available today. The resulting matrices can be reduced (in size) by evaluating their representative convex hulls. The algorithm chosen for the derivation of the convex is the QuickHull (Qhull) algorithm. This is because the algorithm is generally faster and more robust to point dispersion [44]. The computational expense incurred on an Athlon 750 CPU (per Chadnov

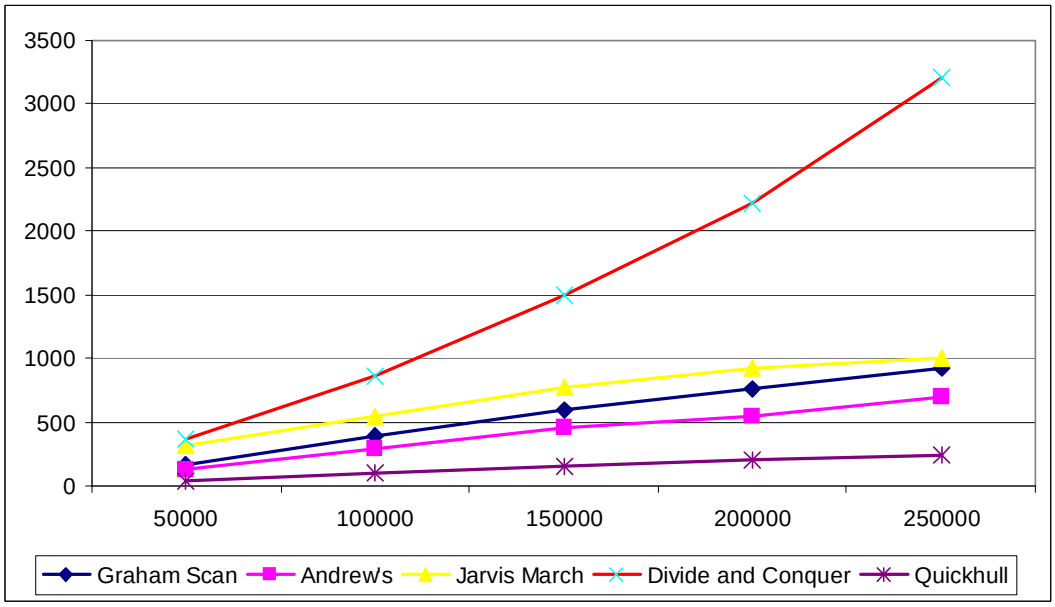

Figure 62: Speed Comparisons of Convex Hull Algorithms for Uniformly Dispersed Points [44]

[44]) is plotted in Figure 63.

Figure 56 showed the subsystem CAD models in VSP [113]. Surface points are harvested from these models in the form of *.hrm* [113] files. Figure 64 shows the approximations of the same components using convex hulls. The convex hulls are visualized in Matlab®.

The benefit of convex hull approximation is not visually intuitive. Two metrics i.e. compression benefit $\frac{\triangle Points}{\#Surface\,Points}$ and approximation cost $\frac{\triangle Volume}{Component\,Volume}$ are used to quantify the costs and benefits of this approach. The former measures the reduction in the number of data points required to represent a component. The latter measures the artificial change in component volume as a result of this approximation. It is seen in Table 10 below that significant reductions in the amount of data required to represent a component can be achieved at no approximation cost. However, for more complex bodies such as the turbo-compressor, cost to benefit ratio of $1:3$ is seen. This can be further improved by decomposing the body into simpler convex sections. This may not always be necessary because complex bodies typically require some clearance around them by virtue of their shape. As a rule of thumb, the approximation cost should be compared to the clearance volume as a percentage of total component volume. Model decomposition is only recommended in the event that the

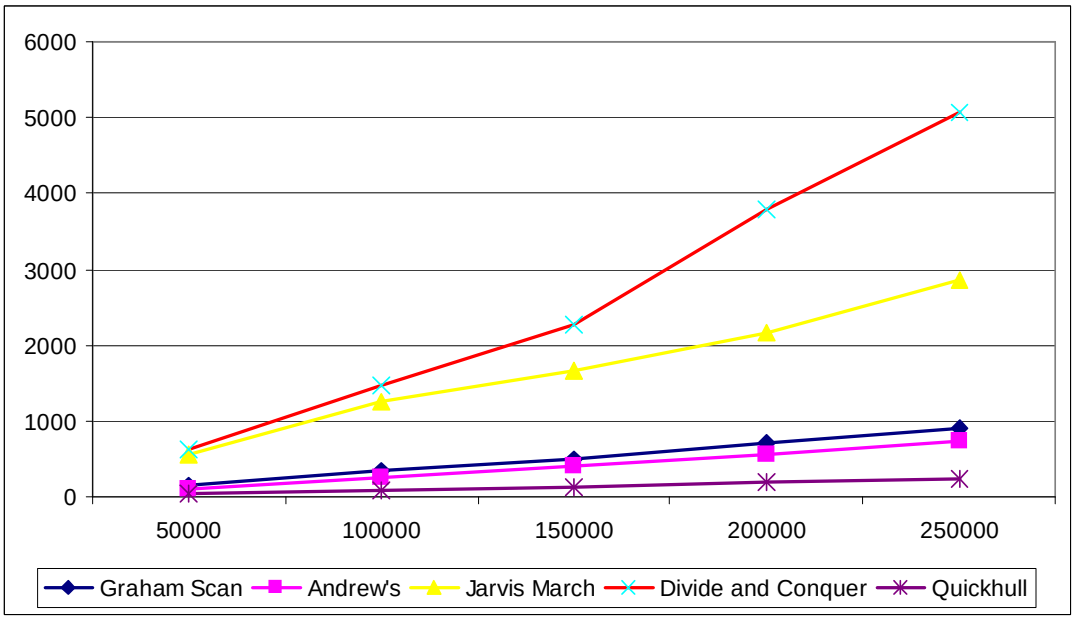

Figure 63: Time Expense Evolution for Points defined by Gaussian Distribution [44]

approximation cost is significantly greater than the clearance volume percentage.

As mentioned earlier, exploring the various layouts of components in space in an automated manner requires some form of collision detection. This can be implemented in a number of ways as described in §7.2.6. The GJK algorithm was selected for the reasons described earlier. A description of the implementation follows.

8.4 Collision Detection

8.4.1 Setting Up the GJK Algorithm

Four sets of data are necessary to implement pairwise collision detection using the GJK algorithm. This data defines the vertices of the component convex hulls as well as the facets of the of the convex hulls. Take for example, the box and cone shown in Figure 65 below.

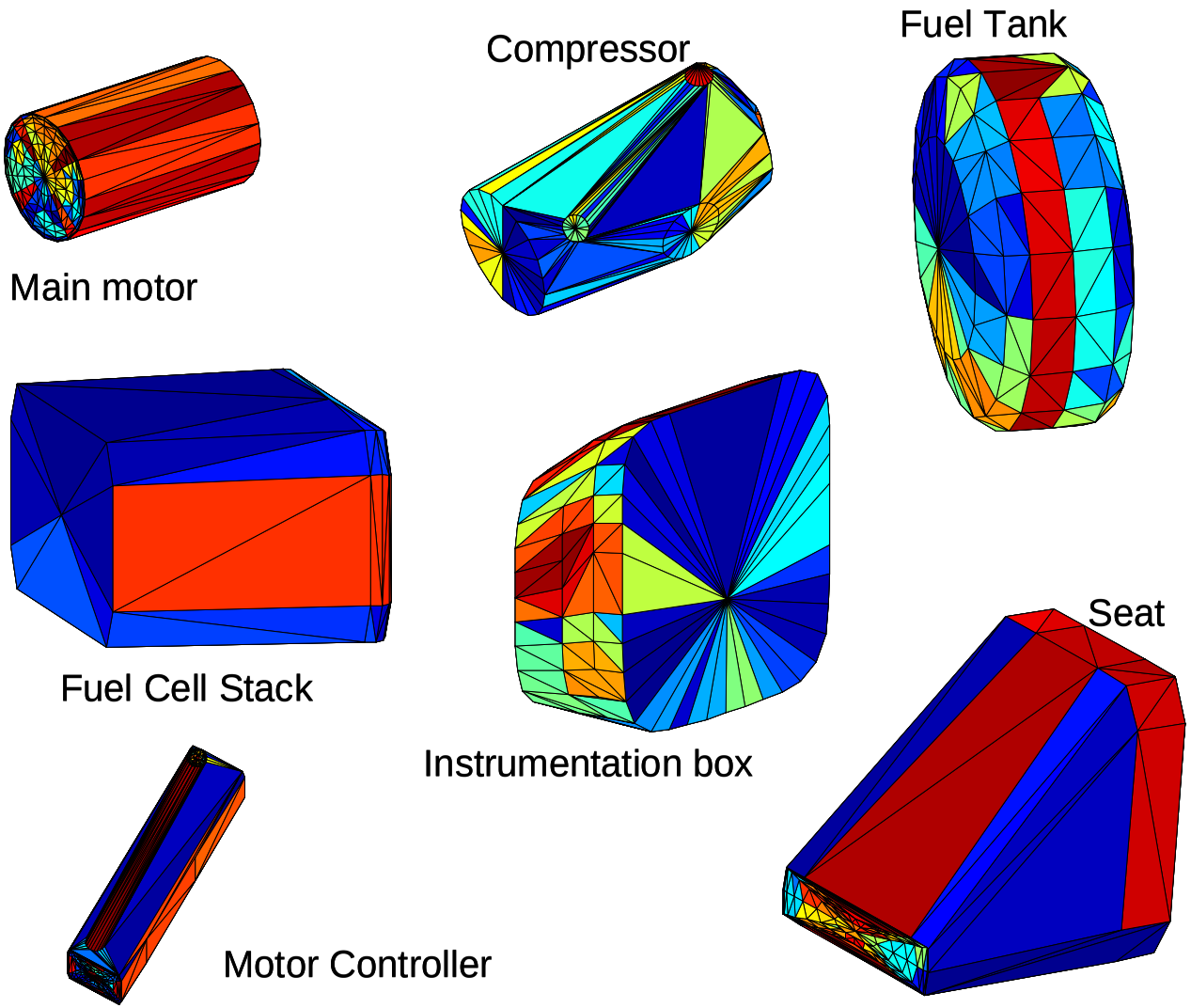

Figure 64: Convex Abstractions of Components

Table 10: Merits of Convex Approximation

Component	Number of Surface Points	Number of Hull Points	Compression Benefit	Compression Cost
Stack	317	124	60%	0%
Fuel Tank	190	140	26%	0%
Main Motor	65	42	35%	0%
Controls	168	139	17%	0.2%
Turbo Compressor	487	123	75%	23%
Motor Controller	1354	233	83%	26%

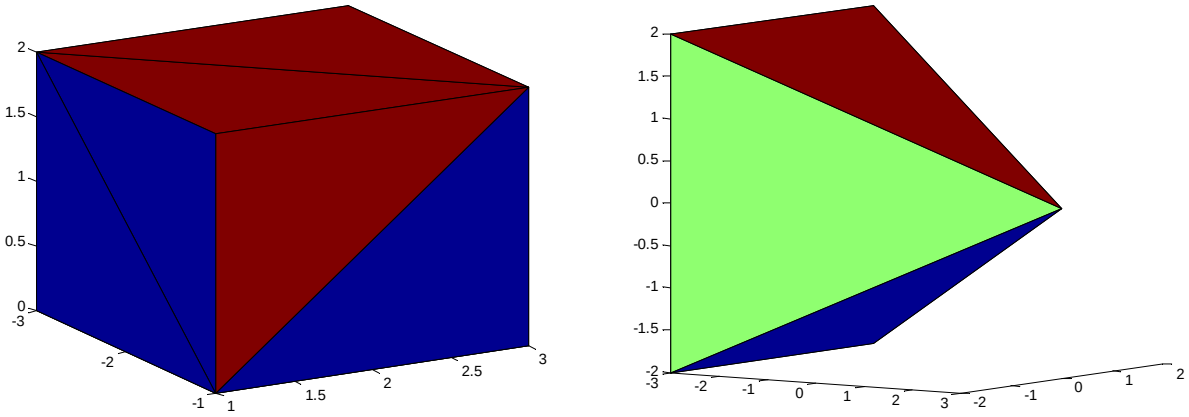

Figure 65: Box and Cone Convex Hulls

The corresponding vertex files are shown in Table 11 below.

-3	3	0
-3	1	2
-1	1	2
-1	3	2
-3	3	0
-3	1	0
-1	1	0
-1	3	0

-3	-2	2
-3	-2	-2
-3	2	2
-3	2	-2
3	0	0

Table 11: Box and Cone Vertex Files

The facets seen in Figure 65 are defined by means of a facets matrix. This matrix defines each facet on the convex hull by the index of the points that constitute its vertices. For the box and cone, the facets matrices are shown in Table 12 .

2	4	3
4	2	1
2	6	1
6	5	1
8	4	1
5	8	1
7	2	3
7	6	2
4	7	3
8	7	4
6	7	5
7	8	5

4	1	2
1	3	2
4	5	1
5	3	1
3	5	2
5	4	2

Table 12: Box and Cone Facet Matrices

By examining the facet matrices, the adjacency of the facets can be evaluated easily. In Table 13 below, each row i corresponds to an individual facet and the numbers in the row denote all other facets which share at least one vertex with this facet i.

4	2	6	5	8	
4	3	1	6	7	
2	4	7			
2	3	1	8	7	
6	1	8	7		
2	1	5	7		
2	3	6	4	8	5
4	1	5	7		

5	4	2	3
4	1	3	5
1	2	5	
1	2	5	
4	1	3	2

Table 13: Box and Cone Adjacency Matrices

By defining this relational data structure, the algorithm is able to reconstruct the simplices of any polyhedron without the need for any additional rules. The reconstruction

process is illustrated in Figure 66 below. Vertices 4, 7 and 8 describe Facet 4. Facet 4 is "neighbored" by Facets 2,3,7 and 8. By consolidating this information, any polyhedron can be reconstructed in mathematical space.

8.4.2 GJK Outputs

Whereas the GJK algorithm can accurately calculate the separation distance between objects, the calculation of overlap or penetration is quite challenging as previously discussed in §7.2.6.2. Buckley [37], Cameron [40], Kim [104], Ong [148] and Zhang [223] all provide methodologies by which this distance may be estimated. The reliability of these estimates varies from case to case. Thus for purposes of guiding an optimizer, these estimates are not very useful.

Figure 67 shows a scenario where two objects are in contact. In this case, the GJK algorithm will accurately return 0 as the separation distance. If the objects are moved closer together along the axis of collision, the algorithm can either return 0 or an estimate for the penetration distance. Since each object has a minimum clearance requirement denoted as C_j, contact is not a necessary condition for a layout to be classified as colliding. In fact the two components i and j are classified as colliding if $d_{ij} < max\{C_i, C_j\}$. To circumvent the problem of unreliable penetration distance estimates, the optimizer can instead track the number of collisions with the goal of reducing this number to 0. In this way, other volumetric metrics such as packing efficiency can be maximized while making sure that there are no collisions. Once a layout has been identified, its implications for system level metrics such as the fineness ratio of the fuselage must be evaluated. This procedure is achieved by using a convex hull of the entire layout i.e super-hull.

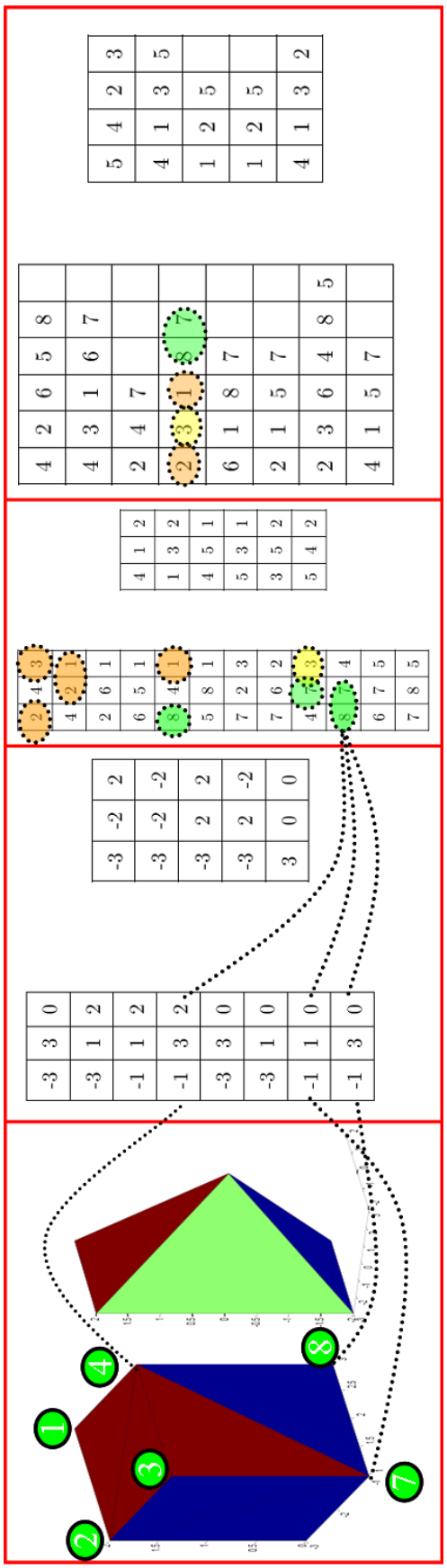

Figure 66: Relationship Between Data Structures

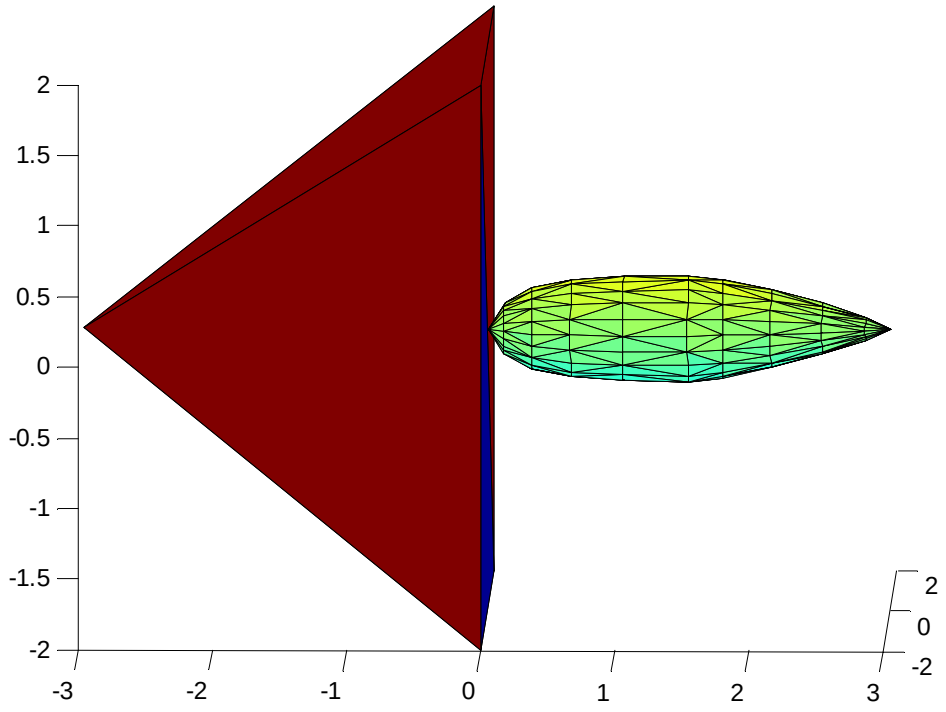

Figure 67: Contact Scenario

In order to test the hypotheses, an integrated modeling and simulation environment was created on the software integration platform, Modelcenter®. A schematic of this environment is shown in Figure 68.

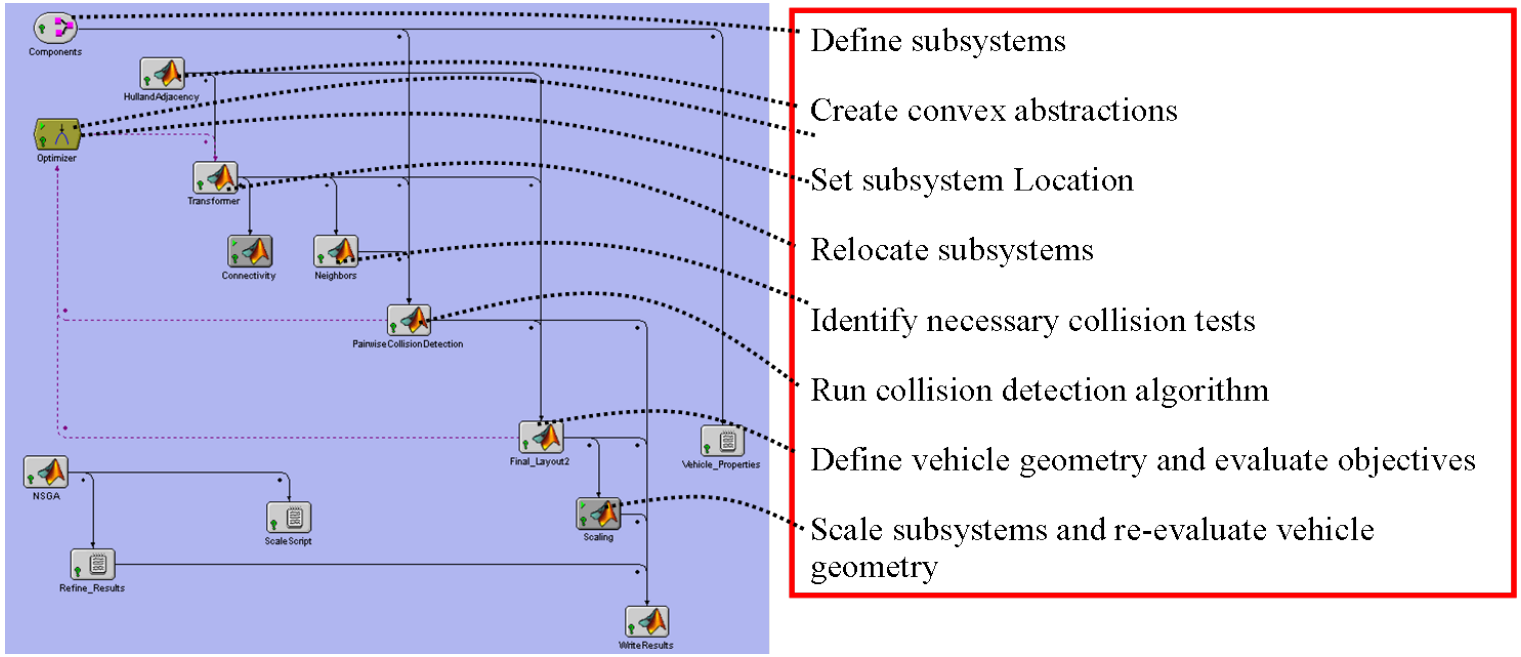

Figure 68: Integrated Modeling and Simulation Environment

Chapter IX

RESULTS AND ANALYSIS

The design of a PEM fuel-cell powered general aviation aircraft was used as a proof-of-concept for the postulated methodology. The two key focus areas were first of all the identification and definition of the appropriate baseline geometry space and second the derivation of custom scaling laws for any chosen configuration. A discussion and an analysis of the results from this research follows.

9.1 Configuration Space Exploration

9.1.1 Exploration of Various Subsystem Layouts in 3D space

Hypothesis : A domain spanning algorithm acting on the location and orientation variables of the subsystems with respect to a fixed axis can be used to explore the design space.

The design space was explored by means of the Non-dominated Sorting Genetic Algorithm (NSGA-II). A number of other domain-spanning techniques such as grid searches or simulated annealing could also be applied to the problem. The main advantage of the NSGA-II algorithm over other competing techniques is the explicit measures against speciation and genetic drift that are critical to ending up with a diverse baseline configuration space . As this is a conceptual stage analysis, it is important that a diverse configuration space be fed to subsequent phases of the design process. Local searches around the diverse members of this population increase the chances of arriving at the optimum.

9.1.2 Mapping Component Level Data to System Level Metrics

Hypothesis: A minimum enclosing envelope can be evaluated for all candidate layouts using convex hulls. This "first order" geometry representation can be used to evaluate constraint/target values for system level metrics and as an indication of the basic shape of the vehicle.

The use of a convex enclosing body or a set of convex enclosing bodies to define the inner mold line of a vehicle fuselage satisfactorily represents the basic shape of the enclosing body. This was illustrated in Figure 64 and Table 10. For situations where the approximation cost i.e. $\frac{Hull\,Volume}{Component\,Volume}$ was too great, a decomposition approach was recommended. Here, a complex shape is broken down into a few simpler shapes for which individually have low approximation cost. The summative approximation cost for the corresponding will decrease accordingly. The computational penalty (in terms of number of extra collision detection analyses) associated with going from n components to $n + \triangle$ components where $\triangle$ is the number of subsets of the complex shape less 1 is less or equal to $\frac{\triangle}{2}(2n - 1 + \triangle)$. A short proof for this claim follows:

Given n components in a layout

$Maximum\,number\,of\,collision\,detection\,analyses = \frac{{}_nC_2}{2}$

$For\,any\,increase\,in\,the\,number\,of\,components\ = \triangle$

$Maximum\,number\,of\,collision\,detection\,analyses = \frac{{}_{(n+\triangle)}C_2}{2}$

$Change\,in\,maximum\,number\,of\,collision\,detection\,analyses = \frac{({}_{(n+\triangle)}C_2 - {}_nC_2)}{2}$

$= \frac{1}{2}((n+\triangle)(n-1+\triangle) - (n)(n-1)) = \frac{\triangle}{2}(2n-1+\triangle)$

Because a convex hull consists of triangular facets, it can be efficiently sliced in order to obtain system level metrics such as maximum cross-sectional area, length and stream-wise growth of cross-sectional area. This is achieved by

9.1.3 Mapping a Layout to a Vehicle Geometry

The final population of the genetic algorithm process forms the basis for the refined configuration space from, which the optimal baseline concept will be derived. A superhull is evaluated for each layout. The superhull is then sliced along the x-axis in sections that lie in the yz plane if x is taken as the flow direction. An offset factor, $0.05\,ft$ in this case, is added to these dimensions in order to define the final fuselage geometry. Once the fuselage is defined, lifting and control surfaces i.e. the wing and the empennage are added to the

vehicle. It should be noted that for this study, these surfaces are not optimized beyond the minimum requirements of having sufficient lift from the wing and maintaining a desirable tail volume coefficient. At this point in the design process, critical contributing analyses such as aerodynamics, stability and control and vehicle structures can be brought on board in order to rate and rank different geometries. Figure 69 to Figure 78 show 10 geometry samples out of a population of 30 in the three hundredth generation of the NSGA-II algorithm. (The wings are cropped in order to allow for a clearer view of the layouts.) The Cartesian co-ordinates of each subsystem are shown in the appendix section §**??**.

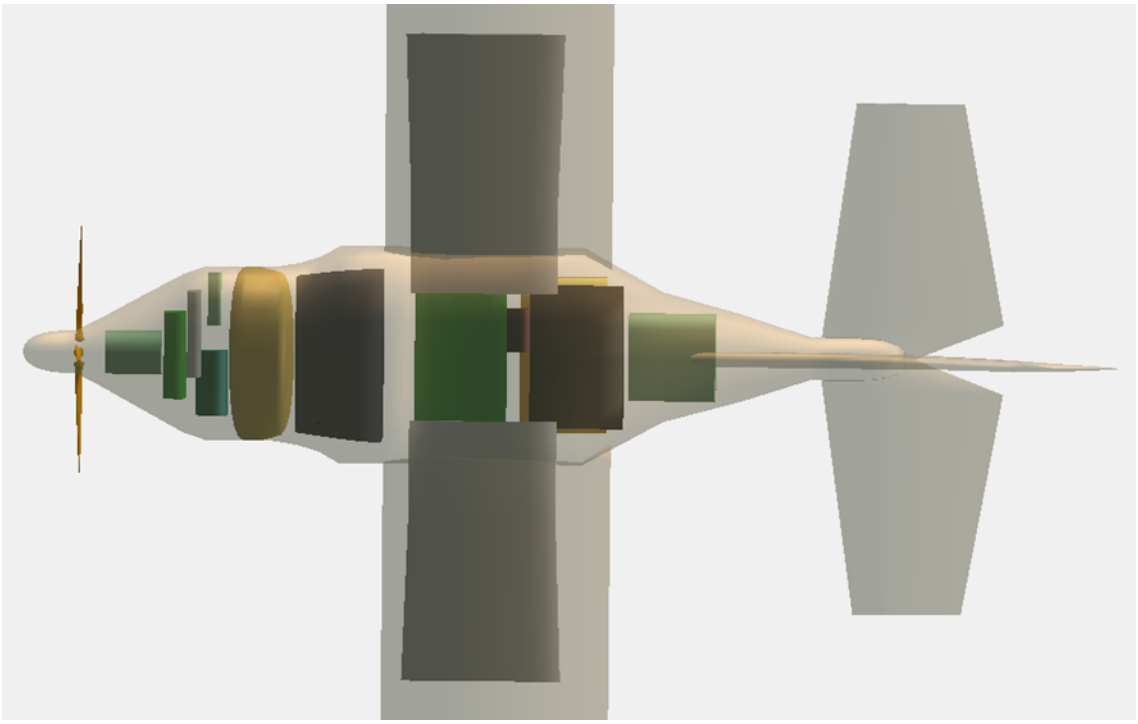

Figure 69: Configuration 1

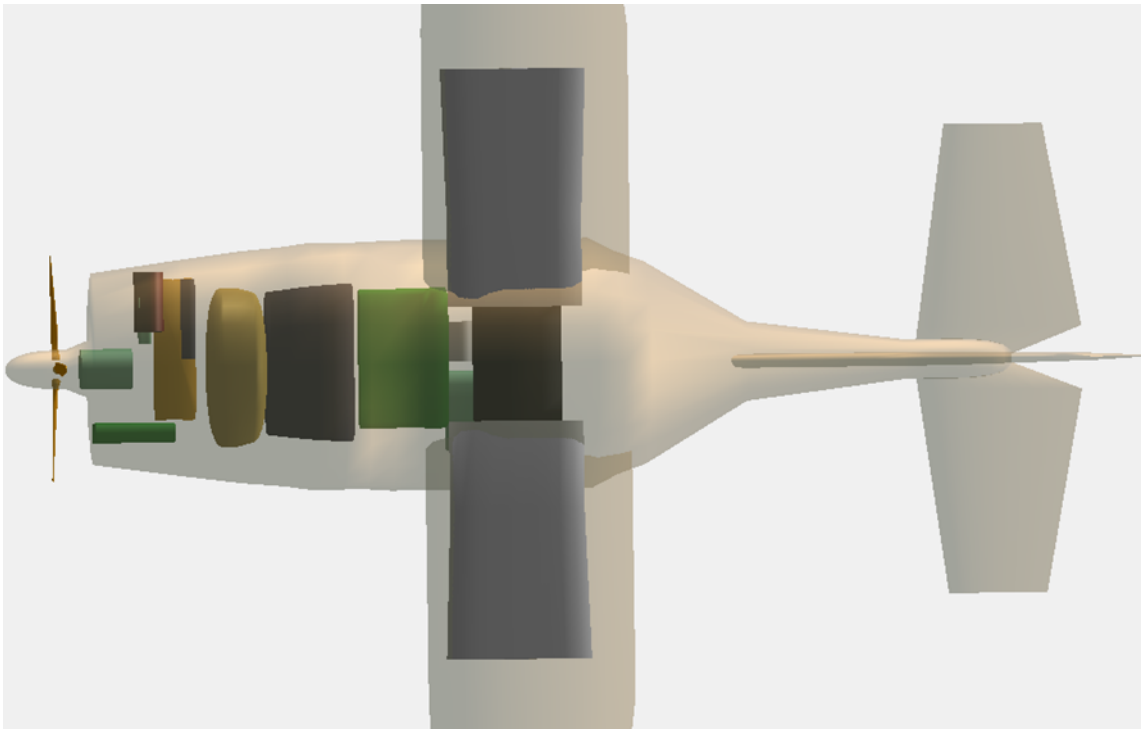

Figure 70: Configuration 2

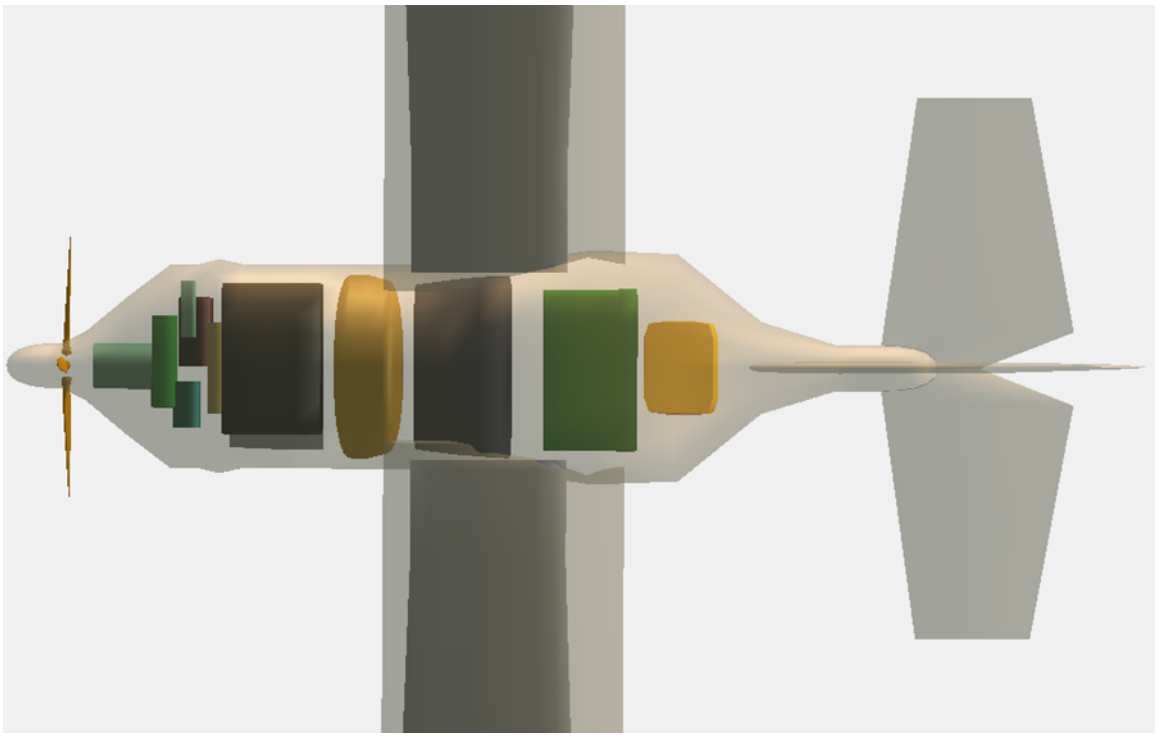

Figure 71: Configuration 3

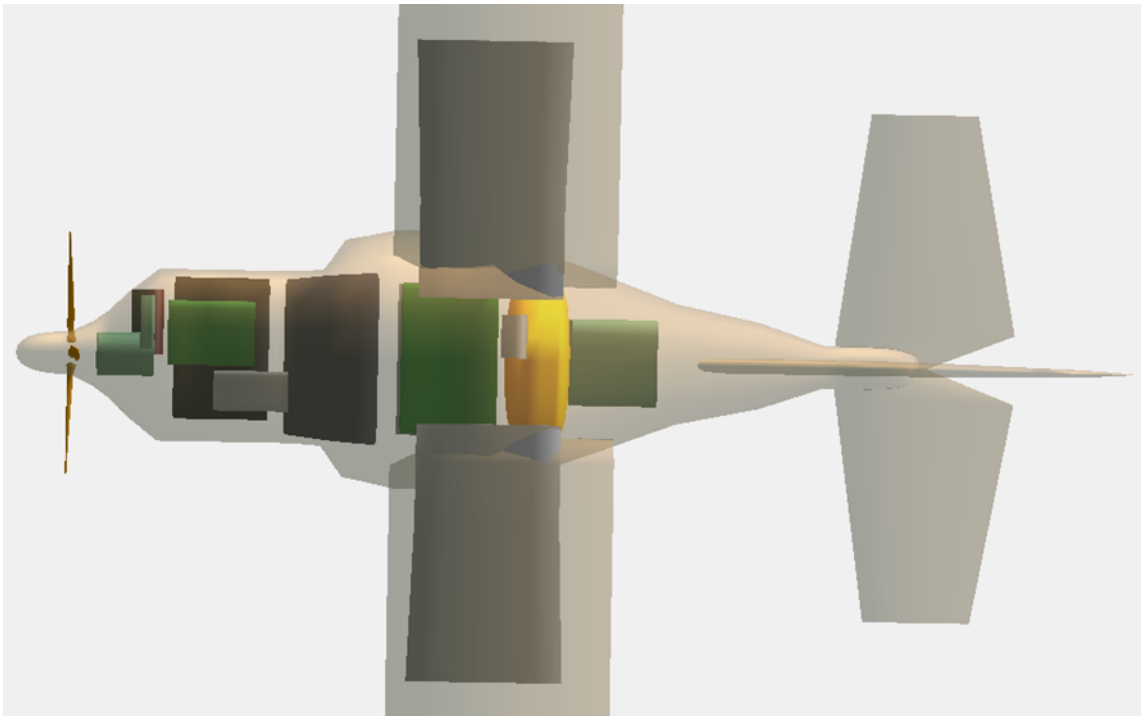

Figure 72: Configuration 4

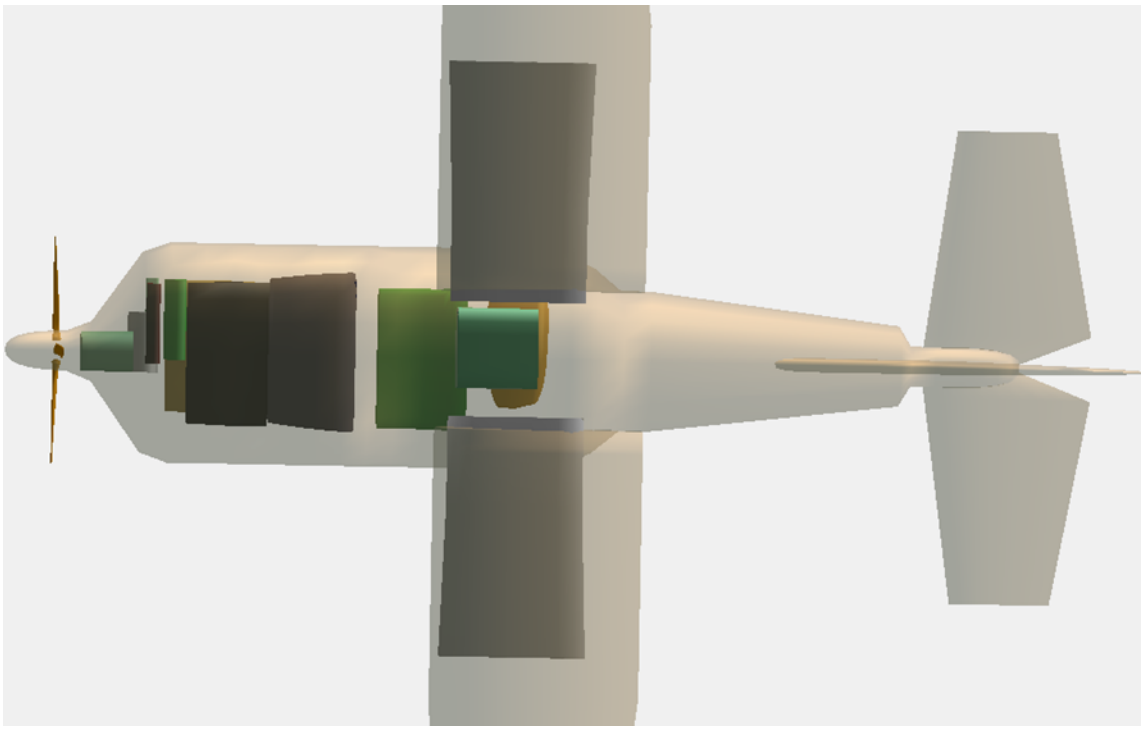

Figure 73: Configuration 5

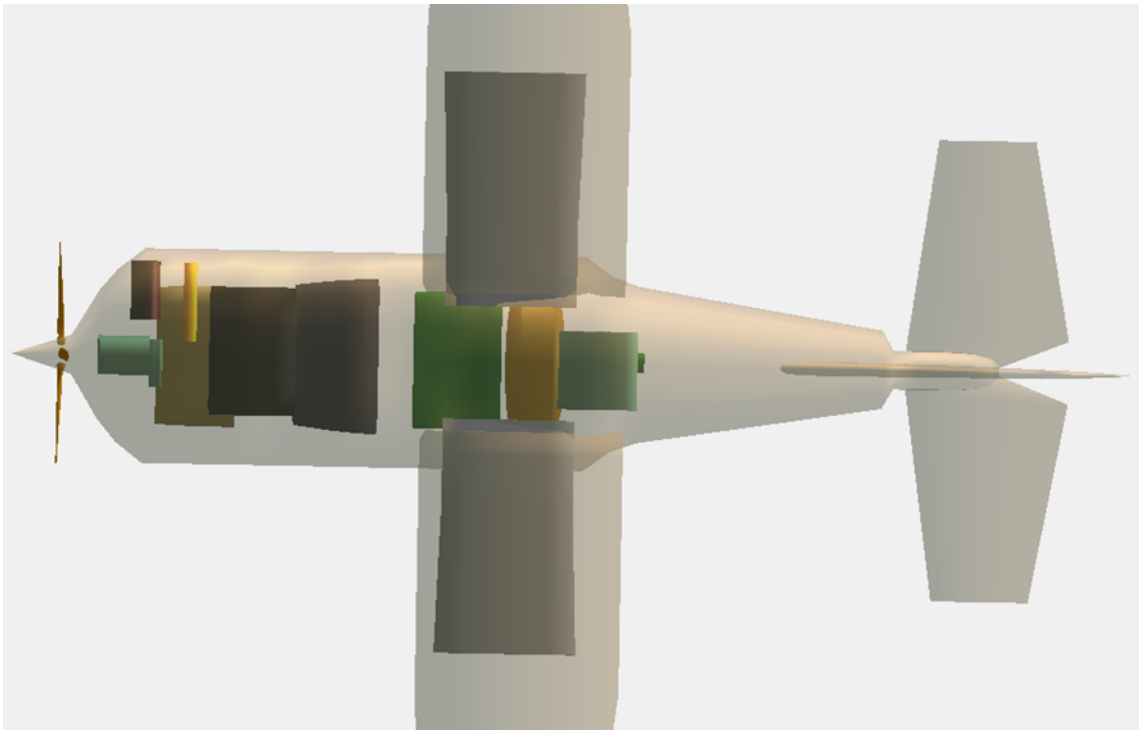

Figure 74: Configuration 6

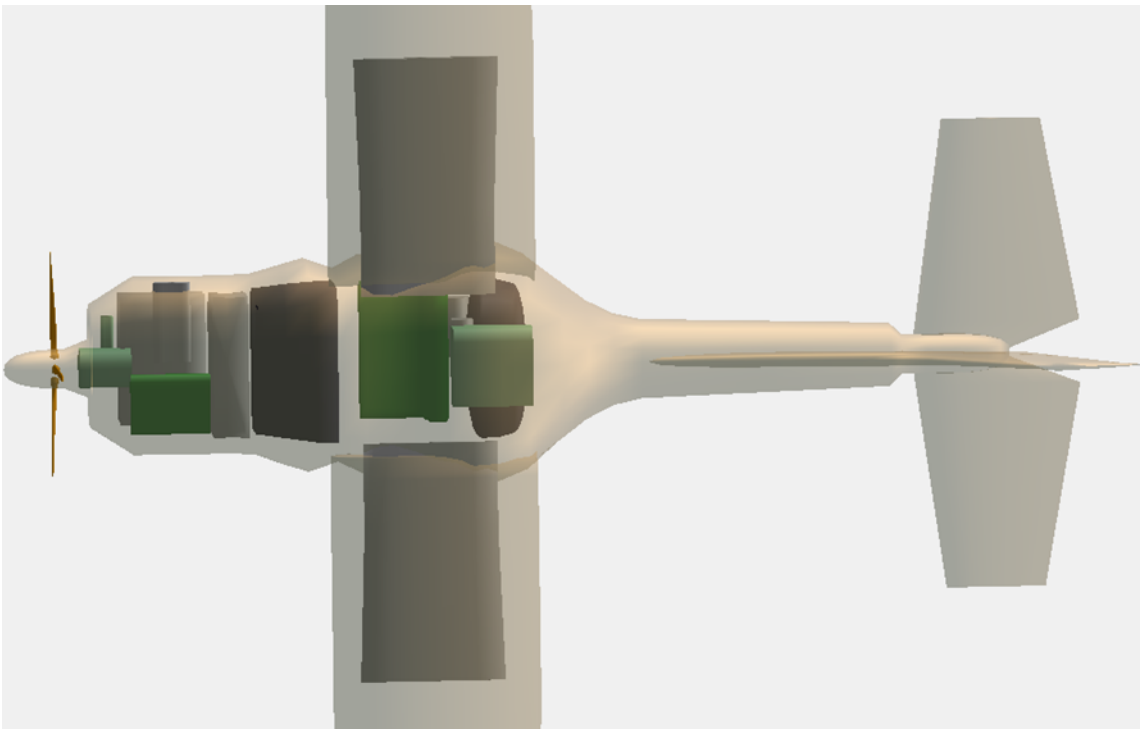

Figure 75: Configuration 7

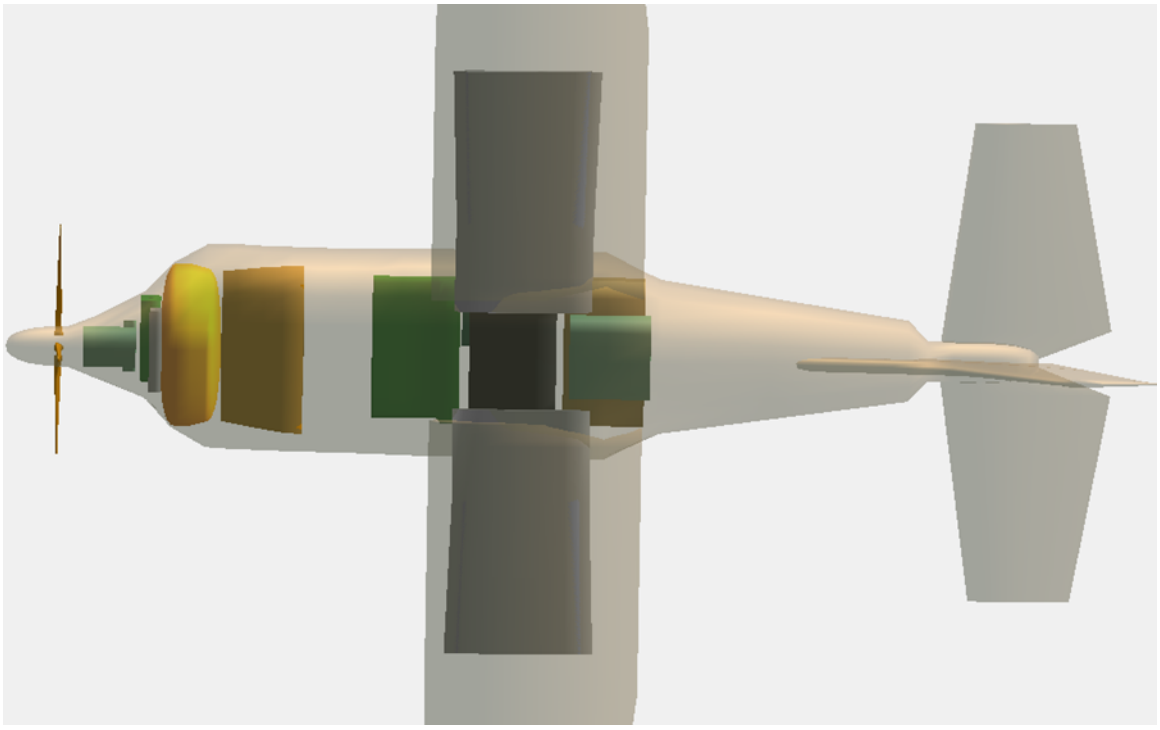

Figure 76: Configuration 8

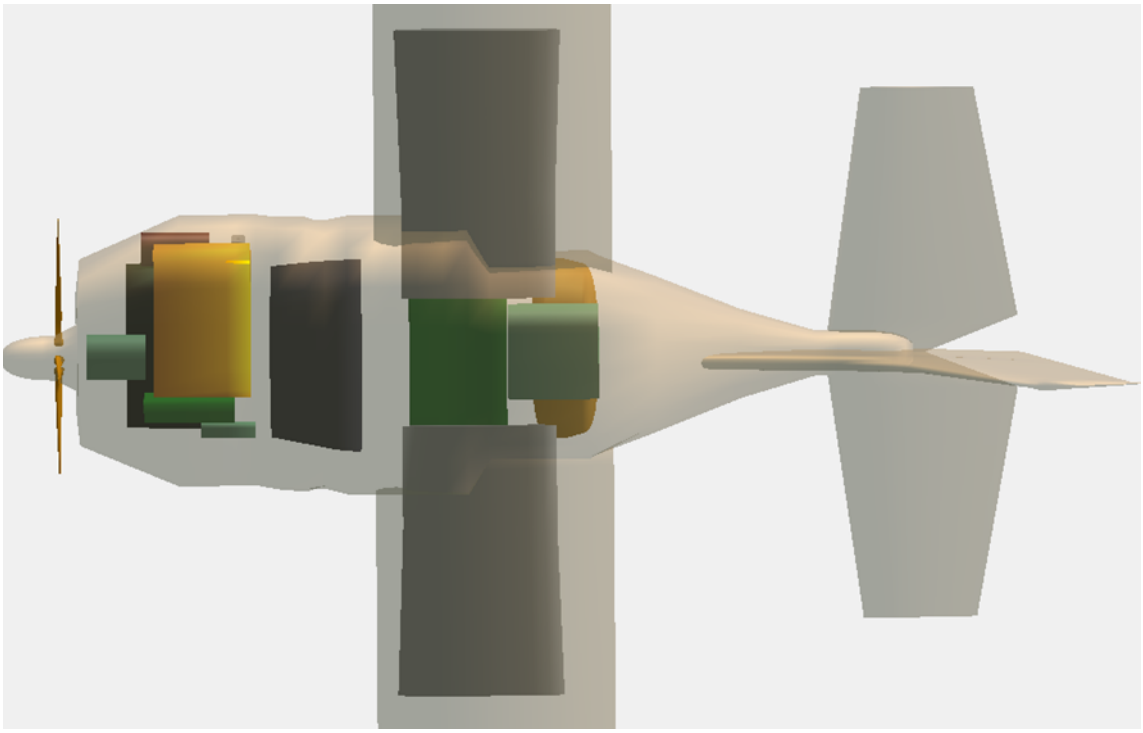

Figure 77: Configuration 9

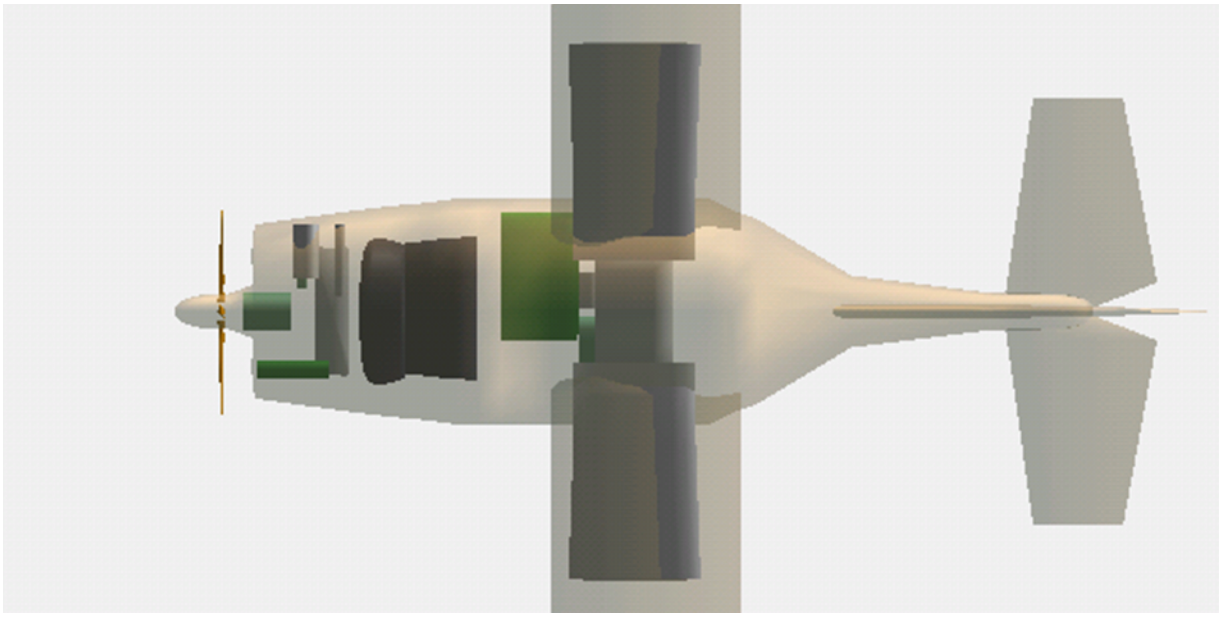

Figure 78: Configuration 10

The corresponding inertial and volumetric characteristics of each configuration are shown in Table 14 below.

Case	Packing Efficiency	TOGW (*lb*)	Rx	Ry	Rz	SM
1	0.54	2659	0.26	0.45	0.34	0.10
2	0.52	2530	0.26	0.43	0.34	-0.06
3	0.67	2412	0.27	0.43	0.34	-0.15
4	0.59	2704	0.25	0.43	0.33	0.42
5	0.44	3019	0.25	0.43	0.33	0.04
6	0.54	2771	0.26	0.44	0.35	0.16
7	0.59	2567	0.27	0.44	0.34	0.08
8	0.68	2240	0.27	0.42	0.33	-0.19
9	0.65	2352	0.28	0.43	0.34	-0.11
10	0.35	3889	0.23	0.39	0.30	0.12

Table 14: Inertial and Volumetric Characteristics of Sample Configurations

9.1.4 Objective Functions

As discussed in §7.4.3.2 , a non-dominated sorting genetic algorithm was used in the exploration of this multimodal design space. The goal was to identify points at or close to non-dominated modes. The following metrics were used in the Pareto genetic algorithm optimization procedure.

9.1.4.1 Lift and Drag Characteristics

The lift and drag characteristics of the various configurations are compared using the maximum lift-to-drag ratio ($\frac{L}{D}$). For the proof of concept study, these characteristics are evaluated by comparing a high-fidelity panel code i.e. PANAIR [119] with a skin friction estimation tool based on empirical form factor relations developed by the Virginia Institute of Technology [120].

It was seen that the Hausdorff distance is not a reliable indicator of the $\frac{L}{D}$ characteristics of a vehicle as seen in Figure 79 below. There is no clear correlation between the similarity measure and the actual metric of interest i.e. the lift-to-drag ratio. Therefore the Hausdorff distance, though cheaper to evaluate can not used as an alternative measure of aerodynamic merit.

9.1.4.2 Stability

Both the static and dynamic stability characteristics of the vehicle must be taken into consideration in attempting to identify an optimal layout. The static stability margin of a configuration as described in Equation 72 was used as the measure of merit. A target of 5% was set as the ideal as this has been shown to be desirable for most aircraft [140].
Moments of inertia along the various force axes may also be estimated based on the component layout and the aircraft structure. A target of $R_t = [0.25,\ 0.38\,, 0.39]$ for the x, y and z radii of gyration is used for the proof of concept study. These targets are based on historical data in Raymer [160].

The following additional figures and assumptions were used in the proof of concept study:

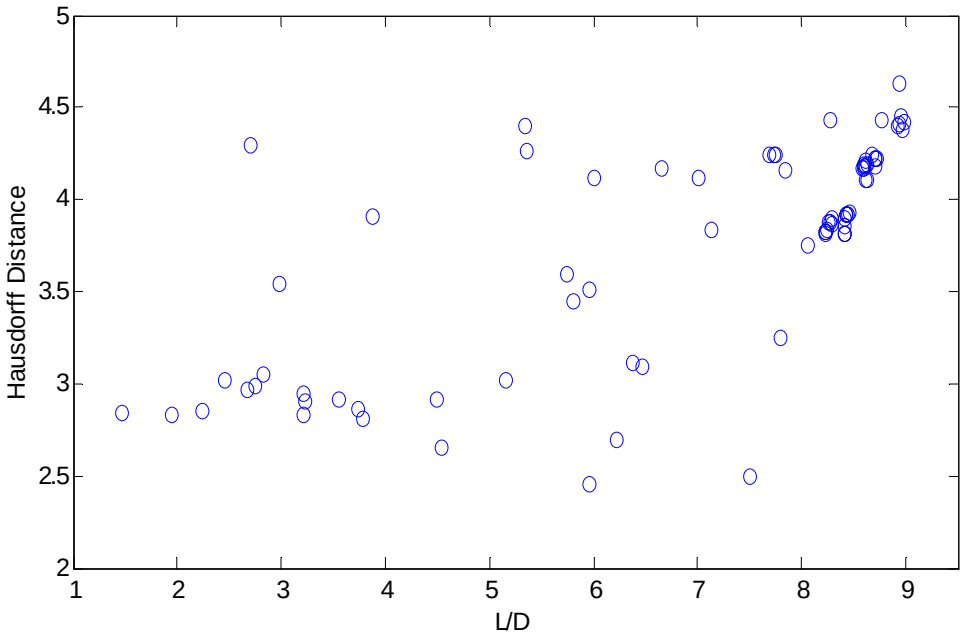

Figure 79: Hausdorff Distance as an indicator for $\frac{L}{D}$

$$\begin{array}{|l|}\hline \eta = 1 \\ C_{L_{\alpha t}} = [0.07, 0.09] \\ C_{L_{\alpha w}} = [0.08, 0.09] \\ \frac{d\varepsilon}{d\alpha} = [0.3, 0.4] \\ \hline \end{array} \quad [160,\ 140]$$

The overall objective function is formulated by aggregating the static and dynamic stability metrics as shown in Equation

$$S = -|R_t - R| - |0.05 - S_m| \tag{85}$$

$$\begin{array}{|l|}\hline where: \\ R = [R_{xx}, R_{yy}, R_{zz}] \\ S_m : Vehicle\ static\ margin \\ \hline \end{array}$$

9.1.4.3 Symmetry

Symmetry in the plane perpendicular to the freestream direction can have a big impact on the aerodynamic and handling characteristics of a vehicle. Though asymmetric vehicles have

been shown to fly just as well with the right control surface design, metrics such as that in Equation 61 can be used to drive the optimization process towards more conventional symmetric designs.

9.1.4.4 Smoothness

Small deviations from the ideal body streamlines do not significantly impact drag as long as the streamwise cross-sectional area distribution is smooth [10]. The mean value of the moving average of the rate change of cross-sectional area was used as measure of the smoothness of a given configuration. This metric forms a second indirect aerodynamic metric for the vehicle. This metric constitutes a partial consideration of some of the higher order effects that the low fidelity panel codes may not capture.

9.1.4.5 Packing Efficiency

This metric is evaluated using Equation 39. The aim is to get this value as close to the target value as possible. When all subsystems are considered, this target would be set at 1. However, as this approach adds significantly to the computational expense incurred, it is recommended that only the major subsystems be modelled and that a target bracket in the range of 0.6 to 0.9 be set based on the class of vehicle and the number of minor subsystems left out. A value greater than one indicates that there are some collisions. It is also worth noting that a value less than one does not necessarily guarantee a collision-free layout.

9.1.4.6 Connectivity

The connectivity metric was used to push components closer together or further apart based on settings in the connectivity or affinity matrix defined by the designer. For this study, the entries used ranged from -1 to 1. The sign is used to indicate if closer is better or vice versa while the magnitude of the entry indicates affinity degree i.e. how close is optimal. For example an entry of 1 indicates that the separation distance of the concerned subsystems should be as close to the minimum required clearance as possible. The metric was mathematically quantified as :

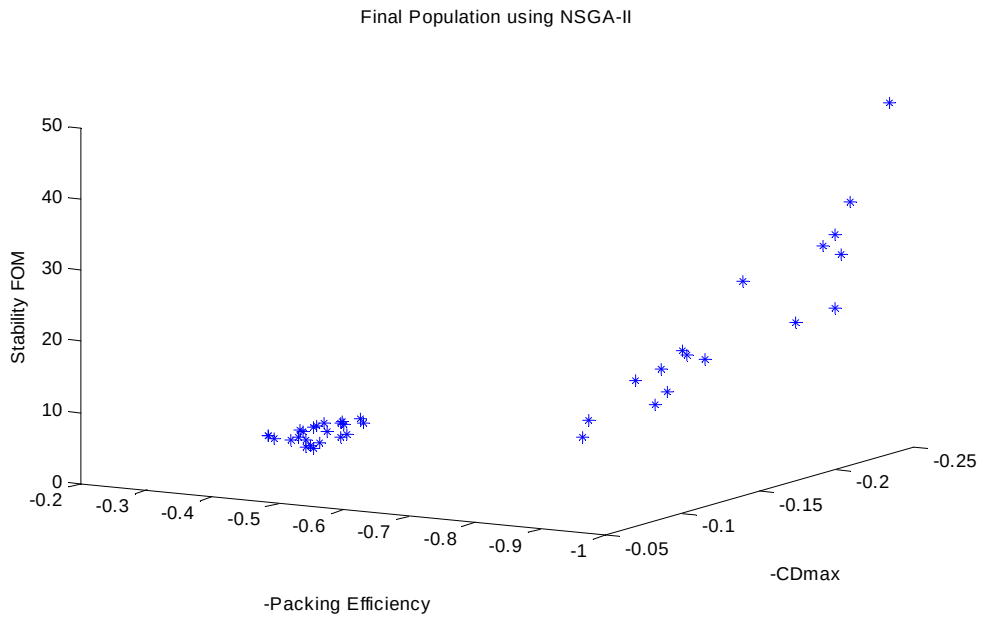

Figure 80: Sample Speciation Graph, Population= 40, Generations= 50

$$C = \sum_{i=1}^{n-1} \sum_{j=i+1}^{n} d'_{i,j} \cdot c_{i,j} \tag{86}$$

$where:$

$d_{i,j} = Distance\, between\, components\, i\, and\, j$

$d'_{i,j} = \left\{ \left[\frac{1}{d_{i,j}}\ if\ c_{ij} > 0,\ Closer\ is\ better \right], [-10000\ if\ d_{ij}\ less\ required\ clearance] \right\}$

$d'_{i,j} = [d_{ij}\, if\ c_{ij} < 0,\ Further\ is\ better]$

$c_{i,j} = Affinity\, matrix\, entry\, i, j$

It was hoped that the penalty for clustering would result in a diverse population in a minimal number of generations (computational expense). It was, however, observed that when the number of generations is less than $O(10^2)$ speciation is likely to occur. This phenomenon is demonstrated in Figure 80. A clear divide based on volumetric packing efficiency emerges after about 50 generations.

To increase the likelihood that a high quality well diversified final population is achieved, a setting of $O(10^3)$ generations is recommended.

9.2 Exploration of Baseline Configuration Space

Hypothesis : The baseline configuration space around a given technology can be rapidly explored by coupling reduced complexity component models with a fast collision detection algorithm.

The exploration of the configuration space entails the creation of various designs and then comparing them to each other by using the appropriate set of objective functions. Key to the success of this process is the mitigation of the inherent compuational expense.

9.2.1 Discussion of Computational Expense

9.2.1.1 Algorithm Speed Test

The algorithm speed was tested on a platform with a 2.4GHz processor and 2 GB of RAM. Models for the battery, balance of plant, a simple box, the compressor, a cone, the controls panel , the fuel cell controller and the pump were tested for collision on a round-robbin basis. The total number of points of each polyhedron pair is plotted against the time take to return a solution in Figure 81. On this platform, the process takes $\sim 2 \cdot 10^{-4}$ seconds per point. Therefore on this platform, the worst expected performance would be $O\left(10^{-4+O(p)+O({}_nC_2)}\right)$. To compensate for the coarseness of the timing clock, each setting was run 100 times and the average time was used for the preceding calculations.

The key take-aways here are first of all that the expected linear time complexity of the GJK algorithm is seen to hold even for this shape-diverse set of component models. The marginal cost of each additional subsystem or increase in subsystem model complexity is not therefore rise exponentially. Second, at $O(10^{-4})$ time expense, $O(10^3)$ generations of an $O(10)$ size population consisting of average subsystem models (10 to 20 components of about 500 points each in the author's opinion) can be readily analyzed in $O(10)$ hours on an average computational platform. This figure will vary based on the computational cost of the additional objective functions.

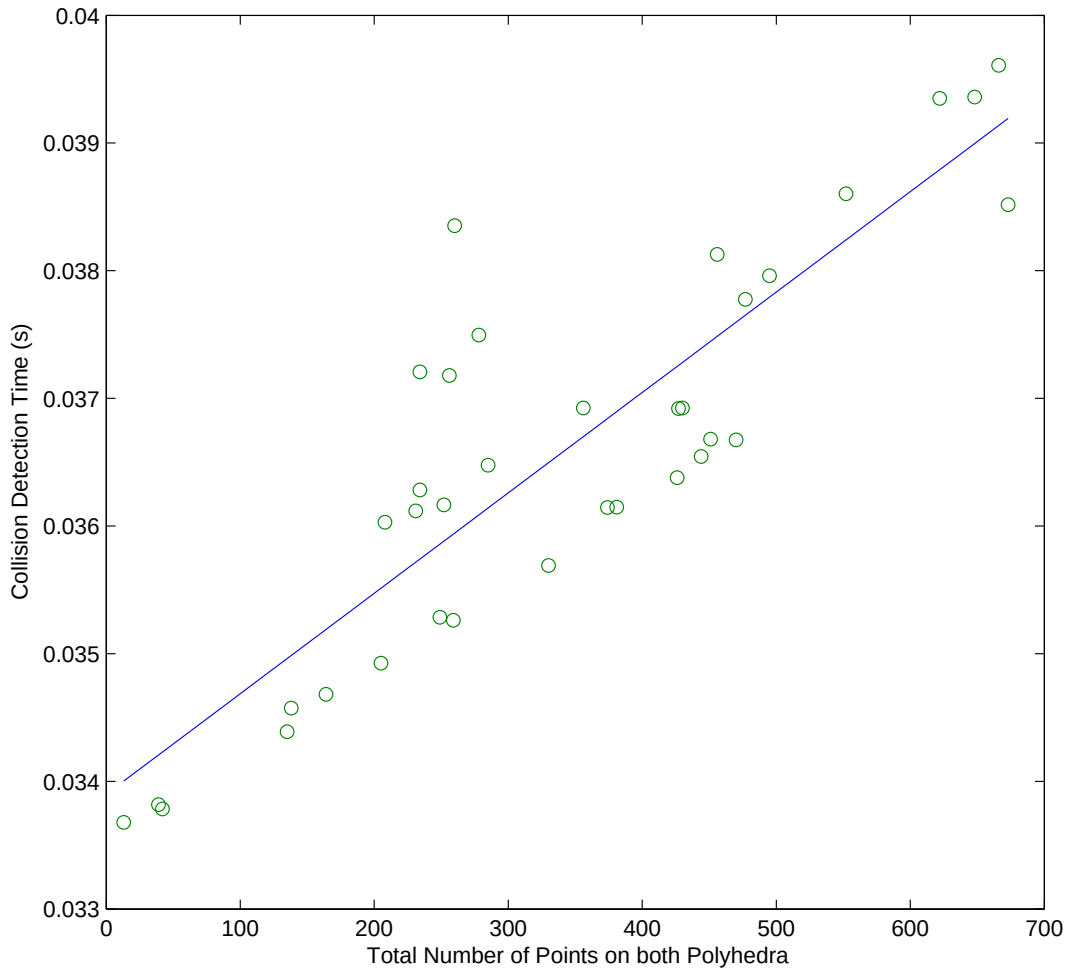

Figure 81: Collision Detection Speed as a function of number of points

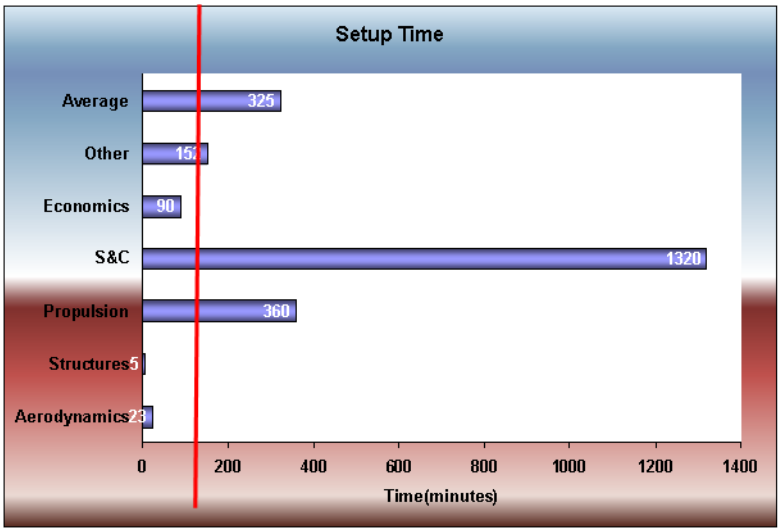

Figure 82: Set-up Time Expense Comparison

9.2.1.2 Time Expense for Proof of Concept

The NSGA-II algorithm was run with a population of 20 configurations over 200 generations. Each configuration consisted of 12 components with up to 6 degrees of freedom depending on the subsystem. The instrumentation box for example had no rotational degrees of freedom whereas the cylindrical fuel tank had two rotational degrees of freedom. Seven objectives were used in the optimization process namely : packing efficiency, maximum lift-to-drag ratio, static margin (target 5%), number of collisions, a connectivity metric, estimated take-off gross weight and superhull symmetry based on the Balinsky distance. The total time expense on this test bed was 4413 minutes. This equates to 1.47 minutes per case. When compared to the results of the conceptual design tools/ methods run time survey results, this approach compares very favorably to the other disciplines as shown in Figure 83.(Note: The vertical line represents the CESM time expense.) A similar comparison for the required set up time is shown in Figure 82. It must be noted that the latter results are subjective. They are used here to show that the time expense incurred can indeed fall within the ball-park defined by other conceptual design analyses.

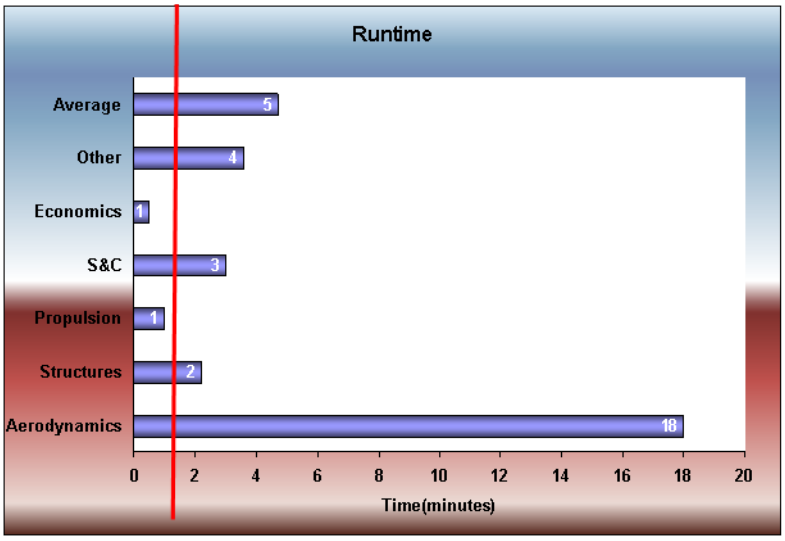

Figure 83: Run Time Expense Comparison

9.2.2 Handling Geometric Uncertainty

Hypothesis: Geometric uncertainty can be incorporated into the search for an optimal geometry by first quantifying the expected uncertainty costs of a volume surplus or deficit either in the design cycle or even in the system life-cycle and then choosing the geometry that minimizes total expected cost of not meeting requirements.

Two major challenges were faced in validating this hypotheses. First of all, the News Vendor model assumes constant unit overage and underage costs.

This cost can be quantified either in the form of redesign costs or changes in vehicle life-cycle costs. A surplus or deficiency in the volume available in a final concept can result increased design and/or life cycle costs. These costs can come in the form of increased design cycle time as design assumptions are re-examined and many analyses are repeated. If the sunk cost is already too great, the selected concept may pass on to prototyping and final design testing. The costs resulting from this decision recur all through the life-cycle of the system. The cost of flying an oversize aircraft will manifest itself in higher operating costs such as fuel and maintenance. Likewise a vehicle that is too small for its intended mission may have to perform multiple sorties to achieve the mission requirements for which it was intended. Thus the designer must do all he can to ensure that by the time the sunk cost is

so high that the process' absorptive capacity for new design information or realizations is really limited, all expected uncertainty costs have been minimized.

Defining the target volume for the vehicle and its subsystems is a direct function of the estimated overage and underage costs. In an aircraft design predicting these costs entails the mapping of requirements violation or over-satisfaction to the affected analyses and thereafter predicting the total cost of re-running each of those analyses. Even though the mean unit cost of each analysis may be reliably predicted via experimentation or past experience, *the total cost of a specific modification may entail multiple iterations the number of which would be hard to predict before hand.* This hypothesis failed based on this observation. The designer could experiment on the candidate layouts in order to determine a distribution of overage or underage costs for the major subsystems and then base the News Vendor analysis on these analyses. Alternatively a probabilistic analysis where the costs could be represented by uniform distributions could also be used. Justifying these distributions or validating these hypotheses would entail building at least one complete vehicle model with sufficient fidelity analyses for all key areas such as structures. Since this is beyond the scope of the research objectives stated herein, it is left to future work.

9.3 Capturing Requirement-induced Geometric Change

Hypothesis : Configuration scaling laws can be used to capture the geometric evolution of a given concept. These laws can be derived through a combination of dimensional analysis and statistical regression techniques. Custom data for the statistical regressions can be obtained via an automated bottom-up parameter space exploration approach.

9.3.0.1 Information Flow

The flow of data through the CESM process to the scaling algorithm is shown in Figure 84.

The parameters listed in Table 15 are used in the scaling law analysis for the proof of concept study. The symbols L, M and T represent units of length, mass and time respectively.

The impact of the PEM fuel cell specific power on fuselage volume is quantified in the

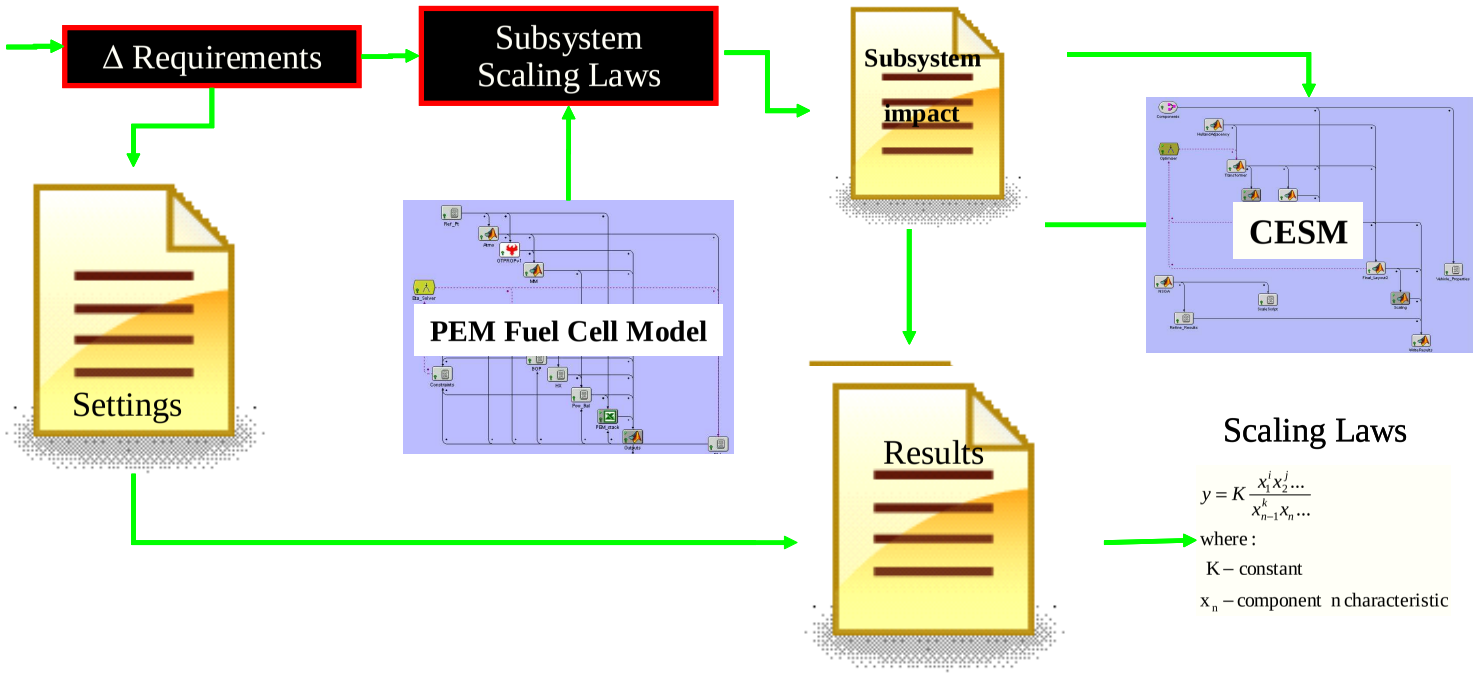

Figure 84: Derivation of Scaling Laws

Parameter	Description	Units
a	Speed of Sound	$\frac{L}{T}$
g	Gravitational Acceleration	$\frac{L}{T^2}$
ρ	Density of Air	$\frac{M}{L^3}$
μ	Viscosity	$\frac{M}{LT}$
c	Wing Chord	L
S	Wing Planform Area	L^2
ϑ	Cruise Speed	$\frac{L}{T}$

Table 15: Scaling Law Dependent Variable Candidates

Equation 87. Using this equation the required specific power to achieve a given fuselage volume, power and altitude combination can be readily and easily evaluated.

$$V_{fus} = e^{-3.6} \cdot \frac{W_{fc}}{\rho_{air} \cdot g} = e^{-3.6} \cdot \frac{W_{fc}}{P} \cdot \frac{P}{\rho_{air} \cdot g} \tag{87}$$

where :

W_{fc} : *Fuel Cell Weight*

ρ_{air} : *Ambient Density*

g : *Gravitational Acceleration*

The predictive power of the scaling law in Equation 87 is validated in Figure 85.

In Equation 88,the specific power of the PEM fuel cell is listed as a predictor for the take-off gross weight of the vehicle. The necessary power density for a given a power, altitude and take-off gross weight combination can be readily evaluated.

$$TOGW = e^{-1.17} \cdot V_{fc} \cdot \rho_{air} \cdot a^2 = e^{-1.17} \cdot \frac{V_{fc}}{P} \cdot P \cdot \rho_{air} \cdot a^2 \tag{88}$$

where :

V_{fc} : *Fuel Cell Volume*

a : *Sound Speed*

ρ_{air} : *Ambient Density*

P : *Power Available*

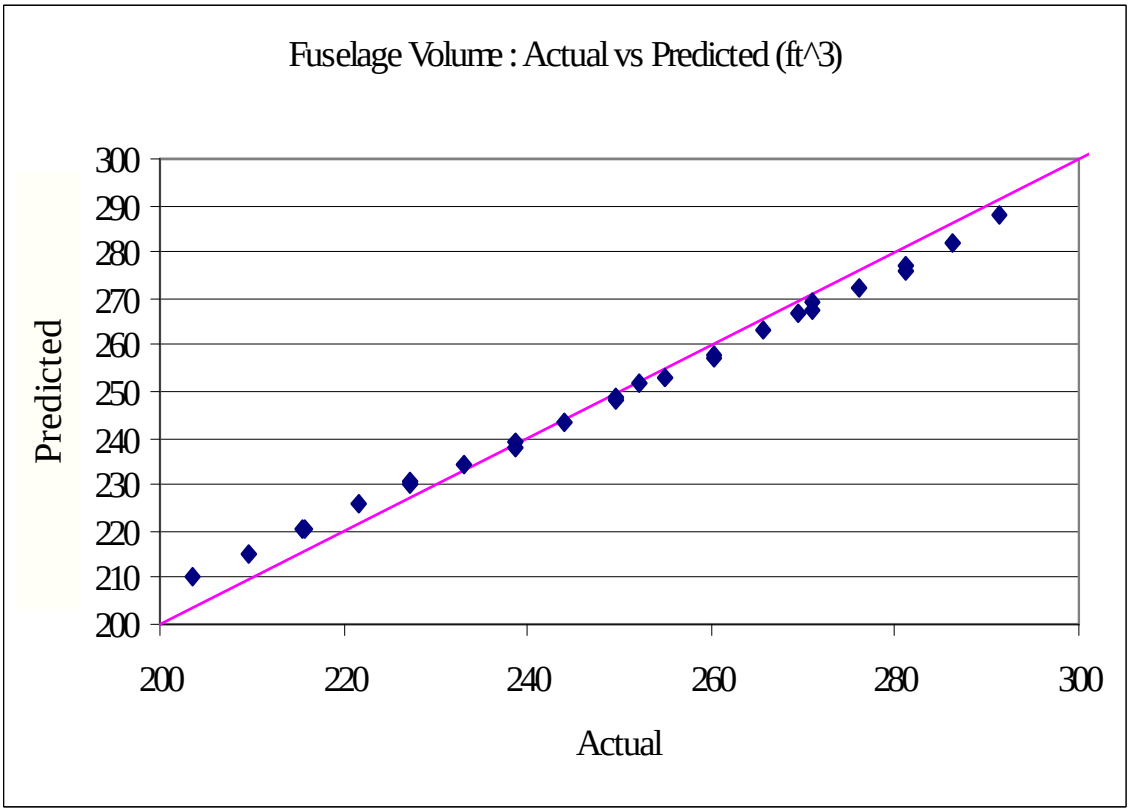

Figure 85: Actual vs Predicted Fuselage Volume

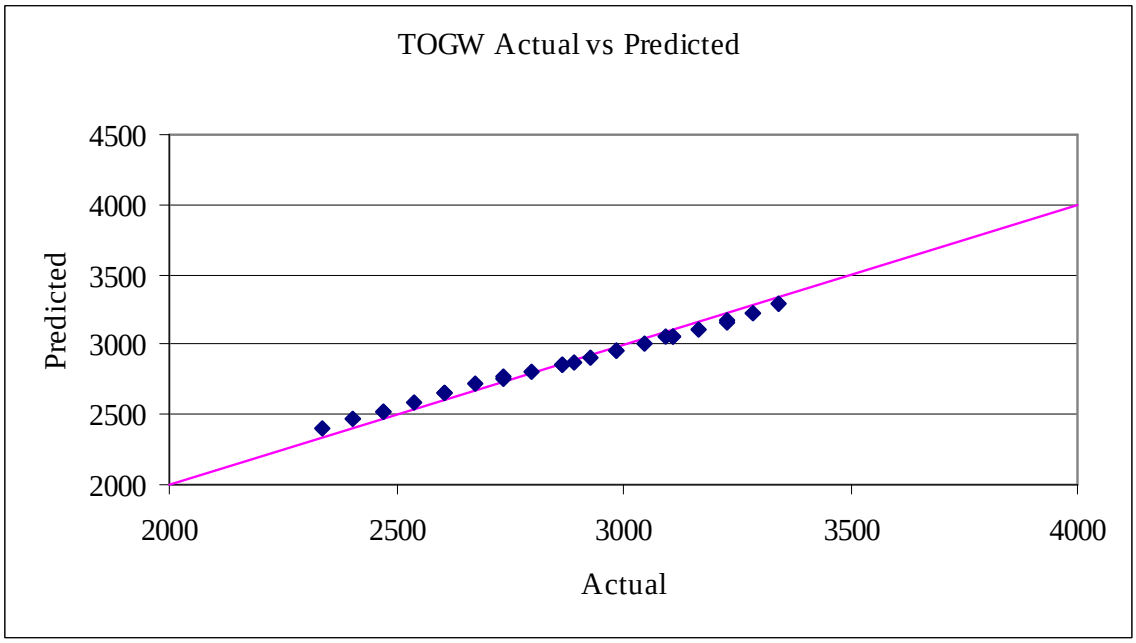

Figure 86: Actual vs Predicted TOGW

The predictive power of the scaling law in Equation 88 is validated in Figure 86.

As expected the more parameters that are considered in the scaling analysis, the higher the number of dimensionally consistent scaling laws that can be derived. Naturally, the predictive power of each scaling law is determined by the pertinence or relative influence of the parameters used in deriving it.

$$V_{fus} = \left(\frac{W_{fc}}{\mu}\right)^{\frac{5}{2}} \frac{1}{\vartheta\sqrt{\vartheta g}} \tag{89}$$

$where$:

W_{fc} : $Fuel\ Cell\ Weight$

ρ_{air} : $Ambient\ Density$

μ_{air} : $Ambient\ Viscosity$

ϑ : $Vehicle\ Speed$

g : $Gravitational\ Acceleration$

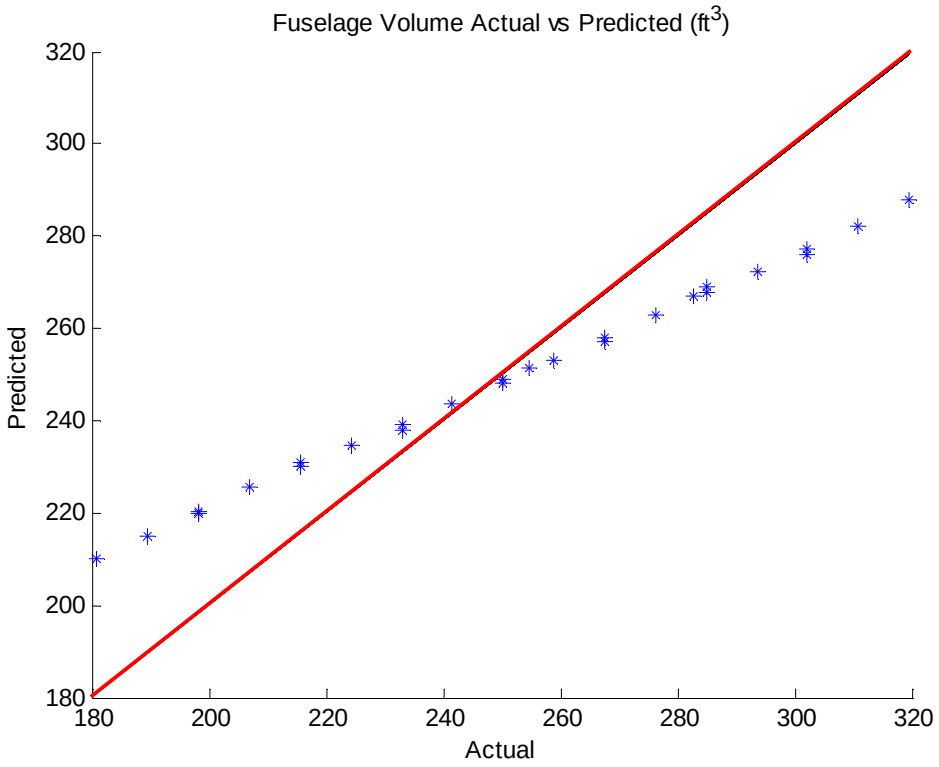

Figure 87: Actual vs Predicted

This scaling law exhibits weaker predictive power as shown in Figure 87. Sequentially weaker scaling laws can be derived depending on the number of parameters considered in the analysis.

Chapter X

CONTRIBUTIONS AND CONCLUSIONS

The key motivation for this research was the need to devise a set of methods with which vehicle architectures could be built around revolutionary technologies. The PEM fuel cell technology was used for the proof-of-concept study. The bodies of work that emerged from this study can be broadly classified into sizing and synthesis of unconventional concepts, unconventional propulsion system modeling and unconvention configuration design. This thesis falls into the latter category i.e. configuration design.

In attempting to retrofit a notional C-172R with a PEM fuel cell power plant, a number of key observations were made. First of all, the design space as defined by the number of possible subsystem layout combinations can be very large. This arises from the fact that each subsystem can have up to six degrees of location and orientation freedom. This observation implies that any exhaustive configuration space exploration technique must first of all, be automated and second, it must be fast enough to allow for exhaustive exploration of the vast design space. Furthermore, if the technology in question has significantly different, weight and/or volume requirements, many historical-data-based analyses that are typically used in conceptual design are rendered unreliable. These analyses include preliminary tasks such as the selection of baseline geometries from existent aircraft as well as sizing and scaling laws. Thus the design of vehicles around volumetrically and gravimetrically disparate technologies requires a new approach to the selection of the appropriate baseline geometry. Historical-data-based scaling laws must also be replaced with higher fidelity custom scaling laws.

Based on the identified needs, two key research questions were formulated. The first question is aimed at identifying a means by which baseline geometries can be defined around a disruptive technology. The second question addresses the challenge of quantifying the impact of requirement changes on the identified geometries. These questions are outlined following :

1. ***How can the contemporary treatment of geometric aspects in conceptual design be enhanced to facilitate the design of revolutionary concepts?***

   (a) *How can the baseline configuration space for a vehicle concept based on a disruptive technology be defined?*

   (b) *How should the subsystems be modeled in order to facilitate fast configuration definition?*

   Which component transformation approach does this approach permit?

   Which collision detection approaches does it permit?

   How fast must a configuration space exploration method/ tool be in order to permit configuration space exploration at the conceptual design level?

   (c) *How can information at the component level be mapped onto meaningful and useful system level metrics?*

   (d) *How can the volumetric uncertainty inherent in new technology immaturity or revolutionary designs be accommodated?*

   Which volume requirement does the designer design for?

   (e) *How can real-world effects such as maximum practical density, subsystem connectivity requirements and aesthetics be incorporated into the configuration space search methodology ?*

   How can they be modeled and quantified in order to be considered in conceptual design?

2. ***How can the evolution of vehicle geometry with requirement changes be captured in conceptual design?***

(a) *How the dominant drivers of system level geometric change be identified?*

(b) *At what threshold does photographic scaling become less viable than "smart scaling" based on scaling laws?*

To answer these questions, a new methodology, the Configuration Space Exploration and Scaling Methodology (CESM), was postulated based on the hypotheses outlined in §5 . The methodology consists of two key blocks namely configuration space exploration and scaling with the former being an enabler for the latter. The former describes a methodology by which vehicle geometries are defined based on the layout of subsystems while the former is used to quantify the changes in these geometries as requirements are altered. These blocks are discussed following :

10.1 Configuration Space Exploration

As defined earlier, the term configuration refers the relative disposition or arrangement of the parts of a thing [112]. In Cartesian space, any element has up to six degrees of location freedom. The number of design variables that must be used for an exhaustive exploration of the design space therefore rises dramatically as the number of elements increases. The enormity of the design space not only precludes most optimization approaches, it also makes it imperative that all key analyses such as component transformation and collision detection, be fast enough in order to permit the exploration of the design space in an acceptable amount of time. These and other showstoppers are summarized in Table 16.

Need	Showstoppers
1. Fast, global configuration space exploration technique	1. Lack of subsystem information i.e. dimensions, weight and scaling behavior 2. Computational expense i.e. subsystem modeling, transformation and collision detection 3. Large design space : potentially many components with up to 6 degrees of freedom each 4. Difficulty in modeling real world effects such as manufacturability, acceptability, connectivity ...

Table 16: Summary of Configuration Space Exploration Needs and Showstoppers

Based on these showstoppers a new methodology was postulated. For this methodology to be effective the choice of component modeling approach is critical as it determines the applicable transformation and collision detection methods. As a result of these choices, the expected expense of these two key processes is essentially "locked in". A discussion of the recommended approach follows.

10.1.1 Rapid Configuration Space Exploration

It was seen that computational expense is one of the major showstoppers to exhaustive geometry space exploration. Approximating subsystems as convex objects or small subsets thereof was shown to help mitigate this expense by enabling fast collision detection. On a 2.4 GHz , 2 GB RAM testbed, the collision detection expense was shown to be $O(10^{-4})$ seconds per surface point.

The second piece of the configuration space exploration approach is the definition of the actual aircraft geometry. It was noted in §2.1 that a good conceptual design tool must deliver information to the designer in a "ready-to-eat" format. Subsystem level information such as locations must be translated into directly useful metrics such as fuselage volume, wet area, take-off gross weight and so on. A super-hull i.e. convex hull of the laid-out subsystems was postulated as an approximation to the inner-mold-line of the design. This approximation relieves the shape optimization burden because ideal aerodynamic bodies are inherently convex. Furthermore convex hulls are by definition, minimum volume enclosing bodies. Thus, the abstraction approach also relieves optimization effort in minimizing dead volume.

The fuselage is defined as a series of cross sections whose dimensions and shapes are dictated by the sectional dimensions of the super-hull plus a designer-defined offset for fuselage thickness. These sectional dimensions are evaluated by sectionally slicing the super-hull. This procedure is implemented efficiently by taking advantage of the triangular facet structure of convex hulls. Once a fuselage is fully defined, the pertinent objective functions can be evaluated and comparisons with other configurations can be made. The size of the design space coupled with the fact that some key constraints such as the number of collisions are discontinuous, dictate that a domain-spanning optimization routine be used. Also, as this is a conceptual design tool, the goal is to provide the designer with a diverse baseline geometry space from which to chose. For these reasons, a domain-spanning algorithm with countermeasures against speciation and genetic drift is the recommended optimization approach. The Non-dominated Sorting Genetic Algorithm (NSGA-II) [60] is shown to work well for the proof of concept study.

By representing the geometries as convex objects, fast collision detection using simplex-based algorithms such as the Gilbert-Johnson-Keerthi algorithm can be performed. Speed is critical for this analysis as there can be up to ${}_nC_2$ analyses per layout (where n is the number of subsystems). The convexity property can be further used to reduce the collision detection expense by eliminating all pairs whose bounding boxes do not intersect along at least one axis as they can not collide. Fast collision detection in turn becomes an enabler for inexpensive

exploration of a large design space. Real world effects such as symmetry, acceptable density range and subsystem proximity requirements are also addressed *a posteriori* as concept selection criteria. The Balinsky distance was shown to be an effective measure of symmetry. A connectivity metric is used to drive component layouts towards more desirable proximity settings. It is acknowledged that not all "real world effects" can be quantitatively modeled and brought online in the concept selection process. The designer would thus still need to inspect final designs for any oddities to which the computational algorithm may have been blind.

10.1.2 Online Volumetric Consideration

When compared to the traditional top-down approach where the external geometry is defined and then checked for volume sufficiency, the bottom-up CESM approach has a higher chance of resulting in volumetrically feasible designs. This is because the top-level metrics such as fuselage length become fall-outs as opposed to design process constraints. When all subsystems are modeled, any resulting configuration is guaranteed to be volumetrically feasible. For vehicles with a large number of subsystems, this approach is not recommended as it would diminish the gains made in mitigating computational expense. For such situations it is recommended that only the major subsystems be used in the configuration space exploration process. An allowance for the volume requirements of the minor subsystems is made by driving the volumetric packing efficiency to a value less than 1. (Typically between 0.6 and 0.9 depending on vehicle class as seen in Figure 46.)

10.2 Custom Scaling Law Derivation

Delivering useful conceptual design metrics to the designer is half the challenge when it comes to the design of vehicles around disruptive technologies. The designer would also need to know how these metrics evolve as requirements change. Such information not only accelerates the design process, it also forms the back-bone of any investment recommendations. Improvements in key metrics such as specific power and power density come with implicit and variant costs per unit improvement. Quantifying the impact of these metrics on the performance of the vehicle as a complete system would enable decision-makers to

Need	Showstoppers
1. Scaling methodology that enables the mapping of design requirements to their impact on vehicle geometry.	1. Lack of information on subsystem scaling behavior 2. Computational expense in collision detection and in translating configuration into useful vehicle level metrics

Table 17: Summary of Configuration Scaling Needs and Showstoppers

identify the least expensive path to achieving the target performance.

There are two major reasons why the need to evaluate higher fidelity, custom geometric scaling laws became a part of this body of work. First of all, historical-data based regressions become implicitly unreliable when the vehicle concept in question is designed around a disruptive technology. The implicit unreliability results from technological and design practice evolution which inherently violates the "single regime" requirement discussed earlier. These noise-effects were illustrated in Figure 25. Second, it was shown in Figure 34 that photographic scaling can result in highly suboptimal concepts even for very small scaling factors.

Comments from Dr. Raymer, a renowned expert in the field of aircraft design, suggested that gains in fidelity could only come from customizing the scaling laws and that this would come at great computational expense [163]. This and other key showstoppers are summarized in Table 17 .

In the postulated methodology, it is assumed that the new technology has matured enough to permit the prediction of the scaling behavior of the various subsystems in response to requirements. Appropriate component abstractions i.e. convex hulls coupled with a simplex-based collision detection algorithm [79] are used to accelerate the key expense in configuration space refinement i.e. collision detection. Evidence was provided in Figure 85 and Figure 86 that higher fidelity custom scaling laws can be derived using data generated from the CESM process. This data is generated by applying the new requirement settings to the affected subsystems. All collisions are then eliminated using the NSGA-II algorithm.

This is done while minimizing the adverse impact on the vehicle packing density. Once all collisions are eliminated, the vehicle geometry is reconstructed and system level data such as fuselage volume can be harvested. This process is repeated for all requirement settings. Dimensional analysis and regression can be carried out using this data and all other pertinent metrics in the manner described by Mendez [124] and Segel [173]. The dominant parameters for each response show up as in the dimensionally consistent groups that form the independent variables. More importantly the impact of changes in any of these variables on system level dependent variables can be easily and rapidly evaluated. In this way, the conceptual design process can be accelerated without sacrificing analysis accuracy.

The next step up from here would be the generalization of these and other scaling laws to specific vehicle classes. This would entail the creation of an integrated modelling simulation in which every key discipline was brought online. In this way, the final solution at every requirement setting could be considered a true optimum. This task is discussed further following.

Chapter XI

FUTURE WORK

11.1 Scaling Laws for Fully Optimized Vehicles

The scope of the proof of concept study was limited to optimizing the fuselage. The wing and tail were only sized for lift and control sufficiency. Other key characteristics such as airfoil sections were fixed for the study. It would be interesting to observe the scaling behavior of the same system, where these and other degrees of freedom were included in the optimization. With this information, conclusions could also be drawn on the impact of these extra degrees on aircraft size and scaling behavior. General requirements for key technology metrics such as specific power could then be set for each vehicle class.

11.2 Incorporating Uncertainty into Analysis

Volumetric and gravimetric uncertainty is an intrinsic characteristic of any maturing technology. The less mature a technology is, the more imperative a treatment of uncertainty in conceptual design becomes. The methodology must, however, accommodate the fact that the design space is typically quite large. The implementation and run-time expense must be minimized to avoid making the entire process computationally prohibitive. Any postulated methodology must minimize the reliance on a priori assumptions as the sources of key probabilistic inputs. As Nemirovski et al [141] and others have shown, attempts to minimize bias by maximizing entropy can become a form of bias when either the uniform distributions are not well-centered or when unbeknownst to the designer, other distributions are more appropriate.

Appendix A

CONFIGURATION DATA FOR FIRST 10 CASES

The tables in this section contain the cartesian co-ordinate locations of the centers of mass of each subsystem for each of the configurations discussed in the results section §9.1.3. Note : Up to six significant figures are included in order to ensure reproducibility of solutions.

Subsystem	X	Y	Z
Main Motor	1.904781	0	-0.08
Motor Controller	4.409168	-1.75541	-0.81137
Compressor	3.123295	2.2	-1.27265
BOP	2.785529	0	-1.68715
Fuel Cell Controller	5.270493	0.3893	-1.56645
Fuel Cell	3.391872	0.7779	-0.24763
LH2 Tank	11.70592	0	-0.92731
Pump	11.529	0.086827	0.06975
Battery	11.213	0.74641	1.4484
Coolant Tank	3.164335	-1.13972	-0.09033
Controls	5.944144	0	0.052731
Seat	9.0326	-1.35701	0.16621
PMAD	10.282	1.70524	1.33905

Table 18: Configuration 1

Subsystem	X	Y	Z
Main Motor	1.904781	0	-0.08
Motor Controller	3.049631	0	0
Compressor	12.42687	0.91892	-1.27265
BOP	13.73521	0.000158	-0.95239
Fuel Cell Controller	3.685187	-1.27738	0
Fuel Cell	11.41814	0	0
LH2 Tank	3.8	0	-0.92731
Pump	11.529	0.086827	-1.12074
Battery	13.88604	0	0.4
Coolant Tank	3.557776	-1.13972	-1.51891
Controls	5.3	0.08697	0
Seat	9.0326	-0.88081	0.16621
PMAD	12.4591	1.48096	1.91575

Table 19: Configuration 2

Subsystem	X	Y	Z
Main Motor	1.904781	0	-0.08
Motor Controller	4.409168	0.62557	-0.33518
Compressor	4.511881	-1.46206	-0.08216
BOP	11.46419	0.000158	-0.97285
Fuel Cell Controller	4.1	-0.56309	0.100237
Fuel Cell	11.72338	0	0.466665
LH2 Tank	4.76299	0	0
Pump	11.529	0.086827	0.06975
Battery	13.99017	0	0.019814
Coolant Tank	3.511482	0.95239	0
Controls	6.29129	-0.15113	0.767024
Seat	9.0326	-0.88081	0.16621
PMAD	10.3681	1.75864	1.44175

Table 20: Configuration 3

Subsystem	X	Y	Z
Main Motor	1.904781	0	-0.08
Motor Controller	2.673437	0	-1.04947
Compressor	11.45481	0	-1.74885
BOP	5.7	0.000158	-1.44905
Fuel Cell Controller	4.229054	0.151202	0.338335
Fuel Cell	2.95	0.16356	-0.72382
LH2 Tank	11.70592	0	-0.92731
Pump	11.529	0.086827	0.06975
Battery	11.213	0	1.4484
Coolant Tank	3.164335	-0.90162	0.45
Controls	6.29129	0.08697	0.528926
Seat	9.0326	-0.64272	0.16621
PMAD	12.4058	2.13956	2.291

Table 21: Configuration 4

Subsystem	X	Y	Z
Main Motor	2.251927	0	-0.08
Motor Controller	3.714876	-0.80302	0.141019
Compressor	3.470442	0.91892	-0.79646
BOP	3.826968	0.000158	-1.44905
Fuel Cell Controller	4.5762	0.3893	0.100237
Fuel Cell	5.127603	0.16356	-0.00953
LH2 Tank	12.74736	0	-0.68921
Pump	11.529	0.086827	-1.83503
Battery	15.03161	-1.15837	0.734107
Coolant Tank	14.27302	0.050766	-0.80462
Controls	7.332729	0.08697	0.052731
Seat	10.42119	-0.88081	0.16621
PMAD	12.4345	1.73016	1.91575

Table 22: Configuration 5

Subsystem	X	Y	Z
Main Motor	1.904781	0	-0.08
Motor Controller	3.714876	0.62557	-1.04947
Compressor	3.470442	-0.50967	-0.55836
BOP	4.521261	0.000158	0.693831
Fuel Cell Controller	3.65	0.3893	0.81453
Fuel Cell	4.086164	0.16356	-0.72382
LH2 Tank	12.05306	0.77181	0
Pump	11.87615	0.086827	-1.35884
Battery	11.213	0.270215	1.4484
Coolant Tank	4.205774	0.050766	0.623968
Controls	6.638437	0.08697	0.290829
Seat	9.379746	-0.95239	0.16621
PMAD	12.4181	1.71592	1.90785

Table 23: Configuration 6

Subsystem	X	Y	Z
Main Motor	1.904781	0	-0.08
Motor Controller	3.020583	0.149375	0.617214
Compressor	3.123295	0	-1.27265
BOP	8.996071	0.000158	-1.44905
Fuel Cell Controller	4.5762	-0.80119	0.81453
Fuel Cell	3.739018	0.16356	-0.48573
LH2 Tank	11.43877	0	-0.92731
Pump	11.529	0.086827	1.498336
Battery	12.94873	0	-0.45638
Coolant Tank	3.511482	0.526961	0.623968
Controls	6.300338	0.08697	0.767024
Seat	9.0326	-0.88081	0.642405
PMAD	10.6633	1.7444	1.93945

Table 24: Configuration 7

Subsystem	X	Y	Z
Main Motor	1.904781	0	-0.08
Motor Controller	3.049631	-0.95239	0.855312
Compressor	3.639491	-1.19049	0.870229
BOP	4.601261	0.000158	0.455733
Fuel Cell Controller	4.100005	-1.42859	0.81453
Fuel Cell	6.894288	0.16356	0.228567
LH2 Tank	11.20067	0	-0.21302
Pump	15.57666	0.086827	0.545945
Battery	15.02256	0	-0.69448
Coolant Tank	4.394824	0.050766	-0.36
Controls	12.7	0.08697	0.528926
Seat	9.0326	-0.95239	0.16621
PMAD	10.61	1.75152	1.9987

Table 25: Configuration 8

Subsystem	X	Y	Z
Main Motor	1.904781	0	-0.08
Motor Controller	4.002021	0.62557	0.617214
Compressor	4.115686	0	-0.32026
BOP	4.839359	0.000158	-0.97285
Fuel Cell Controller	4.5762	-1.03929	0.338335
Fuel Cell	4.751409	0.16356	0.4
LH2 Tank	7.153014	0	0
Pump	3.909876	-1.34176	0.06975
Battery	14.7	0	0.49601
Coolant Tank	3.442433	-0.90162	0
Controls	8.919412	0	0.528926
Seat	11.65167	-0.95239	0.16621
PMAD	10.3394	1.6554	1.9592

Table 26: Configuration 9

Subsystem	X	Y	Z
Main Motor	1.904781	0	-0.08
Motor Controller	3.525826	0.62557	0.141019
Compressor	3.639491	0.91892	0.870229
BOP	4.363164	0.000158	-0.02046
Fuel Cell Controller	4.5762	0.3893	0.81453
Fuel Cell	11.65624	0.16356	0.94286
LH2 Tank	5.109113	0	-0.21302
Pump	11.529	0.086827	0.06975
Battery	11.213	-1.15837	-0.75902
Coolant Tank	2.251945	-1.61592	-0.32842
Controls	6.348039	0.08697	0.528926
Seat	9.0326	0.071577	0.16621
PMAD	12.4591	1.71592	1.91575

Table 27: Configuration 10

Appendix B

COLLISION DETECTION MODULES

B.1 Gilbert-Johnson-Keerthi (GJK) Algorithm Source Code (FORTRAN)

This algorithm calculates the minimum separation distance between two convex objects. For each object a vertex and adjacency data structure must be defined as explained in §8.4.1. An explanation of the GJK procedure can be found in §7.2.6.3.

This code was provided courtesy of Dr. Elmer Gilbert of the University of Michigan and Dr. Ong Chong Jin of the National University of Singapore.

```
SUBROUTINE *DIST3(NVI,NVJ,NZDIM,ZI,ZJ,AVERLSTI,AVERLSTJ,IWANT,EPS,
ZISOL,ZJSOL,ZSOL,DIST,NVS,RIS,RJS,ALS,NCY,FINAL,NZBDIM,ZBI,ZBJ,
NEWORG,DI,DJ,IERROR)
INTEGER NVI, NVJ, NZDIM, IWANT
INTEGER NVS, RIS, RJS
INTEGER NCY, NZBDIM, IERROR, IOUT
INTEGER K, L, NRI, NRJ, NV, RI, RJ, IORD
INTEGER KK, LL, II, JJ, NVSOLD
* INTEGER SVI,SVJ,AVERLSTI,AVERLSTJ
DIMENSION IWANT(4), RIS(4), RJS(4), RI(4), RJ(4), IORD(4)
* DIMENSION AVERSTI(NVI,NVI), AVERLSTJ(NVJ,NVJ)
DOUBLE PRECISION ZI(NZDIM,NVI), ZJ(NZDIM,NVJ), EPS
DOUBLE PRECISION ZISOL(3), ZJSOL(3), ZSOL(3), DIST, ALS(4)
DOUBLE PRECISION GFINAL, ZBI(NZBDIM,NVI), ZBJ(NZBDIM,NVJ)
DOUBLE PRECISION NEWORG(3), DI, DJ, CENT(3), NCENT(3)
DOUBLE PRECISION ZERO, INN, DSUM, EPSDSQ, SFI, SFJ
```

```
DOUBLE PRECISION Y(3,4), DEL(4,4), YOLD(3,4), DELOLD(4,4)
DOUBLE PRECISION DSTSQ, DSTSQP, NZSOL(3), G
LOGICAL BACKUP
======
STEP 1. INITIALIZATION PHASE ...
======
DATA ZERO /0.0D0/ IERROR = 0 NCY = 1
CHECK FOR DIMENSIONING ERRORS :
IF (NVI.LE.0 .OR. NVJ.LE.0 .OR. NZDIM.LT.3 .OR. 1 NZBDIM.LT.3)
GO TO 720
PRINT TITLES IF IWANT(1) .GT. 0 :
IF (IWANT(1) .LE. 0)
GO TO 110
IOUT = IWANT(1)
WRITE(IOUT,1010)
WRITE(IOUT,1020)
WRITE(IOUT,1010)
110 CONTINUE
C FORM ZBI, ZBJ, CENT AND NCENT :
CALL TRANC(NZDIM,NVI,NVJ,ZI,ZJ,NZBDIM,ZBI,ZBJ,
1 IWANT,NEWORG,CENT,NCENT)
C COMPUTE DI, DJ AND EPSDSQ
IF IWANT(3) = 1 : EPSDSQ = EPS
IF (IWANT(3) .NE. 1)
GO TO 115
DI = ZERO
DO 112 K=1,NVI
INN = ZBI(1,K)*ZBI(1,K) + ZBI(2,K)*ZBI(2,K) + 1 ZBI(3,K)*ZBI(3,K)
IF (INN .GT. DI)
```

```
DI = INN
112 CONTINUE
DI = DSQRT(DI)
DJ = ZERO DO
114 K=1,NVJ
INN = ZBJ(1,K)*ZBJ(1,K) + ZBJ(2,K)*ZBJ(2,K) + 1 ZBJ(3,K)*ZBJ(3,K)
IF (INN .GT. DJ) DJ = INN
114 CONTINUE DJ = DSQRT(DJ)
DSUM = DI + DJ EPSDSQ = EPS * DSUM * DSUM
115 CONTINUE
C SET INITIAL NVS, RIS(*) AND RJS(*)
IF IWANT(4) .NE. 1 :
IF (IWANT(4) .EQ. 1)
GO TO 120
NVS = 1
* SVI=1
* SVJ=1
* CALL SCSFCN(NZBDIM,SVI,NVI,ZBI,NCENT,SFI,NRI,AVERLSTI)
* CALL SCSFCN(NZBDIM,SVJ,NVJ,ZBJ,CENT,SFJ,NRJ,AVERLSTJ)
RIS(1) = NRI RJS(1) = NRJ 120 IF (NVS.LE.0 .OR. NVS.GT.4)
GO TO 730
C COMPUTE Y AND DEL FOR INITIAL SET :
DO 130 L=1,NVS
II = RIS(L)
JJ = RJS(L)
Y(1,L) = ZBI(1,II) - ZBJ(1,JJ)
Y(2,L) = ZBI(2,II) - ZBJ(2,JJ)
Y(3,L) = ZBI(3,II) - ZBJ(3,JJ)
DO 125 K=1,L
```

```
      DEL(L,K) = Y(1,K)*Y(1,L) + Y(2,K)*Y(2,L) + Y(3,K)*Y(3,L)
      125 CONTINUE
      130 CONTINUE
      SET DSTSQP = DEL(1,1) + DEL(1,1) + 1.0D0
      C FOR USE IN STEP 4 :
      DSTSQP = DEL(1,1) + DEL(1,1) + 1.0D0
      C====
      C STEP 2. APPLY THE DISTANCE SUBALGORITHM ...
      C====
      200 CONTINUE SET BACKUP = .FALSE. SO THAT THE USUAL DISTANCE SUB-
ALGORITHM IS USED :
      BACKUP = .FALSE.
      C FOR BACKUP PROCEDURE, STATEMENT 220 IS ENTERED WITH
      BACKUP = .TRUE.
      220
      CALL DSBP(NVS,RIS,RJS,Y,DEL,ZSOL,ALS,DSTSQ,BACKUP)
      C====
      C STEP 3. COMPUTE G AND TEST FOR OPTIMALITY ...
      C =
      NZSOL(1) = -ZSOL(1)
      NZSOL(2) = -ZSOL(2)
      NZSOL(3) = -ZSOL(3)
      * SVI=RIS(1)
      * SVJ=RJS(1)
      * CALL CSFCN(NZBDIM,SVI,NVI,ZBI,NZSOL,SFI,NRI,AVERLSTI)
      * CALL CSFCN(NZBDIM,SVJ,NVJ,ZBJ,ZSOL,SFJ,NRJ,AVERLSTJ)
      G = DSTSQ + SFI + SFJ IF (IOUT .GT. 0)
      WRITE(IOUT,1030) NCY, DSTSQ, G IF (G .LE. EPSDSQ)
      GO TO 700
```

```
C ====
C STEP 4. INCLUDE THE NEW POINT AND PREPARE FOR THE NEXT CYCLE
...
C ====
C FIRST CHECK IF THERE IS A NEED FOR STEP 5 :
IF (DSTSQ .GE. DSTSQP .OR. NVS .GE. 4)
GO TO 500
DSTSQP = DSTSQ
C PUT THE FIRST POINT IN THE LAST SPOT :
NVSOLD = NVS
NVS = NVS + 1
RIS(NVS) = RIS(1)
RJS(NVS) = RJS(1)
Y(1,NVS) = Y(1,1)
Y(2,NVS) = Y(2,1)
Y(3,NVS) = Y(3,1)
DO 410 K=2,NVSOLD
DEL(NVS,K) = DEL(K,1)
410 CONTINUE DEL(NVS,NVS) = DEL(1,1)
C PUT THE NEW POINT IN THE FIRST SPOT :
C RIS(1) = NRI RJS(1) = NRJ
Y(1,1) = ZBI(1,NRI) - ZBJ(1,NRJ)
Y(2,1) = ZBI(2,NRI) - ZBJ(2,NRJ)
Y(3,1) = ZBI(3,NRI) - ZBJ(3,NRJ)
DO 420 K=1,NVS
DEL(K,1) = Y(1,K)*Y(1,1) + Y(2,K)*Y(2,1) + Y(3,K)*Y(3,1)
420 CONTINUE
C USE NV, RI(*), RJ(*), YOLD(*,*) AND DELOLD(*,*) FOR TEMPORARY STOR-
AGE. THESE ELEMENTS
```

```
      ARE USEFUL
      C IMMEDIATELY BELOW WHEN NVS = 4, AND ALSO IN STEP 6.
      NV = NVS
      DO 430 K=1,NV
      RI(K) = RIS(K)
      RJ(K) = RJS(K)
      YOLD(1,K) = Y(1,K)
      YOLD(2,K) = Y(2,K)
      YOLD(3,K) = Y(3,K)
      DO 425 L=1,K
      DELOLD(K,L) = DEL(K,L)
      DELOLD(L,K) = DELOLD(K,L)
      425 CONTINUE
      430 CONTINUE
      C IF NVS = 4, REARRANGE DEL(2,1), DEL(3,1) AND DEL(4,1) IN NON DECREAS-
ING ORDER :
      IF (NVS .LE. 3)
      GO TO 490
      IORD(1) = 1
      IORD(2) = 2
      IORD(3) = 3
      IF (DEL(3,1) .GE. DEL(2,1))
      GO TO 435 IORD(2) = 3
      IORD(3) = 2 435
      II = IORD(2)
      IF (DEL(4,1) .GE. DEL(II,1))
      GO TO 440
      IORD(4) = IORD(3)
      IORD(3) = IORD(2)
```

```
IORD(2) = 4
GO TO 450
440 II = IORD(3)
IF (DEL(4,1) .GE. DEL(II,1))
GO TO 445
IORD(4) = IORD(3)
IORD(3) = 4
GO TO 450
445 CONTINUE
IORD(4) = 4
450 CONTINUE
C REORDER RIS(*), Y(*,*) AND DEL(*,*) :
DO 460 K=2,4
KK = IORD(K)
RIS(K) = RI(KK)
RJS(K) = RJ(KK)
Y(1,K) = YOLD(1,KK)
Y(2,K) = YOLD(2,KK)
Y(3,K) = YOLD(3,KK)
DO 455 L=1,K
LL = IORD(L)
DEL(K,L) = DELOLD(KK,LL)
455 CONTINUE
460 CONTINUE
490 NCY = NCY + 1
GO TO 200
C =====
C STEP 5. QUIT IF BACKUP = .TRUE. ...
C =
```

```
500 IF (.NOT.BACKUP)
GO TO 600
IERROR = 3
GO TO 700
C=====
C STEP 6. RE DO THE DISTANCE SUBALGORITHM USING THE BACKUP
C PROCEDURE AND GO TO STEP 3. IN OTHER WORDS, SET
C BACKUP = .TRUE., PUT OLD VALUES IN NVS, RIS(*),
C RJS(*), Y(*,*) AND DEL(*,*), AND GO TO STEP 2 ...
C =====
600 BACKUP = .TRUE.
IF (NCY .EQ. 1)
GO TO 615
NVS = NV
DO 610 K=1,NVS
RIS(K) = RI(K)
RJS(K) = RJ(K)
Y(1,K) = YOLD(1,K)
Y(2,K) = YOLD(2,K)
Y(3,K) = YOLD(3,K)
DO 605 L=1,K
DEL(K,L) = DELOLD(K,L)
605 CONTINUE
610 CONTINUE
615 CONTINUE
IF (IOUT .GT. 0) WRITE(IOUT,1040) NCY
GO TO 220
C =====
C STEP 7. THE FINAL PHASE ...
```

```
C =====
700 CONTINUE
C RETURNING THE SOLUTION WITH IERROR = 0 OR 3 :
DO 710 L=1,3
ZISOL(L) = ZERO
ZJSOL(L) = ZERO
DO 705 K=1,NVS
II = RIS(K)
JJ = RJS(K)
ZISOL(L) = ZISOL(L) + ZI(L,II)*ALS(K)
ZJSOL(L) = ZJSOL(L) + ZJ(L,JJ)*ALS(K)
705 CONTINUE
710 CONTINUE
DIST = DSQRT(DSTSQ)
GFINAL = G IF (IOUT .LE. 0)
GO TO 715 WRITE(IOUT,1010)
IF (IERROR .EQ. 0) WRITE(IOUT,1050)
IF (IERROR .EQ. 3) WRITE(IOUT,1060)
715 RETURN RETURNING WITH IERROR = 1 :
720 IERROR = 1 IF (IOUT .GT. 0) WRITE(IOUT,1070)
RETURN
C RETURNING WITH IERROR = 2 :
730 IERROR = 2 IF (IOUT .GT. 0) WRITE(IOUT,1080)
RETURN
C====
C FORMAT STATEMENTS ...
C =====
1010 FORMAT(1X,40(1H-))
1020 FORMAT(2X,5HCYCLE,2X,15HDISTANCE SQUARE,8X,1HG)
```

1030 FORMAT(4X,I2,4X,D13.7,3X,D13.7)

1040 FORMAT(2X,15H**REDOING CYCLE,1X,I2,1X, 1 28HUSING THE BACKUP PROCEDURE**)

1050 FORMAT(/,2X,36H**SUCCESSFUL TERMINATION: IERROR=0**)

1060 FORMAT(/,2X,30H**EPS IS TOO SMALL: IERROR=3**)

1070 FORMAT(/,2X,38H**INPUT DIMENSIONING ERROR: IERROR=1**)

1080 FORMAT(/,2X,34H**INITIALIZATION ERROR: IERROR=2**)

C ====

C THE LAST LINE OF THE SUBROUTINE DIST3 :

END

SUBROUTINE DSBP(NVS,RIS,RJS,Y,DEL,ZSOL,ALS,DSTSQ,BACKUP)

C ====

DSBP implements, in a very efficient way, the distance subalgorithm of finding the near point to the convex hull of

four or less points in 3-D space. The procedure and its efficient FORTRAN implementation are both due to

D.W.Johnson. Although this subroutine is quite long, only a very small part of it will be executed on each call. Refer

to sections 5 and 6 of the report mentioned in routine DIST3 for details concerning the distance subalgorithm.

Following is a brief description of the parameters in DSBP :

**** ON INPUT :

NVS : The number of points. 1 .LE. NVS .LE. 4 .

Y(*,*) : The array whose columns contain the points.

RIS(*), RJS(*) : Index vectors for Polytope-I and Polytope-J.

For K = 1,...,NVS, Y(.,K) = ZBI(.,RIS(K)) - ZBJ(.,RJS(K)), where A(.,K) denotes the K-th column of the matrix A.

DEL(*,*) : DEL(I,J) = Inner product of Y(.,I) and Y(.,J).

**** ON OUTPUT : ZSOL(*) : Near point to the convex hull of the points in Y.

DSTSQ : Norm of ZSOL.

**** DSBP also determines an affinely independent subset of the points such that ZSOL= near point to the affine hull of

the points in the subset.

The variables NVS, Y, RIS, RJS and DEL are modified so that, on output, they correspond to this subset of points.

ALS(*) : The barycentric coordinates of ZSOL, i.e., ZSOL = ALS(1)*Y(.,1) + ... + ALS(NVS)*Y(.,NVS), ALS(K)

.GT. 0.D0 for K=1,...,NVS, and, ALS(1) + ... + ALS(NVS) = 1.D0 .

========

INTEGER NVS, RIS, RJS, K, L, KK, LL

INTEGER NVSD, RISD, RJSD, IORD

DIMENSION RIS(4), RJS(4), RISD(4), RJSD(4), IORD(4)

DOUBLE PRECISION Y(3,4), DEL(4,4), ZSOL(3)

DOUBLE PRECISION ALS(4), DSTSQ, SUM, ZERO, ONE

DOUBLE PRECISION E132,E142,E123,E143,E213,E243

DOUBLE PRECISION E124,E134,E214,E234,E314,E324

DOUBLE PRECISION D1(15),D2(15),D3(15),D4(15)

DOUBLE PRECISION YD(3,4), DELD(4,4), ZSOLD(3)

DOUBLE PRECISION ALSD(4), DSTSQD LOGICAL BACKUP DATA D1(1),D2(2),D3(4),D4(8) /4*1.D0/

DATA ZERO /0.0D00/ DATA ONE /1.0D00/

C ====

C IF BACKUP = .TRUE. ON INPUT TO THIS ROUTINE, THEN THE SUBALGORITHM WILL BE DONE BY

THE BACKUP PROCEDURE.

C IF BACKUP = .TRUE. ON OUTPUT FROM THIS ROUTINE, THEN IT MEANS THAT THE

SUBALGORITHM WAS DONE USING THE BACKUP

```
C PROCEDURE. GO TO STATEMENT 1000 FOR THE BACKUP PROCEDURE :
C====
IF (BACKUP) GO TO 1000
C====
C THE REGULAR DISTANCE SUBALGORITHM BEGINS ...
C====
GO TO (100, 200, 300, 400), NVS
********* CASE OF A SINGLE POINT ...
100 CONTINUE ALS(1) = D1(1)
ZSOL(1) = Y(1,1)
ZSOL(2) = Y(2,1)
ZSOL(3) = Y(3,1)
DSTSQ = DEL(1,1)
RETURN
*********CASE OF TWO POINTS ...
200 CONTINUE
———— CHECK OPTIMALITY OF VERTEX 1 :
D2(3) = DEL(1,1) - DEL(2,1)
IF (D2(3).GT.ZERO)
GO TO 210
NVS = 1 ALS(1) = D1(1)
ZSOL(1) = Y(1,1)
ZSOL(2) = Y(2,1)
ZSOL(3) = Y(3,1)
DSTSQ = DEL(1,1)
RETURN
210 CONTINUE
———–CHECK OPTIMALITY OF LINE SEGMENT 12 :
D1(3) = DEL(2,2) - DEL(2,1)
```

IF(D1(3).LE.ZERO .OR. D2(3).LE.ZERO)

GO TO 220

SUM = D1(3) + D2(3)

ALS(1) = D1(3)/SUM

ALS(2) = ONE - ALS(1)

ZSOL(1) = Y(1,2) + ALS(1)*(Y(1,1) - Y(1,2))

ZSOL(2) = Y(2,2) + ALS(1)*(Y(2,1) - Y(2,2))

ZSOL(3) = Y(3,2) + ALS(1)*(Y(3,1) - Y(3,2))

DSTSQ = ZSOL(1)*ZSOL(1) + ZSOL(2)*ZSOL(2) + ZSOL(3)*ZSOL(3)

RETURN 220

CONTINUE

————CHECK OPTIMALITY OF VERTEX 2 :

IF (D1(3).GT.ZERO)

GO TO 230 NVS = 1

RIS(1) = RIS(2)

RJS(1) = RJS(2)

ALS(1) = D2(2)

ZSOL(1) = Y(1,2)

ZSOL(2) = Y(2,2)

ZSOL(3) = Y(3,2)

DSTSQ = DEL(2,2)

Y(1,1) = Y(1,2)

Y(2,1) = Y(2,2)

Y(3,1) = Y(3,2)

DEL(1,1) = DEL(2,2)

RETURN

230 CONTINUE

————-NEED TO GO FOR THE BACKUP PROCEDURE : (WITHOUT RECOMPUTING THE DI(*) VALUES)

```
GO TO 1050
**********CASE OF THREE POINTS ...
300 CONTINUE
————————-CHECK OPTIMALITY OF VERTEX 1 :
D2(3) = DEL(1,1) - DEL(2,1)
D3(5) = DEL(1,1) - DEL(3,1)
IF (D2(3).GT.ZERO .OR. D3(5).GT.ZERO)
GO TO 310
NVS = 1 ALS(1) = D1(1)
ZSOL(1) = Y(1,1)
ZSOL(2) = Y(2,1)
ZSOL(3) = Y(3,1)
DSTSQ = DEL(1,1)
RETURN
310 CONTINUE
————————————-CHECK OPTIMALITY OF LINE SEGMENT 12 :
E132 = DEL(2,1) - DEL(3,2)
D1(3) = DEL(2,2) - DEL(2,1)
D3(7) = D1(3)*D3(5) + D2(3)*E132
IF (D1(3).LE.ZERO .OR. D2(3).LE. ZERO .OR. 1 D3(7).GT.ZERO)
GO TO 320 NVS = 2
SUM = D1(3) + D2(3) ALS(1) = D1(3)/SUM
ALS(2) = ONE - ALS(1)
ZSOL(1) = Y(1,2) + ALS(1)*(Y(1,1) - Y(1,2))
ZSOL(2) = Y(2,2) + ALS(1)*(Y(2,1) - Y(2,2))
ZSOL(3) = Y(3,2) + ALS(1)*(Y(3,1) - Y(3,2))
DSTSQ = ZSOL(1)*ZSOL(1) + ZSOL(2)*ZSOL(2) + ZSOL(3)*ZSOL(3)
RETURN
320 CONTINUE
```

————–CHECK OPTIMALITY OF LINE SEGMENT 13 :

E123 = DEL(3,1) - DEL(3,2)

D1(5) = DEL(3,3) - DEL(3,1)

D2(7) = D1(5)*D2(3) + D3(5)*E123

IF (D1(5).LE.ZERO .OR. D2(7).GT.ZERO .OR. 1 D3(5).LE.ZERO)

GO TO 330 NVS = 2

RIS(2) = RIS(3)

RJS(2) = RJS(3)

SUM = D1(5) + D3(5)

ALS(1) = D1(5)/SUM

ALS(2) = ONE - ALS(1)

ZSOL(1) = Y(1,3) + ALS(1)*(Y(1,1) - Y(1,3))

ZSOL(2) = Y(2,3) + ALS(1)*(Y(2,1) - Y(2,3))

ZSOL(3) = Y(3,3) + ALS(1)*(Y(3,1) - Y(3,3))

DSTSQ = ZSOL(1)*ZSOL(1) + ZSOL(2)*ZSOL(2) + ZSOL(3)*ZSOL(3)

Y(1,2) = Y(1,3) Y(2,2) = Y(2,3)

Y(3,2) = Y(3,3)

DEL(2,1) = DEL(3,1)

DEL(2,2) = DEL(3,3)

RETURN

330 CONTINUE

————–CHECK OPTIMALITY OF FACE 123 :

E213 = -E123

D2(6) = DEL(3,3) - DEL(3,2)

D3(6) = DEL(2,2) - DEL(3,2)

D1(7) = D2(6)*D1(3) + D3(6)*E213

IF (D1(7).LE.ZERO .OR. D2(7).LE.ZERO .OR. 1 D3(7).LE.ZERO)

GO TO 340

SUM = D1(7) + D2(7) + D3(7)

```
ALS(1) = D1(7)/SUM
ALS(2) = D2(7)/SUM
ALS(3) = ONE - ALS(1) - ALS(2)
ZSOL(1) = Y(1,3) + ALS(1)*(Y(1,1) - Y(1,3)) + 1 ALS(2)*(Y(1,2) - Y(1,3))
ZSOL(2) = Y(2,3) + ALS(1)*(Y(2,1) - Y(2,3)) + 1 ALS(2)*(Y(2,2) - Y(2,3))
ZSOL(3) = Y(3,3) + ALS(1)*(Y(3,1) - Y(3,3)) + 1 ALS(2)*(Y(3,2) - Y(3,3))
DSTSQ = ZSOL(1)*ZSOL(1) + ZSOL(2)*ZSOL(2) + ZSOL(3)*ZSOL(3)
RETURN
340 CONTINUE
------CHECK OPTIMALITY OF VERTEX 2 :
IF (D1(3).GT.ZERO .OR. D3(6).GT.ZERO)
GO TO 350 NVS = 1
RIS(1) = RIS(2)
RJS(1) = RJS(2)
ALS(1) = D2(2)
ZSOL(1) = Y(1,2)
ZSOL(2) = Y(2,2)
ZSOL(3) = Y(3,2)
DSTSQ = DEL(2,2)
Y(1,1) = Y(1,2)
Y(2,1) = Y(2,2)
Y(3,1) = Y(3,2)
DEL(1,1) = DEL(2,2)
RETURN
350 CONTINUE
-------CHECK OPTIMALITY OF VERTEX 3 :
IF (D1(5).GT.ZERO .OR. D2(6).GT.ZERO)
GO TO 360 NVS = 1
RIS(1) = RIS(3) RJS(1) = RJS(3)
```

```
ALS(1) = D3(4)
ZSOL(1) = Y(1,3)
ZSOL(2) = Y(2,3)
ZSOL(3) = Y(3,3)
DSTSQ = DEL(3,3)
Y(1,1) = Y(1,3)
Y(2,1) = Y(2,3)
Y(3,1) = Y(3,3)
DEL(1,1) = DEL(3,3)
RETURN
360 CONTINUE
————–CHECK OPTIMALITY OF LINE SEGMENT 23 :
IF (D1(7).GT.ZERO .OR. D2(6).LE.ZERO .OR. 1 D3(6).LE.ZERO)
GO TO 370
NVS = 2
RIS(1) = RIS(3)
RJS(1) = RJS(3)
SUM = D2(6) + D3(6)
ALS(2) = D2(6)/SUM
ALS(1) = ONE - ALS(2)
ZSOL(1) = Y(1,3) + ALS(2)*(Y(1,2) - Y(1,3))
ZSOL(2) = Y(2,3) + ALS(2)*(Y(2,2) - Y(2,3))
ZSOL(3) = Y(3,3) + ALS(2)*(Y(3,2) - Y(3,3))
DSTSQ = ZSOL(1)*ZSOL(1) + ZSOL(2)*ZSOL(2) + ZSOL(3)*ZSOL(3)
Y(1,1) = Y(1,3) Y(2,1) = Y(2,3)
Y(3,1) = Y(3,3)
DEL(2,1) = DEL(3,2)
DEL(1,1) = DEL(3,3)
RETURN
```

```
370 CONTINUE
------NEED TO GO FOR THE BACKUP PROCEDURE : (WITHOUT RECOMPUTING THE DI(*) VALUES)
GO TO 1050
********CASE OF FOUR POINTS ...
400 CONTINUE
------CHECK OPTIMALITY OF VERTEX 1 :
D2(3) = DEL(1,1) - DEL(2,1)
D3(5) = DEL(1,1) - DEL(3,1)
D4(9) = DEL(1,1) - DEL(4,1)
IF (D2(3).GT.ZERO .OR. D3(5).GT.ZERO .OR. 1 D4(9).GT.ZERO)
GO TO 405
NVS = 1
ALS(1) = D1(1)
ZSOL(1) = Y(1,1)
ZSOL(2) = Y(2,1)
ZSOL(3) = Y(3,1)
DSTSQ = DEL(1,1)
RETURN 405
CONTINUE
------CHECK OPTIMALITY OF LINE SEGMENT 12 :
E132 = DEL(2,1) - DEL(3,2)
E142 = DEL(2,1) - DEL(4,2)
D1(3) = DEL(2,2) - DEL(2,1)
D3(7) = D1(3)*D3(5) + D2(3)*E132
D4(12) = D1(3)*D4(9) + D2(3)*E142
IF (D1(3).LE.ZERO .OR. D2(3).LE.ZERO .OR. 1
D3(7).GT.ZERO .OR. D4(12).GT.ZERO)
GO TO 410
```

```
NVS = 2
SUM = D1(3) + D2(3)
ALS(1) = D1(3)/SUM
ALS(2) = ONE - ALS(1)
ZSOL(1) = Y(1,2) + ALS(1)*(Y(1,1) - Y(1,2))
ZSOL(2) = Y(2,2) + ALS(1)*(Y(2,1) - Y(2,2))
ZSOL(3) = Y(3,2) + ALS(1)*(Y(3,1) - Y(3,2))
DSTSQ = ZSOL(1)*ZSOL(1) + ZSOL(2)*ZSOL(2) + ZSOL(3)*ZSOL(3)
RETURN
410 CONTINUE
------CHECK OPTIMALITY OF LINE SEGMENT 13 :
E123 = DEL(3,1) - DEL(3,2)
E143 = DEL(3,1) - DEL(4,3)
D1(5) = DEL(3,3) - DEL(3,1)
D2(7) = D1(5)*D2(3) + D3(5)*E123
D4(13) = D1(5)*D4(9) + D3(5)*E143
IF (D1(5).LE.ZERO .OR. D2(7).GT.ZERO .OR. 1
D3(5).LE.ZERO .OR. D4(13).GT.ZERO)
GO TO 415
NVS = 2
RIS(2) = RIS(3)
RJS(2) = RJS(3)
SUM = D1(5) + D3(5)
ALS(1) = D1(5)/SUM
ALS(2) = ONE - ALS(1)
ZSOL(1) = Y(1,3) + ALS(1)*(Y(1,1) - Y(1,3))
ZSOL(2) = Y(2,3) + ALS(1)*(Y(2,1) - Y(2,3))
ZSOL(3) = Y(3,3) + ALS(1)*(Y(3,1) - Y(3,3))
DSTSQ = ZSOL(1)*ZSOL(1) + ZSOL(2)*ZSOL(2) + ZSOL(3)*ZSOL(3)
```

```
Y(1,2) = Y(1,3)

Y(2,2) = Y(2,3)

Y(3,2) = Y(3,3)

DEL(2,1) = DEL(3,1)

DEL(2,2) = DEL(3,3)

RETURN

415 CONTINUE

————————CHECK OPTIMALITY OF FACE 123 :

D2(6) = DEL(3,3) - DEL(3,2)

D3(6) = DEL(2,2) - DEL(3,2)

E213 = -E123

D1(7) = D2(6)*D1(3) + D3(6)*E213

D4(15) = D1(7)*D4(9) + D2(7)*E142 + D3(7)*E143

IF (D1(7).LE.ZERO .OR. D2(7).LE.ZERO .OR. 1 D3(7).LE.ZERO .OR. D4(15).GT.ZERO)

GO TO 420

NVS = 3

SUM = D1(7) + D2(7) + D3(7)

ALS(1) = D1(7)/SUM

ALS(2) = D2(7)/SUM

ALS(3) = ONE - ALS(1) - ALS(2)

ZSOL(1) = Y(1,3) + ALS(1)*(Y(1,1) - Y(1,3)) + 1 ALS(2)*(Y(1,2) - Y(1,3))

ZSOL(2) = Y(2,3) + ALS(1)*(Y(2,1) - Y(2,3)) + 1 ALS(2)*(Y(2,2) - Y(2,3))

ZSOL(3) = Y(3,3) + ALS(1)*(Y(3,1) - Y(3,3)) + 1 ALS(2)*(Y(3,2) - Y(3,3))

DSTSQ = ZSOL(1)*ZSOL(1) + ZSOL(2)*ZSOL(2) + ZSOL(3)*ZSOL(3)

RETURN

420 CONTINUE

————————CHECK OPTIMALITY OF LINE SEGMENT 14 :

E124 = DEL(4,1) - DEL(4,2)

E134 = DEL(4,1) - DEL(4,3)
```

```
      D1(9) = DEL(4,4) - DEL(4,1)
      D2(12) = D1(9)*D2(3) + D4(9)*E124
      D3(13) = D1(9)*D3(5) + D4(9)*E134 IF (D1(9).LE.ZERO .OR. D2(12).GT.ZERO .OR.
     1 D3(13).GT.ZERO .OR.
      D4(9).LE.ZERO)
      GO TO 425
      NVS = 2
      RIS(2) = RIS(4)
      RJS(2) = RJS(4)
      SUM = D1(9) + D4(9)
      ALS(1) = D1(9)/SUM
      ALS(2) = ONE - ALS(1)
      ZSOL(1) = Y(1,4) + ALS(1)*(Y(1,1) - Y(1,4))
      ZSOL(2) = Y(2,4) + ALS(1)*(Y(2,1) - Y(2,4))
      ZSOL(3) = Y(3,4) + ALS(1)*(Y(3,1) - Y(3,4))
      DSTSQ = ZSOL(1)*ZSOL(1) + ZSOL(2)*ZSOL(2) + ZSOL(3)*ZSOL(3)
      Y(1,2) = Y(1,4)
      Y(2,2) = Y(2,4)
      Y(3,2) = Y(3,4)
      DEL(2,1) = DEL(4,1)
      DEL(2,2) = DEL(4,4)
      RETURN
      425 CONTINUE
      ———— CHECK OPTIMALITY OF FACE 124 :
      D2(10) = DEL(4,4) - DEL(4,2)
      D4(10) = DEL(2,2) - DEL(4,2)
      E214 = -E124
      D1(12) = D2(10)*D1(3) + D4(10)*E214
      D3(15) = D1(12)*D3(5) + D2(12)*E132 + D4(12)*E134
```

```
IF (D1(12).LE.ZERO .OR. D2(12).LE.ZERO .OR. 1 D3(15).GT.ZERO .OR. D4(12).LE.ZERO)
GO TO 430
NVS = 3
RIS(3) = RIS(4)
RJS(3) = RJS(4)
SUM = D1(12) + D2(12) + D4(12)
ALS(1) = D1(12)/SUM
ALS(2) = D2(12)/SUM
ALS(3) = ONE - ALS(1) - ALS(2)
ZSOL(1) = Y(1,4) + ALS(1)*(Y(1,1) - Y(1,4)) + 1 ALS(2)*(Y(1,2) - Y(1,4))
ZSOL(2) = Y(2,4) + ALS(1)*(Y(2,1) - Y(2,4)) + 1 ALS(2)*(Y(2,2) - Y(2,4))
ZSOL(3) = Y(3,4) + ALS(1)*(Y(3,1) - Y(3,4)) + 1 ALS(2)*(Y(3,2) - Y(3,4))
DSTSQ = ZSOL(1)*ZSOL(1) + ZSOL(2)*ZSOL(2) + ZSOL(3)*ZSOL(3)
Y(1,3) = Y(1,4)
Y(2,3) = Y(2,4)
Y(3,3) = Y(3,4)
DEL(3,1) = DEL(4,1)
DEL(3,2) = DEL(4,2)
DEL(3,3) = DEL(4,4)
RETURN
430 CONTINUE
————CHECK OPTIMALITY OF FACE 134 :
D3(11) = DEL(4,4) - DEL(4,3)
D4(11) = DEL(3,3) - DEL(4,3)
E314 = -E134
D1(13) = D3(11)*D1(5) + D4(11)*E314
D2(15) = D1(13)*D2(3) + D3(13)*E123 + D4(13)*E124
IF (D1(13).LE.ZERO .OR. D2(15).GT.ZERO .OR. 1 D3(13).LE.ZERO .OR. D4(13).LE.ZERO)
GO TO 435 NVS = 3
```

```
RIS(2) = RIS(4)
RJS(2) = RJS(4)
SUM = D1(13) + D3(13) + D4(13)
ALS(1) = D1(13)/SUM
ALS(3) = D3(13)/SUM
ALS(2) = ONE - ALS(1) - ALS(3)
ZSOL(1) = Y(1,4) + ALS(1)*(Y(1,1) - Y(1,4)) + 1 ALS(3)*(Y(1,3) - Y(1,4))
ZSOL(2) = Y(2,4) + ALS(1)*(Y(2,1) - Y(2,4)) + 1 ALS(3)*(Y(2,3) - Y(2,4))
ZSOL(3) = Y(3,4) + ALS(1)*(Y(3,1) - Y(3,4)) + 1 ALS(3)*(Y(3,3) - Y(3,4))
DSTSQ = ZSOL(1)*ZSOL(1) + ZSOL(2)*ZSOL(2) + ZSOL(3)*ZSOL(3)
Y(1,2) = Y(1,4)
Y(2,2) = Y(2,4)
Y(3,2) = Y(3,4)
DEL(2,1) = DEL(4,1)
DEL(2,2) = DEL(4,4)
DEL(3,2) = DEL(4,3)
RETURN
435 CONTINUE
————CHECK OPTIMALITY OF THE HULL OF ALL 4 POINTS :
E243 = DEL(3,2) - DEL(4,3)
D4(14) = D2(6)*D4(10) + D3(6)*E243
E234 = DEL(4,2) - DEL(4,3)
D3(14) = D2(10)*D3(6) + D4(10)*E234
E324 = -E234
D2(14) = D3(11)*D2(6) + D4(11)*E324
D1(15) = D2(14)*D1(3) + D3(14)*E213 + D4(14)*E214
IF (D1(15).LE.ZERO .OR. D2(15).LE.ZERO .OR. 1 D3(15).LE.ZERO .OR. D4(15).LE.ZERO)
GO TO 440
SUM = D1(15) + D2(15) + D3(15) + D4(15)
```

```
ALS(1) = D1(15)/SUM
ALS(2) = D2(15)/SUM
ALS(3) = D3(15)/SUM
ALS(4) = ONE - ALS(1) - ALS(2) - ALS(3)
ZSOL(1) = ALS(1)*Y(1,1) + ALS(2)*Y(1,2) + 1 ALS(3)*Y(1,3) + ALS(4)*Y(1,4)
ZSOL(2) = ALS(1)*Y(2,1) + ALS(2)*Y(2,2) + 1 ALS(3)*Y(2,3) + ALS(4)*Y(2,4)
ZSOL(3) = ALS(1)*Y(3,1) + ALS(2)*Y(3,2) + 1 ALS(3)*Y(3,3) + ALS(4)*Y(3,4)
DSTSQ = ZSOL(1)*ZSOL(1) + ZSOL(2)*ZSOL(2) + ZSOL(3)*ZSOL(3) RETURN
440 CONTINUE
———-CHECK OPTIMALITY OF VERTEX 2 :
IF (D1(3).GT.ZERO .OR. D3(6).GT.ZERO .OR. 1 D4(10).GT.ZERO)
GO TO 445
NVS = 1
RIS(1) = RIS(2)
RJS(1) = RJS(2)
ALS(1) = D2(2)
ZSOL(1) = Y(1,2)
ZSOL(2) = Y(2,2)
ZSOL(3) = Y(3,2)
DSTSQ = DEL(2,2)
Y(1,1) = Y(1,2)
Y(2,1) = Y(2,2)
Y(3,1) = Y(3,2)
DEL(1,1) = DEL(2,2)
RETURN
445 CONTINUE
———-CHECK OPTIMALITY OF VERTEX 3 :
IF (D1(5).GT.ZERO .OR. D2(6).GT.ZERO .OR. 1 D4(11).GT.ZERO)
GO TO 450 NVS = 1
```

```
RIS(1) = RIS(3) RJS(1) = RJS(3)
ALS(1) = D3(4)
ZSOL(1) = Y(1,3)
ZSOL(2) = Y(2,3)
ZSOL(3) = Y(3,3)
DSTSQ = DEL(3,3)
Y(1,1) = Y(1,3)
Y(2,1) = Y(2,3)
Y(3,1) = Y(3,3)
DEL(1,1) = DEL(3,3)
RETURN
450 CONTINUE
———-CHECK OPTIMALITY OF VERTEX 4 :
IF (D1(9).GT.ZERO .OR. D2(10).GT.ZERO .OR. 1 D3(11).GT.ZERO)
GO TO 455
NVS = 1
RIS(1) = RIS(4)
RJS(1) = RJS(4)
ALS(1) = D4(8)
ZSOL(1) = Y(1,4)
ZSOL(2) = Y(2,4)
ZSOL(3) = Y(3,4)
DSTSQ = DEL(4,4)
Y(1,1) = Y(1,4)
Y(2,1) = Y(2,4)
Y(3,1) = Y(3,4)
DEL(1,1) = DEL(4,4)
RETURN
455 CONTINUE
```

```
———– CHECK OPTIMALITY OF LINE SEGMENT 23 :
IF (D1(7).GT.ZERO .OR. D2(6).LE.ZERO .OR. 1 D3(6).LE.ZERO .OR. D4(14).GT.ZERO)
GO TO 460
NVS = 2
RIS(1) = RIS(3)
RJS(1) = RJS(3)
SUM = D2(6) + D3(6)
ALS(2) = D2(6)/SUM
ALS(1) = ONE - ALS(2)
ZSOL(1) = Y(1,3) + ALS(2)*(Y(1,2) - Y(1,3))
ZSOL(2) = Y(2,3) + ALS(2)*(Y(2,2) - Y(2,3))
ZSOL(3) = Y(3,3) + ALS(2)*(Y(3,2) - Y(3,3))
DSTSQ = ZSOL(1)*ZSOL(1) + ZSOL(2)*ZSOL(2) + ZSOL(3)*ZSOL(3)
Y(1,1) = Y(1,3)
Y(2,1) = Y(2,3)
Y(3,1) = Y(3,3)
DEL(2,1) = DEL(3,2)
DEL(1,1) = DEL(3,3)
RETURN
460 CONTINUE
———- CHECK OPTIMALITY OF LINE SEGMENT 24 :
IF (D1(12).GT.ZERO .OR. D2(10).LE.ZERO .OR. 1 D3(14).GT.ZERO .OR. D4(10).LE.ZERO)
GO TO 465
NVS = 2
RIS(1) = RIS(4)
RJS(1) = RJS(4)
SUM = D2(10) + D4(10)
ALS(2) = D2(10)/SUM
ALS(1) = ONE - ALS(2)
```

```
ZSOL(1) = Y(1,4) + ALS(2)*(Y(1,2) - Y(1,4))
ZSOL(2) = Y(2,4) + ALS(2)*(Y(2,2) - Y(2,4))
ZSOL(3) = Y(3,4) + ALS(2)*(Y(3,2) - Y(3,4))
DSTSQ = ZSOL(1)*ZSOL(1) + ZSOL(2)*ZSOL(2) + ZSOL(3)*ZSOL(3)
Y(1,1) = Y(1,4)
Y(2,1) = Y(2,4)
Y(3,1) = Y(3,4)
DEL(2,1) = DEL(4,2)
DEL(1,1) = DEL(4,4)
RETURN 465
CONTINUE
———CHECK OPTIMALITY OF LINE SEGMENT 34 :
IF (D1(13).GT.ZERO .OR. D2(14).GT.ZERO .OR. 1 D3(11).LE.ZERO .OR. D4(11).LE.ZERO)
GO TO 470
NVS = 2
RIS(1) = RIS(3)
RIS(2) = RIS(4)
RJS(1) = RJS(3)
RJS(2) = RJS(4)
SUM = D3(11) + D4(11)
ALS(1) = D3(11)/SUM
ALS(2) = ONE - ALS(1)
ZSOL(1) = Y(1,4) + ALS(1)*(Y(1,3) - Y(1,4))
ZSOL(2) = Y(2,4) + ALS(1)*(Y(2,3) - Y(2,4))
ZSOL(3) = Y(3,4) + ALS(1)*(Y(3,3) - Y(3,4))
DSTSQ = ZSOL(1)*ZSOL(1) + ZSOL(2)*ZSOL(2) + ZSOL(3)*ZSOL(3)
Y(1,1) = Y(1,3)
Y(2,1) = Y(2,3)
Y(3,1) = Y(3,3)
```

```
Y(1,2) = Y(1,4)
Y(2,2) = Y(2,4)
Y(3,2) = Y(3,4)
DEL(1,1) = DEL(3,3)
DEL(2,1) = DEL(4,3)
DEL(2,2) = DEL(4,4)
RETURN
470 CONTINUE
———- CHECK OPTIMALITY OF FACE 234 :
IF (D1(15).GT.ZERO .OR. D2(14).LE.ZERO .OR. 1 D3(14).LE.ZERO .OR. D4(14).LE.ZERO)
GO TO 475
NVS = 3
RIS(1) = RIS(4)
RJS(1) = RJS(4)
SUM = D2(14) + D3(14) + D4(14)
ALS(2) = D2(14)/SUM
ALS(3) = D3(14)/SUM
ALS(1) = ONE - ALS(2) - ALS(3)
ZSOL(1) = Y(1,4) + ALS(2)*(Y(1,2) - Y(1,4)) + 1 ALS(3)*(Y(1,3) - Y(1,4))
ZSOL(2) = Y(2,4) + ALS(2)*(Y(2,2) - Y(2,4)) + 1 ALS(3)*(Y(2,3) - Y(2,4))
ZSOL(3) = Y(3,4) + ALS(2)*(Y(3,2) - Y(3,4)) + 1 ALS(3)*(Y(3,3) - Y(3,4))
DSTSQ = ZSOL(1)*ZSOL(1) + ZSOL(2)*ZSOL(2) + ZSOL(3)*ZSOL(3)
Y(1,1) = Y(1,4) Y(2,1) = Y(2,4)
Y(3,1) = Y(3,4)
DEL(1,1) = DEL(4,4)
DEL(2,1) = DEL(4,2)
DEL(3,1) = DEL(4,3)
RETURN
475 CONTINUE
```

———NEED TO GO FOR THE BACKUP PROCEDURE :

C(WITHOUT RECOMPUTING THE DI(*) VALUES)

GO TO 1050

C====

C THE BACKUP PROCEDURE BEGINS ...

C====

1000 GO TO (1100, 1200, 1300, 1400), NVS

——-IF THE DI(*) VALUES ARE ALREADY AVAILABLE,

THEN GO TO 1101, 1201, 1301, OR 1401: 1050 GO TO (1101, 1201, 1301, 1401), NVS

*******CASE OF A SINGLE POINT ...

1100 CONTINUE

1101 CONTINUE

DSTSQ = DEL(1,1)

ALS(1) = D1(1)

ZSOL(1) = Y(1,1)

ZSOL(2) = Y(2,1)

ZSOL(3) = Y(3,1)

BACKUP = .TRUE.

RETURN

********CASE OF TWO POINTS ...

1200 CONTINUE D2(3) = DEL(1,1) - DEL(2,1)

D1(3) = DEL(2,2) - DEL(2,1)

1201 CONTINUE

———–CHECK VERTEX 1 :

DSTSQ = DEL(1,1)

NVSD = 1

ALS(1) = D1(1)

ZSOL(1) = Y(1,1)

ZSOL(2) = Y(2,1)

```
ZSOL(3) = Y(3,1)
IORD(1) = 1
1210 CONTINUE
———-CHECK LINE SEGMENT 12 :
IF(D1(3).LE.ZERO .OR. D2(3).LE.ZERO)
GO TO 1220
SUM = D1(3) + D2(3)
ALSD(1) = D1(3)/SUM
ALSD(2) = ONE - ALSD(1)
ZSOLD(1) = Y(1,2) + ALSD(1)*(Y(1,1) - Y(1,2))
ZSOLD(2) = Y(2,2) + ALSD(1)*(Y(2,1) - Y(2,2))
ZSOLD(3) = Y(3,2) + ALSD(1)*(Y(3,1) - Y(3,2))
DSTSQD = ZSOLD(1)*ZSOLD(1) + ZSOLD(2)*ZSOLD(2) + 1 ZSOLD(3)*ZSOLD(3)
IF (DSTSQD .GE. DSTSQ)
GO TO 1220
DSTSQ = DSTSQD
NVSD = 2
ALS(1) = ALSD(1)
ALS(2) = ALSD(2)
ZSOL(1) = ZSOLD(1)
ZSOL(2) = ZSOLD(2)
ZSOL(3) = ZSOLD(3)
IORD(1) = 1
IORD(2) = 2
1220 CONTINUE
——- CHECK VERTEX 2 :
IF (DEL(2,2) .GE. DSTSQ)
GO TO 1230
DSTSQ = DEL(2,2)
```

```
NVSD = 1
ALS(1) = D2(2)
ZSOL(1) = Y(1,2)
ZSOL(2) = Y(2,2)
ZSOL(3) = Y(3,2)
IORD(1) = 2
1230 CONTINUE
——— GO TO 1600
******CASE OF THREE POINTS ...
1300 CONTINUE
D2(3) = DEL(1,1) - DEL(2,1)
D3(5) = DEL(1,1) - DEL(3,1)
E132 = DEL(2,1) - DEL(3,2)
D1(3) = DEL(2,2) - DEL(2,1)
D3(7) = D1(3)*D3(5) + D2(3)*E132
E123 = DEL(3,1) - DEL(3,2)
D1(5) = DEL(3,3) - DEL(3,1)
D2(7) = D1(5)*D2(3) + D3(5)*E123
E213 = -E123
D2(6) = DEL(3,3) - DEL(3,2)
D3(6) = DEL(2,2) - DEL(3,2)
D1(7) = D2(6)*D1(3) + D3(6)*E213
1301 CONTINUE
————–CHECK VERTEX 1 :
DSTSQ = DEL(1,1)
NVSD = 1
ALS(1) = D1(1)
ZSOL(1) = Y(1,1)
ZSOL(2) = Y(2,1)
```

```
ZSOL(3) = Y(3,1)
IORD(1) = 1
1310 CONTINUE
———CHECK LINE SEGMENT 12 :
IF (D1(3).LE.ZERO .OR. D2(3).LE. ZERO)
GO TO 1320
SUM = D1(3) + D2(3)
ALSD(1) = D1(3)/SUM
ALSD(2) = ONE - ALSD(1)
ZSOLD(1) = Y(1,2) + ALSD(1)*(Y(1,1) - Y(1,2))
ZSOLD(2) = Y(2,2) + ALSD(1)*(Y(2,1) - Y(2,2))
ZSOLD(3) = Y(3,2) + ALSD(1)*(Y(3,1) - Y(3,2))
DSTSQD = ZSOLD(1)*ZSOLD(1) + ZSOLD(2)*ZSOLD(2) + 1 ZSOLD(3)*ZSOLD(3)
IF (DSTSQD .GE. DSTSQ)
GO TO 1320
DSTSQ = DSTSQD
NVSD = 2
ALS(1) = ALSD(1)
ALS(2) = ALSD(2)
ZSOL(1) = ZSOLD(1)
ZSOL(2) = ZSOLD(2)
ZSOL(3) = ZSOLD(3)
IORD(1) = 1 IORD(2) = 2
1320 CONTINUE
———CHECK LINE SEGMENT 13 :
IF (D1(5).LE.ZERO .OR. D3(5).LE.ZERO)
GO TO 1330
SUM = D1(5) + D3(5)
ALSD(1) = D1(5)/SUM
```

```
ALSD(2) = ONE - ALSD(1)
ZSOLD(1) = Y(1,3) + ALSD(1)*(Y(1,1) - Y(1,3))
ZSOLD(2) = Y(2,3) + ALSD(1)*(Y(2,1) - Y(2,3))
ZSOLD(3) = Y(3,3) + ALSD(1)*(Y(3,1) - Y(3,3))
DSTSQD = ZSOLD(1)*ZSOLD(1) + ZSOLD(2)*ZSOLD(2) + 1 ZSOLD(3)*ZSOLD(3)
IF (DSTSQD .GE. DSTSQ)
GO TO 1330
DSTSQ = DSTSQD
NVSD = 2
ALS(1) = ALSD(1)
ALS(2) = ALSD(2)
ZSOL(1) = ZSOLD(1)
ZSOL(2) = ZSOLD(2)
ZSOL(3) = ZSOLD(3)
IORD(1) = 1
IORD(2) = 3
1330 CONTINUE
———CHECK FACE 123 :
IF (D1(7).LE.ZERO .OR. D2(7).LE.ZERO .OR. 1 D3(7).LE.ZERO)
GO TO 1340
SUM = D1(7) + D2(7) + D3(7)
ALSD(1) = D1(7)/SUM
ALSD(2) = D2(7)/SUM
ALSD(3) = ONE - ALSD(1) - ALSD(2)
ZSOLD(1) = Y(1,3) + ALSD(1)*(Y(1,1) - Y(1,3)) + 1 ALSD(2)*(Y(1,2) - Y(1,3))
ZSOLD(2) = Y(2,3) + ALSD(1)*(Y(2,1) - Y(2,3)) + 1 ALSD(2)*(Y(2,2) - Y(2,3))
ZSOLD(3) = Y(3,3) + ALSD(1)*(Y(3,1) - Y(3,3)) + 1 ALSD(2)*(Y(3,2) - Y(3,3))
DSTSQD = ZSOLD(1)*ZSOLD(1) + ZSOLD(2)*ZSOLD(2) + 1 ZSOLD(3)*ZSOLD(3)
IF (DSTSQD .GE. DSTSQ)
```

```
GO TO 1340
DSTSQ = DSTSQD
NVSD = 3
ALS(1) = ALSD(1)
ALS(2) = ALSD(2)
ALS(3) = ALSD(3)
ZSOL(1) = ZSOLD(1)
ZSOL(2) = ZSOLD(2)
ZSOL(3) = ZSOLD(3)
IORD(1) = 1
IORD(2) = 2
IORD(3) = 3
1340 CONTINUE
———————-CHECK VERTEX 2 :
IF (DEL(2,2) .GE. DSTSQ)
GO TO 1350 NVSD = 1
DSTSQ = DEL(2,2)
ALS(1) = D2(2)
ZSOL(1) = Y(1,2)
ZSOL(2) = Y(2,2)
ZSOL(3) = Y(3,2)
IORD(1) = 2
1350 CONTINUE
———————-CHECK VERTEX 3 :
IF (DEL(3,3) .GE. DSTSQ)
GO TO 1360
NVSD = 1
DSTSQ = DEL(3,3)
ALS(1) = D3(4)
```

```
ZSOL(1) = Y(1,3)
ZSOL(2) = Y(2,3)
ZSOL(3) = Y(3,3)
IORD(1) = 3
1360 CONTINUE
———- CHECK LINE SEGMENT 23 :
IF (D2(6).LE.ZERO .OR. D3(6).LE.ZERO)
GO TO 1370 SUM = D2(6) + D3(6)
ALSD(2) = D2(6)/SUM
ALSD(1) = ONE - ALSD(2)
ZSOLD(1) = Y(1,3) + ALSD(2)*(Y(1,2) - Y(1,3))
ZSOLD(2) = Y(2,3) + ALSD(2)*(Y(2,2) - Y(2,3))
ZSOLD(3) = Y(3,3) + ALSD(2)*(Y(3,2) - Y(3,3))
DSTSQD = ZSOLD(1)*ZSOLD(1) + ZSOLD(2)*ZSOLD(2) + 1
ZSOLD(3)*ZSOLD(3) IF (DSTSQD .GE. DSTSQ)
GO TO 1370
DSTSQ = DSTSQD
NVSD = 2
ALS(1) = ALSD(1)
ALS(2) = ALSD(2)
ZSOL(1) = ZSOLD(1)
ZSOL(2) = ZSOLD(2)
ZSOL(3) = ZSOLD(3)
IORD(1) = 3
IORD(2) = 2
1370 CONTINUE
GO TO 1600
***** CASE OF FOUR POINTS ...
1400 CONTINUE
```

D2(3) = DEL(1,1) - DEL(2,1)

D3(5) = DEL(1,1) - DEL(3,1)

D4(9) = DEL(1,1) - DEL(4,1)

E132 = DEL(2,1) - DEL(3,2)

E142 = DEL(2,1) - DEL(4,2)

D1(3) = DEL(2,2) - DEL(2,1)

D3(7) = D1(3)*D3(5) + D2(3)*E132

D4(12) = D1(3)*D4(9) + D2(3)*E142

E123 = DEL(3,1) - DEL(3,2)

E143 = DEL(3,1) - DEL(4,3)

D1(5) = DEL(3,3) - DEL(3,1)

D2(7) = D1(5)*D2(3) + D3(5)*E123

D4(13) = D1(5)*D4(9) + D3(5)*E143

D2(6) = DEL(3,3) - DEL(3,2)

D3(6) = DEL(2,2) - DEL(3,2)

E213 = -E123 D1(7) = D2(6)*D1(3) + D3(6)*E213

D4(15) = D1(7)*D4(9) + D2(7)*E142 + D3(7)*E143

E124 = DEL(4,1) - DEL(4,2)

E134 = DEL(4,1) - DEL(4,3)

D1(9) = DEL(4,4) - DEL(4,1)

D2(12) = D1(9)*D2(3) + D4(9)*E124

D3(13) = D1(9)*D3(5) + D4(9)*E134

D2(10) = DEL(4,4) - DEL(4,2)

D4(10) = DEL(2,2) - DEL(4,2)

E214 = -E124

D1(12) = D2(10)*D1(3) + D4(10)*E214

D3(15) = D1(12)*D3(5) + D2(12)*E132 + D4(12)*E134

D3(11) = DEL(4,4) - DEL(4,3)

D4(11) = DEL(3,3) - DEL(4,3)

```
E314 = -E134
D1(13) = D3(11)*D1(5) + D4(11)*E314
D2(15) = D1(13)*D2(3) + D3(13)*E123 + D4(13)*E124
E243 = DEL(3,2) - DEL(4,3)
D4(14) = D2(6)*D4(10) + D3(6)*E243
E234 = DEL(4,2) - DEL(4,3)
D3(14) = D2(10)*D3(6) + D4(10)*E234
E324 = -E234
D2(14) = D3(11)*D2(6) + D4(11)*E324
D1(15) = D2(14)*D1(3) + D3(14)*E213 + D4(14)*E214
1401 CONTINUE
——– CHECK VERTEX 1 :
DSTSQ = DEL(1,1) NVSD = 1
ALS(1) = D1(1)
ZSOL(1) = Y(1,1)
ZSOL(2) = Y(2,1)
ZSOL(3) = Y(3,1)
IORD(1) = 1
1405 CONTINUE
——— CHECK LINE SEGMENT 12 :
IF (D1(3).LE.ZERO .OR. D2(3).LE.ZERO)
GO TO 1410
SUM = D1(3) + D2(3)
ALSD(1) = D1(3)/SUM
ALSD(2) = ONE - ALSD(1)
ZSOLD(1) = Y(1,2) + ALSD(1)*(Y(1,1) - Y(1,2))
ZSOLD(2) = Y(2,2) + ALSD(1)*(Y(2,1) - Y(2,2))
ZSOLD(3) = Y(3,2) + ALSD(1)*(Y(3,1) - Y(3,2))
DSTSQD = ZSOLD(1)*ZSOLD(1) + ZSOLD(2)*ZSOLD(2) + 1 ZSOLD(3)*ZSOLD(3)
```

```
IF (DSTSQD .GE. DSTSQ)
GO TO 1410
DSTSQ = DSTSQD
NVSD = 2
ALS(1) = ALSD(1)
ALS(2) = ALSD(2)
ZSOL(1) = ZSOLD(1)
ZSOL(2) = ZSOLD(2)
ZSOL(3) = ZSOLD(3)
IORD(1) = 1
IORD(2) = 2
1410 CONTINUE
——— CHECK LINE SEGMENT 13 :
IF (D1(5).LE.ZERO .OR. D3(5).LE.ZERO)
GO TO 1415
SUM = D1(5) + D3(5)
ALSD(1) = D1(5)/SUM
ALSD(2) = ONE - ALSD(1)
ZSOLD(1) = Y(1,3) + ALSD(1)*(Y(1,1) - Y(1,3))
ZSOLD(2) = Y(2,3) + ALSD(1)*(Y(2,1) - Y(2,3))
ZSOLD(3) = Y(3,3) + ALSD(1)*(Y(3,1) - Y(3,3))
DSTSQD = ZSOLD(1)*ZSOLD(1) + ZSOLD(2)*ZSOLD(2) + 1 ZSOLD(3)*ZSOLD(3)
IF (DSTSQD .GE. DSTSQ)
GO TO 1415 DSTSQ = DSTSQD
NVSD = 2
ALS(1) = ALSD(1)
ALS(2) = ALSD(2)
ZSOL(1) = ZSOLD(1)
ZSOL(2) = ZSOLD(2)
```

```
ZSOL(3) = ZSOLD(3)
IORD(1) = 1
IORD(2) = 3
1415 CONTINUE
——— CHECK FACE 123 :
IF (D1(7).LE.ZERO .OR. D2(7).LE.ZERO .OR. 1 D3(7).LE.ZERO)
GO TO 1420
SUM = D1(7) + D2(7) + D3(7)
ALSD(1) = D1(7)/SUM
ALSD(2) = D2(7)/SUM
ALSD(3) = ONE - ALSD(1) - ALSD(2)
ZSOLD(1) = Y(1,3) + ALSD(1)*(Y(1,1) - Y(1,3)) + 1 ALSD(2)*(Y(1,2) - Y(1,3))
ZSOLD(2) = Y(2,3) + ALSD(1)*(Y(2,1) - Y(2,3)) + 1 ALSD(2)*(Y(2,2) - Y(2,3))
ZSOLD(3) = Y(3,3) + ALSD(1)*(Y(3,1) - Y(3,3)) + 1 ALSD(2)*(Y(3,2) - Y(3,3))
DSTSQD = ZSOLD(1)*ZSOLD(1) + ZSOLD(2)*ZSOLD(2) + 1 ZSOLD(3)*ZSOLD(3)
IF (DSTSQD .GE. DSTSQ)
GO TO 1420
DSTSQ = DSTSQD
NVSD = 3
ALS(1) = ALSD(1)
ALS(2) = ALSD(2)
ALS(3) = ALSD(3)
ZSOL(1) = ZSOLD(1)
ZSOL(2) = ZSOLD(2)
ZSOL(3) = ZSOLD(3)
IORD(1) = 1
IORD(2) = 2
IORD(3) = 3
1420 CONTINUE
```

———- CHECK LINE SEGMENT 14 :

IF (D1(9).LE.ZERO .OR. D4(9).LE.ZERO)

GO TO 1425

SUM = D1(9) + D4(9)

ALSD(1) = D1(9)/SUM

ALSD(2) = ONE - ALSD(1)

ZSOLD(1) = Y(1,4) + ALSD(1)*(Y(1,1) - Y(1,4))

ZSOLD(2) = Y(2,4) + ALSD(1)*(Y(2,1) - Y(2,4))

ZSOLD(3) = Y(3,4) + ALSD(1)*(Y(3,1) - Y(3,4))

DSTSQD = ZSOLD(1)*ZSOLD(1) + ZSOLD(2)*ZSOLD(2) + 1 ZSOLD(3)*ZSOLD(3)

IF (DSTSQD .GE. DSTSQ)

GO TO 1425

DSTSQ = DSTSQD

NVSD = 2

ALS(1) = ALSD(1)

ALS(2) = ALSD(2)

ZSOL(1) = ZSOLD(1)

ZSOL(2) = ZSOLD(2)

ZSOL(3) = ZSOLD(3)

IORD(1) = 1

IORD(2) = 4

1425 CONTINUE

——– CHECK FACE 124 :

IF (D1(12).LE.ZERO .OR. D2(12).LE.ZERO .OR. 1

D4(12).LE.ZERO)

GO TO 1430

SUM = D1(12) + D2(12) + D4(12)

ALSD(1) = D1(12)/SUM

ALSD(2) = D2(12)/SUM

```
ALSD(3) = ONE - ALSD(1) - ALSD(2)
ZSOLD(1) = Y(1,4) + ALSD(1)*(Y(1,1) - Y(1,4)) + 1 ALSD(2)*(Y(1,2) - Y(1,4))
ZSOLD(2) = Y(2,4) + ALSD(1)*(Y(2,1) - Y(2,4)) + 1 ALSD(2)*(Y(2,2) - Y(2,4))
ZSOLD(3) = Y(3,4) + ALSD(1)*(Y(3,1) - Y(3,4)) + 1 ALSD(2)*(Y(3,2) - Y(3,4))
DSTSQD = ZSOLD(1)*ZSOLD(1) + ZSOLD(2)*ZSOLD(2) + 1 ZSOLD(3)*ZSOLD(3)
IF (DSTSQD .GE. DSTSQ)
GO TO 1430
DSTSQ = DSTSQD
NVSD = 3
ALS(1) = ALSD(1)
ALS(2) = ALSD(2)
ALS(3) = ALSD(3)
ZSOL(1) = ZSOLD(1)
ZSOL(2) = ZSOLD(2)
ZSOL(3) = ZSOLD(3)
IORD(1) = 1
IORD(2) = 2
IORD(3) = 4
1430 CONTINUE
—— CHECK FACE 134 :
IF (D1(13).LE.ZERO .OR. 1 D3(13).LE.ZERO .OR. D4(13).LE.ZERO)
GO TO 1435
SUM = D1(13) + D3(13) + D4(13)
ALSD(1) = D1(13)/SUM
ALSD(3) = D3(13)/SUM
ALSD(2) = ONE - ALSD(1) - ALSD(3)
ZSOLD(1) = Y(1,4) + ALSD(1)*(Y(1,1) - Y(1,4)) + 1 ALSD(3)*(Y(1,3) - Y(1,4))
ZSOLD(2) = Y(2,4) + ALSD(1)*(Y(2,1) - Y(2,4)) + 1 ALSD(3)*(Y(2,3) - Y(2,4))
ZSOLD(3) = Y(3,4) + ALSD(1)*(Y(3,1) - Y(3,4)) + 1 ALSD(3)*(Y(3,3) - Y(3,4))
```

```
DSTSQD = ZSOLD(1)*ZSOLD(1) + ZSOLD(2)*ZSOLD(2) + 1 ZSOLD(3)*ZSOLD(3)
IF (DSTSQD .GE. DSTSQ)
GO TO 1435
DSTSQ = DSTSQD
NVSD = 3
ALS(1) = ALSD(1)
ALS(2) = ALSD(2)
ALS(3) = ALSD(3)
ZSOL(1) = ZSOLD(1)
ZSOL(2) = ZSOLD(2)
ZSOL(3) = ZSOLD(3)
IORD(1) = 1
IORD(2) = 4
IORD(3) = 3
1435 CONTINUE
————-CHECK THE HULL OF ALL 4 POINTS :
IF (D1(15).LE.ZERO .OR. D2(15).LE.ZERO .OR. 1 D3(15).LE.ZERO .OR. D4(15).LE.ZERO)
GO TO 1440 SUM = D1(15) + D2(15) + D3(15) + D4(15)
ALSD(1) = D1(15)/SUM
ALSD(2) = D2(15)/SUM
ALSD(3) = D3(15)/SUM
ALSD(4) = ONE - ALSD(1) - ALSD(2) - ALSD(3)
ZSOLD(1) = ALSD(1)*Y(1,1) + ALSD(2)*Y(1,2) + 1 ALSD(3)*Y(1,3) + ALSD(4)*Y(1,4)
ZSOLD(2) = ALSD(1)*Y(2,1) + ALSD(2)*Y(2,2) + 1 ALSD(3)*Y(2,3) + ALSD(4)*Y(2,4)
ZSOLD(3) = ALSD(1)*Y(3,1) + ALSD(2)*Y(3,2) + 1 ALSD(3)*Y(3,3) + ALSD(4)*Y(3,4)
DSTSQD = ZSOLD(1)*ZSOLD(1) + ZSOLD(2)*ZSOLD(2) + 1 ZSOLD(3)*ZSOLD(3)
IF (DSTSQD .GE. DSTSQ)
GO TO 1440
DSTSQ = DSTSQD
```

```
NVSD = 4
ALS(1) = ALSD(1)
ALS(2) = ALSD(2)
ALS(3) = ALSD(3)
ALS(4) = ALSD(4)
ZSOL(1) = ZSOLD(1)
ZSOL(2) = ZSOLD(2)
ZSOL(3) = ZSOLD(3)
IORD(1) = 1
IORD(2) = 2
IORD(3) = 3
IORD(4) = 4
1440 CONTINUE
—— CHECK VERTEX 2 :
IF (DEL(2,2) .GE. DSTSQ)
GO TO 1445
NVSD = 1
DSTSQ = DEL(2,2)
ALS(1) = D2(2)
ZSOL(1) = Y(1,2)
ZSOL(2) = Y(2,2)
ZSOL(3) = Y(3,2)
IORD(1) = 2
1445 CONTINUE
—— CHECK VERTEX 3 :
IF (DEL(3,3) .GE. DSTSQ)
GO TO 1450
NVSD = 1
DSTSQ = DEL(3,3)
```

```
ALS(1) = D3(4)
ZSOL(1) = Y(1,3)
ZSOL(2) = Y(2,3)
ZSOL(3) = Y(3,3)
IORD(1) = 3
1450 CONTINUE
—– CHECK VERTEX 4 :
IF (DEL(4,4) .GE. DSTSQ)
GO TO 1455
NVSD = 1
DSTSQ = DEL(4,4)
ALS(1) = D4(8)
ZSOL(1) = Y(1,4)
ZSOL(2) = Y(2,4)
ZSOL(3) = Y(3,4)
IORD(1) = 4
1455 CONTINUE
—— CHECK LINE SEGMENT 23 :
IF (D2(6).LE.ZERO .OR. D3(6).LE.ZERO)
GO TO 1460
SUM = D2(6) + D3(6)
ALSD(2) = D2(6)/SUM
ALSD(1) = ONE - ALSD(2)
ZSOLD(1) = Y(1,3) + ALSD(2)*(Y(1,2) - Y(1,3))
ZSOLD(2) = Y(2,3) + ALSD(2)*(Y(2,2) - Y(2,3))
ZSOLD(3) = Y(3,3) + ALSD(2)*(Y(3,2) - Y(3,3))
DSTSQD = ZSOLD(1)*ZSOLD(1) + ZSOLD(2)*ZSOLD(2) + 1 ZSOLD(3)*ZSOLD(3)
IF (DSTSQD .GE. DSTSQ)
GO TO 1460
```

```
DSTSQ = DSTSQD
NVSD = 2
ALS(1) = ALSD(1)
ALS(2) = ALSD(2)
ZSOL(1) = ZSOLD(1)
ZSOL(2) = ZSOLD(2)
ZSOL(3) = ZSOLD(3)
IORD(1) = 3
IORD(2) = 2
1460 CONTINUE
——— CHECK LINE SEGMENT 24 :
IF (D2(10).LE.ZERO .OR. D4(10).LE.ZERO)
GO TO 1465
SUM = D2(10) + D4(10)
ALSD(2) = D2(10)/SUM
ALSD(1) = ONE - ALSD(2)
ZSOLD(1) = Y(1,4) + ALSD(2)*(Y(1,2) - Y(1,4))
ZSOLD(2) = Y(2,4) + ALSD(2)*(Y(2,2) - Y(2,4))
ZSOLD(3) = Y(3,4) + ALSD(2)*(Y(3,2) - Y(3,4))
DSTSQD = ZSOLD(1)*ZSOLD(1) + ZSOLD(2)*ZSOLD(2) + 1 ZSOLD(3)*ZSOLD(3)
IF (DSTSQD .GE. DSTSQ)
GO TO 1465
DSTSQ = DSTSQD
NVSD = 2
ALS(1) = ALSD(1)
ALS(2) = ALSD(2)
ZSOL(1) = ZSOLD(1)
ZSOL(2) = ZSOLD(2)
ZSOL(3) = ZSOLD(3)
```

```
IORD(1) = 4
IORD(2) = 2
1465 CONTINUE
------ CHECK LINE SEGMENT 34 :
IF (D3(11).LE.ZERO .OR. D4(11).LE.ZERO)
GO TO 1470
SUM = D3(11) + D4(11)
ALSD(1) = D3(11)/SUM
ALSD(2) = ONE - ALSD(1)
ZSOLD(1) = Y(1,4) + ALSD(1)*(Y(1,3) - Y(1,4))
ZSOLD(2) = Y(2,4) + ALSD(1)*(Y(2,3) - Y(2,4))
ZSOLD(3) = Y(3,4) + ALSD(1)*(Y(3,3) - Y(3,4))
DSTSQD = ZSOLD(1)*ZSOLD(1) + ZSOLD(2)*ZSOLD(2) + 1 ZSOLD(3)*ZSOLD(3)
IF (DSTSQD .GE. DSTSQ)
GO TO 1470
DSTSQ = DSTSQD
NVSD = 2
ALS(1) = ALSD(1)
ALS(2) = ALSD(2)
ZSOL(1) = ZSOLD(1)
ZSOL(2) = ZSOLD(2)
ZSOL(3) = ZSOLD(3)
IORD(1) = 3
IORD(2) = 4
1470 CONTINUE
------ CHECK FACE 234 :
IF (D2(14).LE.ZERO .OR. 1 D3(14).LE.ZERO .OR. D4(14).LE.ZERO)
GO TO 1475
SUM = D2(14) + D3(14) + D4(14)
```

```
ALSD(2) = D2(14)/SUM
ALSD(3) = D3(14)/SUM
ALSD(1) = ONE - ALSD(2) - ALSD(3)
ZSOLD(1) = Y(1,4) + ALSD(2)*(Y(1,2) - Y(1,4)) + 1 ALSD(3)*(Y(1,3) - Y(1,4))
ZSOLD(2) = Y(2,4) + ALSD(2)*(Y(2,2) - Y(2,4)) + 1 ALSD(3)*(Y(2,3) - Y(2,4))
ZSOLD(3) = Y(3,4) + ALSD(2)*(Y(3,2) - Y(3,4)) + 1 ALSD(3)*(Y(3,3) - Y(3,4))
DSTSQD = ZSOLD(1)*ZSOLD(1) + ZSOLD(2)*ZSOLD(2) + 1 ZSOLD(3)*ZSOLD(3)
IF (DSTSQD .GE. DSTSQ)
GO TO 1475
DSTSQ = DSTSQD
NVSD = 3
ALS(1) = ALSD(1)
ALS(2) = ALSD(2)
ALS(3) = ALSD(3)
ZSOL(1) = ZSOLD(1)
ZSOL(2) = ZSOLD(2)
ZSOL(3) = ZSOLD(3)
IORD(1) = 4
IORD(2) = 2
IORD(3) = 3
1475 CONTINUE
——– THE FINAL REORDERING :
1600 CONTINUE
DO 1620 K=1,NVS
RISD(K) = RIS(K)
RJSD(K) = RJS(K)
YD(1,K) = Y(1,K)
YD(2,K) = Y(2,K)
YD(3,K) = Y(3,K)
```

```
DO 1610 L=1,K
DELD(K,L) = DEL(K,L)
DELD(L,K) = DEL(K,L)
1610 CONTINUE 1620
CONTINUE
NVS = NVSD
DO 1640 K=1,NVS
KK = IORD(K)
RIS(K) = RISD(KK)
RJS(K) = RJSD(KK)
Y(1,K) = YD(1,KK)
Y(2,K) = YD(2,KK)
Y(3,K) = YD(3,KK)
DO 1630 L=1,K
LL = IORD(L)
DEL(K,L) = DELD(KK,LL)
1630 CONTINUE
1640 CONTINUE
BACKUP = .TRUE.
RETURN
C====
C THE LAST LINE OF THE SUBROUTINE DSBP :
END
C====
SUBROUTINE TRANC(NZDIM,NVI,NVJ,ZI,ZJ,NZBDIM,ZBI,ZBJ,
1 IWANT,NEWORG,CENT,NCENT)
C ====
C THIS ROUTINE IS USED FOR FORMING THE CENTROIDAL DIRECTION
AND FORMING ZBI(*,*),ZBJ(*,*) AND NEWORG(*).
```

```
=====
      INTEGER NZDIM, NVI, NVJ, NZBDIM, IWANT, L
      DIMENSION IWANT(4)
      DOUBLE PRECISION ZI(NZDIM,NVI), ZJ(NZDIM,NVJ)
      DOUBLE PRECISION ZBI(NZBDIM,NVI), ZBJ(NZBDIM,NVJ)
      DOUBLE PRECISION PI(3), PJ(3), NEWORG(3), CENT(3), NCENT(3)
      IF (IWANT(2) .EQ. 0 .AND. IWANT(4) .EQ. 1)
      GO TO 50
      C FORM THE CENTROIDS PI(*) AND PJ(*) :
      PI(1) = 0.D0 PI(2) = 0.D0 PI(3) = 0.D0
      PJ(1) = 0.D0 PJ(2) = 0.D0
      PJ(3) = 0.D0 DO 10 L=1,NVI
      PI(1) = PI(1) + ZI(1,L)
      PI(2) = PI(2) + ZI(2,L)
      PI(3) = PI(3) + ZI(3,L)
      10 CONTINUE
      DO 20 L=1,NVJ
      PJ(1) = PJ(1) + ZJ(1,L)
      PJ(2) = PJ(2) + ZJ(2,L)
      PJ(3) = PJ(3) + ZJ(3,L)
      20 CONTINUE
      PI(1) = PI(1) / DFLOAT(NVI)
      PI(2) = PI(2) / DFLOAT(NVI)
      PI(3) = PI(3) / DFLOAT(NVI)
      PJ(1) = PJ(1) / DFLOAT(NVJ)
      PJ(2) = PJ(2) / DFLOAT(NVJ)
      PJ(3) = PJ(3) / DFLOAT(NVJ)
      C FORM THE CENTROIDAL AND NEGATIVE CENTROIDAL DIRECTIONS, CENT(*)
AND NCENT(*) :
```

```
CENT(1) = PI(1) - PJ(1)
CENT(2) = PI(2) - PJ(2)
CENT(3) = PI(3) - PJ(3)
NCENT(1) = -CENT(1)
NCENT(2) = -CENT(2)
NCENT(3) = -CENT(3)
C FORM ZBI(*,*), ZBJ(*,*) AND OPTIONALLY NEWORG :
IF (IWANT(2) .EQ. 0)
GO TO 50
NEWORG(1) = ( PI(1) + PJ(1) )/2.D0
NEWORG(2) = ( PI(2) + PJ(2) )/2.D0
NEWORG(3) = ( PI(3) + PJ(3) )/2.D0
DO 30 L=1,NVI
ZBI(1,L) = ZI(1,L) - NEWORG(1)
ZBI(2,L) = ZI(2,L) - NEWORG(2)
ZBI(3,L) = ZI(3,L) - NEWORG(3)
30 CONTINUE
DO 40 L=1,NVJ
ZBJ(1,L) = ZJ(1,L) - NEWORG(1)
ZBJ(2,L) = ZJ(2,L) - NEWORG(2)
ZBJ(3,L) = ZJ(3,L) - NEWORG(3)
40 CONTINUE
RETURN
50 CONTINUE
DO 60 L=1,NVI
ZBI(1,L) = ZI(1,L)
ZBI(2,L) = ZI(2,L)
ZBI(3,L) = ZI(3,L)
60 CONTINUE
```

```
      DO 70 L=1,NVJ
      ZBJ(1,L) = ZJ(1,L)
      ZBJ(2,L) = ZJ(2,L)
      ZBJ(3,L) = ZJ(3,L)
      70 CONTINUE
      RETURN
      C ===
      THE LAST LINE OF THE SUBROUTINE TRANC :
      END
      C ===
      SUBROUTINE CSFCN(NZBDIM,NVK,ZBK,ETA,SFK,NRK)
      ====
      C THIS ROUTINE COMPUTES THE CONTACT AND SUPPORT FUNCTIONS FOR
A POLYTOPE.
      C======
      INTEGER NZBDIM, NVK, NRK, L
      DOUBLE PRECISION ZBK(NZBDIM,NVK), ETA(3), SFK
      DOUBLE PRECISION INN NRK = 1
      SFK = ZBK(1,1)*ETA(1) + ZBK(2,1)*ETA(2) + ZBK(3,1)*ETA(3)
      IF (NVK .LE. 1)
      GO TO 20
      DO 10 L=2,NVK
      INN = ZBK(1,L)*ETA(1) + ZBK(2,L)*ETA(2) + ZBK(3,L)*ETA(3)
      IF (INN .LE. SFK)
      GO TO 5
      NRK = L
      SFK = INN
      5 CONTINUE
      10 CONTINUE
```

```
20 CONTINUE
RETURN
C====
C THE LAST LINE OF THE SUBROUTINE CSFCN :
C====
* SUBROUTINE SCSFCN(NZBDIM,SVK,NVK,ZBK,ETA,SFK,NRK, * 1 AVERLSTK)
C ====
C * THIS ROUTINE COMPUTES THE SEQUENTIAL CONTACT AND
C * SUPPORT FUNCTIONS FOR A POLYTOPE.
C ====
INTEGER NZBDIM, NVK, NRK, L
DOUBLE PRECISION ZBK(NZBDIM,NVK), ETA(3), SFK
* DOUBLE PRECISION INN,INN1,INN2
* INTEGER SVK,AVERLSTK(NVK,NVK),FLAG(NVK)/SHOULD BE ALL 0/
* NRK = SVK * INN1=ETA(1)
*ZBK(1,NRK)+ETA(2)
*ZBK(2,NRK)+ETA(3)
*ZBK(3,NRK)
* DO 10 I=1,NVK
* IF(AVERLSTK(NRK,I).EQ.0) THEN "FOUND SUPPORT FUNCTION"
* GETOUT OF LOOP
* IF(FLAG(AVERLSTK(NRK,I).EQ.1) THEN
GOTO 10
* FLAG(AVERLSTK(NRK,I)=1
* INN2=ETA(1)*ZBK(1,AVERLSTK(NRK,I))+
* 1 ETA(2)*ZBK(2,AVERLSTK(NRK,I))+
* 2 ETA(3)*ZBK(3,AVERLSTK(NRK,I))
* INN=INN1-INN2 * IF(INN.GT.0.0) THEN
* NRK=AVERLSTK(NRK,I)
```

```
* INN1=ETA(1)*ZBK(1,NRK)+ETA(2)
*ZBK(2,NRK)+ETA(3)*ZBK(3,NRK)
* ENDIF
* 10 CONTINUE
* SFK=INN1
* RETURN
C=====
C THE LAST LINE OF THE SUBROUTINE SCSFCN :
END
C=====
```

B.2 GJK Driver Program (FORTRAN)

This programs reads in the necessary data structures for the two convex objects in question. It then calls the GJK program to calculate the minimum separation distance between the two objects.

```
program GJKdriver
c c This program reads n points from a data file and stores them in c 3 arrays x, y, z. c
integer nmax, u , v, i, j, p,ll
parameter (nmax=1000, u=20, v=20)
real x(nmax), y(nmax), z(nmax)
real ZI(3,nmax) real ZJ(3,nmax)
INTEGER AVERLSTI(nmax,nmax)
INTEGER AVERLSTJ(nmax,nmax)
INTEGER NVI, NVJ, NZDIM, IWANT
INTEGER NVS, RIS, RJS, NCY,SUMCOUNT,TOTCOUNT
INTEGER IERROR, K, L, M, KK DIMENSION IWANT(4), RIS(4), RJS(4)
DOUBLE PRECISION EPS
DOUBLE PRECISION ZISOL(3), ZJSOL(3), ZSOL(3), DIST
DOUBLE PRECISION ALS(4), GFINAL
```

```
DOUBLE PRECISION NEWORG(3), DI, DJ, PJ(3,8), CENTJ(3)
DOUBLE PRECISION ZERO
DOUBLE PRECISION DIEST, DJEST
DOUBLE PRECISION BSEC,ESEC,TTIME
NZDIM = 3
SUMCOUNT=0
TOTCOUNT=0
IWANT(1) = 0
EPS = 20.D0 * 1.D-11
IWANT(4) = 0
c OPEN HULL CO-ORDINATE FILES
do 5 j=1, 2
if (j.eq.1) then
open (u, FILE='componenti.txt', STATUS='OLD')
else
open (u, FILE='componentj.txt', STATUS='OLD')
endif
c Read the number of points and co-ordinates for first component
read(u,*) n
if (n.GT.nmax) then
write(*,*) 'Error: n = ', n, 'is larger than nmax =', nmax
goto 9999
endif
c Loop over the data points and write data to GJK nomenclature
do 10 i= 1, n
read(u,*) x(i), y(i), z(i)
if (j.eq.1) then
ZI(1,i)= x(i)
ZI(2,i)= y(i)
```

```
ZI(3,i)= z(i)
else
ZJ(1,i)= x(i)
ZJ(2,i)= y(i)
ZJ(3,i)= z(i)
endif
write(*,*) 'X= ', x(i), 'Y= ', y(i), 'Z= ', z(i)
10 enddo
5 enddo
c OPEN ADJACENCY FILES
do ll=1,2
if (ll==1) then
open (u, FILE='Adjacencyi.txt', STATUS='OLD')
else
open (u, FILE='Adjacencyj.txt', STATUS='OLD')
end if
c Read the number of points and co-ordinates for first component
read(u,*) n
read(u,*) m
if (ll==1) then
NVI=n
DO 11 i=1,NVI
DO 12 j=1,NVI
AVERLSTI(i,j)=0
12 enddo
11 enddo
else
NVJ=n
DO 13 i=1,NVJ
```

```
DO 13 j=1,NVJ
AVERLSTJ(i,j)=0
13 CONTINUE
end if
if (n.GT.nmax) then
write(*,*) 'Error: n = ', n, 'is larger than nmax =', nmax
goto 9999
endif
c Loop over the data points and write data to GJK nomenclature
do 105 i= 1, n
do 55 p= 1, m
if (ll==1) then
read(u,*) AVERLSTI(i,p)
if (AVERLSTI(i,p)== 0) then
exit
end if
write(*,*) 'X= ',AVERLSTI(i,p)
else read(u,*) AVERLSTJ(i,p)
if (AVERLSTJ(i,p)== 0) then
exit
end if
write(*,*) 'X= ',AVERLSTJ(i,p)
end if
55 enddo
105 enddo
c Close the file close (u) enddo !file switch looop
* CALL DISTANCE SUBROUTINE
CALL DIST3(NVI,NVJ,NZDIM,ZI,ZJ,AVERLSTI,AVERLSTJ,
1 IWANT,EPS,ZISOL,ZJSOL,ZSOL,DIST,NVS, RIS,RJS, ALS,
```

2 NCY,GFINAL,IERROR,SUMCOUNT)

OPEN (UNIT=7,FILE='DISTANCE.TXT',STATUS='OLD') WRITE (7,*) DIST CLOSE(7)

9999 stop end

B.3 Pairwise Collision Detection Algorithm

This algorithm calls the collision detection algorithm for each relevant pair of objects.

function [Distance]=PWCD(Neighbors, Component, clearance)

%Component is the list of subsystem files

%NumComps is the number of subsystems

NumComps=length(Component);

[nn,max_neighbors]= size(Neighbors);

n=1; i=0; j=0; t=0;

Tracker= eye(NumComps);

for i=1: NumComps

A = Component(i,:) ;

for j=1 : max_neighbors

nei= Neighbors(i,j);

if nei==0 break

elseif (Tracker(i,nei)==0)

Tracker(i,nei)=1;

Tracker(nei,i)=1;

B = Component(nei,:);

%% Copy convex Hull files

component1=['TransHull',A];

component2=['TransHull',B];

copyfile(component1,'componenti.txt');

copyfile(component2,'componentj.txt');

%% Copy Adjacency Files

adjacency1=['Adjacencyfacets',A];

```
adjacency2=['Adjacencyfacets',B];
copyfile(adjacency1,'Adjacencyi.txt');
copyfile(adjacency2,'Adjacencyj.txt');
%% Run Collision Detection and measure runtime
% tic; % GJK driver outputs a text file "distance.txt" that contains the collision data
!GJKdriver.exe
% toc;
% t=t+toc;
file= ['distance',num2str(n), '.txt'];
copyfile( 'distance.txt', file);
d=dlmread('distance.txt');
Distance(n)= d(1,1);
n=n+1;
end
end %% End j
end %% End i
```

Appendix C

SLICING FUNCTION (MATLAB)

This algorithm evaluates the cross-sectional dimensions of the super-hull. Given the required number of cross-sections in each dimensions, a 3D grid is created. Each line in the grid is set to be at least as long as the dimension of the bounding box in the parallel axis. This is done to ensure that each line intersects the super-hull. The intersection points are evaluated using the 180 degree interior angle sum criterion since the facets of the super-hull are all triangular.

```
function [terminator,Hull]= slice2(H,Adj,facet,xmini,xmaxi,ymini,ymaxi,zmini,zmaxi,type,step)
%% Sweep across y-range to find points on facets at each x- location
clear Hull;
Hull=[]; count =0;
x= linspace(min(H(:,1))-2,max(H(:,1))+2,step);
y= linspace(min(H(:,2))-2,max(H(:,2))+2,step);
z= linspace(min(H(:,3))-2,max(H(:,3))+2,step);
terminator= zeros(step,1);
for i=1 : length(xmini)
% x= linspace(xmini(i),xmaxi(i),step);
% y= linspace(ymini(i),ymaxi(i),step);
% z= linspace(zmini(i),zmaxi(i),step); icount=0;
for j=1 : length(y)
if type==1
dummy1=min(H(:,1));
dummy2=max(H(:,1));
LP1= [ dummy1, y(j), z(i)];
LP2= [ dummy2, y(j), z(i),];
```

```
% color= 'red ';
elseif type==2
dummy1=min(H(:,2)) ;
dummy2=max(H(:,2)) ;
LP1= [x(i), dummy1 , z(j)]; LP2= [x(i), dummy2 , z(j)];
% color= 'green';
else dummy1=min(H(:,3));
dummy2=max(H(:,3));
LP1= [x(i), y(j), dummy1];
LP2= [x(i), y(j), dummy2];
% color= 'blue ';
end
for k= 1 : length(facet(i,:))
% Extract Facet Points
if facet(i,k)>0
P1=H(Adj(facet(i,k),1),:);
P2=H(Adj(facet(i,k),2),:);
P3=H(Adj(facet(i,k),3),:);
% Calculate Plane's normal
normal=cross(P1-P2,P1-P3) ;
orient = dot(normal,(LP1-LP2));
if orient ~= 0
D = -dot(normal,P3);
mu= (D + dot(normal,LP1))/orient;
P = LP1 - mu*(LP1-LP2);
% Calculate Facet vertex Vectors
Pa= P1-P ;
Pa= Pa/norm(Pa);
Pb= P2-P ;
```

```
Pb= Pb/norm(Pb);
Pc= P3-P ;
Pc= Pc/norm(Pc);
% Calculate Interior Angles
a1= dot(Pa,Pb);
a2= dot(Pa,Pc);
a3= dot(Pb,Pc);
a = acos(a1) + acos(a2) + acos(a3);
% Check if sum=360 i.e. point lies on facet if (abs(a-2*pi)< 0.00001)
icount= icount+1;
count= count+1;
Hull(count,:)= P;
end
end
end
end
%%%%%%%%%%%%%%%%%%%%%%%%%%%%%%%%%%%%%%%%%%%%%%%%%%%%%%
if j==length(y)
terminator(i)=icount;
end
end
end
```

C.1 *Collision Culling Function (matlab)*

This is a simple function that identifies the "neighbors" of a given component by employing the visibility criterion i.e. There must be some overlap within the extremeties of any component pair, without any other component lying between the said pair, for a chance of collision to exist. Any pair that does not meet this criterion need not be tested for collision.

```
% The variable "Component" is a list of the names of all subsystem models.
```

```
function [Neighbors]= Neighbors(Component)
%%clear sum;
clear Neindex;
clear Neibax;
clear Neibay;
clear Neibaz;
%% Initialize Neighbor matrices along each axis
NumComps=length(Component);
neibax= zeros(NumComps,NumComps);
neibay= zeros(NumComps,NumComps);
neibaz= zeros(NumComps,NumComps);
neiba = zeros(3*(NumComps-1),3*(NumComps-1));
neiba2= zeros(NumComps,3*(NumComps-1));
Mini = zeros(NumComps,4); Maxi = zeros(NumComps,4);
for i =1: NumComps
C= strvcat(Component(i,:));
File= ['TransHull',C];
H=dlmread(File);
HH=H((2:length(H)),:);
Hx= sortrows(HH,1);
Hy= sortrows(HH,2);
Hz= sortrows(HH,3);
Mini(i,:)=[Hx(1,1), Hy(1,2),Hz(1,3),i];
Maxi(i,:)=[Hx(length(HH),1), Hy(length(HH),2),Hz(length(HH),3),i];
end
%% Construct sorted matrices of X,Y,Z minima and maxima
N=[Mini;Maxi];
Hx=sortrows(N,1);
Hy=sortrows(N,2);
```

```
Hz=sortrows(N,3);
%% Identify component neighbors by sequentially sweeping through each axis
for i=1 : NumComps
neibax=vecino(Hx,i,neibax);
neibay=vecino(Hy,i,neibay);
neibaz=vecino(Hz,i,neibaz);
end
neiba=[neibax, neibay,neibaz];
max=0;
for i=1 : NumComps
M= unique(neiba(i,:));
lm= length(M);
if (lm > max)
max=lm; end
for j=1 : lm
neiba2(i,j)=M(j);
end
end
Neighbors=zeros(NumComps,max-1);
for i=1 : NumComps
for j=2: max
Neighbors(i,j-1)=neiba2(i,j);
end
end
%% Count preceding neighbors (for use in refinement)
Neindex= zeros(12,1);
sum=0;
for i=1 : NumComps
Neindex(i,1)= sum;
```

```
sum2=0;
for j= 1 : max-1
if Neighbors(i,j) >i
sum2= sum2+1;
end
end
sum=sum2+ sum;
end
```

C.2 Convex Hull and Adjacency Matrix Algorithm (matlab)

This algorithm evaluates the subsystem convex hulls and calls the adjacency matrix algorithm. This operation is performed once for each subsystem. The convex hulls and adjacency matrices remain unchanged under translation, rotation and scaling.

```
function Hullpoint= HullGen(A)
format long;
i=0; k=0; v1=0; v2=0; point=1;
%% Read in Surface data
Hullpoints= dlmread(A);
X= Hullpoints(2:length(Hullpoints),:);
%% Create convex Hull
[H, v] = convhulln(X);
%% Extract Hullpoints
dummy =[H(:,1);H(:,2);H(:,3)];
dummy = sort(dummy);
i=1;
Hullindex(1)=dummy(1);
for j=2 : length(dummy)
if dummy(j)> dummy(j-1)
i=i+1;
```

```
Hullindex(i)=dummy(j);
end
end
Hullpoint= X(Hullindex,:);
%% Re-index Convex Hull
[n,m]=size(Hullpoint);
H= convhulln(Hullpoint)
hull=['Hull',A];
fid= fopen(hull,'wt');
fprintf(fid,'%d \n',n);
fclose(fid);
dummy =[H(:,1);H(:,2);H(:,3)];
dummy = sort(dummy); i=1;
Hullindex(1)=dummy(1);
for j=2 : length(dummy)
if dummy(j)> dummy(j-1)
i=i+1;
Hullindex(i)=dummy(j);
end
end
Hullpoint= Hullpoint(Hullindex,:);
dlmwrite(hull,Hullpoint,'-append');
facets=['facets',A];
dlmwrite(facets,H,',');
Adjacency(facets);
```

C.2.1 Adjacency Matrix Algorithm (matlab)

```
function Adjacency(A) format long;
    res=0; i=0; k=0; v1=0; v2=0; point=1;
```

```
%% Read in Surface data
facets= dlmread(A);
for i=1 : length(facets)
H(i,:)=facets(i,:);
end
%% Extract Connectivity data
v1=0; v2=0; max=0;
fid = fopen('connectivity.txt','wt');
rows=0; for i=1 : length(H)
count=0;
connectivity = zeros(200);
for k=1 : length(H)
p1=0; p2=0;
for j=1: 3
if H(k,j)== i
if j==1
v1=H(k,2);
v2=H(k,3);
elseif j==2
v1=H(k,1);
v2=H(k,3);
else
v1=H(k,1);
v2=H(k,2);
end
for l=1: count
%% Check if already vertex already stored
if connectivity(l)==v1
p1=1;
```

```
elseif connectivity(l)==v2
p2=1;
end
end
% Check if already stored
%% Add new vertices to list
if p1==0 && p2==0
connectivity(count+1)= v1; %#ok<AGROW>
connectivity(count+2)= v2; %#ok<AGROW>
count= count + 2;
elseif p1==0 && p2==1
connectivity(count+1)= v1; %#ok<AGROW>
count= count + 1;
elseif p1==1 && p2==0
connectivity(count+1)= v2;
count= count + 1;
end
end %% End Row Check
end % End Row
%% Update maximum number of adjacent vertices
if count > max
max=count;
end
end
for l=1: count
fprintf(fid,'%d \n',connectivity(l));
end
end
if(l==count) rows=rows+1;
```

```
fprintf(fid,'0 \n');
end
end
fclose(fid);
fid = fopen('connectivity.txt','r');
H= fscanf(fid,'%d');
fclose(fid);
[n,m]=size(H);
storage = ['Adjacency',A];
fid = fopen(storage,'wt');
fprintf(fid,'%d \n%d \n',rows,max);
fprintf(fid,'%d \n',H);
fclose(fid);
```

REFERENCES

[1] "Aerospace systems design laboratory." `http://www.asdl.gatech.edu/`.

[2] *Qhull Code for Convex Hull, Delaunay Triangulation, Voronoi Diagram, and Halfspace Intersection*, May 1995. `http://www.qhull.org/`.

[3] *Curve-based Stereo Matching Using the Minimum Hausdorff Distance*, 1996.

[4] *Nash Genetic Algorithms: Examples and Applications*, (La Jolla Marriott Hotel La Jolla, California, USA), IEEE Press, 6-9 2000.

[5] *NATOPS Flight Manual Navy Model F/A-18A /B/C/D 161353 and Up Aircraft, McDonnell Douglas Corporation*, February 2000.

[6] *NATOPS Flight Manual Navy Model F/A-18A /B/C/D 165533 and Up Aircraft, McDonnell Douglas Corporation*, February 2000.

[7] Abbott, I. and von Deonhoff, A., *Theory of Airfoil Sections*. Dover Publications Inc. New York, 1959.

[8] Abhyankar, S. S., *Algebraic Geometry for Scientists and Engineers*. AMS Bookstore, 1990.

[9] Airbus, "Super Jumbo." `http://images.surclaro.com/Screenshots/FS2004/Beluga1.jpg`, 2000. Image of Airbus Beluga.

[10] Ashley, H. and Landahl, M., *Aerodynamics of Wings and Bodies*. Dover Publications Inc. New York, 1965.

[11] Badrocke, M. and Gunston, W., *Boeing Aircraft Cutaways: The History of Boeing Aircraft Company*. Osprey Publishing Ltd. through Barnes & Noble Books, 2001.

[12] Badrocke, M. and Gunston, W., *Lockheed Aircraft Cutaways: The History of Lockheed Martin*. Osprey Publishing Ltd. through Barnes & Noble Books, 2001.

[13] Badrocke, M. and Gunston, W., *The Illustrated History of McDonnell Douglas Aircraft: From Cloudster to Boeing*. Osprey Publishing Ltd. through Barnes & Noble Books, 2001.

[14] Balaba, D., "A Survey of State-of-the Art Conceptual Design Disciplinary Set Up and Run Time Requirements." Source of Benchmarking Data for New Methodology.

[15] Balaba, D., "A General Aviation Aircraft Retrofit with an LH2-PEM Fuel Cell Power-plant," in *2008-01-2914*, vol. 01, (Aerospace Systems Design Laboratory, School of Aerospace Engineering), 2008.

[16] Balaba, Davis et al, "QuEST: Quiet Efficient Subsonic Transport," tech. rep., AIAA, 2003.

[17] Balinsky, H., "Evaluating Interface Aesthetics: a measure of symmetry," *International Symposium on Electronic Imaging*, vol. 1, pp. 1–7, 2006.

[18] Ballard Power Systems, "Fuel Cell Technology." `http://www.ballard.com/be_informed/fuel_cell_technology/roadmap`, 2005.

[19] Ballard Systems Inc, "Fuel Cell Roadmap." `http://www.ballard.com/be_informed/fuel_cell_technology/roadmap`, 2005.

[20] Ballard Transportation Products, "Xcellsis HY-205 Light Duty Fuel Cell Engine," 2003.

[21] Ballard Transportation Products, "Xcellsis HY-80 Light Duty Fuel Cell Engine," 2003.

[22] Barnsley, M., *Fractals Everywhere*. Academic Press Professional, 1993.

[23] Bennett, G., "Probability Inequalities for the Sum of Independent Random Variables," *Journal of the American Statistical Association*, vol. 57 no.297, pp. 33–45, 1962.

[24] Bertin, J. J. e. a., *Hypersonics*. Birkhaeuser, Boston, 1989.

[25] Berton, J., L. A. and Freeh, J., "Electrical Systems Analysis at NASA Glenn Research Center: Status and Prospects," in *NASA -TM*, 2003-212520.

[26] Beukers, A. e. a., "Multi-Disciplinary Design Philosophy for Aircraft Fuselages.," *Applied Composite Materials*, vol. 12, pp. 3–11, 2005.

[27] Bisplinghoff, R. L. e. a., *Aeroelasticity*. Dover Science Books, 1996.

[28] Blohm and Voss, "Bv111." `http://www.luft46.com/bv/bvp111.html`, January 2000. Blohm and Voss BV111 Aircraft.

[29] Blohm and Voss, "Bv144." `http://www.luft46.com/bv/bvp144.html`, January 2000. Blohm and Voss BV144 Aircraft.

[30] Blohm and Voss, "Bv204." `http://www.luft46.com/bv/bvp204.html`, January 2000. Blohm and Voss BV204 Aircraft.

[31] Blohm and Voss, "Bv237." `http://www.luft46.com/bv/bvp237.html`, January 2000. Blohm and Voss BV204 Aircraft.

[32] Bloor, M. and Wilson, M., "The Efficient Parameterization of Generic Aircraft Geometry," *Journal of Aircraft*, vol. 6, pp. 1269–1275, 1995.

[33] Borwein, P. and Erdélyi, T., *Polynomials and Polynomial Inequalities*. Springer-Verlag, 1995.

[34] Bower, J. L. and Christensen, C. M., "Disruptive Technologies: Catching the Wave," *Harvard Business Review*, vol. 73, no. 1, pp. 43–53, 1995.

[35] Bradley, T., M. B. M. D. and Parekh, D., "Test Results for a Fuel Cell-Powered Demonstration Aircraft ," *Society of Automotive Engineers Power Systems Conference*, vol. 1, pp. 1–8, 2006.

[36] Buckingham, E., "On physically similar systems; Illustrations of the use of dimensional equations," *Physics Review*, vol. 4, pp. 345–376, 1914.

[37] Buckley, C. and Leifer, L. J., "A Proximity Query for Continuum Path Planning," *9th International Joint Conference on Artificial Intelligence*, vol. 1, pp. 1096–1102, 1985.

[38] Bushnell, D., "SCALING: Wind Tunnel to Flight," *Annual Review of Fluid Mechanics*, vol. 38, pp. 111–128, 2006.

[39] Caddell, W. E., "On the use of aircraft density in preliminary design," *SAWE*, vol. 813, pp. 8–39, May 1969.

[40] Cameron, S., "Enhancing GJK: Computing Minimum and Penetration Distances between Convex Polyhedra," in *International Conference on Robotics and Automation*, April 1997.

[41] Cameron, S. and Culley, R., "Determining the Minimum Translation Distance Between Two Convex Polyhedra," *IEEE International Conference on Robotics and Automation*, vol. 1, pp. 591–596, 1986.

[42] Carafoli, E., *Wing Theory in Supersonic Flow* . Elsevier, 1969.

[43] Carty, A. and Davies, C., "Fusion of Aircraft Synthesis and Computer Aided Design," in *10th AIAA/ISSMO Multidisciplinary Analysis and Optimization Conference*, 2004.

[44] Chadnov, R. V., "Convex Hull Algorithms Review," *KORUS*, pp. 112–115, 2004.

[45] Chaput, A., "Preliminary Sizing Methodology for Hypersonic Vehicles," *Journal of Aircraft*, vol. Vol. 29, No. 2,, pp. 20–33, March-April 1992.

[46] Choi, T., N. T. and Soban, D., "Novel Synthesis and Analysis Methods Development towards the Design of Revolutionary Electric Propulsion and Aircraft Architectures," in *AIAA Infotech@Aerospace*, 2005.

[47] Choi, T., S. D. and Mavris, D., "Creation of a Design Framework for All-Electric Aircraft Propulsion Architectures," in *AIAA 2005-5581*, 2005.

[48] Choi, T., *A Recourse-Based Approach to the Design of Rapidly Evolving Aerospace Systems*. PhD thesis, Georgia Institute of Technology, 2008.

[49] Chu, M.-Y. e. a., "High Specific Power Lithium Polymer Battery," *Eleventh Annual Battery Conference on Applications and Advances*, vol. 1 Issue 9, pp. 163–165, 1996.

[50] Chui, C. K. and Schumaker, L. L., *Approximation Theory IX, Volume I, Theoretical Aspects*. Vanderbilt University Press, 1989.

[51] Cleveland, F. A., "Size effects in conventional aircraft," *Journal of Aircraft*, vol. 7 No. 6, pp. 483–512, 1970.

[52] Crossley, W. e. a., "A study of Adaptive Penalty Functions for Constrained Genetic Algorithm-based Optimization." In AIAA 35th Aerospace Sciences Meeting and Exhibit, Reno, Nevada, January 1997. AIAA Paper 97-0083., 1997.

[53] Daggett, D., "Hydrogen Fueled Airplanes," in *The Boeing Company*, 2003.

[54] Darnell, M., *Communications and Coding*. Taunton, Somerset, England, 1998.

[55] Das, A. e. a., *Quantum Annealing and Related Optimization Methods*. Springer, 2005.

[56] Dassault Systemes, "CATIA Design Excellence For Product Success." `http://www.3ds.com/products/catia/catia-discovery`, 2008.

[57] Datorro., J., *Convex Optimization and Euclidean Distance Geometry*. Meboo Publishing USA, 2005.

[58] de Berg, Mart ., e. a., *Computational Geometry: Algorithms and Applications*. Springer-Verlag, 2000.

[59] Deb, K. and Srinivas, N., "Multi-Objective Function Optimization Using Non-dominated Sorting Genetic Algorithms," *IEEE Transactions on Evolutionary Computation*, vol. 2 no. 3, pp. 221–248, 1995.

[60] Deb, K. e. a., "A Fast Elitist Multiobjective Genetic Algorithm : NSGA-II," *IEEE Transactions on Evolutionary Computation*, vol. 6 no.2, pp. 181–197, 2002.

[61] DeJong, K., *Analysis of the Behavior of a Class of Genetic Adaptive Systems*. PhD thesis, The University of Michigan, 1975.

[62] Donlan, C. J., "An Assessment of the Airplane Drag Problem at Transonic and Supersonic Speeds," tech. rep., National Advisory Committee for Aeronatics, 1954.

[63] Dorrance, W., *Viscous Hypersonic Flow: Theory of Reacting and Hypersonic Boundary Layers*. McGraw Hill, 1962.

[64] Drexler, E., *Nanosystems: Molecular Machinery, Manufacturing and Computation*. A. Wiley Interscience Publication, 1992.

[65] Econometrics.Com, "Oil Price Volatility." `www.wtrg.com`, August 2007. Study of Oil Price Volatility and the Major World Events that Exacerbate it.

[66] Elsenaar, A., "On Reynolds Number Effects and Simulation. In Aerodynamic Data Quality and Accuracy: Requirements and Capabilities in Wind Tunnel Testing," *AGARD*, vol. CP-429, p. 20, 1988.

[67] Elsenaar, A., "Reynolds Number Effects in Transonic Flow," *AGARD*, vol. AG-303, pp. 1–23, 1988.

[68] Farin, G. E., *NURBS: From Geometry to Practical Use*. A. K. Peters, 1999.

[69] Fleming, P. and Pashkevich, A., "Computer Aided Control System Design Using a Multiobjective Optimization Approach," *Proceedings of the IEEE Control Conference*, vol. 1, pp. 174–179, 1985.

[70] Folland, G., *Real Analysis: Modern Techniques and their Applications*. John Wiley & Sons, 1999.

[71] Fonseca, C. and Fleming, P., "Genetic Algorithms for Multi-objective Optimization: Formulation, Discussion and Generalization," *Proceedings of the Fifth International Conference on Genetic Algorithms*, vol. 1, pp. 416–423, 1993.

[72] Fonseca, C. and Fleming, P., "An Overview of Evolutionary Algorithms in Multiobjective Optimization," *Evolutionary Computation*, vol. 3 No.1, pp. 1–16, 1995.

[73] General Motors Corporation, "The Best Emissions Strategy is a Zero Emissions Strategy." `http://www.chevrolet.com/fuelcell/`, January 2008.

[74] Georgia Institute of Technology, System Realization Lab, "Optimization in Engineering Design." `www.srl.gatech.edu/education/ME6103/Pareto_ME6103.ppt`, January 2006. Pareto Optimality.

[75] Germundsson, R., "Understanding 2D Scaling." `http://demonstrations.wolfram.com/Understanding2DScaling/`, January 2008.

[76] Germundsson, R., "Understanding 2D Translation." `http://demonstrations.wolfram.com/Understanding2DTranslation/`, January 2008.

[77] Germundsson, R., "Understanding 3D Scaling." `http://demonstrations.wolfram.com/Understanding3DScaling/`, January 2008.

[78] Germundsson, R., "Understanding 3D Translation." `http://demonstrations.wolfram.com/Understanding3DTranslation/`, January 2008.

[79] Gilbert, Elmer, J. W., "A Fast Procedure for Computing the Distance Between Complex Objects in Three-Dimensional Space," *IEEE Journal of Robotics and Automation*, vol. Vol. 2., Issue 4, pp. 193–203, 1988.

[80] Goldberg, D., *Genetic Algorithms in Search, Optimization and Machine Learning.* Addison Wesley Longman, 1989.

[81] Goldberg, D. and Segrest, P., "Finite Markov Chain Analysis of Genetic Algorithms," *Proceedings of the Second International Conference on Genetic Algorithms*, vol. 1, pp. 1–8, 1987.

[82] Graham, R., "An efficient algorithm for determining the convex hull of a finite planar set," *Information Processing Letters*, vol. 1, Issue 4, pp. 132–133, 1972.

[83] Guderley, K., *The Theory of Transonic Flow.* Pergamon Press, 1962.

[84] Haack, W., "Geschoßformen kleinsten wellenwiderstandes," *Lilienthal-Gesellschaft*, vol. 139, pp. 14–28, 1941.

[85] Haines, A., "Further Evidence and Thoughts on Scale Effects at High Subsoni Speeds," *AGARD*, vol. CP-174, p. 43, 1976.

[86] Haldane, J., "On Being the Right Size," in *A Treasury of Science*, 1958.

[87] Hartzuiker, J., "On the Flow Quality Necessary for large European High Reynolds Number Wind Tunnel LEHRT," *AGARD*, vol. R-644, pp. 1–9, 1976.

[88] Heaslet, M. A. and Lomax, H., "The Calculation of Pressure on Slender Airplanes in Subsonic and Supersonic Flow," tech. rep., National Advisory Committee for Aeronautics, NACA, 1956.

[89] Heijmanns, H. and Tuzikov, A., "Similarity and Symmetry Measures for Convex Shapes Using Minkowski Addition," *International Transactions on Pattern Analysis and Machine Intelligence*, vol. 20 Issue 9, pp. 980–992, 1998.

[90] Hemaspaandra, L. A. and Selman, A. L., *Complexity Theory Retrospective II.* Springer, 1997.

[91] Hill, P., *Mechanics and Thermodynamics of Propulsion.* Addison Wesley, 1992.

[92] Holland, J., *Adaptation in Natural and Artificial Systems: an introductory analysis with applications to biology, control and artificial intelligence.* university of Michigan Press, 1975.

[93] Honda Motor Company Ltd, "Honda Fuel Cell Vehicle." `http://world.honda.com/FuelCell/`, January 2007.

[94] Hong, Q., "Physics based geometric design," tech. rep., Department of Computer Science, University of Toronto, 2005.

[95] Horn, J. and Nafpliotis, N., "Multiobjective Optimization Using Niched Pareto Genetic Algorithm," tech. rep., University of Illinois at Urbana-Champaign, 1993.

[96] Jackson, P., *Jane's All The World's Aircraft 1991-1992.* Bath Press, Bath and Glasgow, 1992.

[97] Jackson, P., *Jane's All The World's Aircraft 1994-1995.* Bath Press, Bath and Glasgow, 1995.

[98] Jackson, P., *Jane's All The World's Aircraft 1997-1998.* Bath Press, Bath and Glasgow, 1998.

[99] Jackson, P., *Jane's All The World's Aircraft 2002-2003.* Bath Press, Bath and Glasgow, 2002.

[100] Jakob, W. e. a., "Application of Genetic Algorithms to Task Plannning and Learning," *Parallel Problem Solving From Nature*, vol. 2, pp. 291–300, 1992.

[101] Jarvis, R. A., "On the identification of the convex hull of a finite set of points in the plane," *Information Processing Letters*, vol. 2, Issue 1, pp. 18–21, 1973.

[102] Joines, J. and Houck, C., "On the Use of Non-Stationary Penalty Functions to Solve Nonlinerar Constrained Optimization Problems with GA's," in *IEEE, International Conference on Evolutionary Computation*, 1994.

[103] Jones, W. e. a., "Searching Databases of Two-dimensional and Three-dimensional Data Chemical Structures Using Genetic Algorithms," *Proceedings of the Fifth International Conference on Genetic Algorithms*, vol. 1, pp. 597–602, 1993.

[104] Kim, Y. e. a., "Incremental Penetration Depth Estimation Between Convex Polytopes Using Dual-Space Expansion," *IEEE Transcations on Visualization and Computer Graphics*, vol. 10 No. 2, pp. 152–163, 2004.

[105] Kirby, M., *A Methodology for Technology Identification, Evaluation and Selection in Conceptual and Preliminary Aircraft Design.* PhD thesis, Georgia Institute of Technology, 2001.

[106] Knuth, D. E., *Lectures in Computer Science: Axioms and Hulls.* Springer- Verlag, 1992.

[107] Korner, H. e. a., "The Role of Flight Tests and Wind Tunnels in Laminar Flow Research," *ICAS 19*, vol. 1, p. 3.1.1, 1995.

[108] Kreyszig, E., *Advanced Engineering Mathematics.* John Wiley & Sons, 2005.

[109] Kuhl, F. and Giardina, C., "Elliptic Features of a Closed Contour," *Computer Vision, Graphics and Image Processing*, vol. 18, pp. 236–258, 1982.

[110] Kulfan, B., "Recent extensions and applications of the cst universal parametric geometry representation method," in *7th AIAA Aviation Technology, Integration and Operations Conference,ATIO*, 2007-7708.

[111] Kuri-Morales, A. F. and Gutierrez-Garcia, J., "Penalty Function Methods for Constrained Optimization with Genetic Algorithms: a Statistical Analysis," tech. rep., Instituto Tecnologico Autonomo de Mexico, Kuri.

[112] Laird, C., *Webster's New World Dictionary*, second edition ed., 1999.

[113] LANGLEY, N., "Vehicle sketch pad." `http://www.sbir.nasa.gov/SBIR/abstracts/05/sttr/phase1/STTR-05-1-T7.01-9925.html?solicitationId=`

STTR_05_P1, 2005. NASA Langley Software Platform for Rapid Aircraft Geometry Modeling.

[114] Lapygin, V. and Fofonov, D., "Absolutely Optimal Configurations with Maximum Lift-to-Drag Ratio at High Supersonic Flow Velocity," in *West-East High Speed Flow Field Conference*, 2007.

[115] Li, C.-C. and Lee, Y.-C., "A statistical Procedure for model building in dimensional analysis," *International Journal of Heat and Mass Transfer*, vol. 33 No. 7, pp. 1566–1567, 1990.

[116] Lin, C. and Chellapa, R., "Classification of Partial 2D Shapes Using Fourier Descriptors," *IEEE Transactions on Pattern Analysis and Machine Intelligence*, vol. 9, pp. 690–696, 1987.

[117] Lin, M., *Efficient Collision Detection for Animation and Robotics*. PhD thesis, University of California Berkeley, December 1993.

[118] Liu, J.-S. e. a., "Geometric interpretation and comparisons of enhancements of gjk algorithm for computing euclidean distance between convex polyhedra," *Academia Sinica*, 2001.

[119] Magnus, A. and Epton, E., *PANAIR, Predicting Subsonic Or Supersonic Linear Potential Flows About Arbitrary Configurations Using a Higher Order Panel Method*. NASA, 1 ed., 1980.

[120] Mason, F., "Friction." http://www.aoe.vt.edu/~mason/Mason_f/MRsoft.html/SkinFriction, 2002. A skin Friction Drag estimation Tool based on Form Factor.

[121] Mattingly, J., *Aircraft Engine Design*. AIAA Educational Series, 2002.

[122] McCullers, A., *Flight Optimization System, FLOPS Release 5.9.4*. NASA Langley Research Center, December 1998.

[123] Mehta, U., "Strategy for developing air-breathing aerospace planes," *Journal of Aircraft*, vol. 33 No. 2, pp. 377–385, 1996.

[124] Mendez, P. and Ordóñez, F., "Scaling laws from statistical data and dimensional analysis," in *Transactions of the ASME, Volume 72*, 2005.

[125] Michalewicz, J. and Fogel, D., *How to Solve it: Modern Heuristics*. Springer, 2000.

[126] Miles, J., *The Potential Theory of Unsteady Supersonic Flow* . Cambridge University Press, 1959.

[127] Milstein, M., "Superduperjumbo." `http://www.airspacemag.com/flight-today/Superduperjumbo.html?c=y&page=2`, July 2006.

[128] Mitlitsky, F. e. a., "Vehicular Hydrogen Storage Using Lightweight Tanks," in *Proceedings of the 2000 U.S DOE Hydrogen Program Review*, 2000.

[129] Moffitt, B., B. T. M. D. and Parekh, D., "Design and Performance Validation of a Fuel Cell Unmanned Aerial Vehicle ," in *7th AIAA Aviation Technology, Integration and Operations Conference (ATIO)*, 2006.

[130] Moffitt, B, B. T. M. D. and Parekh, D., "Validated Modeling and Synthesis of Medium-scale PEM Fuel Cell Aircraft ," in *4th International ASME Conference on Fuel Cell Science, Engineering and Technology*, 2006.

[131] Moffitt, B, B. T. M. D. and Parekh, D., "Development and Experimental Characterization of a Fuel Cell Powered Aircraft ," in *Journal Of Power Sources*, 2007.

[132] Moffitt, B, B. T. M. D. and Parekh, D., "Reducing Design Error of a Fuel Cell UAV through Variable Fidelity Optimization," in *7th AIAA Aviation Technology, Integration and Operations Conference (ATIO)*, 2007.

[133] Moore, F., *Theory of Laminar Flows*. Princeton University Press, 1964.

[134] Mukres, J., *Topology: A first Course*. Prentice-Hall, 1975.

[135] Multhopp, H., "The Aerodynamics of the Fuselage," tech. rep., NACA, 1924.

[136] Munk, M., "The Aerodynamics of Airship Hulls," tech. rep., NACA, 1924.

[137] Nam, T., *A generalized Sizing Methodology for Revolutionary Concepts Under Probabilistic Constraints*. PhD thesis, Georgia Institute of Technology, 2007.

[138] Nash, J. F., "Non-cooperative games," *Annals of Mathematics*, vol. 54, p. 289, 1951.

[139] Needham, L., *Aircraft Design and Construction*. Chapman & Hall, 1975.

[140] Nelson, R. C., *Flight Stability and Automatic Control*. McGraw Hill, 1989.

[141] Nemirovski, A. and Shapiro, A., "Robust Stochastic Approximation Approach," *SIAM Journal of Optimization*, vol. 1, pp. 1–35, 2008.

[142] Nickol, C., "Conceptual Design Shop," in *Conceptual Aircraft Design Working Group (CADWG21)*, 2004.

[143] Nicolai, M. L., *Fundamentals of Aircraft Design*. Dayton, Ohio, University School of Engineering, 1975.

[144] Nishida, T., "Stable marker-particle method for the Voronoi diagram in a flow field," *Journal of Computational and Applied Mathematics*, vol. 202 issue 2, pp. 377–391, 2007.

[145] Observatory, N., "Mount kilimanjaro ice cap." `http://earthobservatory.nasa.gov/Newsroom/NewImages/Images/kilimanjaro_etm_93_00.jpg`, March 2000.

[146] of Automotive Engineers, S., "Hydrogen IC Engines," in *SAE Technical Series*, Society of Automotive Engineers, 2006.

[147] Olds, J., "Class Notes on Stochastic Optimization." Georgia Institute of Technology, 2002.

[148] Ong, C.-J., "On the Quantification of Penetration Between General Objects," *International Journal of Robotics Research*, vol. 16 No. 3, pp. 400–409, 1997.

[149] PACE GmBH, "Pacelab Suite." `http://www.pace.de/en/group.php?myid=2&subid=0&mydataid=5`, 2007. Description of Engineering Workbench and Knowledge Designer Products.

[150] Parker, H. M., "Minimum Drag Ducted and Closed Three Point Body of Revolution," tech. rep., National Advisory Committee for Aeronatics, 1955.

[151] Passos, G. M., "Xmlsmart." `http://search.cpan.org/dist/XML-Smart/`, December 2004.

[152] Perakis, G. and Roels, G., "Regret in the News Vendor Model." Comparison of Regret Models, 2006.

[153] Persoon, E. and Fu, K., "Shape Descrimination Using Fourier Descriptors," *IEEE Transactions on Systems, Man and Cybernetics* , vol. 7, pp. 170–179, 1977.

[154] Phoenix, C., "Scaling Laws : Back to Basics." `http://crnano.typepad.com/crnblog/2004/08/scaling_lawsbac.html`, August 2006.

[155] Picket, R. M. e. a., "Automated structural synthesis of using a reduced number of design coordinates," *AIAA Journal*, vol. 11 no. 4, pp. 489–494, 1973.

[156] Price, M. e. a., "A Geometry Centered Process in Airframe Design," in *AIAA 5th Aviation, Technology, Integration and Operations Conference*, 2005.

[157] Rabbitz, R., *Fast Collision Detection of Moving Convex Polyhedra, Graphics Gems IV*. Academic Press Inc., 1994.

[158] Rapoport, A., *A two-person Game Theory*. Dover Publications Inc. New York, 1966.

[159] Rapoport, A., *Coalition by Sophisticated Players*. Springer-Verlag, 1979.

[160] Raymer, D., *Aircraft Design: A conceptual Approach*. AIAA, 1999.

[161] Raymer, D., "Vehicle Scaling Laws for MDO: Use of Net Design Volume to improve Optimization Realism," in *1st AIAA ATIO Forum, Los Angeles, CA.*, 2001.

[162] Raymer, D., *Enhancing Aircraft Conceptual Design Using Multidisciplinary Optimization*. PhD thesis, Department of Aeronautics, Royal Institute of Technology Stockholm, Sweden, 2002.

[163] Raymer, D., "Email: RE: Vehicle Scaling Laws for MDO," January 2007.

[164] Rogers, C. A., *Hausdorff Measures*. Cambridge University Press, 1970.

[165] Rogers, E. M., *Diffusion of Innovations*. New York Free Press, 2003.

[166] Samareh, J., " A Survey of Shape Parametrization Techniques ," *CEAS/AIAA/ICASE/NASA Langley International Forum on Aeroelasticity and Structural Dynamics*, vol. 1, pp. 333–343, June 1999.

[167] Samareh, J., "Survey of Shape Parametrization Techniques for High-Fidelity Multidisciplinary Shape Optimization," *AIAA Journal*, vol. 39, No. 5, pp. 877–884, May 2001.

[168] Sambridge, M. e. a., "Geophysical parameterization and interpolation of irregular data using natural neighbours," *Geophysical Journal International*, vol. 122, pp. 837–857, 1995.

[169] Scaled Inc, "Ares." `www.scaled.com`, 2003.

[170] Schaffer, J. and Grefenstette, J., "Multi-objective Learning via Genetic Algorithms," *Proceedings of the Ninth International Conference on Artificial Intelligence*, vol. 1, pp. 593–595, 1985.

[171] Sears, W. R., "On Projectiles of Minimum Drag," *Quaterly of Applied Mathematics*, vol. 4, pp. 303–310, 1947.

[172] Sears, W., *Small Perturbation Theory*. Princeton University Press, 1960.

[173] Segel, L., "Simplification and scaling," *SIAM review*, vol. 14, No. 4, pp. 547–571, October 1972.

[174] Sensmeier, M., "A survey of structural layouts of Post-WWII aircraft," *45th AIAA/ASME/ASCE/AHS/ASC Structures, Structural Dynamics & Materials Conference , Palm Springs, California*, vol. AIAA 2004-1624, pp. 877–884, 2004.

[175] Shane, D., "Agile responsive effective support - Design and testing of the ARES concept demonstrator aircraft ," *Aerospace Design Conference*, vol. 1, pp. 1–10, 1992.

[176] Shevell, R., "Aircraft Design: Synthesis and Analysis." `http://adg.stanford.edu/aa241/AircraftDesign.html`, September 2006.

[177] Shiffman, "Voronoi." `http://www.truveo.com/Voronoi/id/2471404506`, April 2006.

[178] Smith, A. E. and Coit, D., *"Constraint-Handling Techniques - Penalty Functions" in Handbook of Evolutionary Computation.* Institute of Physics Publishing and Oxford University Press, 1997.

[179] Soban, D., "2003 NASA/DoD UAPT PROGRAM ANNUAL REVIEW: Formulation & Development of Physics-Based Methods," tech. rep., Georgia Institute of Technology, 2003.

[180] Sobieczky, H., *New Design Concepts for High Speed Air Transport.* Springer, 1997.

[181] Sonin, A. and Probstein, R., "A generalization of the À-theorem and Dimensional Analysis," *Proceedings of the National Academy of Sciences of the United States of America*, vol. 101, pp. 8525–8526, June 2004.

[182] Srinivasan, V. and Newman, J., "A model-based comparison of various Li-ion Chemistries," tech. rep., Lawrence National Laboratory, 2005.

[183] Systems, L. M. T. A., "Best Practices: Modelling and Simulation." `http://www.bmpcoe.org/bestpractices/internal/lmtas/lmtas_6.html`, 2007. Lockheed Martin Computer Mock Up.

[184] Syswerda, G. and Palmucci, J., "The Application of Genetic Algorithms to Resource Scheduling," *Proceedings of the Forth Internation Conference on Genetic Algorithms*, vol. 1, pp. 502–508, 1991.

[185] Technology Transfer Department, "Zinc-Nickel Batteries." url/http://www.lbl.gov/tt/techs/lbnl0868.html, 1998.

[186] Terwiesch, C. and Cachon, G., *Matching Supply with Demand : An Introduction to Operations Management*. McGraw Hill Primis Custom Publishing, 2003.

[187] The Boeing Company, "Boeing 747 airplane description." www.boeing.com, December 1969.

[188] The Cessna Aircraft Company, *Information Manual Skyhawk Model 172* . Cessna, 1981.

[189] The Toyota Corporation, "Toyota FCHV." `http://www.toyota.co.jp/en/tech/environment/fchv/`, January 2008. Description of Toyota Echo-Car Initiatives.

[190] Torenbeek, E., *Synthesis of a Subsonic Airplane Design*. Kluwer Academic Publishers, 1982.

[191] Toro, E., *Riemann Solvers and Numerical Methods for Fluid Dynamics*. Springer-Verlag, 1999.

[192] Trefethen, L. and Bau, D., *Numerical Linear Algebra*. SIAM, 1997.

[193] Upton, E., *An Intelligent, Robust Approach to Volumetric Aircraft Sizing*. PhD thesis, Georgia Institute of Technology, 2007.

[194] U.S Department of Energy, "Hydrogen, Fuel Cells, & Infrastructure Technologies Program; Multi-Year Research, Development and Demonstration Plan:Planned program activities for 2003-2010.." `www.nrel.gov/docs/fy05osti/34289.pdf,March2005.`, March 2005.

[195] Van den Bergen, G., *Collision Detection*. Morgan Kaufman Publishers Inc., 2003.

[196] van der Waerden, B. L., *Algebra*. Springer-Verlag, 1993.

[197] van Otterloo, P. J., *A Contour-Oriented Approach to Digital Shape Analysis*. PhD thesis, Delft University of Technology, 1988.

[198] Vanderplaats, G. N., *Numerical Optimization Techniques For Engineering Optimization*. Vanderplaats Research and Development, Inc., 2001.

[199] Vignaux, G.A et al, "Simplifying Regression Models Using Dimensional Analysis," *Australia & New Zealand Journal of Statistics*, vol. 41, pp. 31–41, 1991.

[200] Von Karman, T., *Collected Works of Theodore Von Karman 1940-1956*. New York: Butterworths Scientific Publications, 1956.

[201] W., W. and R., M., "Hydrogen Fueled General Aviation Airplanes," in *AIAA*, 2005.

[202] Waldo, O. and Wallace, S., "Bodies of Revolution Having Minimum Total Drag in Hypersonic Flow," tech. rep., National Aeronautics and Space Administration, 1969.

[203] Warsi, Z., *Fluid Dynamics: Theoretical and Computational Approaches*. Taylor & Francis, 2006.

[204] Way, D. and Olds, J., "Sirius: A new Launch Vehicle Option for Mega-LEO Constellation Deployment," in *AIAA*, 1997.

[205] Weir, A., *Lebesgue Integration and Measure*. Cambridge University Press, 1973.

[206] Werner, R. and Wislicenus, G. F., "Analysis of Airplane Design by Similarity Considerations," in *AIAA*, 1968.

[207] Whitcomb, R., "Development of a Supersonic Area Rule and an Application to the Design of a Wing-Body Configuration," tech. rep., National Advisory Committee for Aeronatics, 1953.

[208] Whitcomb, R., "Some Considerations Regarding the Application of the Supersonic Area Rule to the Design of Airplane Fuselages," tech. rep., National Advisory Committee for Aeronatics, 1956.

[209] Wikipedia, "4.5 v." `http://en.wikipedia.org/wiki/4.5V`, May 2008.

[210] Wikipedia, "9v batteries." `http://en.wikipedia.org/wiki/9v`, May 2008.

[211] Wikipedia, ""a" batteries." `http://en.wikipedia.org/wiki/A_battery`, May 2008.

[212] Wikipedia, "Aa batteries." http://en.wikipedia.org/wiki/AA_battery, May 2008.

[213] Wikipedia, "Aaa batteries." http://en.wikipedia.org/wiki/AAA_battery, May 2008.

[214] Wikipedia, "List of battery sizes." http://en.wikipedia.org/wiki/List_of_battery_sizes, June 2008.

[215] Wikipedia, "Nils Aall Barricelli." http://en.wikipedia.org/wiki/Nils_Aall_Barricelli, April 2008.

[216] Wilf, H., *Algorithms and Complexity.* A. K. Peters, 2002.

[217] Wilkinson., H., *Aircraft Engines of the World 1970.* Paul H. Wilkinson, Washington D.C ., 1970.

[218] Will, F., "Recent Advances in Zinc-air Batteries," *Thirteenth Annual Battery Conference on Applications and Advances*, vol. 1 Issue 13, pp. 1–6, 1998.

[219] Williams, G., *Linear Algebra with Applications.* Jones & Bartlett Publishers, 2007.

[220] Woyak, S., "CAD Fusion: Bridging the hand-off from Conceptual to Preliminary Design," tech. rep., Phoenix Integration, 2007.

[221] Yakunina, Y., "Three-Dimensional Bodies of Minimum Total Drag in Hypersonic Flow," *Journal of Optimization Theory and Applications*, vol. 115, pp. 241–265, 2002.

[222] Zahn, C. and Roskies, R., "Fourier Descriptors for Plane Closed Curves," *IEEE Transactions on Computers*, vol. 21, pp. 269–281, 1972.

[223] Zhang, L. e. a., "Generalized Penetration Depth Computation," *Computer Aided Design*, vol. 39 Issue 8, pp. 625–638, 2007.

[224] Zweber, J., "Towards an Integrated Modeling Environment for Hypersonic Vehicle Design and Synthesis," in *AIAA/AAAF 11th International Space Planes and Hypersonic Systems and Technology Conference*, 2002.

VITA

Davis Balaba was born in Kampala, Uganda. For the better part of his first decade on earth, Uganda was in and out of civil wars. It was not unusual for class to get interrupted by gun fire. At this point the teacher would say "if your parents are not coming to get you, please go home." He was one of those kids that had to navigate their own way home as his mothers office was located on the opposite side of the war zone. Children were not typically harmed by the warring factions but the sights and sounds were enough to disorient even the most stoic of individuals. At school he was infamous for always solving the toughest maths problem on the test and then failing the simplest one. A sign of things to come, he always opted for the most challenging subjects and themes. The resulting excellence in themes less addressed earned him a scholarship to the United World College of The Atlantic in Wales, U.K. With students from over 100 countries, this college helped him develop a deeper understanding of cultures different from his own. He proceeded to pursue half of his undergraduate degree in aerospace engineering in Madrid, Spain ; a very rich cultural experience. He completed this degree in St. Louis, Missouri. In 2002 he began what would be a six stint at the Georgia Institute of Technology. A master's degree in aerospace engineering and an MBA later, he has arrived at this point. A point he only dared to dream about, growing up in war torn Kampala. After all, what is a life without dreams, but a wingless bird? He remains eternally grateful to his mother who was the insatiable coach that fuelled his drive to excel.